Universidade do Minho
Escola de Engenharia

Mohammad Kheradmand

Incorporation of hybrid phase change
materials in plastering mortars for
increased energy efficiency in buildings

Universidade do Minho
Escola de Engenharia

Mohammad Kheradmand

Incorporation of hybrid phase change materials in plastering mortars for increased energy efficiency in buildings

fevereiro de 2016

## STATEMENT OF INTEGRITY

I hereby declare having conducted my thesis with integrity. I confirm that I have not used plagiarism or any form of falsification of results in the process of the thesis elaboration.
I further declare that I have fully acknowledged the Code of Ethical Conduct of the University of Minho.


University of Minho, _____

Full name: _____

Signature: _____

# Acknowledgements

# Abstract

This thesis proposes the development of a new technology for improved energy efficiency in buildings by incorporation of more than one type of phase change material (hybrid PCM) in plastering mortars for façade walls. Such approach provides added benefits in regard to recent proposals of single PCM usage. Their application as lining of walls contributes to keep the indoor air temperature within acceptable comfort levels, and consequently reduce energy consumption associated to acclimatization. The focus was the strategy for minimizing heating/cooling energy consumption by applying mortars containing adequate proportions of PCMs with distinct melting temperatures and phase change enthalpies. The overall work methodology involved experimental (laboratory level, small scale testing) and numerical research with hybrid PCM, and aimed to develop a guideline for energy efficiency.

This thesis initially started with experimental part aimed characterization of the used materials (material level investigations). Then, the feasibility of hybrid PCM (i.e. incorporating more than one types of PCM with distinct melting temperature and enthalpies in the same mortar) to enhance the efficiency of PCM system was assessed through laboratory scale prototypes and real scale simulation. The experimental part of the work aimed to demonstrate the effectiveness of PCM incorporated into the plastering mortars used as internal coatings of building spaces. Two small scale prototypes were prepared with distinct interior coatings: (1) one with common plastering mortars; (2) another mortar incorporated with hybrid PCM. Both test cells have been subjected to realistic daily temperature profile, and the effect of the coatings has been assessed with recourse to internal temperature monitoring. The collected results for daily cycles showed that hybrid PCM acts reducing inside temperature amplitudes during the day and turning them closer to comfort temperature levels. Numerical thermal model was conducted to verify the experimental results. The numerical predictions for the temperature profiles were almost similar to those obtained from experimental observations. The obtained results and their comparison with monitored temperatures have shown that the numerical simulation methodology can provide feasible estimates of temperature in elements containing mortar with incorporated hybrid PCM. This confidence in the numerical framework for this purpose allows the possibility of evaluating alternative scenarios, both in terms of climate condition and melting temperature solutions of the PCM. Development and experimental evaluation were conducted for this two laboratory scale prototypes, as to enhance the

thermal energy storage potential of buildings. The prototypes were internally equipped with a heater that was programmed to keep the comfort temperature in the enclosure. A reference mortar without PCM was also applied in a prototype for comparative purposes. The hybrid PCM mortar development work has experimentally shown that the concept is feasible on the small scale and that the thermal storage of the hybrid PCM can be successfully reduces the energy consumption about 20%. It was further observed that the HPCMM plays a role in reducing the temperature variation of indoor environment, which assists to significantly decrease the energy consumption for buildings. Then, it is considered advisable to test the hybrid PCM concept in a real scale application, in order to assess thermal behaviour as well as energy saving potential of hybrid PCM mortar. The results further confirmed the energy saving potential of the hybrid PCM and consequently, provided the ground for better understanding the phase change phenomena and modelling approaches.

# Resumo

Esta tese propõe uma nova tecnologia para melhorar a eficiência energética de edifícios através da incorporação de um tipo de material de mudança de fase (PCM híbrido) em argamassas de revestimento de paredes. Esta tecnologia conduz a maiores benefícios comparando com as propostas recentes para a utilização de PCM simples. A sua aplicação no revestimento de paredes contribui para manter a temperatura interior em níveis de conforto aceitáveis e consequentemente reduzir o consumo de energia associado ao aquecimento/arrefecimento. A estratégia foi minimizar o consumo desta energia aplicando argamassas contendo adequadas proporções de PCMs com distintas temperaturas de fusão e entalpias associadas à mudança de fase. A metodologia do trabalho envolveu investigação experimental (laboratorial, testes a escala reduzida) e numérica, com PCM híbrido, com o objetivo de desenvolver um guia para a eficiência energética.

Esta tese começou com a parte experimental com vista à caraterização dos materiais utilizados (investigação ao nível do material). Depois, foi investigada a viabilidade de utilização de PCM híbrido (i.e. com incorporação de mais do que um tipo de PCM, com diferentes temperaturas de fusão e entalpias, na mesma argamassa) para aumentar a eficiência do sistema. Para o efito foram desenvolvidos protótipos à escala laboratorial e simulações numéricas à escala real. A parte experimental do trabalho teve como objetivo a demonstração das vantagens da incorporação de PCM em argamassas de revestimento interior de edifícios. Dois protótipos de pequena escala foram preparados com diferentes revestimentos interiores: (1) um com argamassa convencional; (2) um com argamassa com PCM híbrido. As duas células foram submetidas a perfis de temperatura diários reais. A influência dos revestimentos foi avaliada com recurso a monitoração das temperaturas interiores. Os resultados obtidos para ciclos diários mostraram que o PCM híbrido reduz as amplitudes térmicas interiores durante o dia e coloca-as próximas dos níveis de conforto térmico. Um modelo numérico térmico foi desenvolvido adaptando-se aos resultados experimentais. As previsões numéricas dos perfis de temperatura revelaram-se similares aos observados experimentalmente. Os resultados obtidos e a sua comparação com as temperaturas monitoradas mostraram que a metodologia seguida na simulação numérica permite estimativas corretas das temperaturas nos elementos que contêm argamassa com PCM híbrido. Esta confiança no estudo numérico permite a possibilidade de avaliar cenários alternativos, quer em termos de condições climáticas quer de temperaturas de fusão do PCM. O desenvolvimento e a avaliação experimental foram conduzidos para os dois protótipos à escala laboratorial, de forma a avaliar o potencial de armazenamento de

energia térmica de edifícios. Os protótipos foram equipados internamente com uma resistência programada para manter a temperatura de conforto no interior. Uma argamassa de referência sem PCM foi também aplicada em um protótipo para efetuar comparações. O desenvolvimento do trabalho com argamassa com PCM híbrido mostrou experimentalmente que o conceito é vantajoso a escala reduzida e que o armazenamento térmico do PCM híbrido pode reduzir o consumo de energia em cerca de 20%. Também foi observado que a HPCMM reduz a variação de temperatura no ambiente interior, o que contribui para o significativo decréscimo do consumo energético em edifícios. Assim, for considerado importante ensaiar o conceito do PCM híbrido numa aplicação à escala real, para avaliar o comportamento térmico e o potencial de poupança de energia da argamassa com PCM híbrido. Os resultados confirmaram o potencial de poupança de energia do PCM híbrido e consequentemente são uma base para melhor entender os fenómenos de mudança de fase e das representações com modelos.

# Contents

# List of Figures

# List of Tables

# Nomenclature

| | |
|---|---|
| $C_{specimen}$ | Specific heat capacity of the specimen (J/kg K) |
| $C_{PCM}$ | Specific heat capacity of the PCM (J/kg K) |
| $W_{PCM}$ | Weight ratio of the PCM to the specimen |
| $C_{mortar}$ | Specific heat capacity of the plain material (J/kg K) |
| $W_{mortar}$ | Mass fraction of the plain mortar |
| $U$ | Thermal transmittance (W/m$^2$ K) |
| $T_{Sol-Air}$ | Sol–air temperature (°C) |
| $T_{Air}$ | Exterior temperature (°C) |
| $\alpha$ | Absorption coefficient of the surface |
| $I_g$ | Global solar radiation (W/m$^2$) |
| $R_{se}$ | External surface resistance ((m$^2$ K)/W) |
| $\rho$ | Density of the material (kg/m$^3$) |
| $C(T)$ | Specific heat capacity dependent of temperature (J/kg K) |
| $T$ | Static temperature(°C) |
| $k$ | Thermal conductivity (W/m K) |
| $DSC(T)_s$ | The heat flow across the specimen at temperature $T$ from the thermogram (mW/mg) |
| $\varphi$ | Heating rate (°C/s) |
| $\Delta t$ | Time step (s) |
| $q$ | Heat flow (W/m) |
| $h_{eq}$ | Convection/radiation coefficient (W/m K) |
| $T_s$ | Surface temperature (°C) |
| $C_p$ | Specific heat capacity (J/kg K) |
| $I$ | Thermal inertia (J/m$^2$ K s$^{1/2}$) |
| $T$ | Time (h) |
| $DSC(T)_{sample}$ | Value of DSC signal at temperature $T$ from the thermogram (mW/mg) |

| | |
|---|---|
| $DSC(T)_{baseline}$ | Value of DSC signal at temperature $T$ from the baseline of the thermogram for the phase change (mW/mg) |
| $H(T)$ | Specific enthalpy over temperature |
| $T_{onset}$ | The onset temperature (˚C) |
| $N$ | The calibration factor that relates the voltage signal of the heat flow to the heat flux through the sample |
| $V$ | Voltage signal of the heat flow sensor |
| $\Delta X$ | Thickness of the specimen |
| $\Delta T$ | Temperature difference across the specimen |
| $\Delta w$ | Increment of water content measured in the composite after three freeze/thaw cycles |
| $w_0$ | The water content in the reference composite |
| $m$ | The weight of the cubes (g) |
| $V_1$ | The volumes of the cubes ($cm^3$) |
| $Si$ | The solid–liquid interface location (m) |
| $k_s$ | The thermal conductivity at solid stage (W/mK) |
| $k_l$ | The thermal conductivity at liquid stage (W/mK) |
| $L_f$ | The latent heat (J/kg) |
| $\beta$ | liquid fraction |
| $h_{ref}$ | Reference enthalpy |
| $T_{ref}$ | Reference temperature |
| $Cp_{eff}$ | Effective heat capacity (J/kg K) |
| $\eta$ | Thermal expansion coefficient |
| $g$ | Gravitational acceleration |
| $P$ | Pressure |
| $S$ | Source term |
| $t$ | Time |
| $u$ | Velocity component along x-axes |
| $v$ | Velocity component along y-axes |

| | |
|---|---|
| $w$ | Velocity component along z-axes |
| $\mu_{Air}$ | Dynamic viscosity for the air |
| $\rho_{Air}$ | Density for the air |
| $R$ | Universal gas |

# Acronyms

| | |
|---|---|
| *LWAs* | Lightweight aggregates |
| *PCMs* | Phase change materials |
| *TES* | Thermal energy storage |
| *SHS* | Sensible heat storage |
| *LHS* | Latent heat storage |
| *DSC* | Differential scanning calorimetry |
| *DTA* | Differential thermal analysis |
| *MC*18 | Microencapsulated PCM with melting temperature of 18°C |
| *MC*24 | Microencapsulated PCM with melting temperature of 24°C |
| *MC*28 | Microencapsulated PCM with melting temperature of 28°C |
| *MC*18_28 | Hybrid Microencapsulated PCM blends of 50% MC18 and 50% MC28 |
| *R*3 | Paraffin PCM with melting temperature of 3°C |
| *R*5 | Paraffin PCM with melting temperature of 5°C |
| *IC* | Expanded clay |
| *GC* | Granulated expanded cork |
| *EV* | Expanded vermiculite |
| *AP* | Expanded perlite |
| *CEP* | Water proofing material, CEPSA-ECM2 |
| *MCB* | Water proofing material, MC-Bauchemie (Makote3) |
| *WEB* | Water proofing material, Weber dry lastic |
| *SIK* | Water proofing material, Sikalastic-490T |
| *IUPAC* | International union of pure and applied chemistry |
| *IC_R*3 | Impregnated Paraffin PCM with melting temperature of 3°C into the expanded clay |
| *GC_R*3 | Impregnated Paraffin PCM with melting temperature of 3°C into the granulated expanded cork |

| | |
|---|---|
| *EV _ R*3 | Impregnated Paraffin PCM with melting temperature of 3°C into the expanded vermiculite |
| *AP _ R*3 | Impregnated Paraffin PCM with melting temperature of 3°C into the expanded perlite |
| *IC _ R*5 | Impregnated Paraffin PCM with melting temperature of 5°C into the expanded clay |
| *GC _ R*5 | Impregnated Paraffin PCM with melting temperature of 5°C into the granulated expanded cork |
| *EV _ R*5 | Impregnated Paraffin PCM with melting temperature of 5°C into the expanded vermiculite |
| *AP _ R*5 | Impregnated Paraffin PCM with melting temperature of 5°C into the expanded perlite |
| *SEM* | Scanning electron microscopy |
| | |
| *IC _ R*3_*REF* | Impregnated Paraffin PCM with melting temperature of 3°C into expanded clay without waterproofing |
| *IC _ R*3_*SIK* | Impregnated Paraffin PCM with melting temperature of 3°C into expanded clay coated with Sikalastic-490T |
| *IC _ R*3_*WEB* | Impregnated Paraffin PCM with melting temperature of 3°C into expanded clay coated with Weber dry lastic |
| *IC _ R*3_MCB | Impregnated Paraffin PCM with melting temperature of 3°C into expanded clay coated with MC-Bauchemie (Makote3) |
| *IC _ R*3_*CEP* | Impregnated Paraffin PCM with melting temperature of 3°C into expanded clay coated with CEPSA-ECM2 |
| *IC _ R*5_*REF* | Impregnated Paraffin PCM with melting temperature of 5°C into expanded clay without waterproofing |
| *IC _ R*5_*SIK* | Impregnated Paraffin PCM with melting temperature of 5°C into expanded clay coated with Sikalastic-490T |
| *IC _ R*5_*WEB* | Impregnated Paraffin PCM with melting temperature of 5°C into expanded clay coated with Weber dry lastic |
| *IC _ R*5_MCB | Impregnated Paraffin PCM with melting temperature of 5°C into expanded clay coated with MC-Bauchemie (Makote3) |
| *IC _ R*5_*CEP* | Impregnated Paraffin PCM with melting temperature of 5°C into expanded clay coated with CEPSA-ECM2 |
| *EV _ R*3_*REF* | Impregnated Paraffin PCM with melting temperature of 3°C into expanded vermiculite without waterproofing |
| *EV _ R*3_*SIK* | Impregnated Paraffin PCM with melting temperature of 3°C into expanded vermiculite coated with Sikalastic-490T |
| *EV _ R*3_*WEB* | Impregnated Paraffin PCM with melting temperature of 3°C into expanded vermiculite coated with Weber dry lastic |
| *EV _ R*3_MCB | Impregnated Paraffin PCM with melting temperature of 3°C into expanded vermiculite coated with MC-Bauchemie (Makote3) |
| *EV _ R*3_*CEP* | Impregnated Paraffin PCM with melting temperature of 3°C into expanded vermiculite coated with CEPSA-ECM2 |
| *EV _ R*5_*REF* | Impregnated Paraffin PCM with melting temperature of 5°C into expanded vermiculite without waterproofing |
| *EV _ R*5_*SIK* | Impregnated Paraffin PCM with melting temperature of 5°C into expanded vermiculite coated with Sikalastic-490T |
| *EV _ R*5_*WEB* | Impregnated Paraffin PCM with melting temperature of 5°C into expanded vermiculite coated with Weber dry lastic |

| | |
|---|---|
| *EV_R5_MCB* | Impregnated Paraffin PCM with melting temperature of 5°C into expanded vermiculite coated with MC-Bauchemie (Makote3) |
| *EV_R5_CEP* | Impregnated Paraffin PCM with melting temperature of 5°C into expanded vermiculite coated with CEPSA-ECM2 |
| *GC_R3_REF* | Impregnated Paraffin PCM with melting temperature of 3°C into Granulated expanded cork without waterproofing |
| *GC_R3_SIK* | Impregnated Paraffin PCM with melting temperature of 3°C into Granulated expanded cork coated with Sikalastic-490T |
| *GC_R3_WEB* | Impregnated Paraffin PCM with melting temperature of 3°C into Granulated expanded cork coated with Weber dry lastic |
| *GC_R3_MCB* | Impregnated Paraffin PCM with melting temperature of 3°C into Granulated expanded cork coated with MC-Bauchemie (Makote3) |
| *GC_R3_CEP* | Impregnated Paraffin PCM with melting temperature of 3°C into Granulated expanded cork coated with CEPSA-ECM2 |
| *GC_R5_REF* | Impregnated Paraffin PCM with melting temperature of 5°C into Granulated expanded cork without waterproofing |
| *GC_R5_SIK* | Impregnated Paraffin PCM with melting temperature of 5°C into Granulated expanded cork coated with Sikalastic-490T |
| *GC_R5_WEB* | Impregnated Paraffin PCM with melting temperature of 5°C into Granulated expanded cork coated with Weber dry lastic |
| *GC_R5_MCB* | Impregnated Paraffin PCM with melting temperature of 5°C into Granulated expanded cork coated with MC-Bauchemie (Makote3) |
| *GC_R5_CEP* | Impregnated Paraffin PCM with melting temperature of 5°C into Granulated expanded cork coated with CEPSA-ECM2 |
| *AP_R3_REF* | Impregnated Paraffin PCM with melting temperature of 3°C into expanded perlite without waterproofing |
| *AP_R3_SIK* | Impregnated Paraffin PCM with melting temperature of 3°C into expanded perlite coated with Sikalastic-490T |
| *AP_R3_WEB* | Impregnated Paraffin PCM with melting temperature of 3°C into expanded perlite coated with Weber dry lastic |
| *AP_R3_MCB* | Impregnated Paraffin PCM with melting temperature of 3°C into expanded perlite coated with MC-Bauchemie (Makote3) |
| *AP_R3_CEP* | Impregnated Paraffin PCM with melting temperature of 3°C into expanded perlite coated with CEPSA-ECM2 |
| *AP_R5_REF* | Impregnated Paraffin PCM with melting temperature of 5°C into expanded perlite without waterproofing |
| *AP_R5_SIK* | Impregnated Paraffin PCM with melting temperature of 5°C into expanded perlite coated with Sikalastic-490T |
| *AP_R5_WEB* | Impregnated Paraffin PCM with melting temperature of 5°C into expanded perlite coated with Weber dry lastic |
| *AP_R5_MCB* | Impregnated Paraffin PCM with melting temperature of 5°C into expanded perlite coated with MC-Bauchemie (Makote3) |
| *AP_R5_CEP* | Impregnated Paraffin PCM with melting temperature of 5°C into expanded perlite coated with CEPSA-ECM2 |
| *HPCMM18_28* | Hybrid PCM mortar blends of 50% Microencapsulated PCM with melting temperature of 18°C and 50% Microencapsulated PCM with melting temperature of 28°C with total mass fraction of PCMs ~20% |
| *SPCMM24* | Single PCM mortar with incorporation ~20% mass fraction of Microencapsulated PCM with melting temperature of 24°C |

| | |
|---|---|
| *REFM* | Conventional mortar without PCM |
| *ITZ* | Interstitial transition zone |
| *C* | Carbon element |
| *Si* | Silicate element |
| *Ca* | Calcium element |
| *PCMM10\** | Single PCM mortar with incorporation ~10% mass fraction of impregnated PCM with melting temperature of 5°C into expanded clay |
| *PCMM20\** | Single PCM mortar with incorporation ~20% mass fraction of impregnated PCM with melting temperature of 5°C into expanded clay |
| *REFM0* | Reference mortar without PCM |
| *DFM* | Delayed freezing mortar |
| *RT10* | Paraffin PCM with melting temperature of 10°C |
| *BSF26* | Microencapsulated PCM with melting temperature of 26°C |
| *HPCMM* | Hybrid PCM mortar blends of 33% Paraffin PCM with melting temperature of 10°C, 33% Microencapsulated PCM with melting temperature of 26°C and 33% Microencapsulated PCM with melting temperature of 28°C with total mass fraction of PCMs ~20% |
| *IT* | Interior temperature (°C) |
| *FEM* | Finite element method |
| *CFD* | Computational fluid dynamic |
| *IEA* | International energy agency |
| *UDF* | User defined function |
| *SPCMM10* | Single PCM mortar with incorporation ~20% mass fraction of Microencapsulated PCM with melting temperature of 10°C |
| *SPCMM26* | Single PCM mortar with incorporation ~20% mass fraction of Microencapsulated PCM with melting temperature of 26°C |
| *SPCMM28* | Single PCM mortar with incorporation ~20% mass fraction of Microencapsulated PCM with melting temperature of 28°C |
| *SPCMM* | Single PCM mortar with incorporation ~20% mass fraction of Microencapsulated PCM with melting temperature of 24°C |
| *XPS* | Extruded polystyrene insulation board |
| *PID* | Proportional integrated derivative |
| *TOU* | Time of use (classified in the demand response programs) |

*RTP*        Real time pricing (classified in the demand response programs)

*CPP*        Critical peak pricing (classified in the demand response programs)

*DRPs*       Demand response programs

# Chapter 1  Introduction

## 1.1   General context

Energy consumption in buildings and the corresponding costs are two major challenging concerns in most countries worldwide. Therefore, decisions and measures aimed to increased energy efficiency are becoming frequent in view of the global awareness of the importance of this issue. In buildings, a large portion of energy consumption is used for heating and cooling. The energy consumption of any building is critically dependent on indoor air temperature which the building must maintain. The heat lost from the building, is through its surfaces or by ventilation, depends on the difference between the inside and outside temperature (Hensen J 2011). The sensitivity of occupants to indoor climate also has implication for how closely we need to control the environment and this again has the energy implication. The challenge is to have the benefits from a construction with minimum energy demand for cooling/heating. In order to move towards sustainability in the buildings it is important to investigate methods that can reduce the cooling/heating energy demand.

One such method that can help in the reduction of peak cooling loads and stabilization of indoor temperature is the use of Phase Change Materials (PCMs) in a building construction, which takes advantage of air temperature inside a building to moderate thermal comfort. ASHRAE55 (2004), which is used to judge thermal comfort in buildings, recommended that air temperature inside building can be minimum 20℃ and maximum 25℃. The addition of PCMs allows the building envelope to become an effective thermal energy storage system (Baetens *et al.* 2010). A well designed building

envelope thermal energy storage system can improve building operation by reducing the energy required to maintain the temperature ranges in comfort level and shifting the time of the peak load on the electrical grid (Sarı *et al.* 2004).

## 1.2   Objectives and research methodology

The purpose of this research is to develop a thermal energy storage system for increased energy efficiency in buildings. The lack of knowledge of the general public on this subject has prevented the use of phase change materials as a common building material. The research of this thesis was part of a project that aims at developing a set of practical design guidelines for integrating PCM in buildings.

Apart from contributing to a better understanding and knowledge on PCMs behaviour and application in the scope of building construction, this thesis had the further objective of verifying the feasibility of a new generation of hybrid PCM systems for construction, to be applied in plastering mortars of building façades (proposed in the scope of the thesis). Such hybrid system is expected to have the potential to control internal building temperatures with minimized energy consumption for both heating and cooling seasons. Energy saving by hybrid PCM concept can provide better profit of the thermal properties of such materials, when compared to their separate individual use.

The thesis initially was focused on the experimental characterization of pure materials and mortars at material level investigation. Next, designation of small scale tests of PCM-integrated building materials and then on the development and validation of a numerical simulation strategy for the thermal analysis of plaster mortar without PCM, with single PCM and with hybrid PCM-integrated into building envelopes. The numerical simulation approach was validated by the small scale test results, and such capacity was used to deploy "virtual laboratories" for real scale applications and provide the grounds for an energy saving assessment of real scale application in the scope of this work. Experimental and numerical research with incorporation of hybrid PCM mortars was carried out, in order to provide solid grounds for the development of a guideline for the sustainable construction and design of buildings. Based on the knowledge acquired in this study, the concept of hybrid PCM system can be easily extended to distinct scopes of building elements, such as reinforced concrete or pre-fabricated facades. A series of experiments were conducted in order to understand the effect of the

introduction of PCM into plastering mortars used as internal coatings of building spaces as a passive system. In this way, extensive efforts were performed on the material level investigations. Next, two categories of small scale cells was designed and prepared with distinct interior coating corresponding to the experimental works of flow diagram presented in Figure 1-1: (i) one with common plastering mortars; (ii) one with hybrid PCM mortar. Each of prototypes was subjected to realistic daily temperature variation by using controlled climatic chamber. The effectiveness of the coatings was assessed with recourse to internal temperature monitoring. A series of experimental works with incorporation of a heating system was considered inside the small scale prototypes as active systems. The numerical simulations tool was deployed to simulate the results of the small-scale test cells, and therefore attained a validated numerical modelling strategy. The experimental results and the availability of adequate simulation tools was used to provide the grounds for preparation of the performance of the proposed hybrid PCM in view of real conditions (real scale test). Upon availability of robust and reliable numerical simulation model, real-scale simulations in order to assess the energy saving benefits of using PCM mortars in building envelopes were developed. The real scale dimension of a middle store building was designed and simulated by the tools. The daily energy saving opportunities by using hybrid PCM was calculated by energy simulation method for a typical winter day between two cases without PCM and hybrid PCM.
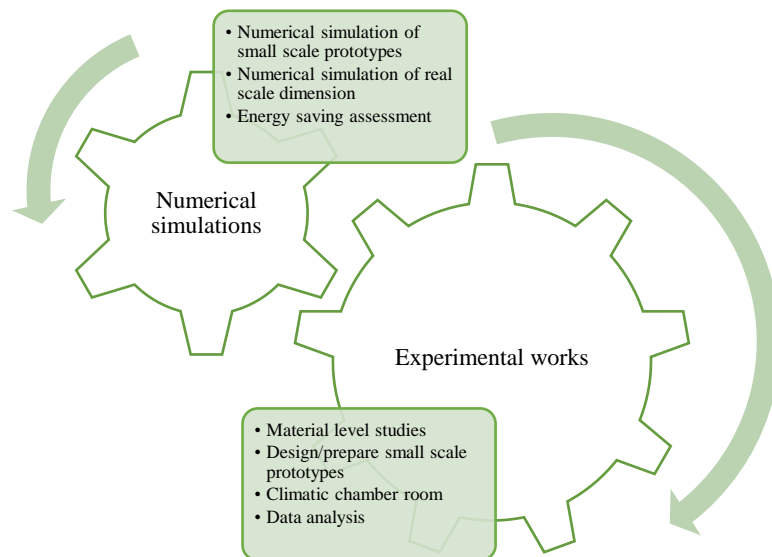


Figure 1-1: Diagram of the research methodology.

## 1.3 Thesis outlines

This thesis consists of seven chapters. ***Chapter 1*** describes an introduction and general context of the work carried out in three research projects, including the scopes and objectives of the study. ***Chapter 2*** deals with overview of the phase change materials and their application in the context of building envelopes which evaluates different studies related to the PCM-based systems used in the building sectors. This leads to the next stage of the thesis: selection of suitable PCMs for enhanced thermal comfort purposes.

***Chapter 3*** describes the materials used in this thesis as well as adopted methodologies to characterize the materials. This leads not only insights to the thermal characterization, chemical characterization of the materials, but it also shows the leakage analysis of the developed thermal energy storage composites under which they have to scope with.

***Chapter 4*** deals with the experimental set up of developed mortars incorporated with microencapsulated PCMs. They were tested under thermal loads in order to conduct their required thermo-physical parameters for the numerical simulation inputs. The final study in this chapter includes feasibility assessment of impregnating paraffin PCM in LWAs for development of thermal energy storage systems and the corresponding advantages that may be achieved cost effectively.

***Chapter 5*** describes the thermal performance of the small scale prototypes that are internally coated with plastering mortars in order to evaluate the potential advantage of PCM based system as passive and active solutions synonymous of thermal efficiency of buildings. Additionally, a study on PCM impregnated LWAs in cement based mortar targeted bound to contribute for the minimizing of potential freeze-thaw effect upon applications, such as: pavement structures.

***Chapter 6*** describes suitable numerical simulation tools that can handle the both PCM modelling and air flow predictions within context of buildings. Then, discusses the general introduction and modelling approaches used in CFD, and presents the validation of the CFD upon experimental results of small scale prototypes in both terms of phase change process and indoor environment (air modelling). The chapter also portrays the benefits of using CFD in the building design process, particularly when PCMs are

included throughout real scale dimension. This depicted the evaluation of direct energy saving potential of the PCM based systems compared with conventional buildings.

*Chapter 7* finally concludes the research work by describing the outcomes of the study, and makes recommendations for future work in this field.

# Chapter 2  PCMs and Their Applications

# to Building Envelopes

## 2.1   Phase change materials: definition and principle of operation

Before introducing phase change materials (PCMs) it is desirable to define some relevant concepts: Thermal energy storage (TES) can be defined as the temporary storage of thermal energy at high or low temperatures. Storage of energy improves the energy efficiency and the higher efficiency would lead to energy conservation. There are mainly two types of TES systems, sensible heat storage (SHS) and latent heat storage (LHS), used for heat storage in the built environment (Hassan E 1991). The method called sensible heat storage consists in heating a liquid or a solid, without phase change. In SHS, energy is stored or extracted by heating or cooling a liquid or solid. LHS is usually based on the heat absorption of a material when it changes phase from solid to liquid and on the heat release when it changes phase from liquid to solid. The principle of LHS is that, when ambient temperature rises, the chemical bonds of PCM will break up and it will change phase from solid to liquid. This phase change is an endothermic process and it will absorb heat regard to the heat capacity of the PCM. When the temperature drops again, the PCM will return to the solid state and it releases the heat (Duffie J 1980). In the solid-liquid phase change, storage of heat results in a change of phase and not in an increase in temperature. This storage in latent form has the advantage of greater heat storage capacity per unit volume compared to SHS. Thus, by selecting PCM with a melting temperature close to the optimum indoor comfort temperature, the indoor temperature can stabilize and cut off peak cooling loads. In this

way, a reduction in the cooling energy demand and improvement in thermal comfort can be achieved.

The materials that take advantages of latent heat storage are called phase change materials (Duffie J 1980). The objective of the PCM is illustrated in Figure 2-1, as can be seen, when ambient temperature increased, the PCM absorbs heat by melting. Conversely, when the ambient temperature goes below the melting temperature of PCM, it solidifies with energy release. Thus, the thermal exchanges inward/outward from the building decrease. This leads to an indoor thermal behaviour that tends to remain in the vicinity of the PCM's melting point, thus increasing the thermal efficiency of the building. The PCM absorb heat during the day and then release it at night. This makes the entire energy cycle more efficient due to maintaining a constant comfortable temperature. Consequently, less energy is used to heat and cool buildings while PCM intelligently captures and releases otherwise wasted energy.
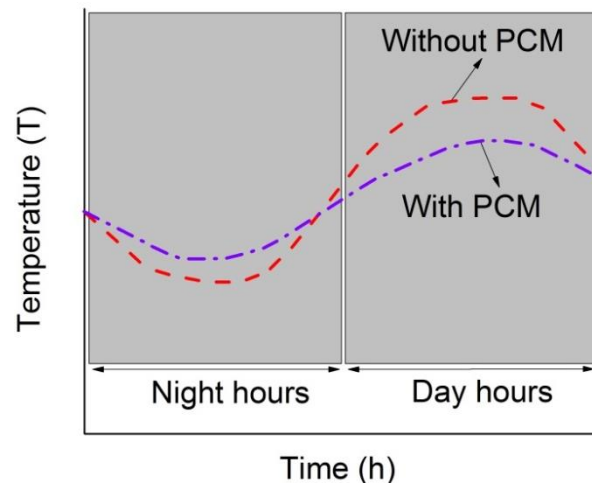


Figure 2-1: The function of PCM.

Phenomenological definition of the PCM can be explained by: when the PCM material is in the solid state and the surrounding air is hotter than it, heat is absorbed from the air as sensible heat. This heat causes a continuous rise in the PCM temperature up till the melting temperature $T_{ml}$ at point B in Figure 2-2. At this point, the heat being absorbed is solely utilized in breaking down the molecular structure of the solid PCM. The material is in the mushy $\Delta T$ region here and is capable of absorbing large amounts of

8

---------------------------------------------------------------------------------------------------------------

latent heat energy from the surroundings without significant rise in its surface temperature. When the PCM melts completely, it becomes fully liquid and it is incapable of latent heat storage. At this condition (point C), the material is completely liquid and experiences a progressive rise in temperature as sensible heat. During solidification, these processes are reversed (from point D to point A) for a PCM.
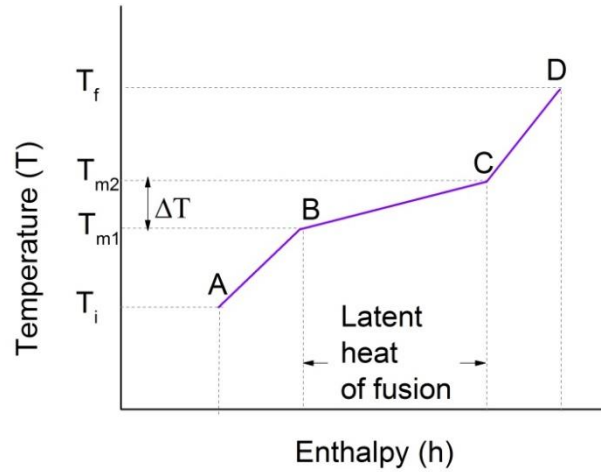


Figure 2-2: Practical curves for enthalpy as a function of temperature for PCM.

## 2.2   Classification of PCMs

PCMs can be classified in three different categories based on their chemical composition. The three different groups of PCMs are: (1) organic compounds, (2) inorganic compounds and (3) eutectics (Sharma *et al.* 2009). Each different group has a typical range of melting temperature and melting enthalpy.

Organic PCMs can be further divided into paraffins and fatty acids, and eutectics can be organic and inorganic combinations. The only type of inorganic PCMs is salt hydrates (Zhou *et al.* 2012). Figure 2-3 presents a wide variety of PCMs within each of the three groups in any required temperature ranges.
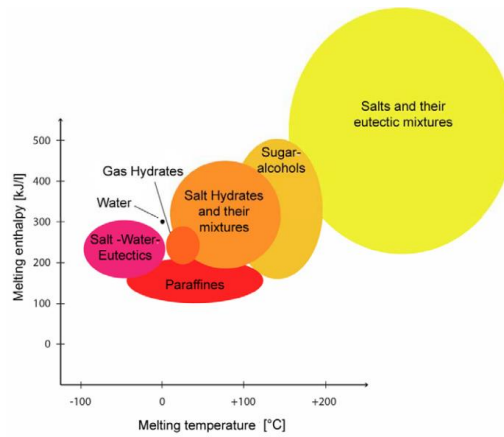
Figure 2-3: Melting enthalpy versus melting temperature for various materials used as PCMs (Kalnæs *et al.* 2015).

## 2.2.1 Organic PCMs

Organic PCMs are divided into two large groups: (1) paraffins and (2) non-paraffins. Paraffins have the advantage that they are available in a range of melting temperatures between 20-70°C and therefore can be used for indoor temperature stabilization (Zhou *et al.* 2012). Another advantage is that they are chemically inert and they can be easily implemented in building construction (Sharma *et al.* 2009). Also, their thermal performance is not affected by the number of cycles (Cabeza *et al.* 2011). Their thermal storage capacity is between 100-210 kJ/kg. Also, paraffins have a thermal conductivity about 0.2 W/m K, (Baetens *et al.* 2010). Flammability of organic PCMs is a problem that has been hindering their wider implementation for the last 20 years. However, Kosny *et al.* (2010) developed an encapsulation of cellulose and fiberglass that improved the fire resistivity. The non-paraffin organics, include a wide selection of organic materials such as fatty acids, esters, alcohols and glycols (Sunliang 2010). They have certain advantages compared to paraffins, such as higher latent heat of fusion and a smaller volume change during their phase transition which could make them a comparably preferable material (Velraj *et al.* 2009). However, there is a lack of materials with a melting point near 21°C, which is ideal for indoor comfort. Their melting points are between 16°C and 65°C and freezing points between 17°C and 64°C, with a heat of fusion between 155-180 kJ/kg, Also their price is almost three times higher than the price of paraffins (Baetens *et al.* 2010).

### 2.2.2   Inorganic PCMs

In comparison with organic PCMs they have better thermal properties, because they have a high latent heat of fusion between 180-440 kJ/kg approximately. Also, they have a higher thermal conductivity (about 0.5 W/mK) when compared with paraffins. Another important advantage for their implementation in the built environment is their low price and also the fact that they are non-flammable (Cabeza *et al.* 2011). The main disadvantage of inorganic PCMs is the phase segregation they show after a relatively short number of cycles (1000 melt/freeze cycles) (Sharma *et al.* 2009). This happens because hydrated salts melt congruently with formation of lower salts, making the process irreversible after a number of cycles, resulting in reduction of their heat storage capacity and their robustness (Abhat 1983).

### 2.2.3   Eutectics

Eutectics, or eutectic mixtures, are mixtures of multiple solids in certain proportion in order to have the lowest melting point possible. They have a sharp melting point (small melting–solidification temperature range) which enables them to be used to maintain a specific indoor temperature and their volumetric storage density is slightly higher than that of organic compounds. Eutectics are divided into three categories: (1) organic–organic, (2) inorganic–inorganic, (3) inorganic- organic (Cabeza *et al.* 2011).

## 2.3   Desirable PCM features for building applications

A suitable phase change temperature and a large melting enthalpy are two obvious requirements for a phase change material. They have to be fulfilled in order to store and release heat at all. However, there are more requirements for most, but not all applications. These requirements can be grouped into: thermal, physical, kinetic, chemical and economical (Sunliang 2010, Dutil *et al.* 2011, Zhou *et al.* 2012). For the sack of brevity, a review of such properties relevant to this thesis is made in the following text.

### 2.3.1   Thermal properties

PCMs must have a suitable phase change temperature range for their predictable application. For the built environment this range will determine the indoor temperature levels that can be achieved with the selected PCM. The optimal phase change

temperature depends on the comfort temperature desired by the building user and also by the climatic conditions (Dutil *et al.* 2011). Another important thermal property of a PCM is the latent heat of fusion. The higher latent heat is, the higher energy demand for the change of phase, and therefore the higher energy can be absorbed by the PCM. Also, a PCM must have an adequate conductivity rate to be able to react fast to indoor temperature variations. For example, when employed enormous masses of PCM inside a building with low thermal conductivity (not in a wall), they can fail to activate because they do not meet temperature variations. Defining density of a material as its mass per unit volume, it can be stated that materials with higher density tend to have higher volumetric energy storage capacity, due to the higher amount of matter that endures phase change per volume unit (Zhou *et al.* 2012).

### 2.3.2 Chemical properties

PCM application in the built environment requires long term durability from the material in order to assure robust long term performance. There must be a high chemical stability of the melting and solidification procedure and a completely reversible cycle. In the scope of usage in the built environment, it is very important for a PCM to be compatible with construction materials, and other chemical properties of the PCMs such as: non-toxic, non-flammable, non-corrosive and non-explosive can be found in details at (Eissenberg A 1980, Sharma *et al.* 2009).

### 2.3.3 Economic issues

An important selection criterion for a PCM is their cost. This comprises the initial cost for purchasing the PCM and for the installation in the built environment. The economic value of a PCM depends on the effect it has on the building energy consumption.

## 2.4 Thermal characterization techniques for PCM/composite PCM

The performance of a thermal energy storage system such as pure PCM is directly associated with the phase change properties of PCM. It has been shown in (Kheradmand *et al.* 2015) that the data indicated by the supplier could be incorrect, doubtful and over optimized. Therefore, it is necessary to make measurements so as to get the correct phase change properties of PCM. Several measurement techniques such as Differential Scanning Calorimetry (DSC) and Differential Thermal Analysis (DTA) exist; however,

DSC is the most common one and therefore would be extensively discussed in this chapter.

## 2.4.1   Differential Scanning Calorimetry (DSC)

Firstly, a brief introduction on differential scanning calorimetry is given which is an analytical technique that was developed by Kalnæs *et al.* (2015). The term was used to describe equipment having the capability to measure the specific enthalpy and allow accurate measurement of specific heat capacity. DSC measures the temperatures and heat flows associated with material changes as a function of time and temperature in a controlled environment. The measurements provide qualitative and quantitative data about physical and chemical changes that involve endothermic or exothermic processes (Denner T 2012). It is interesting to mention the mean of each word of differential scanning calorimetry according to (Hawes *et al.* 1989):

**Differential:** The above measurements on a sample are done with respect to a reference sample with known properties;

**Scanning:** The thermal excitation with a linear temperature ramp;

**Calorimetry:** The measurement of the quantity of heat absorbed or released by a sample subjected to temperature change.

The analysis procedure in pictorial form is shown Figure 2-4 is explained herein. Basically, heat flow and temperature calibrations of the DSC should be done periodically (Denner T 2012). Typically indium is used as a calibrating material. In order to obtain accurate results, baseline slope and offset calibrations require heating an empty pan through expected temperature range in the experiment. Calibration program is then used to flatten the baseline and zero the heat flow signal. In the next step, sample preparation, includes selecting the appropriate weight and size of the sample, selecting the pan type and material and encapsulating the sample pan. Larger samples will increase sensitivity but it will decrease the resolution. Therefore, the goal is to have heat flow rate in between 0.1 and 10 m W. Normally, the sample weight is in between 5 and 20 mg (Memon Shazim A 2014).
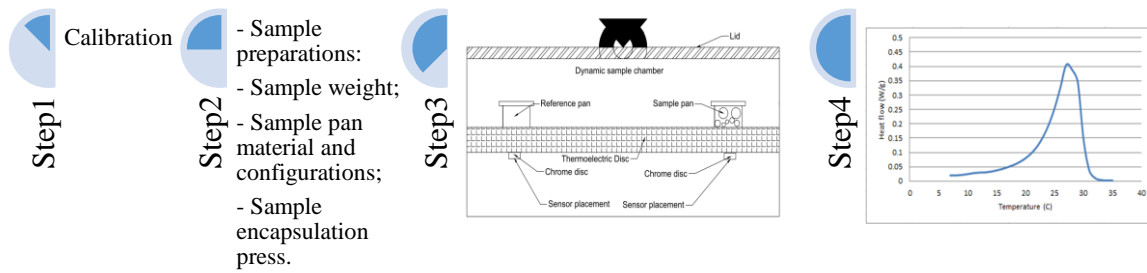
Figure 2-4: DSC analysis protocol.

Typically used DSC equipment is presented in Figure 2-5(a). Regarding the sample pan, in most cases, aluminium ones can be used in the temperature ranges 180 to 600°C (Figure 2-5(b)). As far as the sample pan configuration is concerned, the pan can be hermetic, non-hermetic or open. However, hermetic pan is preferred due to obvious advantages such as better thermal contact, reduced thermal gradient in the sample, higher internal pressure resistance due to air tight seal and preservation of sample for further study.



**(a)**          **(b)**          **(c)**
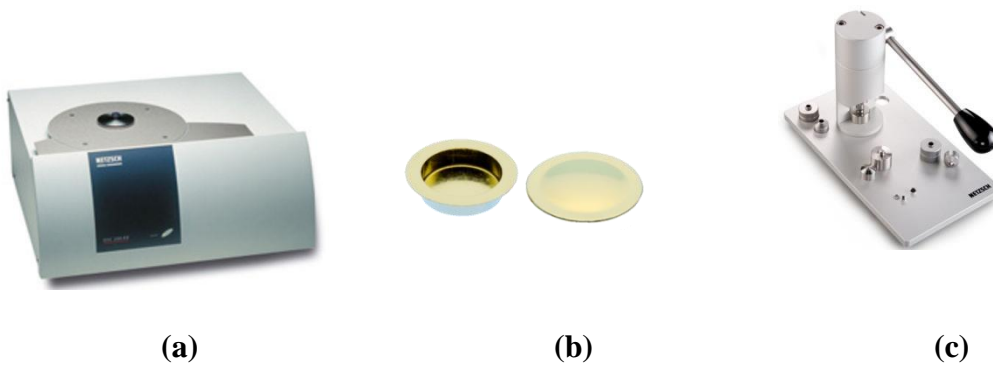
Figure 2-5: (a) DSC equipment; (b) Hermetic aluminium sample pan and lid set; (c) Sample encapsulating press used to hermetically seal sample pan (Denner T 2012).

In addition, when contact with cell atmosphere or the reaction of the sample gas is required, hermetic pan can be used by making a pin hole in the lid before sealing. After deciding the sample pan material and configuration, and keeping the sample in the sample pan, both the hermetic and non-hermetic pan should be sealed with the sample encapsulating press (Figure 2-5(c)). The sample and reference pan are then loaded into the heat flux DSC cell. In heat flux DSC, the sample and reference pans sit on the same thermoelectric disc, which transfers the heat to these pans (Denner T 2012).

14

The heat capacity of the sample will cause a temperature difference between the sample and reference pans. This temperature difference leads to voltage difference which after making adjustments for thermocouple response is proportional to heat flow (Denner T 2012).

The thermal properties such as phase change temperature and thermal energy stored in unit weight can be determined by using commercially available software's such as Thermal Analysis Proteus (Denner T 2012). The schematic DSC, specific heat capacity and specific enthalpy plots are shown in Figure 2-6. The phase change temperature is divided into starting, peak and ending temperatures. The specific heat capacity curve can be obtained by removing baseline part of the DSC and consequently, the specific enthalpy in the unit weight of PCM can be obtained by dividing the integrated area of specific heat capacity curve with a temperature rising rate. This value can be calculated automatically by the software (Denner T 2012).



**(a)**                                    **(b)**                                    **(c)**
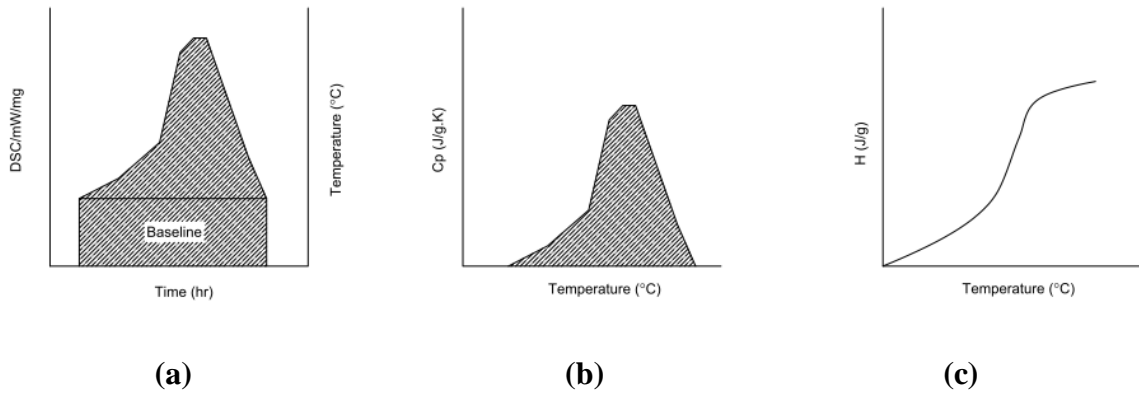
Figure 2-6: (a) DSC curve; (b) Specific heat capacity versus temperature; (c) Specific enthalpy versus temperature.

In practice, the specific enthalpy for the materials can follow the strategy proposed by (Kheradmand *et al.* 2014). From the DSC output, the specific enthalpy is calculated for each phase transition based on following method: (i) the onset and end temperatures are defined according to EN ISO 11357-1 (1997); (ii) a linear baseline is selected for the calculation of the specific enthalpy by tracing a line from the onset to the end temperature; (iii) the computation of the specific heat capacity of the sample along the tested temperatures $Cp(T)$ (J/g.K) is made according to Eq.(2.1) :

15

$$Cp(T) = \frac{\left[ DSC(T)_{sample} - DSC(T)_{baseline} \right]}{\varphi} \qquad (2.1)$$

Where $DSC(T)_{sample}$ is value of DSC signal at temperature $T$ from the thermogram (m W/mg); $DSC(T)_{baseline}$ is value of DSC signal at temperature $T$ from the baseline of the thermogram for the phase change (m W/mg), and $\varphi$ is the heating or cooling rate (˚C/s).

The specific enthalpy at temperature $T$ corresponds to the integral of $Cp(T)$ that can be obtained according to Eq.(2.2) as follows:

$$H(T) = \int_{T_{onset}}^{T} Cp(T)dT \qquad (2.2)$$

Where $H(T)$ is specific enthalpy over temperature and $T_{onset}$ is the onset temperature (˚C).

### 2.4.2 Differential thermal analysis (DTA)

Differential Thermal Analysis (DTA), a thermo-analytic technique, appears to have been first employed by Murphy C. B (1958). In DTA, the heat supplied to the sample and the inert reference remains the same while measuring the temperature and temperature differences (between the sample and the reference) associated with material changes as a function of time and temperature in a controlled atmosphere. The plot of differential temperature versus temperature or time is known as a DTA curve.

## 2.5 Measurement of thermal conductivity of PCM/composite PCM

In order to measure the performance of PCM in terms of heat transfer effect, it is necessary to determine the thermal conductivity of the PCM/composite PCM. The thermal conductivity of a sample can be measured by steady-state and non-steady steady methods. In the steady state method, the measurements are made when the temperature of the material does not vary with time, i.e. at constant signal. Therefore, the signal analysis is simple and straightforward (Catalina *et al.* 2009). Heat flow meter method is

typical steady-state measurement which is simple in concept, quick and appropriate for a wide range of test specimens such as solid materials. It is applicable to materials having low thermal conductivity for example building insulations in the range 0.005 to 0.5 W/(m K) and provides highly accurate results if it has been calibrated properly according to ISO:8301 (1991). In this method, the test sample is placed between two parallel plates set at different temperatures (Figure 2-7). The principle of the first version of this instrument depends in the application of heat flow sensor, which is attached to a metal block with constant temperature, which differs from the sample temperature. When the measurement starts, the measuring head containing the mentioned heat flow sensor drops down and touches the planar measured specimen, which is located on the instrument base under the measuring head. In this moment, the surface temperature of the sample suddenly changes and the instrument computer registers the heat flow. Simultaneously, a sensor measures the sample thickness. The thermal conductivity of the sample is calculated using Fourier's law of heat conduction by the following formula (Eq.(2.3)):

$$k = N \times (V \times \Delta X / \Delta T) \tag{2.3}$$

Where $k$ is thermal conductivity of the sample, $N$ is the calibration factor that relates the voltage signal of the heat flow to the heat flux through the sample, $V$ is voltage signal of the heat flow sensor, $\Delta X$ is thickness of the specimen, $\Delta T$ is temperature difference across the specimen.

In non-steady state method, the measurement is made during the process of heating up i.e. the signal is studied as a function of time. It can be performed more quickly, however, in general, the mathematical analysis of the data is more difficult (Barreneche *et al.* 2016).
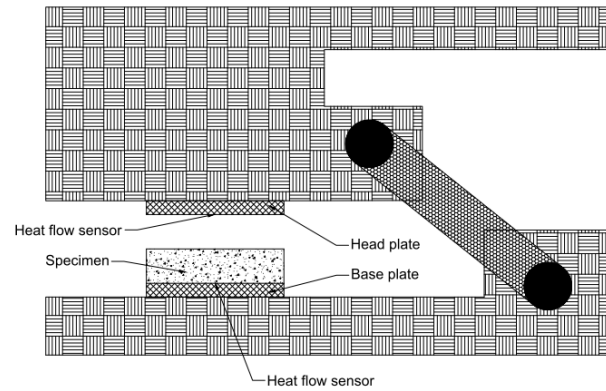
Figure 2-7: Schematic of heat flow meter apparatus.

## 2.6   Strategies for PCM incorporation in cement-based materials

Recently, integration of PCM in cement based materials has regained interest. The incorporation of PCM can be as part of separate building components, or as additive to ordinary building materials. Therefore, this section focus on experimental investigations carried out on PCM incorporation in cement based materials for building applications. The main containment methods that have been used are immersion, direct incorporation and encapsulation (micro and macro) pointed out by (Zhou *et al.* 2012).

### 2.6.1   Direct incorporation

In this method, liquid or powdered PCMs are directly added to building materials such as gypsum, concrete or plaster during production. No extra equipment is needed in this method but incompatibility with construction materials may be the biggest problem (Shrestha M 2012).

### 2.6.2   Immersion

Immersion is a technology in which the building structure components, such as gypsum, brick or concrete, are dipped into melted PCMs and then absorb PCMs into their internal pores with the help of capillary elevation. However, some researchers pointed out this method may have a leakage problem which is not good for long-term use (Yinping *et al.* 2006). Direct incorporation and immersion have different operation processes, but they both incorporate PCMs in contact with conventional construction materials (Barreneche *et al.* 2016) and (Shrestha M 2012).

## 2.6.3 Encapsulation

Encapsulation is the method of containing PCMs within a capsule of various materials, forms and sizes prior to incorporation so that it may be introduced into the building construction in a convenient manner (Cabeza *et al.* 2011). Because of the fact that PCM is stored before implemented in a construction material, encapsulation prevents unwanted compatibility problems between the two. There are two methodologies developed for encapsulation:

*Macroencapsulation of PCM*, which is encapsulation in containers usually larger than 1 cm in diameter, is the most common form of encapsulation. Tubes, spheres or panels are examples of macroencapsulation. Previous experiments with large volume containment or macroencapsulation failed due to the poor conductivity of the PCM (Hensen J 2011). When it was time to regain the heat from the liquid phase, the PCM solidified around the edges and prevented effective heat transfer.

*Microencapsulation of PCM,* it is the process by which individual particles or droplets of solid or liquid material (the core) are surrounded or coated with a continuous film of polymeric material (the shell) to produce capsules in the 300 micrometer to 1 millimeter range, are known as microcapsules (Tyagi *et al.* 2011). Microencapsulation allows the PCM to be incorporated simply and into conventional construction materials. Simple spherical particles are the most common ones being fabricated and utilized (Hawladera *et al.* 2003). Microencapsulated phase change material overcomes the following problems in comparison to the direct incorporation and immersion methods: corrosive to metal, decomposition and leakage (Zhao *et al.* 2011).

## 2.6.4 Shape stabilized PCMs

In recent years, a new kind of compound PCM, the so-called shape-stabilized PCMs, has been attracting the interest due to the fact that they have large apparent specific heat, and suitable thermal conductivity, the ability to keep the shape of PCM stabilized in phase-change process, and a good performance of long-term multiple thermal cycles (Zhou *et al.* 2012). In this technique the PCM (like paraffin) is dispersed in another phase of supporting material (like high-density polyethylene) to form a stable composite material (Soares *et al.* 2013). Since the mass percentage of paraffin can be as much as 80%, the total energy is comparable to that of traditional PCMs (Khudhair *et al.* 2004). Some applications of shape-stabilized PCMs in building walls, ceilings and floors have

been studied by following authors (Gellings 2009, de Gracia *et al.* 2013, Shafie-khah M *et al.* 2015) showing that interest in this new kind of PCMs is rising. All of these techniques deal with the solid-liquid phase-change for potential integration in building materials.

## 2.7  PCM enhanced cement- based materials

Usually, cement based materials such as: concrete and mortar are widely used as construction materials (Zhang *et al.* 2014). Due to the fact that, they have large thermal mass this can be advantageous, especially in moderate climates where it can be used to store energy during the day and release it during night time therefore reducing the need for auxiliary cooling and heating (Song *et al.* 2014). Moreover, the energy storage capacity of concrete or mortar can further be enhanced by the incorporation of PCM into the mixtures. Plastering PCM enhanced mortar, combines an appropriate PCM with a mortar matrix producing mortar with thermo-physical properties (Vaz Sá *et al.* 2012). Cement based materials are considered suitable for incorporation of PCM because of the following reasons (Hawes *et al.* 1989, Tyagi *et al.* 2011): 1) they are the most widely used construction materials; 2) they can be formed into a variety of shapes and sizes; 3) they have a larger heat exchange area and smaller heat exchange depth; 4) production and quality control can be easily achieved and 5) ease of testing.

In order to plan our PCM plastering mortar experiments for energy saving, it is desirable to review some of the representative experiments done by researchers in the past. Shilei L *et al.* (2007) experimentally studied PCM based wallboards that could reduce cooling load in buildings. Capric acid (CA) and lauric acid (LA), as PCM for low temperature latent heat storage were applied to the building's wallboards for energy storage. The melting-freezing temperature of CA–LA PCM mixture was 20.4 °C and 19.1 °C and the latent heat of fusion was 150.3 J/g and 144.2 J/g, respectively. During the experiment, when the indoor temperature exceeded 18.6 °C, the PCM in wallboards melted and absorbed 39.2 kJ/kg before completely melting at 24.3 °C. They concluded that wallboard based on PCM has excellent latent heat storage capability and can shift energy consumption from peak load to an off-peak load period. A PCM based wallboard was experimentally investigated to test the thermal behaviour of light weight building internal partition wall by Kuznik  F *et al.* (2008). The experimental study was carried

-------------------------------------------------------------------------------------------------------

out in a full-scale test room which was completely controlled. The external temperature and radiated flux dynamically simulate a summer repetitive day. The result of this study showed that the overheating effect was lower with PCM material and the energy absorbed was released to heat the air room when the temperature was at its minimum. The wall's surface temperatures were reduced using PCM material, enhancing the thermal comfort by radiated effects. Castell A *et al.* (2010) constructed PCM brick and experimentally studied if it is suitable for passive cooling. Experiments under free-floating conditions showed lower peak temperatures (up to 1 °C) and more constant conditions in the cubicles with PCM, smoothing out the daily temperature fluctuations. The results of this work were similar as those observed in previous works done with microencapsulated PCM in concrete and gypsum. However, some problems with the solidification of the PCM during the night were observed. Therefore, a cooling strategy (either natural or mechanical) must be defined to improve the performance of the PCM under free-floating conditions. Additional experiments using a heat pump to set and control the inside temperature of the cubicles were performed. The experiments demonstrated that the energy consumption of the cubicles containing PCM was reduced by about 15% compared with the cubicles without PCM. This demonstrated the significant contribution and potential of the use of PCM in building envelopes for energy savings and thermal comfort in a real house-shaped cubicle.

In research by Kuznik *et al.* (2009), the PCM experiments in a small scale test cells MICROBAT were performed. The PCM influence and impact with respect to the change of conditions in the climatic chamber. The test cell MICROBAT was completely placed inside the climatic chamber and was examined. They designed an active face, which is used to enhance the heat transfer between the exterior and interior of the test cell. Kuznik *et al.* (2009) recommended that the PCM wallboard should be constructed in the way that directly expose the PCM layer to the air.

Ahmad *et al.* (2006) reported that using a vacuum isolation panel (VIP) in a wallboard can reduce the thermal loss and improve efficiency for lightweight buildings. Two test cells were designed and each cell consisted of one glazed face and five opaque faces insulated with VIPs. One of the cells was equipped with five PCM panels (PCM type of polyethylene glycol (PEG) 600 with melting point of 21–25°C; latent heat of fusion 148 kJ/kg; density 1128 kg/m$^3$ and specific heat capacity of 2490 J/kgK). During summer, the efficiency of PCM test cell was found to be remarkable with a reduction in

temperature amplitude of 20 °C. In winter, the PCM cell helped to prevent negative indoor efficiently. Moreover, the PCM panels still showed a good thermal storage capability even after more than 480 thermal cycles (Tyagi *et al.* 2011).

Thermal performance of plastering mortar was assessed by Vaz Sá *et al.* (2012) with the purpose of enhancing the thermal comfort inside buildings. Their research presents the development and characterization of a new composite construction material that consists in embedding 25% microencapsulated PCM with melting point of 23°C, enthalpy of 100–110 kJ/kg and 300 kg/m$^3$ density in plastering mortar. The experimental part of their research was the first application of the new composite material with the goal of highlighting behavioural differences in regard to common mortars. For that propose two small-scale test cells were built: one with recourse to conventional mortar; and other with PCM plastering mortar.

Two small size closed test cells (hollow cubes with outer edge of 40 cm) were built with distinct interior coatings: (i) one with common plastering mortars (REFM); (ii) another with the developed PCM mortar (PCMM). Each pilot test cell was placed inside a controlled climatic chamber. The temperature cycles inside the climatic chamber were programmed to match the sol–air temperature corresponding to the surface temperature of a vertical wall facing south, which is considered to be the most unfavourable situation for Spring/Summer time in Portugal.

The results for both spring and summer days turn clear that PCM acts by reducing inside temperature amplitudes during the day, levelling them and turning them closer to comfort temperature levels. The results showed that the climates with warm to hot and dry summers (in Portugal) are ideal for utilizing microencapsulated PCM with melting temperature of 23°C.

Test results showed that the difference in the maximum internal temperature between the reference and PCM mortar cell was 2.6 °C for the spring day while this difference was 2 °C for the summer day. The PCMM test cell had a larger corresponding delay of approximately 4 h.

Gómez *et al.* (2012) performed an experimental research with precast self-compacting concrete panels containing 5% of PCM (melting point 23°C, latent heat of 110kJ/kg and density of 980 kg/m$^3$). The cubicle rests on a base made of conventional concrete; the roof was also constructed with conventional concrete and contains expanded

polystyrene insulation. The enclosure also contains a heat pump, which functions to maintain a constant temperature inside the cubicle. Regarding the electrical installation of the cubicle, an electrical breaker box is installed outside the cubicle to separate the electrical installation of the cubicle and the electric network. The consumption meter allows an evaluation of the variation in energy consumption when the heat pump operates in cooling or heating mode. Temperature range of climate conditions all during 10 days of the test was with minimum of 14°C and maximum of 32°C. The main conclusion of their work was the lower energy consumption during day time because PCM stores part of the energy received by cubicle. The difference observed during the night when PCM releases the energy stored, thereby producing a greater consumption of the heat pump, is less significant. The amount of the overall electricity energy saved in the case of PCM was approximately 8% (Gómez *et al.* 2012).

The research by Baetens *et al.* (2010) showed that enhancing thermal mass of concrete buildings seemed better than the use of PCM wallboards; however, the high cost of PCMs was the biggest concern. The research by Pasupathy (2008) showed the effect of the building with PCM panel on the roof from the aspect of the location and thickness. He recommended a double layer of PCM to be incorporated in the roof to narrow indoor air temperature variation and to better suit the comfort demands for all seasons.

An experimental investigation by Bentz *et al.* (2007) showed the effect of incorporation of PCM on temperature variations within 2 days of hydration of cement mortars at semi-adiabatic conditions. In their research three types of cement mortars were produced with water to cement ratio of 0.4. These mixes were: 1) a control mix having no PCM produced with a non-porous coarse silica sand; 2) a mix containing pre-impregnated expanded shale lightweight aggregate with 13.8% (by mass of dry LWA) paraffin wax as 100% replacement of sand; and 3) a mix containing 100% paraffin wax particles (1 mm in size) as replacement of sand. They founded, the use of PCM lowered the peak temperature by approximately 8 °C and delayed it by around 1 h. Therefore, the heat evolution in mortar with PCM was strongly influenced by the presence of PCM.

Sakulich *et al.* (2012) studied the incorporation of PCM into cementitious mortar via fine lightweight aggregates in order to extend the service life of bridge decks, by reducing the freeze/thaw damage. Two types of lightweight aggregates (expanded clay and pumice) and four types of PCM (a paraffin wax, vegetable oil based PCM, PEG400 and PEG600) were studied. A fix dosage of 50 kg/m$^3$ of PCM has been investigated.

Test results showed that the compressive strength was lower in all PCM mortars with polyethylene glycol cement mortar showing a substantial reduction in compressive strength. The decrease in compressive strength was due to the mechanical (the relative weakness of LWA) and chemical reasons (polyethylene glycol interfering in hydration). Moreover, paraffin showed no effect on hydration reaction while polyethylene and vegetable oil-based PCM significantly retarded and suppressed the hydration of the cement mortar. This suggests that the PCM sticking to the aggregate surface were likely to be a problem during cement hydration. It is noteworthy to mention here that the focus of this section is on building application for PCM however, this research was discussed here due to its important contribution. Moreover, the findings could be positively used for building applications.

## 2.8  Summary of chapter 2

This chapter introduced the concept of phase change materials. The important aspect of high heat content at narrow ranges of temperature supports the use of PCM in buildings, but various other thermophysical, kinetic and chemical properties have also been identified as essential to the proper utilisation of PCMs. The classification of PCMs into organic, inorganic and eutectics has been presented. Classical thermal analysis techniques consisting of the DSC, T-history, and heat flow for thermal conductivity measurements have also been described. Organic PCMs are found to have poor heat transfer properties and hence are not used directly as a heat transfer medium. Microencapsulation is popular method to improve the heat transfer properties, resulting in heat transfer enhancements and efficient system designs. The application of PCMs to buildings has mainly been made through their incorporation into the building envelopes in order to shift the thermal loads by providing additional thermal inertia. They have also been incorporated in cement based materials with very encouraging results by overall reduction energy consumption in buildings for example.

Most of the PCM systems designed in the literature have been studied for relatively small indoor spaces such as offices, and for intermittently occupied buildings. The performance of PCM systems were found to be heavily dependent on the phase change temperatures, thermo-physical properties, melting enthalpy, amount and type of PCM, orientation of the building, climatic conditions, type of systems (passive, active).

Therefore, this highlights the use of numerical simulations in the prediction and optimization of the performance of PCM systems.

# Chapter 3 Materials Characterization

## 3.1 General overview

The materials used in this thesis and corresponding characterization are described in the present chapter. Two types of PCM were studied, paraffin PCMs and microencapsulated PCMs. Each type of PCMs has a specific characterization procedure such as thermal energy storage testing.

Regarding aggregates, three types of aggregates were studied, lightweight aggregates, river aggregates and artificial aggregates. The characterization procedure for the aggregates was selected due to their final application.

Furthermore, two types of cement were studied as binders. The characterization of each binder is based on the final application of the cement.

A schematic of the experimental plan is shown in Figure 3-1. The main aim of this plan was first to estimate specific enthalpy temperature functions for the studied pure PCMs by using advanced measurement technique. The DSC tests were adopted to investigate the thermal behaviour and corresponding specific enthalpy values. In fact, the heat flow evolution versus temperature/time during the test was monitored and corresponding enthalpy values were determined as explained in this chapter.

Furthermore, SEM/EDS technique was used in order to investigate the chemical composition of the studied materials including: microencapsulated PCMs, cements and artificial sand. Consequently, elemental composition of each material was determined.

Finally, impregnation potential of PCM into lightweight aggregates was addressed. An impregnation process was adopted to carry out the impregnation study of two different

---------------------------------------------------------------------------------------------------------------

PCMs in four different LWAs. In fact, the leakage of the impregnated PCMs was studied when they were submitted to freeze/thawing and oven drying tests, separately.
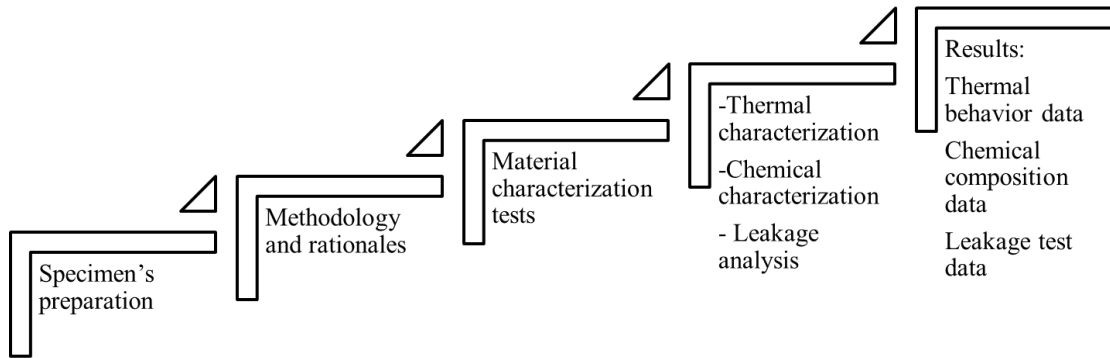


Figure 3-1: Experimental plan.

## 3.2 Materials

Two types of PCMs were used in this research, commercially microencapsulated PCMs and paraffin PCMs. Moreover, two types of cement, and three types of aggregates were studied, a type of cement with a type of aggregate for production of plastering mortar targeted for building applications and a type of cement together with two types of aggregates for production of delayed freezing mortar targeted for pavement applications.

### 3.2.1 PCMs

*Microencapsulated PCMs*

The studied materials were sourced as ready-to-use from commercial microencapsulated PCM. Three types of encapsulated organic PCM paraffins were considered (Devan Mikrathermic D series): MC18 (melting temperature of 18ºC), MC24 (melting temperature of 24ºC) and MC28 (melting temperature of 28ºC) as given in Table 3-1.

Table 3-1: Properties of PCMs, provided by supplier (Microthermic 2012).

| Properties | Melting point (°C) | Latent heat of fusion (kJ/kg) |
|:---:|:---:|:---:|
| MC18 | 18 | 180.40 |
| MC24 | 24 | 147.90 |
| MC28 | 28 | 170.10 |

According to the supplier, the selected PCM materials show very similar texture characteristics such as grain size and shape (Microthermic 2012). The technical specifications of the PCMs (Microthermic 2012) report a mean size of the encapsulated spherical paraffin particles of around 18 μm for MC18, MC24 and MC28. SEM imaging of these materials revealed a large variation of the particle size around the average value, as seen in Figure 3-2a. In fact, the smallest paraffin particles were around 3 μm in diameter and the largest reached approximately 26 μm. With these three types of PCMs, four samples were prepared for DSC tests: three samples that solely contained one type of PCM (MC18, MC24 or MC28) and one sample that contained a 50%−50% mass proportion mix of MC18 and MC28, here termed as MC18_28. The tested samples had average weight of ~4mg. The morphology of bulk PCM can be observed in Figure 3-2a, where only PCM particles can be seen without any extra substances. It should be note that, the EDS/SEM analysis of the pure microencapsulated PCMs has a strong peak appeared in the elemental analysis of the PCM is the carbon element (C) which is the main component of the PCM material (see Figure 3-2b).



**(a)**                                        **(b)**
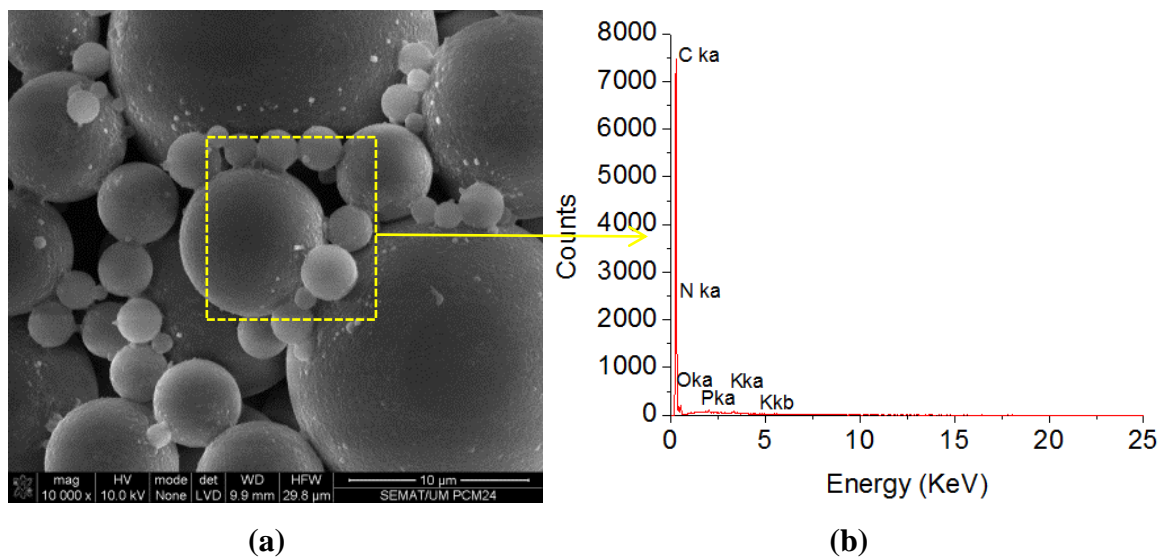
Figure 3-2: (a) Particle size characteristics of microencapsulated PCM powder (MC24); (b) EDS spectrum of the PCM (MC24).

*Paraffin PCMs*

Two types of organic PCM paraffins were considered: R3 Rubitherm RT series (melting temperature of 3°C) and R5 Rubitherm RT series (melting temperature of 5°C) (Rubitherm GmbH 2012). The properties of the PCMs selected for this study were provided by the manufacturer: Rubitherm GmbH (2012) and are presented in Table 3-2. Selection of melting temperatures for the paraffin PCMs under study was based on the target application of reducing freeze-thaw cycles in pavement structures.

Table 3-2: Properties of paraffin PCMs (Rubitherm GmbH 2012).

| Materials | Melting area (°C) | Density-liquid phase at 15°C (kg/m$^3$) | Latent heat capacity ±7.5% (kJ/kg) |
|---|---|---|---|
| R3 | 2-5 | 770 | 198.0 |
| R5 | 1-6 | 770 | 180.0 |

Therefore, the melting temperatures were selected to be slightly above 0ºC as to attenuate the enduring of such temperature within the mortars into which the PCMs are to be applied. Furthermore, chemical compatibility with the porous materials was taken into account, as well as the range of available PCMs products in the market. Figure 3-3 presents the paraffin PCM in the solid and liquid stages. This type of paraffin PCM can be used in container, while paraffin PCM generally implies the PCM being embedded in building wallboards, using various ways, depending on the design of the building, but are usually added in the building envelope or as its substitution.



Figure 3-3: The paraffin PCM at solid and liquid stages that adapted from (Rubitherm GmbH 2012).

### 3.2.2   Aggregates

*Lightweight aggregates (LWAs)*

Geometrical features of the pore structure (including porosity, pore diameter distribution, pore connectivity and pore shape) and chemical compatibility are some of the important factors to be considered when selecting porous materials for impregnation with organic paraffin PCM. Four LWAs were chosen for this study, both inorganic and organic lightweight aggregates were adopted: Expanded Clay (IC) supplied by ARGEX-SA (Portugal) (ARGEX 2013); Granulated Expanded Cork (GC) supplied by SOFALCA/ISOCOR Co., Ltd. (BRANCO 2014); Expanded Perlite (AP) and Expanded Vermiculite (EV) supplied by URBICULT Unipessoal Ltd (URBICULT 2012).



**(a)**                    **(b)**



**(c)**                    **(d)**
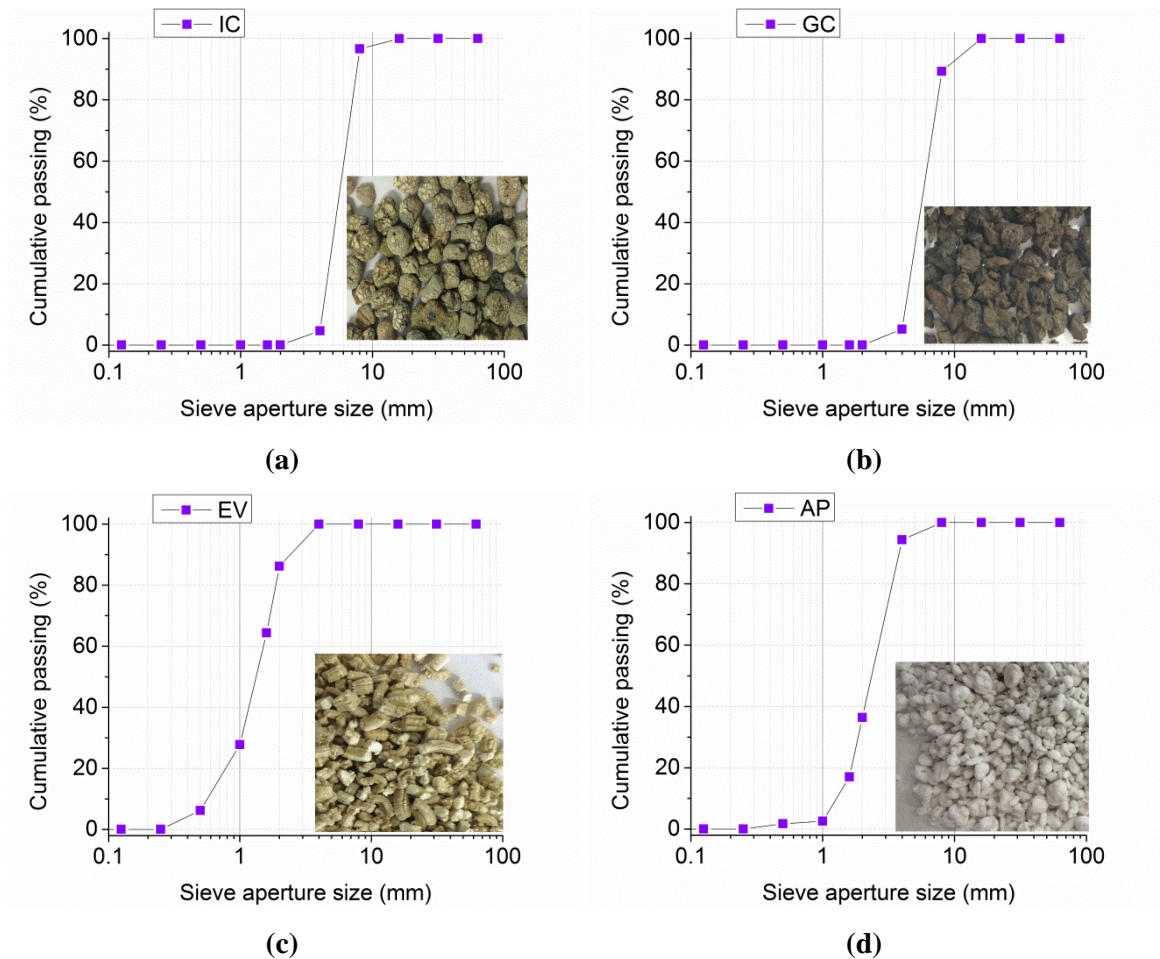
Figure 3-4: Distribution of particle size of the LWAs with the representative shot of LWAs presented in the insets: (a) Expanded Clay (IC); (b) Granulated Expanded Cork (GC); (c) Expanded Vermiculite (EV); and (d) Expanded Perlite (AP).

Such materials have been considered suitable for impregnation in previous works (Nóvoa *et al.* 2004, Karaipekli *et al.* 2009, Lu *et al.* 2014, Barreneche *et al.* 2016). The particle grain size distributions of LWAs was assessed with sieving method (EN 933-1 2012), and the results are presented in Figure 3-4.

*Artificial sand*

Industrial sand with mean particle size around 440 μm was used as aggregate. The detailed grain size distribution of the sand is presented in Figure 3-5a. Regarding sand materials, the EDS results shows the silicium element (Si) as the main component (Figure 3-5b). The element content of the zoomed regions was performed and the main component of the artificial sand material was determined.



**(a)** **(b)**
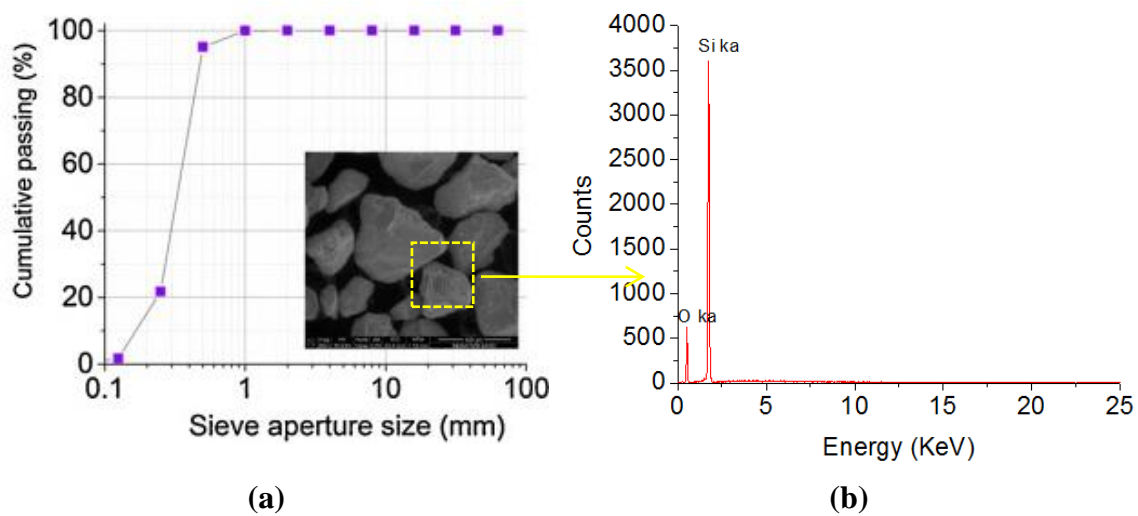
Figure 3-5: (a) Particle size distribution of the sand with the granulometry curve presented in the inset; (b) EDS spectrum of the artificial sand.

*River sand*

For the production of set delayed freezing mortar, the natural aggregate was composed of fine grain size and mean grain size portions, which had been used in previous studies (Barreneche *et al.* 2016). The particle size distributions of aggregates were assessed through sieving (EN 933-1 2012), and the corresponding results are presented in Figure 3-6.

---
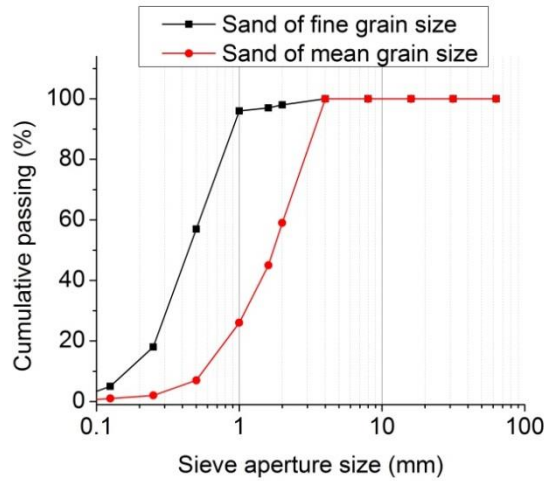


Figure 3-6: Grading curves of river aggregates.

### 3.2.3 Waterproofing materials

For the production of delayed freezing mortar that will be described in the next chapter, it was decided to use waterproofing materials due to the fact that, impregnation of LWAs with PCM at material level investigation showed leakage problem of the PCM.

It is worth to mentioned that, the importance of adequately coating the impregnated LWAs to avoid possible leakages of the PCMs, four different coating solutions were trialled (Table 3-3), namely: Sikalastic-490T (a polyurethane, transparent waterproofing liquid membrane) (Sika 2011), Weber Dry Lastic (a liquid membrane used for waterproofing roofs) (Weber 2009), Makote 3 (a waterproofing bituminous emulsion from MC-Bauchemie) (MC-Bauchemie 2011) and ECM-2 from CEPSA (a cationic bituminous emulsion for cold asphalt mixtures) (CEPSA 2010). These waterproofing coating solutions need to have service temperature ranges adequate for the end applications aimed in this research.

Table 3-3: Technical data of waterproofing materials (Weber 2009, CEPSA 2010, MC-Bauchemie 2011, Sika 2011).

| Materials | Application Temperature (°C) | Service Temperature (°C) | Density (kg/m3) | Drying time (hour) | Colour | Names |
|---|---|---|---|---|---|---|
| CEPSA (ECM-2) | 30 to 60 | - | - | - | Black | CEP |
| MC-Bauchemie (Makote 3) | 5 to 40 | * | 1080 | 48 | Black | MCB |
| Weber Dry Lastic | 10 to 40 | −15 to +70 | 1300 | 24-36 | White | WEB |
| Sikalastic -490T | 5 to 40 | −30 to +90 | 990 | 8-12 | Transparent | SIK |

* No information available on behalf of the supplier. The product is a bituminous emulsion that is recommended for protection of buried concrete elements or as a primer for asphaltic fabric.

### 3.2.4 Cements

*Cement for plastering mortars*

The binder adopted to be used for the production of plastering mortars (will be also discussed in next chapter), is Portland cement type I class 42.5R and SEM image of the cements illustrated in Figure 3-7a. The SEM image and corresponding energy spectrum of the materials used as substance materials for plastering mortar were investigated and are shown in Figure 3-7b. As it can be seen, the unhydrated particles are bare, with debris lying of particles in the microstructure of the cement as well as chemical elements of the cement (Figure 3-7a, b).



**(a)**         **(b)**
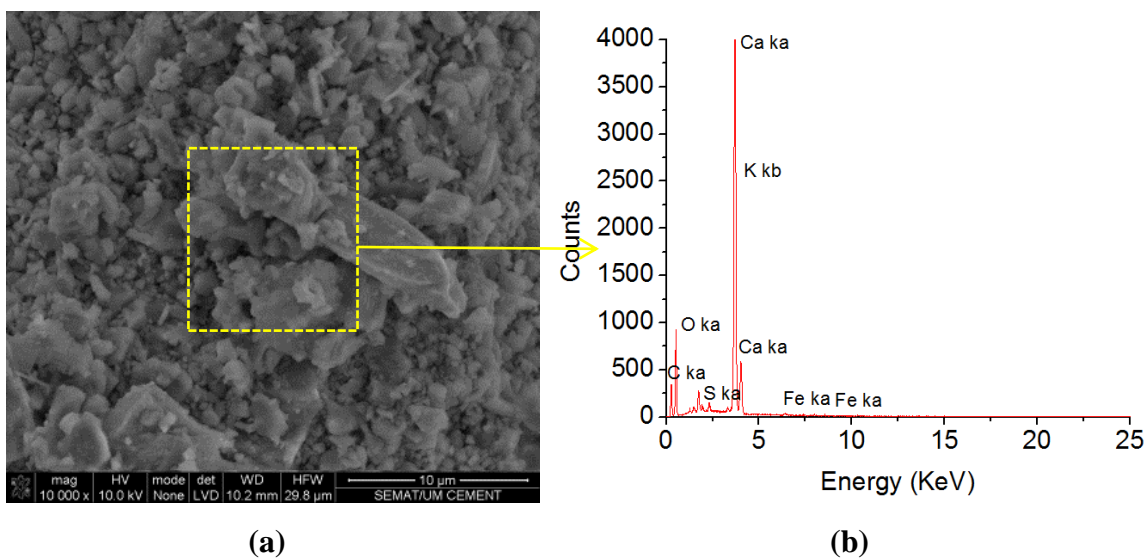
Figure 3-7: (a) Particle size characteristics of the cement powder (42.5R); (b) EDS spectrum of the cement.

*Cement for delayed freezing mortars*

For the preparation of the set delayed freezing mortars, a commercially available Portland cement CEMII-32.5N was used. This binder was Portland cement CEM II/B-L 32.5N provided by Secil-Companhia Geral de Cal e Cimento, SA in Portugal.

### 3.2.5 Superplasticizer

For workability control of the mortars it is recommended to use superplasticizer (Silva *et al.* 2013, Barreneche *et al.* 2016). Therefore, a commercial superplasticizer that was provided by BASF Construction Chemicals was considered. Regarding the properties of the superplasticizer, composed by a polycarboxylate product (dry maximum loss of 4.0%), containing from 1.0% to 5.0% of sodium sulfate and <0.195% of formaldehyde, and it is characterized by a specific density of 500–800 kg/m$^3$ and a pH range of 9–11.4 (200 g/l, 20 °C).

## 3.3 Evaluation of thermal energy storage of PCMs

The DSC calorimeter submits the sample to controlled temperatures and records the corresponding heat fluxes, thus providing information about temperatures and enthalpies associated to phase changes. From the heat flux, the specific heat as a function of temperature can be obtained, and the enthalpy is determined by integration procedures. In this thesis, the methodology of enthalpy calculation follows the strategy mentioned in Chapter 2.

### 3.3.1 DSC procedure for pure microencapsulated PCMs

The melting and freezing behaviours of the PCM were analysed by a DSC model Mettler Toledo DSC 822e. The DSC has an accuracy of ±0.2ºC for temperature measurements. All the samples were tested within aluminium crucibles with volume of 40 μL under nitrogen ($N_2$) atmosphere flow of 80ml.min$^{-1}$. The samples were weighted by an analytical balance with accuracy of ±0.01mg. The weights for samples MC18, MC24, MC28 and MC18_28 were 3.5 mg, 4.4 mg, 3.8 mg and 4.3 mg, respectively. A constant heating/cooling rate of 1ºC.min$^{-1}$ was applied for all the samples, as recommended by (Barreneche *et al.* 2013). The applied program steps for the test procedure of samples are presented in Figure 3-8. Samples of each material were analysed and each sample was cycled once (heating and cooling).
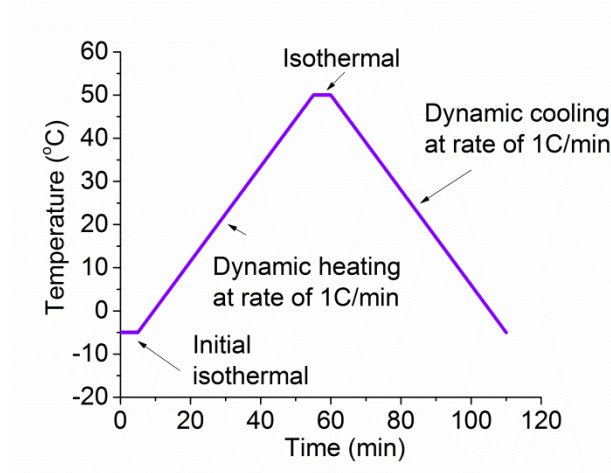
Figure 3-8: DSC program for testing of pure microencapsulated PCMs.

### 3.3.2   DSC results for pure microencapsulated PCMs

The results of the DSC experiments for the pure PCMs are discussed in the following sections and presented in Table 3-4. None of the tested PCMs revealed melting temperatures (peak points) coinciding with the reference value indicated by the supplier, with maximum deviations reaching 3.74 K. Furthermore, the difference between the melting peak temperature and the freezing peak temperature was of 3.29, 4.5 and 2.42 K for MC18, MC24 and MC28, respectively. This is coherent with reports of hysteretic behaviour of the phase change by (Castellón *et al.* 2008). For the sample of MC18_28, the difference between the melting peak temperatures and the freezing peak temperatures was of 2.7 and 1.86 K for the phase changes corresponding to MC18 and MC28, respectively. In the MC18_28 sample, the phase change melting temperatures were coherent with those of the components of the mix (MC18 and MC28). This indicates that, the mixing of two PCMs had similar behaviour to the independent PCMs and it can be inferred that they have not endured unexpected interactions with each other.

Table 3-4: Pure PCM enthalpy, onset and end temperatures for different PCM samples.

| Designation | Melting | | | | Freezing | | | |
|---|---|---|---|---|---|---|---|---|
| | Onset temp. (ºC) | End Temp. (ºC) | Enthalpy (kJ/kg) | Peak temp. (ºC) | Onset temp. (ºC) | End temp. (ºC) | Enthalpy (kJ/kg) | Peak temp. (ºC) |
| MC18 | 15.67 | 18.97 | 270.63 | 17.75 | 15.4 | 12.44 | 275.08 | 14.32 |
| MC24 | 18.21 | 23.86 | 162.4 | 22.74 | 22.36 | 15.67 | 136.53 | 17.94 |
| MC28 | 24.19 | 28.79 | 253.89 | 24.26 | 25.96 | 13.42 | 256.89 | 27.08 |
| MC18_28 | 15.8 , 24.72 | 18.29 , 27.8 | 134.17, 100.5 | 17.61, 27.08 | 15.31, 25.96 | 13.51, 22.62 | 139.59, 82.23 | 14.7, 24.78 |

--------------------------------------------------------------------------------------------------------

For illustrative purposes, Figure 3-9a shows the DSC heating curves of MC18 and MC28 separately and also, superimposed graphically to the result of MC18_28 sample.
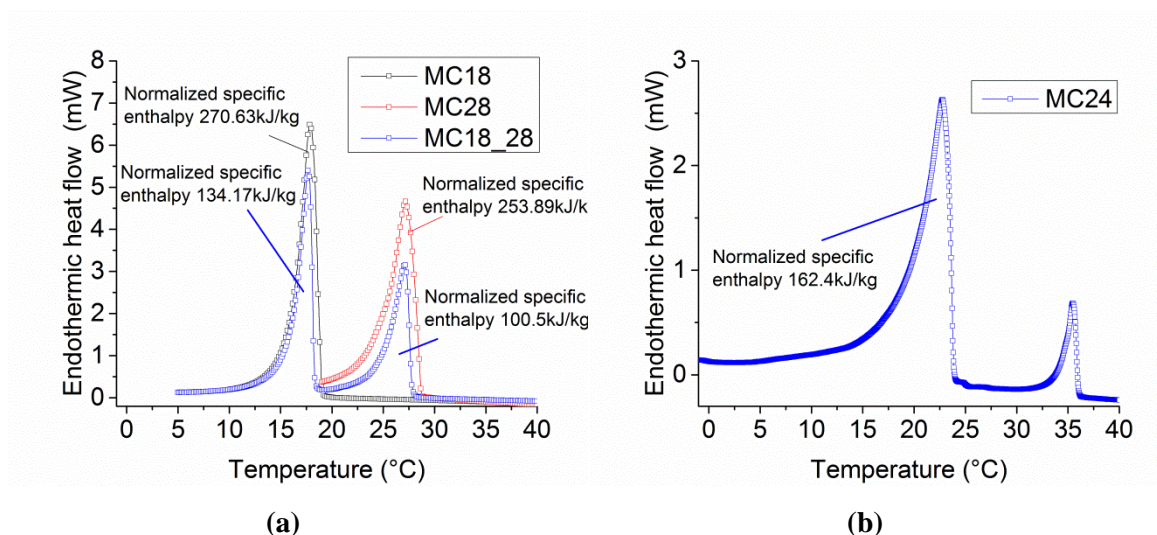


Figure 3-9: Heating DSC curves for: (a) MC18, MC28 and MC18_28; and (b) MC24.

It can be observed that, the specific enthalpy value of MC18_28 at ~18ºC is almost half of the specific enthalpy of the MC18 sample at the same transition temperature. This is coherent with the fact that MC18_28 has half of the quantity of 18ºC PCM when compared with MC18. A similar tendency is observed for the 28ºC transition (however with slightly higher deviation). Figure 3-9b shows the results obtained by DSC have the same thermal behaviour during the heating process: highest peak at 24°C in a melting temperature range between ≈18°C and ≈24°C. The melting enthalpy of MC24 sample analysed has a value 162.4 kJ/kg.

### 3.3.3 DSC procedure for pure paraffin PCMs

The melting and freezing behaviours of the paraffin PCMs were analysed by a DSC model NETZSCH 200 F3 Maia. The DSC has an accuracy of ±0.2°C for temperature measurements. All the samples were tested in 40 µl capacity aluminium crucibles under nitrogen ($N_2$) atmosphere with a flow of 50 ml.min$^{-1}$. The weights for samples R3 and R5 were 5.35 mg and 5.68 mg respectively, measured to an accuracy of ±0.01mg. Each sample was sealed in the pan by using an encapsulating press. An empty aluminium crucible was used as a reference in all measurements.

The effect of thermal cycles and heating/cooling rates on the phase change processes and specific enthalpy values was examined. In this way, different heating/cooling rates

------------------------------------------------------------------------------------------------------

of 0.5°Cmin[-1], 1°Cmin[-1], 2°Cmin[-1], 5°Cmin[-1] and 10°Cmin[-1] were considered. The applied program steps for the test procedure of samples were as follows: (i) initial isothermal period at −20°C for 5 minutes; (ii) dynamic heating up to +20°C according to the proposed rate (0.5°Cmin[-1], 1°Cmin[-1], 2°Cmin[-1], 5°Cmin[-1] or 10°Cmin[-1]); (iii) stabilization at +20ºC for 5 minutes; (iv) dynamic cooling to −20ºC with proposed rate (0.5°Cmin[-1], 1°Cmin[-1], 2°Cmin[-1], 5°Cmin[-1] or 10°Cmin[-1]). For the PCMs analysed, each sample endured one full cycle (each full cycle consisted of the steps (i) to (iv) as detailed earlier). The DSC peaks for each PCM were evaluated for a cycle of heating/cooling curves in terms of latent heat storage and phase change temperatures, in line with references (Melhing *et al.* 2008, Denner T 2012, Biwan *et al.* 2013).

### 3.3.4  DSC results for pure paraffin PCMs

In order to quantify the thermal energy storage capacity of the paraffin PCMs, DSC was deployed. In view of the acknowledged dependency of DSC results on the heating/cooling rates (Dumas *et al.* 2014, Jin *et al.* 2014), the assessment of the influence of heating/cooling rates on the DSC thermograms as well as specific enthalpy calculation has been analysed and separated into two main sections: 1) effect of the heating/cooling rates; 2) specific enthalpy analysis.

*Effect of the heating/cooling rates*

The experimental curves for R3 at different heating/cooling rates are shown in Figure 3-10.



(a)                                                             (b)
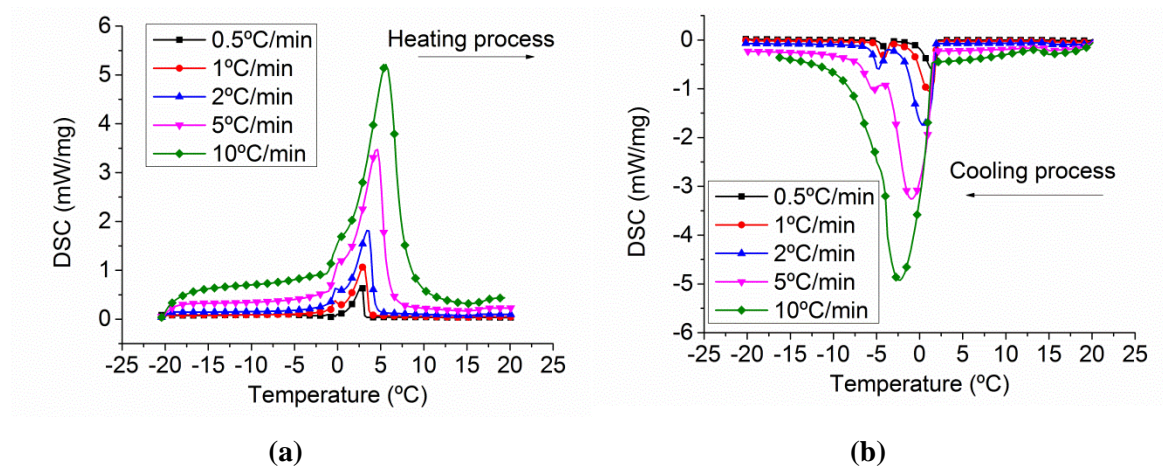
Figure 3-10: DSC thermograms for R3 specimen with different heating/cooling rates: (a) heating process at several rates; (b) cooling process at several rates.

-------------------------------------------------------------------------------------------------------

The peak temperatures in the thermograms of the heating process (Figure 3-10a) are consistently being increased as the heating rate increases. Conversely, in the case of cooling (Figure 3-10b), the peak temperatures decreases with increased cooling rates. Overall, it was observed that the PCM peak response shifts in the direction of the imposed flux; i.e. higher peaks for heating and lower peak temperatures for cooling. This type of behaviour has been reported in earlier investigations (Kousksou *et al.* 2013), and it can be explained by an increasing thermal gradient in the sample.

The DSC curves for the R5 specimen at several heating and cooling rates are shown in Figure 3-11. The observations are quite similar to those already made for R3, except for the fact that this new PCM (R5) exhibits shifted phase transition in terms of peak temperatures compared to R3. It is interesting to note that, for samples R3 and R5, at a heating rate of 2°C/min, the phase change melting temperatures were in direct agreement with those specified by the material supplier (see Table 3-2).



**(a)**    **(b)**
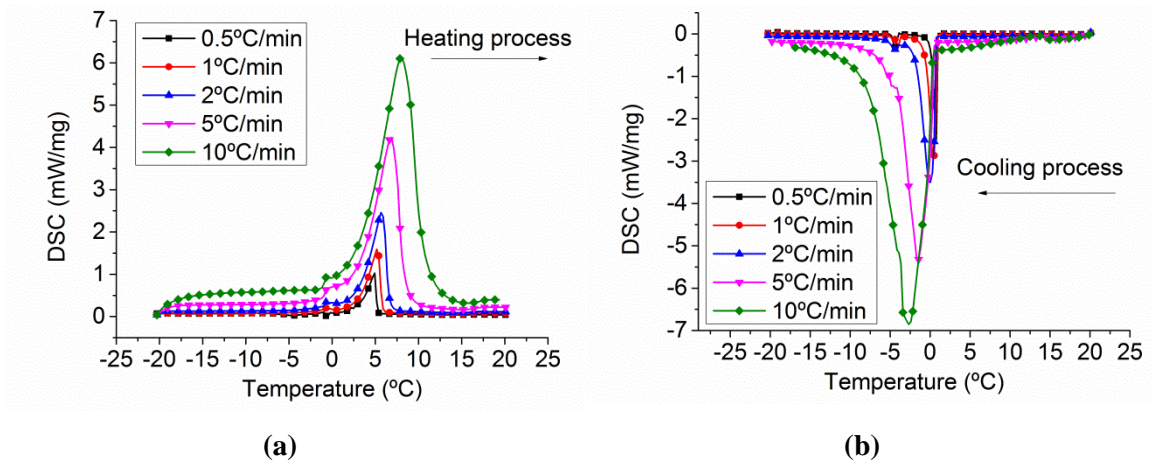
Figure 3-11: DSC thermograms for R5 specimen with different heating/cooling rates: (a) heating process at several rates; (b) cooling process at several rates.

*Specific enthalpies of PCMs*

The specific enthalpy assessment for the three mortars is discussed hereafter. The methodology for the specific enthalpy calculation was based on the proposed method by (Kheradmand *et al.* 2014) as mentioned in Chapter 2.

The results of the calculation of specific enthalpy evolution along temperature for R3 are shown in Figure 3-12a) and b), which present the results for heating and cooling

---

processes, respectively. It can be observed that the accumulated specific enthalpy is almost constant (nearly 130 J/g) regardless of the heating/cooling rate. However, it should be noted that, the obtained specific enthalpy for R3 has a lower value (about 25% less) in comparison with the material supplier data.



(a)                  (b)
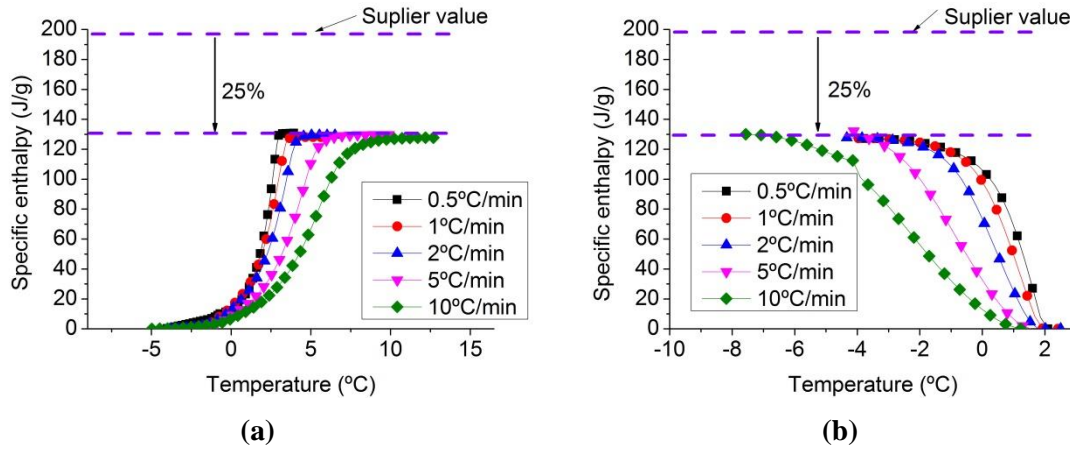
Figure 3-12: Specific enthalpy curves for R3 with different heating rates of 0.5 °C/min, 1°C/min, 2 °C/min, 5 °C/min and 10 °C/min : (a) heating process and (b) cooling process.

Figure 3-13 shows the specific enthalpy evolution for R5, and as expected, the accumulated enthalpy is almost independent of the heating/cooling rate. The obtained specific enthalpy value obtained for R5 (approx.180 J/g) was consistent with the information provided by the supplier (see Table 3-2).



(a)                  (b)
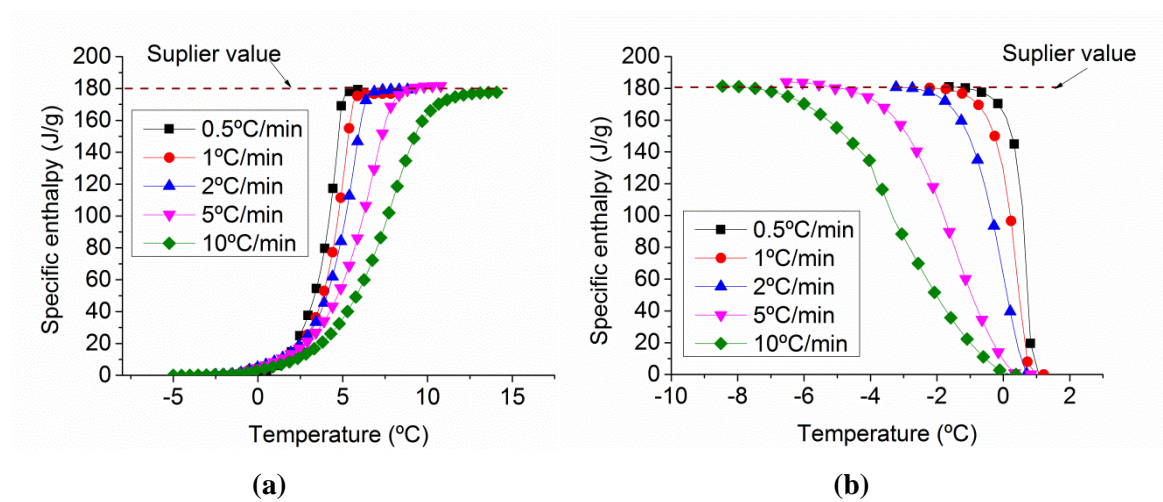
Figure 3-13: Specific enthalpy curves for R5 with different heating rates of 0.5°C/min, 1°C/min, 2 °C/min, 5 °C/min and 10 °C/min: (a) heating process and (b) cooling process.

## 3.4 Lightweight aggregate characterization and impregnation potential

### 3.4.1 Lightweight aggregate characterizations

First, the LWAs particle density and pore structure were studied as to infer the potential of their impregnation. In the first phase of material testing, each type of non-impregnated LWAs (IC, AP, EV and GC) was submitted to the following tests in order to characterize their capacity for impregnation: 1) density analysis, 2) pore structure analysis and 3) absorption amount test.

*Specimen preparations*

Regarding the particle density testing, a total number of 12 specimens were considered for determining density of saturated LWAs with dried surface and that was compared with density of dried LWAs. This included 4 representative samples of each LWAs system (IC, AP, EV or GC) with 3 repeating specimens of each LWA for the particle density measurement. The particle density determination of LWAs was carried on according to EN 1097-6 (2003): (i) first, LWAs samples were oven-dried at 80°C for 24 hours; (ii) then, LWAs samples were immersed in water at temperature of 22°C; (iii) after water immersion, LWAs samples were placed over a filter for 2 hours to drain the excess of superficial water at room temperature (about 22°C); (iv) then, the surface of the samples was dried with an absorbent sheet of paper. Finally LWAs samples with dried surface were placed inside various densimeters with 500ml water and weighted. Regarding pore structure testing, a total number of 12 specimens were considered for the pore structure analysis of LWAs. This includes 4 representative samples of each LWAs system (IC, AP, EV or GC) with 3 repeating specimens of each LWA type for the pore structure investigation. Specific total surface area and pore size distribution of the LWAs was measured using a Quantachrome Instrument, model NOVA 2200e.

Total specific surface area (external surface area and pore surface of particles) determinations were conducted using Multi-point Brunauer-Emmett-Teller (B.E.T) method which is suitable for solid materials (Nova Win 2008). Furthermore, the Barrett, Joyner and Halenda's (B.J.H) method was used to determine pore size distribution, which relates pore volume with pore size, also allowing porosity analysis. In this test

-----------------------------------------------------------------------------------------------------------

nitrogen was used for adsorption and desorption processes with an accuracy of ±0.1% and liquid nitrogen was used to maintain a controlled environment. Also in this phase, a series of tests have been performed to assess the absorption capacity of PCM on behalf of the LWAs. In this way, a total number of 24 specimens were considered for testing absorption rate of PCM by LWAs. This includes 8 representative specimens of each LWA type (IC, AP, EV or GC) with each type of PCM (R3 or R5) with 3 repeating specimens of each mixture for the absorption amount investigation. Specific nomenclature has been given to each composite material in order facilitate identification. In this way a designation type was created in which the two first characters stand for the name of the corresponding LWA (IC, AP, EV or GC), followed by two characters correspond to the PCMs type (R3 or R5). Therefore, as an example, IC_R3 corresponds to expanded clay containing PCM with melting temperature of 3ºC.

*Dry and water saturated densities*

Dry and water saturated LWAs particle density results, as well as percentages masses of water absorption of LWAs are presented in Figure 3-14. The saturated density difference between the four LWAs is related with the volume of existing voids that can be filled in with water.



**(a)**                                                                 **(b)**
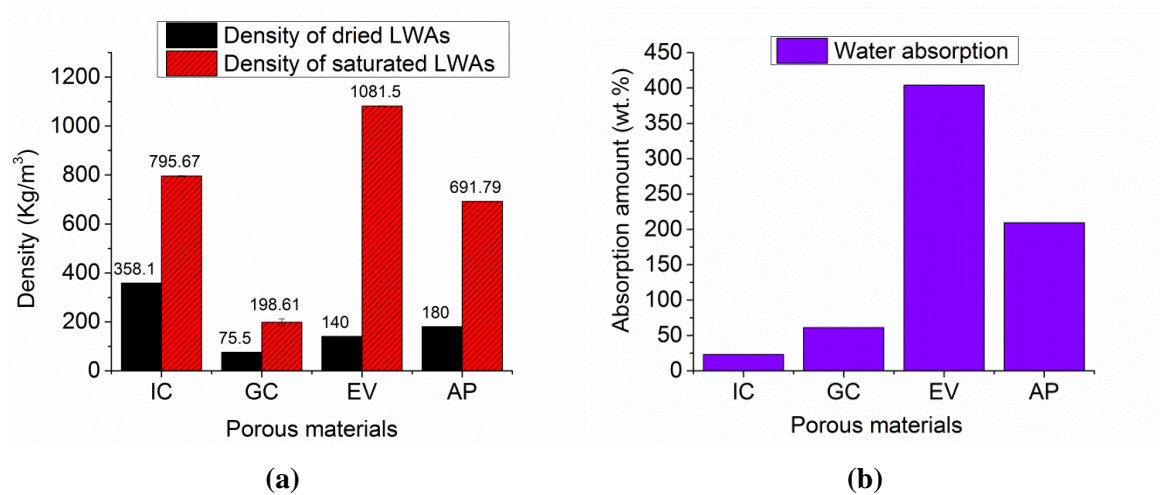
Figure 3-14: (a) Density comparison between dried and water saturated LWAs; (b) Percentage of mass water absorption of the porous materials.

As it can be seen from the results, the EV has the highest saturated particle density (see Figure 3-14a), which means it can absorb the highest amount of water in open pores when compared to the other studied LWAs, as seen in Figure 3-14b. Density of saturated LWAs increased by 1.22, 1.64, 6.72 and 2.83 times when compared with dried densities, respectively for IC, GC, EV and AP. This indicates that the water penetrating in open pores (water absorption) within LWAs is different. The EV particles absorbed much more water than the other LWA materials and have higher open porosity.

It is important to note that the absorption characteristics of an aggregate can also depend on the aggregate size. Large lightweight aggregate have larger voids (like IC and GC). As a result, these large pores effectively become part of the texture of the aggregate, and then they are no longer considered as internal porosity in the aggregate (Castro *et al.* 2011). Comparison between studied LWAs reveals that, smaller particles (like EV and AP) tend to have more porosity simply because they have expanded more than a larger particle. Therefore, in the tested LAWs using different size particles it is observed that the absorption of the smaller aggregate particle sizes is higher than the absorption of larger particle sizes. These results give adequate information regarding the pore volume of the studied LWAs.

*Pore size distributions of lightweight aggregates*

The pore size distributions of IC, GC, AP and EV, was analysed and the results, are shown in Figure 3-15.



(a)                                                                                      (b)
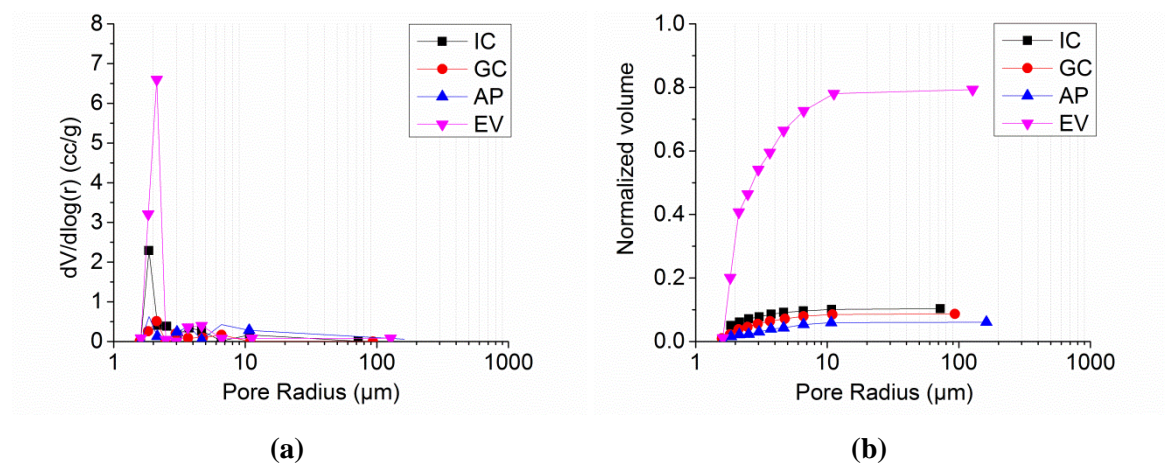
Figure 3-15: Pore size distribution of IC, GC, AP and EV: (a) differential curves; (b) cumulative curves.

---------------------------------------------------------------------------------------------------------------

The Figure presents the LWAs pore size distribution in terms of log differential intrusion volume in dV/dlog(r), where V is the volume intruded into the pores of the sample. The log differential intrusion volume is the derivative of the intruded volume. The derivative plots show clearly identified points of inflection, which highlight zones where clusters of pores of a particular radius occur. Figure 3-15b, depicts the relative distribution of each LWA in terms of the cumulative intruded pore volume to the weight of the sample.

As shown in Figure 3-15a, EV LWAs have more volume of pores per unit weight when compared with the other LWA materials. The strong peak indicated that most pores have approximately 2.1µm radius, for the EV and 2.0 µm radius, for the IC. On the other hand, GC and AP have less volume of pores, having approximately 1.9µm of radius. According to the International Union of Pure and Applied Chemistry (IUPAC) pore-size classification (Collins *et al.* 2000), which classifies pores into macro, meso and micropores, the pores of the IC and EV LWAs are mesopores, as they are equal or larger than 2µm. Furthermore, GC and AP LWAs have micropores since sizes are lower than 2µm. The total specific surface areas values were 0.321 $m^2$/g, 0.188 $m^2$/g, 5.817$m^2$/g and 0.437$m^2$/g for IC, GC, EV and AP respectively. The EV has much larger total specific surface area than other LWAs. The results of pore size analysis are coherent with previous information regarding the capacity to absorb water, which indirectly indicated the porosities (see Figure 3-14). Consequently, the pore structure plays an important factor in the absorption capacity of the LWAs. The LWAs with greater pore volumes and larger pore radiuses are bound to be capable of absorbing higher water or paraffin content. Nevertheless, it should be noted that, the viscosity of paraffin and water are slightly different, and also that the corresponding surface tension properties and hence impregnation potential can also be different.

*Paraffin PCM absorption in lightweight aggregates*

The results of absorption amounts of both R3 and R5 PCMs into the four different LWAs are presented in Figure 3-16. Comparing these results to the water saturated density test results (Figure 3-14), the data shows that the PCMs (R3 or R5) absorption is not reaching the maximum possible absorption of the water. It is interesting to highlight the quantitative differences between the capacity of absorption water and PCM into LWAs. For instance, in the cases of IC, EV and AP increases by 21%, 55% and 52% the percentage of water absorptions when compared with the cases with R3 absorption

-----------------------------------------------------------------------------------------------------------------

(wt.%) respectively. In the case of GC the water absorption (wt.%) is about 7% less than that obtained with R3. However, it should be noted that, there is a slightly difference between PCM absorption (wt.%) in the cases with R3 and R5. In which more quantity of R3 can be absorbed in LWAs by 5%, 10% and 23% for GC, EV and AP rather than R5 respectively. These differences might be due to the difference of PCMs specific gravity, viscosity, and liquid surface tension.

As it can be seen, the absorption amounts with different LWAs follow the same trend. The absorption amounts for IC is generally lower than that for the GC, EV and AP, possibly due to the more homogenous (narrow particle size distribution of the IC particles). For the EV mixes with PCMs of R3 and R5, the increments are about 290 wt. % and 240 wt. % respectively. In fact, there are both types of meso and micropores in EV than in the other three kinds of LWAs. However, the impregnation of liquid part into the pore space of LWAs with smaller diameter becomes more difficult than those with larger diameter. Therefore, the adopted impregnation method may be more feasible in porous materials that encompass both fine and large pores.



(a)  (b)
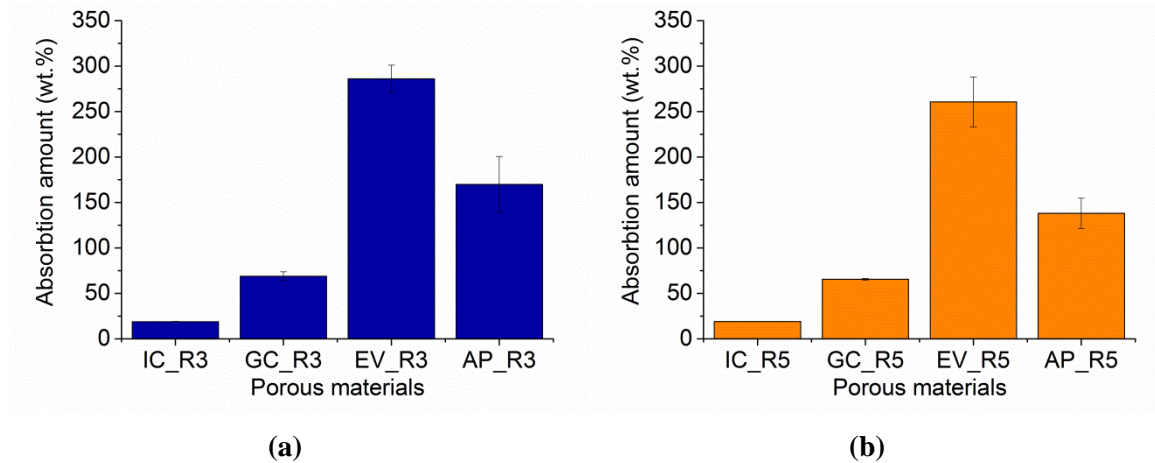
Figure 3-16: Absorption amount for the studied PCMs impregnated into the LWAs: (a) PCM with melting temperature of 3ºC; (b) PCM with melting temperature of 5ºC.

### 3.4.2   Encasement of PCM in lightweight aggregates

*Materials*

Two types of organic PCM paraffins were considered: R3 Rubitherm RT series (melting temperature of 3°C) and R5 Rubitherm RT series (melting temperature of 5°C)

--------------------------------------------------------------------------------

(Rubitherm GmbH 2012). The properties of the PCMs selected for this study were provided by the manufacturer (Rubitherm GmbH 2012), and were characterized in material level investigation.

Four LWAs were chosen for this study, were both inorganic and organic lightweight aggregates adopted: Expanded Clay (IC) supplied by ARGEX- SA (Portugal) (ARGEX 2013); Granulated Expanded Cork (GC) supplied by SOFALCA/ISOCOR Co., Ltd. (BRANCO 2014); Expanded Perlite (AP) and Expanded Vermiculite (EV) supplied by URBICULT Unipessoal Ltd. (URBICULT 2012). Bearing in mind the importance of adequately coating the impregnated LWAs to avoid possible leakages of the PCMs, four different coating solutions were trialled, namely: Sikalastic-490T (a polyurethane, transparent waterproofing liquid membrane) (Sika 2011), Weber Dry Lastic (a liquid membrane used for waterproofing roofs) (Weber 2009), Makote 3 (a waterproofing bituminous emulsion from MC-Bauchemie) (MC-Bauchemie 2011) and ECM-2 from CEPSA (a cationic bituminous emulsion for cold asphalt mixtures) (CEPSA 2010).

*Proposed procedures for encasement of PCMs and surface waterproofing*

The absorption of different PCMs paraffin waxes into different LWAs was measured in accordance with EN 1097-6 (2003). The preparation of encased thermal energy storage LWAs regardless of PCM types are shown in Figure 3-17. In the first stage, all lightweight aggregates were exposed to a jet of compressed air to remove dust and any loose superficial residue from the particles (Figure 3-17a). The lightweight aggregates were next dried in a ventilated oven until a constant weight was achieved. The duration of drying was a minimum of 24 hours at temperatures of 110°C, 80°C, 80°C and 65°C for the IC, AP, EV and GC, respectively. The temperature adopted to dry the granulated expanded cork (GC) was slightly lower than the rest, in order to cause minimal damage to the cork internal structure. It should be noted that, the imposed drying temperatures on the LWAs were adequate, since each types of LWAs was conducted, after drying, into an electronic moisture meter (model KERN MLB_N). The water content of the LWAs showed less than 1 mg. This was considered as dried LWAs (see Figure 3-17b). The LWAs were subsequently cooled down to room temperature (approx. 22°C) for 2 hours. Following drying, a representative sample from each LWA was completely immersed in each PCM for 24 hours (Figure 3-17c). Impregnated LWAs samples were next drained over filter paper to remove the excess of PCM for 2 hours at room temperature, which is above the phase change temperature (Figure 3-17d). The surfaces

----------------------------------------------------------------------------------------------------------------------
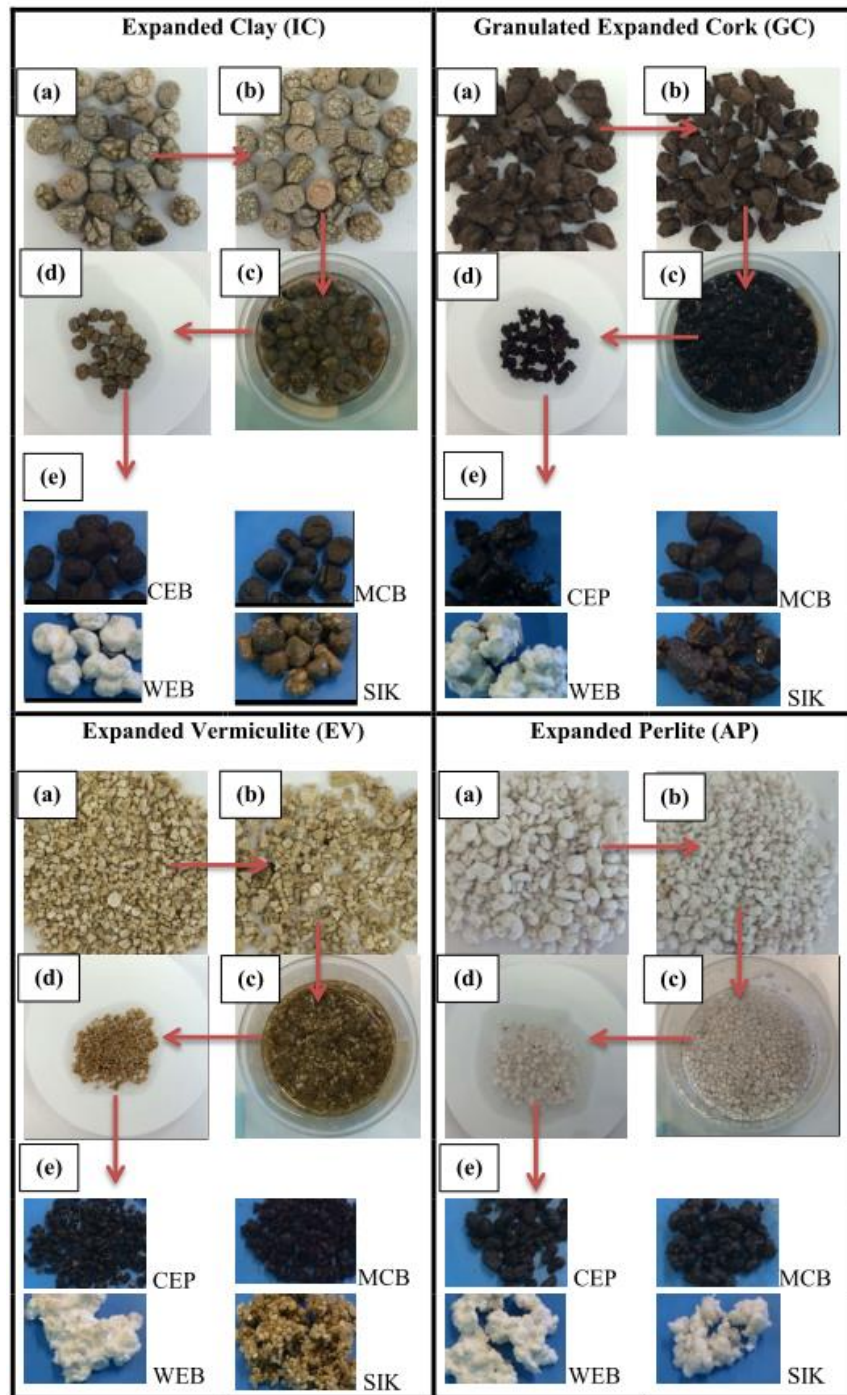


Figure 3-17: Production of thermal energy storage LWAs (a) cleaned surfaces of the particles after using a jet of compressed air; (b) dried LWAs after using a ventilated oven; (c) impregnation of LWA in PCM; (d) drainage procedure over a filter paper (e) PCM+LWA samples coated with different waterproofing materials.

of the impregnated LWAs were then dried with an absorbent sheet of paper. The impregnated LWAs were subsequently soaked with different waterproof coating solutions until the surface of the particles was fully coated. This waterproof coating

procedure was performed at room temperature, i.e., above the phase change temperature of the PCMs. Afterwards, the encased LWAs were allowed to dry in the laboratory environment (room temperature/humidity). Then, the samples were oven dried at 60ºC for 24 hours and left curing at the laboratory environment for further 7 days. Weight variations were monitored during the entire process, and it could be confirmed that all samples had weight variations of less than 0.1 %, during the last three days of the process, thus pointing to a complete hydrothermal equilibrium state. Therefore, the product obtained at the end could be considered as emulating an industrial process of encapsulation of PCMs.

*Testing procedure of thermal energy storage LWAs*

In this phase, two series of tests were performed on thermal energy storage LWAs: freeze/thaw cycle tests and drying tests. A total of 40 specimens were tested under freeze/thaw cycles. This included 8 representative specimens from each LWAs system (IC, AP, EV or GC) with each type of PCM (R3 or R5) with or without a waterproofing solution (REF, SIK, WEB, MCB or CEP). Additionally a total of 40 specimens (same distribution as used for the freeze/thaw cycles) were tested by oven drying. Specific nomenclature has been given to each composite material in order facilitate identification. In this way a designation type was created in which the first two characters stand for the name of corresponding LWAs (IC, AP, EV or GC), the following two characters correspond to the PCMs type (R3 or R5), and the last three characters represents the type of water proofing solution (REF, SIK, WEB, MCB or CEP). For samples with no waterproofing layer, the three letters "REF" stands for reference material. As an example, the IC LWA impregnated with R3 and waterproofed with the Sika product is termed IC_R3_SIK. Conversely, the corresponding impregnated LWA without waterproofing is termed IC_R3_REF. Reference and coated specimens were left at room temperature for 7 days curing, prior to conducting the freeze/thawing tests. For these tests the temperature range was selected to be between – 7°C and +16°C. This range is slightly larger than the range of temperatures that is recorded during Winter in Portugal, particularly in the mountain regions of Guarda (The World Weather Online 2014). To carry out the experiments, four sets of specimens were used. Each set contained five particles of different types of encased PCMs with and without waterproofing coating. At the start of each test, the initial weight of the specimens was recorded.

Specimens were next exposed to 3 freeze/thaw cycles (1 cycle consisting of 0.25 hours of freezing in air inside an automatic conventional freezer, followed by 1.5 hours of thawing in water). Each specimen was subsequently weighed at the conclusion of the third cycle, thus monitoring the process of desiccation. A dimensionless parameter $S$ has been introduced to evaluate the effect of freeze/thaw cycles on the percentage of mass loss, as follows:

$$S = \frac{\Delta w}{w_0} \times 100\% \tag{3.1}$$

Where $\Delta w$ is increment of water content measured in the composite after three freeze/thaw cycles, and $w_0$ is the water content in the reference composite.

To measure the leakage of PCM from encased LWAs, a drying test was adopted according to Refs.(Sakulich *et al.* 2012, Kheradmand *et al.* 2015). In this test, the specimens were first weighed and then placed in an oven at 40 °C, and repeatedly weighed with at least 24 hour intervals between measurements for at least seven days thereafter. Since, the waterproofing materials include water and this will influence the correct measurement of the leaked PCM from LWAs, separate drying tests were performed on the waterproofing materials themselves. The water content in each waterproofing material was determined by placing a few grams of waterproofing material in an oven and conducting a drying test (following a similar test procedure as mentioned earlier for thermal energy storage LWAs). The average amount of PCM retained by the aggregate was considered the encased capacity of the coated LWA in regard to the amount of the water loss of waterproofing materials. Any residue remaining on the surface of the aggregates was only quantified with visual observations of whether the aggregate appeared wet or dry. Similar methodology has been attempted in terms of number of specimens, consideration as freeze/thawing test.

*Result of mass loss of thermal energy storage LWAs under freeze/thaw cycles*

From now on, for the sake of brevity, the term of "composite" will be used to address the thermal energy storage LWAs. The maximum percentage of mass loss was evaluated after concluding three freeze/thawing test cycles and the results are shown in Figure 3-18.

----------------------------------------------------------------------------------------------------------------



(a)



(b)



(c)



(d)
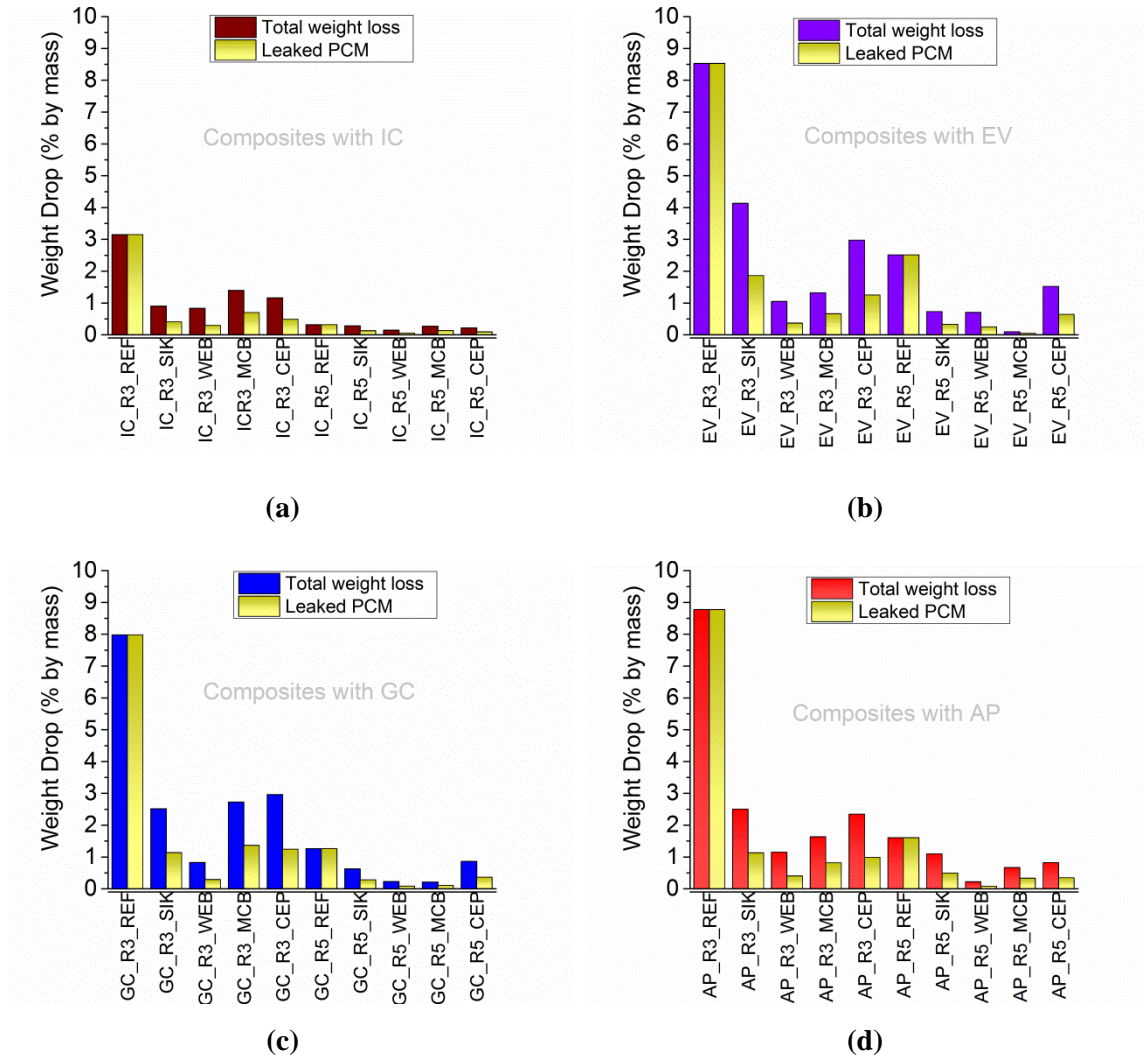
Figure 3-18: Ratio of specimen's desiccation after three cycles of freeze-thaw test for the composites with different coated LWAs: (a) IC; (b) EV; (c) GC and (d) AP.

It is interesting to note that the percentage of mass loss of each composite varies with different waterproofing material. This can be explained by the fact that, the waterproofing material loses weight during the freeze thawing process and its thickness is not homogeneous in each particle and LWA. Thus, the non-homogeneity of waterproofing thickness is most responsible for the mass losses discrepancies found for each different composite.

In order to illustrate the non-homogeneity of the thickness of waterproofing coating a scanning electron microscopy (SEM) study was carried on IC particles. The IC particles were mixed with a cement-based mortar, and cured for 28 days. A specimen of hardened mortar composite was then embedded in resin and surface polished for the microscopy study. The general view of the microstructure of the specimen is presented

in Figure 3-19, which shows a cross section of IC particles surrounded by waterproof coating. It is evident that the thickness of the waterproofing coating layer around the IC particles is not uniform. In terms of waterproofing type effect on mass loss of the composites, a significant reduction can be observed in all composites with all four different waterproofing solutions. Taking into account weight loss of the different composites with different PCMs, the smallest value was recorded for the cases of composites with R5 (about 0.7%, 1.5%, 0.5% and 1% by mass for the composites with IC, EV, GC and AP, respectively).

In contrast, the composites with R3 exhibited a greater drop in mass of about 1%, 2.5%, 2% and 2% for IC, EV, GC and AP, respectively. At this stage, the results revealed that, the influence of the porous lightweight aggregate on the development of physical property values has dependency on the waterproofing type. The water loss percentage of the waterproofing itself was determined, and then it was subtracted from corresponding total weight loss of each composite. The results of drying test on the waterproofing materials showed that the waterproofing material can lose water by 65, 50, 58, 55 percentage weight losses for the WEB, MCB, CEB and SIK, respectively.
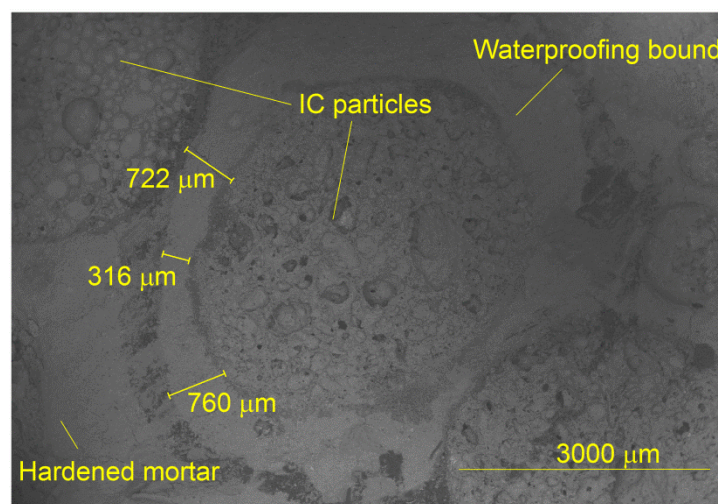


Figure 3-19: SEM micrograph of the IC particle embedded in cement-based hardened mortar showing waterproofing bound thickness variation.

The increase or decrease of the PCM absorption amount depends on the porous aggregates and PCM type. It can be stated that the percentage mass drop for the impregnated/coated LWAs with EV is related to the pore structure size of particles as well as their absorption capacity. Additionally, it should be remarked that the weight losses of composites with respect to the leaked PCM after freeze/thaw cycles are less than 0.5% for different coating solutions (except in the cases with SIK waterproofing with slightly higher leaked PCM), which indicates that such coating materials minimizes the potential for leakage of the PCM. It should be stressed that, visual observation of the composites after testing confirmed that no leakage of the PCM was evident.

*Results of mass loss of composites under oven drying test*

The percentage weight loss of composites dried at 40°C temperature was calculated with the same formula explained in the above section. The weight drop values in percentage by mass were calculated for three different drying temperatures and the results for each composite are shown in Figure 3-20.

Generally speaking, it can be observed in Figure 3-20, that the leaked PCM percentage of mass loss in all the composites with waterproofing was less than 1% when composites are subjected to the drying temperature of 40°C. Considering that, when mass loss is less than 1%, the potential for leakage of the PCM is low. Visual observation of the composites after testing confirmed that no leakage of the PCM occurred.

--------------------------------------------------------------------------------



**(a)**                                                    **(b)**



**(c)**                                                    **(d)**
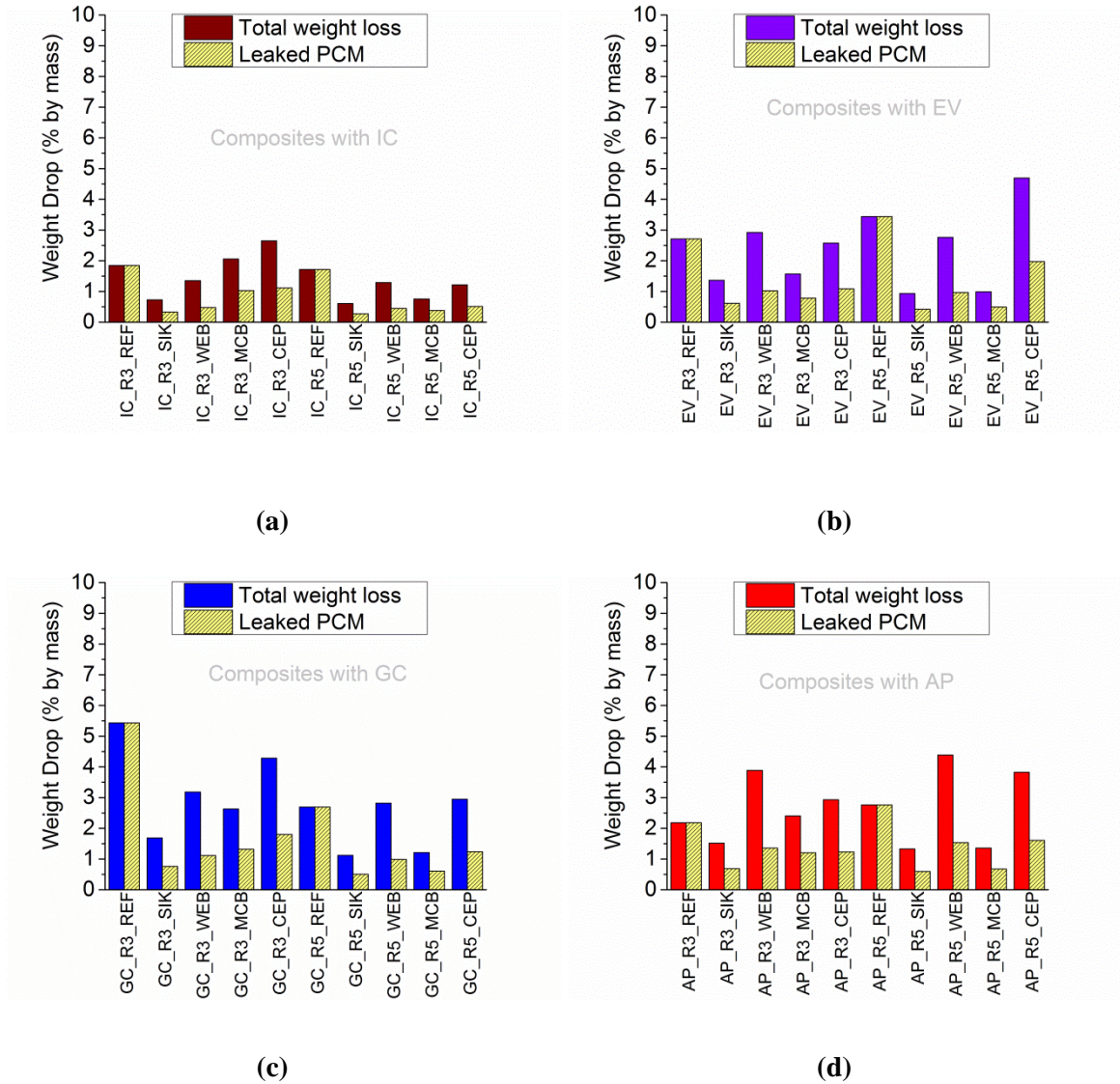
Figure 3-20: Ratio of specimen's desiccation after the drying test temperatures of 40°C for composites with different coated LWAs: (a) IC; (b) EV; (c) GC and (d) AP.

## 3.5 General remarks

The characterization of the used materials demonstrates that:

- The DSC analysis of the pure microencapsulated PCM samples conducted to specific enthalpy and phase change temperature determination as important parameters for thermal characterization.
- Dependency of the DSC thermograms to the heating/cooling rates of testing on several PCMs was investigated, both in terms of the peak temperatures and the overall shape of the curve.

- The chemical elements of materials as substance materials for plastering mortar were determined. This chemical composition can assist to distinguish counts of each element of a composite system such as mortars.

- The influence of different waterproofing solutions on the weight loss of the composites under freeze/thaw cycles has been analysed, namely in regard to the weight drop percentage by mass as well as amount of leaked PCM from studied composites. Weight loss percentages of total mass of the composites were dependent to the used type of waterproofing materials. In fact, the thickness of the waterproofing (bounded LWAs) was non-homogeneous.

- The observations for drying test of the composites were also analogous to those already made for freeze/thaw test, allowing again observing that, as expected, weight loss percentages of the composites with and without waterproofing.

# Chapter 4   Thermal Mortars

## 4.1   General overview

The present chapter describes the production of thermal mortars and corresponding tests. A schematic of the experimental plan is shown in Figure 4-1. In the scope of this chapter, two series of mortars are presented. The first series includes cement based mortars with and without incorporation of microencapsulated PCM, here termed as plastering mortars. The second series includes a type of LWAs, with and without impregnation of a type of paraffin PCM, incorporated into the cement based materials, here termed as delayed freezing mortars.

The main aim of this plan was first to evaluate thermal performance of the mortars when subjected to the thermal loads. Estimation of specific enthalpy temperature functions for studied plastering mortars by mean of DSC tests as well as investigation of thermal behaviour. In fact, the heat flow evolution versus temperature/time during the test was monitored and corresponding enthalpy values were determined as explained in this chapter. Furthermore, SEM/EDS technique was used in order to investigate the chemical composition of the studied plastering mortars.

The studied delayed freezing mortar systems involve mechanical and thermal behaviours aspects. However, this chapter deals only with mechanical properties such as: compressive strength and flexural strength in order to assess the effectiveness of the PCM together with LWAs incorporation into the cement based mortar.

Experimental Plan
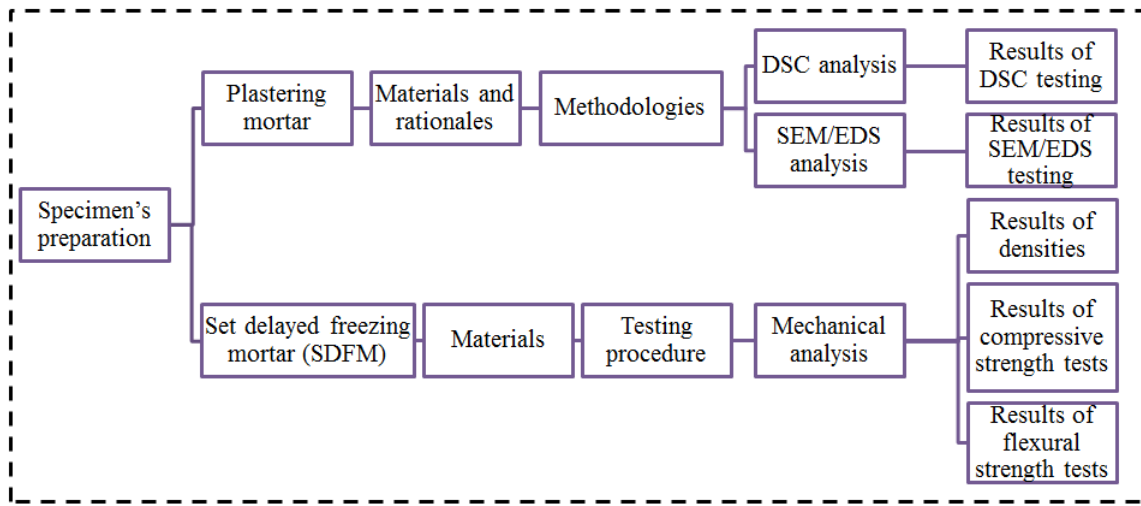


Figure 4-1: Experimental plan methodology.

## 4.2 Study of plastering mortars

### 4.2.1 Materials and rationales

The mix designs of the investigated plastering mortars together with their adopted designations are listed in Table 4-1.

Table 4-1: Mix proportions of formulations SPCMM24, HPCMM18_28 and REFM.

| Materials | Formulations (percentage of the total weight of mortar) | | |
|---|---|---|---|
| | REFM | SPCMM24 | HPCMM18_28 |
| Cement type I -42.5R | 22.64 | 31.32 | 31.32 |
| Sand | 64.23 | 30.59 | 30.59 |
| Water | 12.45 | 18.79 | 18.79 |
| Super plasticizer | 0.63 | 0.94 | 0.94 |
| MC18 | - | - | 9.18 |
| MC24 | - | 18.34 | - |
| MC28 | - | - | 9.18 |

The investigation includes a reference plain mortar (mortar REFM) and two mortar systems which incorporate respectively a single type of PCM with 24°C of melting temperature (mortar SPCMM24), or the combination of two PCMs with melting temperatures of 18°C and 28°C (mortar HPCMM18_28). Mortar SPCMM24 contains 18.34% in weight of MC24, whereas HPCMM18_28 has the same total percentage of PCM, evenly distributed among MC18 and MC28 (see Table 4-1). The formulation of

the mortars was selected based on recent developments that allowed nearly 20% mass fractions of PCM to be incorporated in mortar, while maintaining satisfactory performance in terms of mechanical properties/behaviour (Cunha *et al.* 2013, Cunha *et al.* 2015).

It should be noted that, the formulation of mortars with incorporation of PCM, should comply with the standards before considering for such an application. Therefore, extensive experimental campaign was trailed by a colleague, Sandra Cunha (another PhD student focused on development mortar pertained with microencapsulated PCM). In fact, she tried to have as high as feasible incorporation of PCM that can be introduced into the plastering mortar while respecting the standards. Finally, a formulation of cement based mortar with and without incorporation of PCM was adopted for this research regarding maximum PCM incorporation into the cement based mortar (nearly 20wt.%). In fact, the adopted formulations for mortar with and without PCM was successfully encompassed the problem related with the mortar shrinkage and consequent cracking, by adding superplasticizer into the mixture (Cunha *et al.* 2015).

## 4.2.2 Specimen preparations

*Specimen preparation for DSC analysis*

The samples for DSC testing were collected from the cylinders that gathering at the age of 28 days (see schematic sample gathering description in Figure 4-2). The central part of the disk was cut out with a diamond drop saw, resulting in a slice with approximate size of $100 \times 10 \times 4$ mm (Figure 4-2b).

Subsequently, the few milligrams of mortars samples necessary for DSC testing were gathered with dimensions of $4 \times 4 \times 1$ mm by using slow speed diamond saw (WELL 3242) as shown in Figure 4-2c. One sample was prepared for each type of mortar: REFM, SPCMM24 and HPCMM18_28. Finally, each sample placed in an aluminium crucible for DSC testing. The weight of the prepared samples was 24mg, 25.29mg and 15.99mg for REFM, SPCMM24 and HPCMM18_28, respectively.

------------------------------------------------------------------------------------------------------



2R=100 mm      100×10×4 mm      4×4×1 mm

**(a)**      **(b)**      **(c)**
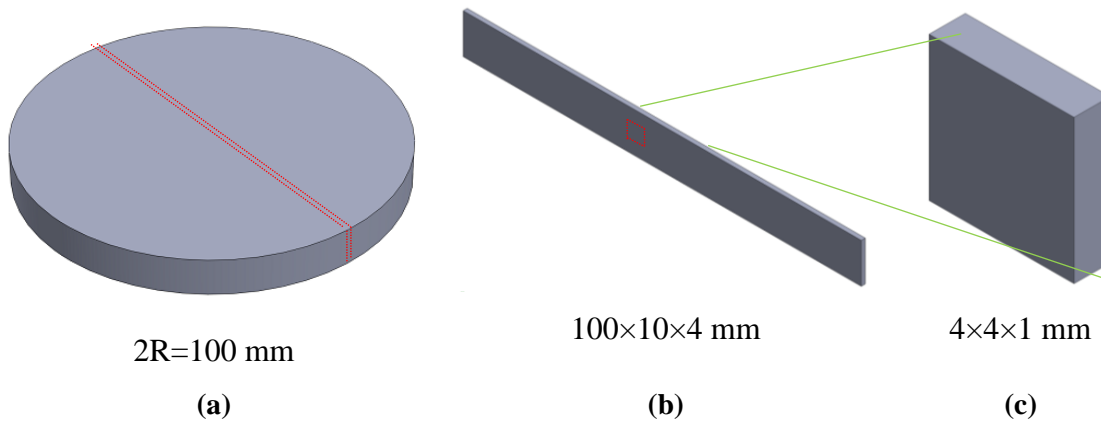
Figure 4-2: Schematic of specimen preparation for DSC test: (a) fabricated sample in the shape of disk; (b) the thin layer of 4 mm width were cut from middle of the disk in the form of slice; (c) finalized sample for DSC testing, extracted from the centre of the slice.

*Specimen preparation for SEM/EDS analysis*

In the scope of SEM/EDS analysis, a total number of 12 specimens were involved. This includes four representative specimens of each mortar system for the SEM/EDS investigation focused on the assessment of the spatial homogeneity of the mortar. All test samples were obtained from mortar casted in cylindrical moulds with diameter of 100 mm, which were cured for 28 days, before the process of sampling. Figure 4-3 shows a general view of the mortar cylinders with identification of zones for surface study (labelled as zone 1 to 4). For zones 1 to 4, a small sub-sample with 15 mm diameter and 10 mm height was extracted with a diamond saw for SEM/EDS testing. The detailed of specimen preparation is explained next.
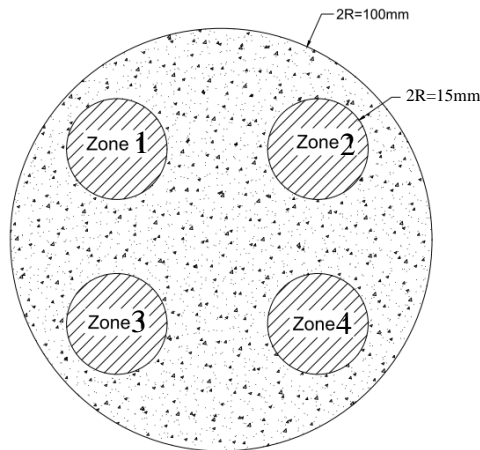


Figure 4-3: Generic view of the sample with identification of the zone for surface study of the plastering mortars (Zone1-4).

Upper and lower surfaces of specimens were prepared, cylindrical sub-samples 10 mm in diameter and 5 mm in height were cut from small volume samples by use of low speed diamond saw WELL 3242.

Figure 4-4 shows the sample placement, fixation and cutting the surface, with subsequent ground faces of samples from upper and lower sides. After mounting separately with cyanoacrylate glue on the Strues Pedemin griding and polishing machine (DAP-7), they were levelled and grounded.



(a)                                              (b)
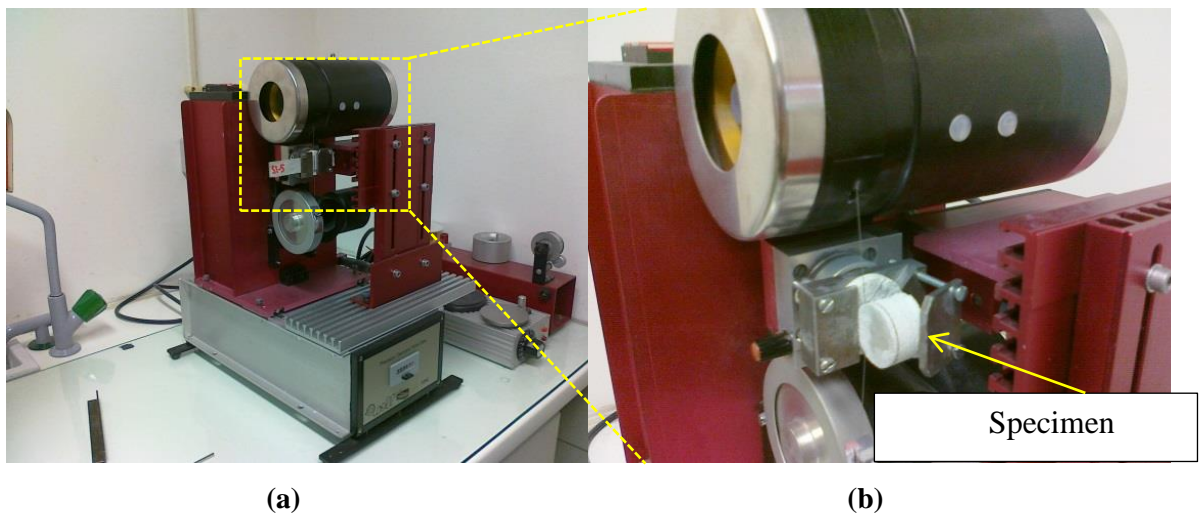
Figure 4-4: (a) Diamond saw instrument; (b) zoomed surface preparation of the specimen.

Figure 4-5 shows, the sample placement in the specially designed space with an opening drilled through to match the diameter of the specimen disk. An interior cylinder fits closely inside, and rests on the back of the specimen disk apply a light weight to the sample.

Each of the samples was ground by using an abrasive disk with grit size 180 µm abrasive paper. The amount of materials was removed from surface by gridding process until entire surface has been ground.

--------------------------------------------------------------------------------



<div align="center">(a)        (b)</div>
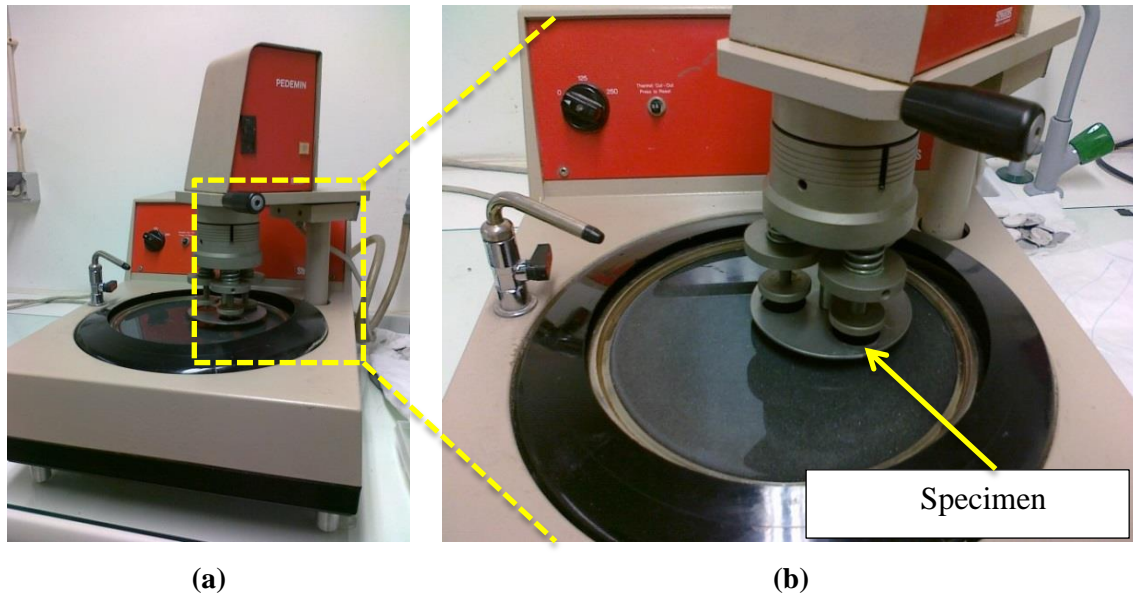
Figure 4-5: (a) Struers Pedemin DAP-7 grinding and polishing machine; (b) zoomed surface polishing preparation of the specimen.

The last step is polishing step. After trial and error for polishing purpose, one combination gave us repeated success which explained next. The detailed classification of the type of specimen, selected test method as well as the location of the region of interest for the SEM/EDS studies of the mortars are presented in Table 4-2. A ground and cleaned surface were polished on the abrasive disks, with the reducing abrasive size meshed 180 µm, 600 µm, 1200 µm and 2500 µm. Each pad of different abrasive size, were used by lasting 1 min. cleaning of the sample by using propanol in the ultrasonic bath for 3 min and after the sample dried by hot air, then SEM images were taken.

Table 4-2: Required test method and region with respect to the materials identification.

| Names | Material | Region | Test method |
|---|---|---|---|
| REFMZ1 | Conventional mortar | Zone 1 | SEM/EDS test |
| REFMZ2 | Conventional mortar | Zone 2 | SEM/EDS test |
| REFMZ3 | Conventional mortar | Zone 3 | SEM/EDS test |
| REFMZ4 | Conventional mortar | Zone 4 | SEM/EDS test |
| SPCMZ1 | Mortar contains MC24 | Zone 1 | SEM/EDS test |
| SPCMZ2 | Mortar contains MC24 | Zone 2 | SEM/EDS test |
| SPCMZ3 | Mortar contains MC24 | Zone 3 | SEM/EDS test |
| SPCMZ4 | Mortar contains MC24 | Zone 4 | SEM/EDS test |
| HPCMZ1 | Mortar contains MC18 and MC28 | Zone 1 | SEM/EDS test |
| HPCMZ2 | Mortar contains MC18 and MC28 | Zone 2 | SEM/EDS test |
| HPCMZ3 | Mortar contains MC18 and MC28 | Zone 3 | SEM/EDS test |
| HPCMZ4 | Mortar contains MC18 and MC28 | Zone 4 | SEM/EDS test |

### 4.2.3  Evaluation of thermal energy storage

The melting and freezing behaviours of the PCM were analysed by a DSC model NETZSCH 200 F3 Maia. The DSC has an accuracy of ±0.2˚C for temperature measurements. All the samples were tested within aluminium crucibles with volume of 40 µl under nitrogen ($N_2$) atmosphere with a flow of 50 ml.min$^{-1}$. The samples were weighted by an analytical balance model Perkin-Elmer AD-4 with accuracy of ±0.01mg. Each sample was sealed in the pan by using an encapsulating press. An empty aluminium crucible was used as a reference in all measurements.

The effect of the thermal cycles and heating/cooling rates on the phase change processes and specific enthalpy values was examined. In this way, different heating/cooling rates of 0.1ºCmin$^{-1}$, 1ºCmin$^{-1}$, 2ºCmin$^{-1}$, 4ºCmin$^{-1}$ and 6ºCmin$^{-1}$ were considered. The applied program steps for the test procedure of samples were the following: (i) initial isothermal period at 5ºC for 5 minutes; (ii) dynamic heating up to 40ºC according to the proposed rate (0.1ºCmin$^{-1}$, 1ºCmin$^{-1}$, 2ºCmin$^{-1}$, 4ºCmin$^{-1}$ or 6ºCmin$^{-1}$); (iii) stabilization at 40ºC for 5 minutes; (iv) dynamic cooling to 5ºC with proposed rate (0.1ºCmin$^{-1}$, 1ºCmin$^{-1}$, 2ºCmin$^{-1}$, 4ºCmin$^{-1}$ or 6ºCmin$^{-1}$). The three materials were analysed, and each sample endured three full cycles (each full cycle included the steps (i) to (iv) mentioned before). The DSC peaks for each composite PCM were evaluated for the second cycle of heating/cooling curves in terms of latent heat storage studies and phase change temperatures, in coherence with Ref. (Biwan *et al.* 2013). Evaluation of the resulting DSC curves was performed through Proteus analysis v.6.0.0 Software from NETZSCH (Denner T 2012). Phase change enthalpy and temperature were obtained from the DSC heat flux signal response by integration. The peak temperatures of heating and cooling have been considered as the representative temperature of a phase change transition. The onset and end temperature for each transition were determined with respect to the recommendation of the standard EN ISO 11357-1 (1997).

### 4.2.4  DSC analysis

*Effect of the heating/cooling cycles*

The results of three consecutive heating and cooling cycles on the REFM sample are shown in Figure 4-6. The absence of phase changes can be confirmed, together with coincident results among the three performed cycles.

----------------------------------------------------------------------------------------------------------------
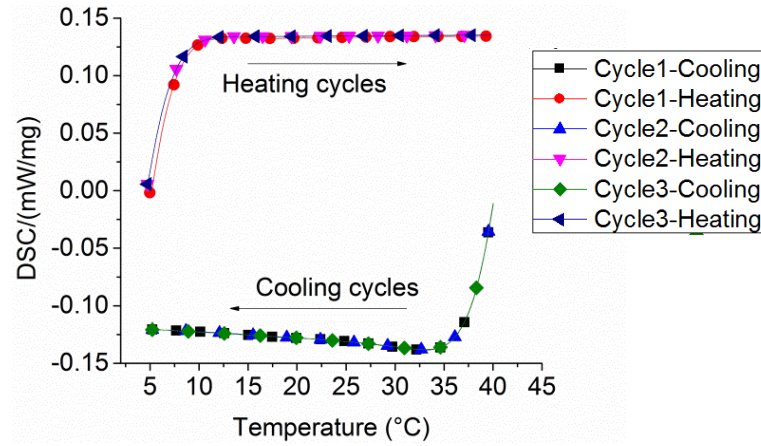


Figure 4-6: DSC thermograms for three thermal cycles on REFM with heating/cooling rate of 6⁰C/min.

The DSC curves for sample SPCMM24 over 3 heating cycles are given in Figure 4-7.



**(a)**



**(b)**



**(c)**
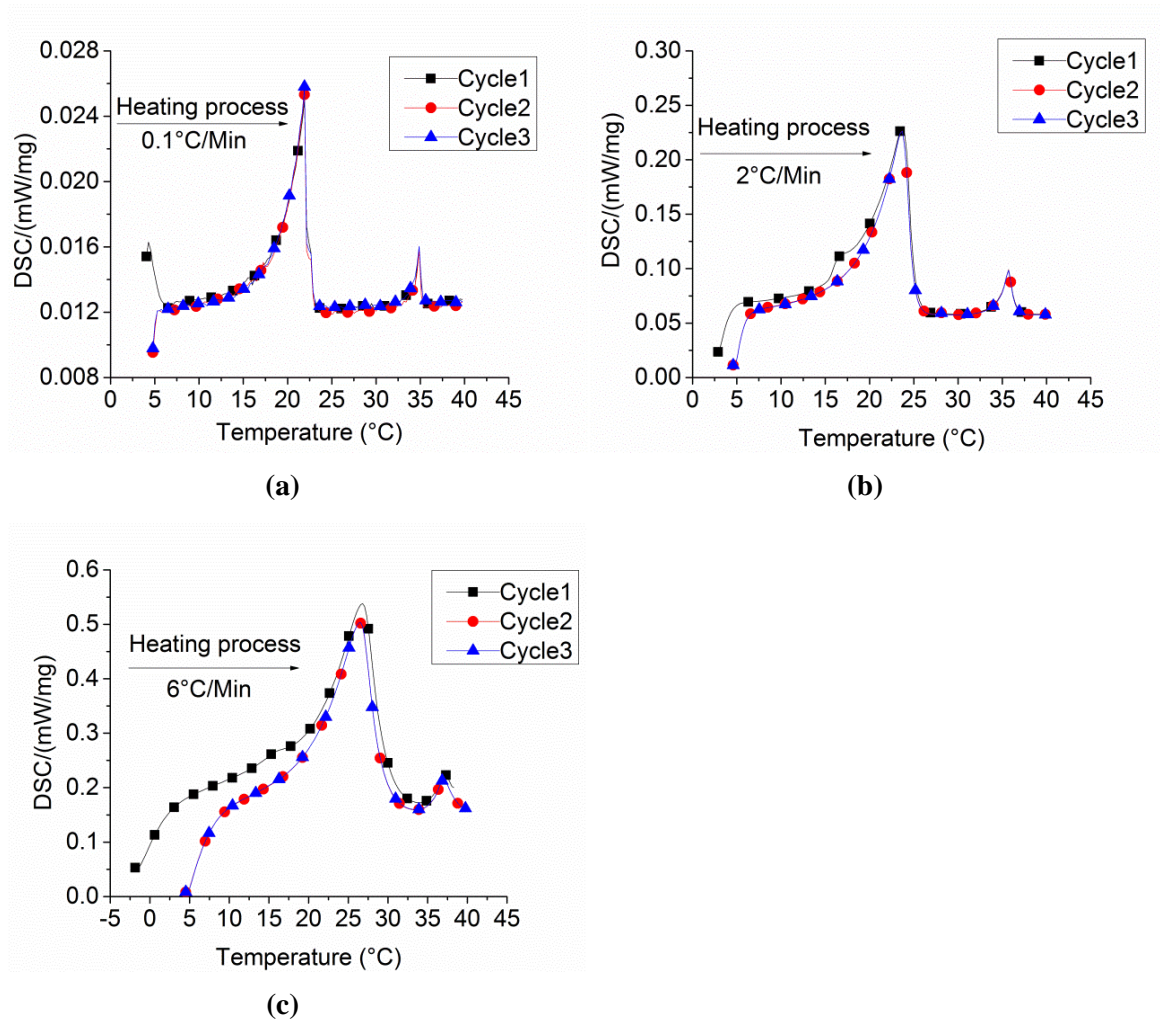
Figure 4-7: DSC thermograms for three thermal cycles with SPCMM24 at the following heating rates:(a) 0.1⁰C/min; (b) 2⁰C/min; (c) 6⁰C/min.

For the purpose of illustration, this Figure solely plots the results for three chosen heating rates, comprising the lowest, the intermediate and the highest studied rates: 0.1, 2 and 6°C/min. In all situations the second and third cycle follow same trend (see Figure 4-7a, b, c), whereas the first cycle consistently exhibits a slightly different behaviour. This distinct behaviour was only observed in the first cycle of heating (not on cooling), and appears to be more evident in the higher heating rates. The results of DSC thermal cycling in the hybrid PCM mortar (HPCMM18_28) are shown in Figure 4-8. The results seem to be more homogeneous among the three cycles (in comparison to SPCMM24), a slight disturbance in the results of the first cycle can still be noticed. Overall, the results suggests that maximum accuracy and homogeneity of results can be achieved by always performing at least two cycles, and operate on the results of the second cycle.



**(a)**



**(b)**



**(c)**
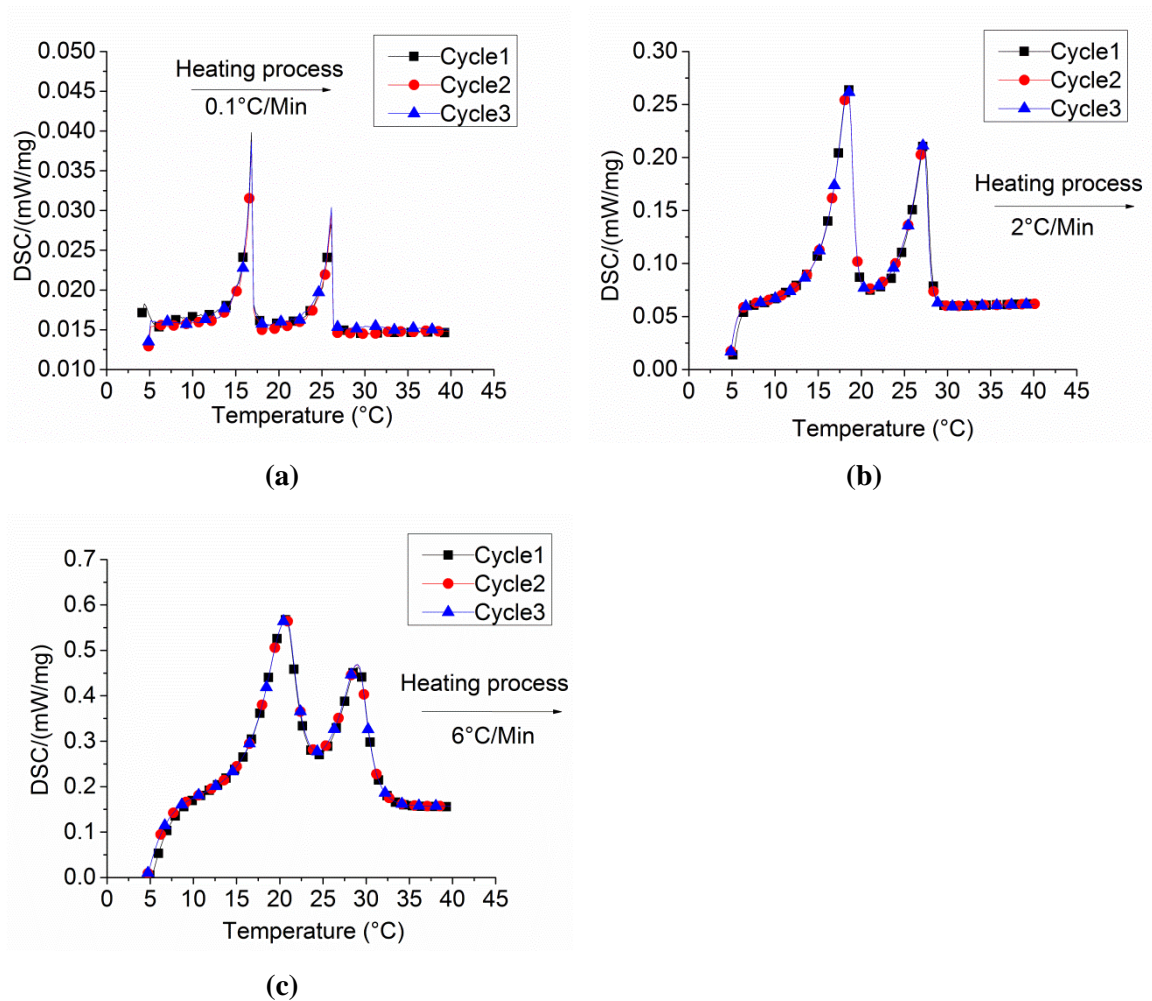
Figure 4-8: DSC thermograms for three thermal cycles on HPCMM18_28 at the following heating rates: (a) 0.1℃/min; (b) 2℃/min; (c) 6℃/min.

*Effect of the heating/cooling rates*

The effect of adopting distinct heating/cooling rates is now discussed, with basis on results collected at the second heating/cooling cycle on each sample. The experimental curves for SPCMM24 different heating/cooling rates are shown in Figure 4-9.



**(a)**                                     **(b)**
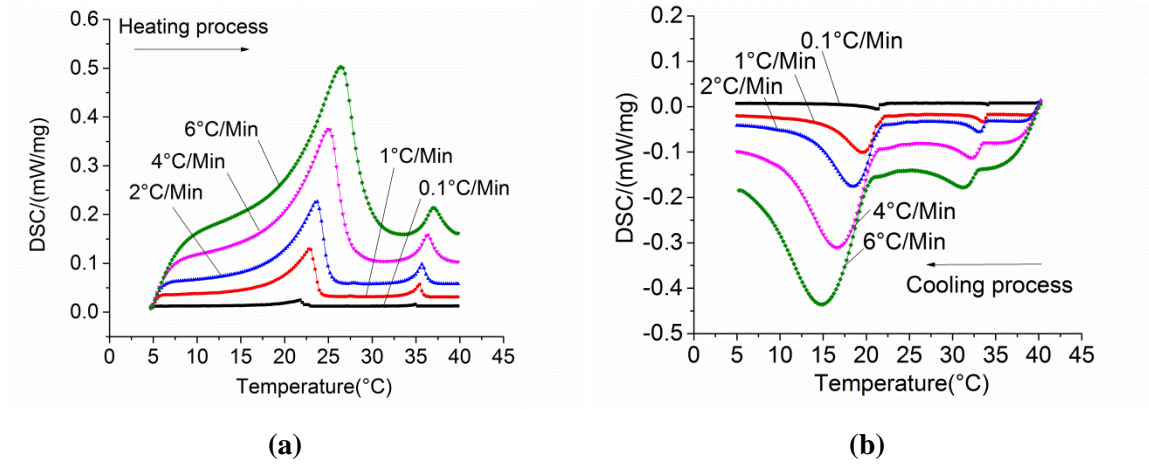
Figure 4-9: DSC thermograms for SPCMM24 specimen: (a) heating process at several rates; (b) cooling process at several rates.

The peak temperatures in the thermograms of the heating process (Figure 4-9a) are consistently being increased as the heating rate increases. Conversely, in the case of cooling (Figure 4-9b), the peak temperatures decreases with increased cooling rates. Overall, it can be stated that the PCM peak response shifts in the direction of the imposed flux: higher peaks for heating and lower peak temperature for cooling. This kind of trend has been observed in the past (kousksou T *et al.* 2012, Kousksou *et al.* 2013), and it can be explained by an increasing thermal gradient in the sample. The phase change lags the heat exchange and delays the entry of heat, thus creating an internal thermal gradient on the sample that can justify the observed differences.

It is interesting to observe that the peak temperature announced by the supplier of the PCM embedded into the mortar (MC24) is of 24ºC, which is almost coincident with the peak temperature of 23.6ºC observed for the heating process of 2ºC/min (as seen in Figure 4-10a). In fact, most of the results presented in the literature for PCM behaviour with DSC testing pertain to this testing situation (2ºC/min; heating) (Melhing *et al.* 2008, Vaz Sá *et al.* 2012, Soares *et al.* 2013, Ventolà *et al.* 2013).

----------------------------------------------------------------------------------------------------

The representation of peak temperatures versus heating/cooling rates made in Figure 4-10, evidences a clear linear relationship in terms of peak temperatures for both heating and cooling processes. Moreover, Figure 4-10 also shows onset and end temperatures computed according to EN ISO 11357-1 (1997). It is further confirmed that the peak temperatures of both processes (heating and cooling) tend to approximate themselves as the heating/cooling rate diminishes. Also, onset and end temperatures are dependent to the heating/cooling rates in a similar fashion to that already reported for peak temperatures. The tendency is though less clear, probably due to the process of calculation of onset/end temperatures.



**(a)**                                                          **(b)**
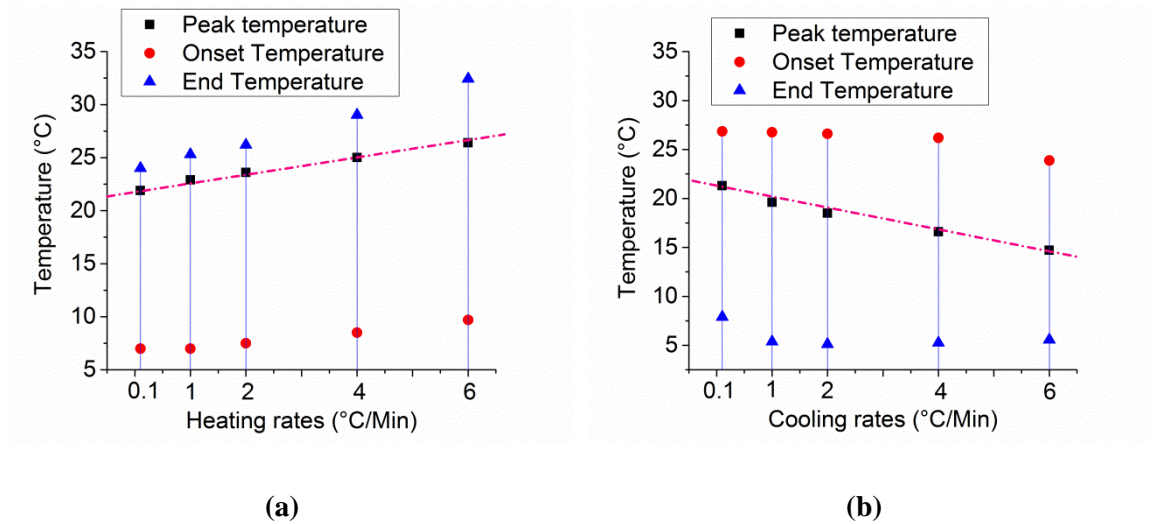
Figure 4-10: Onset, peak and end temperatures for the phase transitions in SPCMM24: (a) heating process; (b) cooling process.

It is further interesting to remark, that the overall differences in the thermograms for each rate heating/cooling are smaller as the rate decreases, with an almost negligible hysteretic behaviour being observed at the heating/cooling rate of 0.1ºC/min. An example of such a case for the SPCMM24 sample is presented in Figure 4-11a, where a negligible shift is generally observed in the case of 0.1ºC/min rate, in opposition to the observable situation for 1ºC/min (Figure 4-11b). It should be noted that the DSC fluxes have been normalized to their peaks in order to facilitate the simultaneous observation of the shape of the thermograms for 0.1ºC/min and 1ºC/min.

-----------------------------------------------------------------------------------------------------------



**(a)**                                                                                         **(b)**
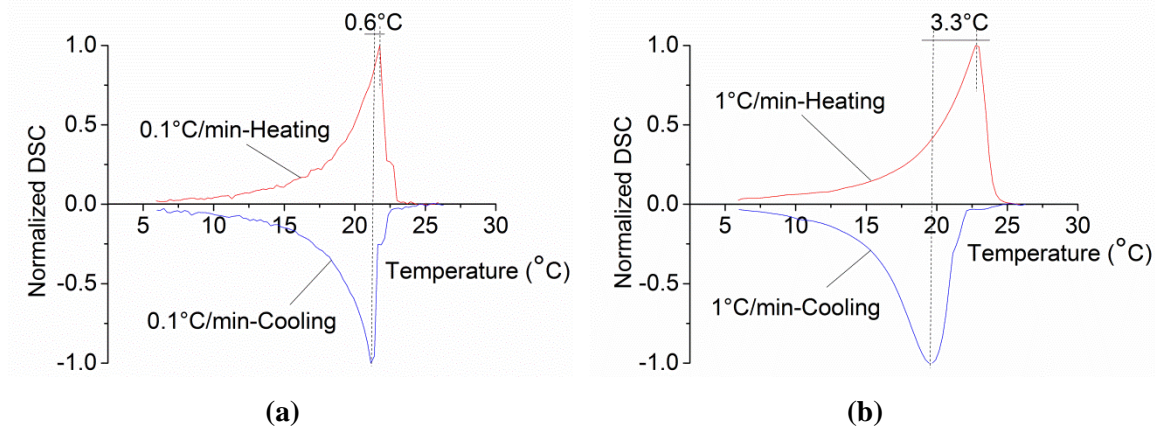
Figure 4-11: Comparison between normalized DSC curves for SPCMM24 for heating/cooling rates of: (a) 0.1ºC/min and (b) 1ºC/min.

The DSC curves for testing of HPCMM18_28 at several heating cooling rates are shown in Figure 4-12. The observations are quite similar to those already made for SPCMM24, with the single difference that this new mortar exhibits two distinctive peaks in correspondence to the incorporation of MC18 and MC28. The linear relationship between the peak temperatures in the thermograms and the heating cooling rates is also observed for both embedded PCMs in HPCMM18_28 as shown in Figure 4-13.



**(a)**                                                                                         **(b)**
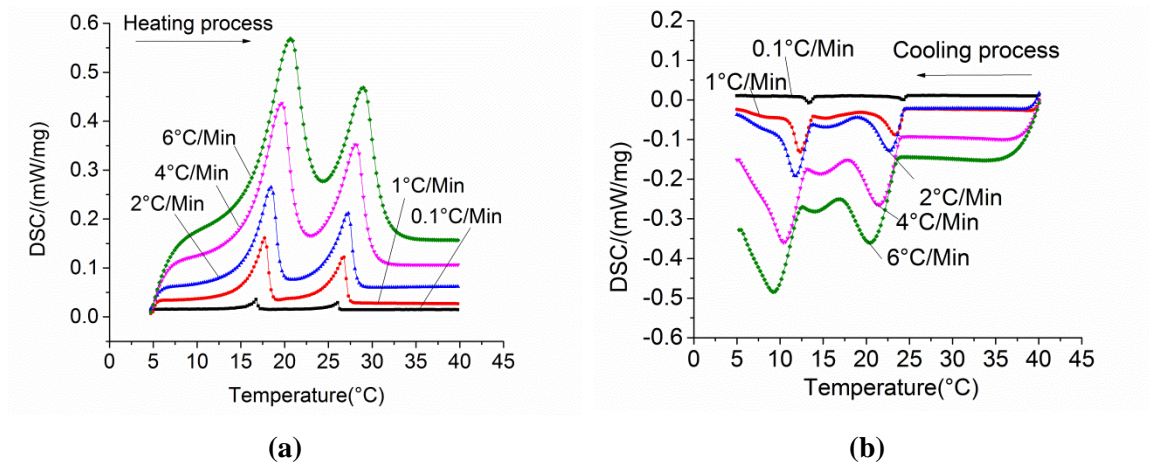
Figure 4-12: DSC thermogram curves for HPCMM18_28 specimen: (a) effect of the heating rates on the shape of the thermogram; (b) effect of the cooling rates on the shape of the thermogram.

It is interesting to observe that the temperature difference between each of the two peak temperatures in the thermogram remains constant for all tested heating rates, amounting to approximately 8.9ºC (labelled as Delta1 in Figure 4-13a).

-------------------------------------------------------------------------------------------------------------------



**(a)**                                                              **(b)**
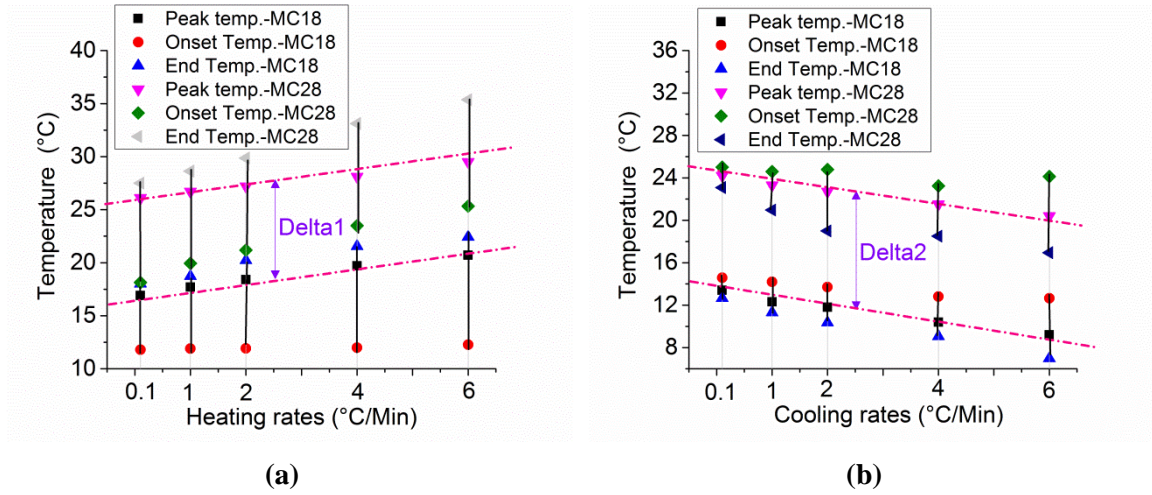
Figure 4-13: Onset, peak and end temperatures for the phase transitions in HPCM18_24: (a) heating process; (b) cooling process.

A similar situation is observed in Figure 4-13b for the cooling process, with an average difference (labelled as Delta2) of 10.8ºC. These differences are coherent with the differences in melting points appointed by the PCM supplier: 28ºC−18ºC=10ºC. Also, similar behaviours to those observed for the SPCMM24 sample can be seen in terms of the onset and the end temperatures for the embedded MC18 and MC28 within HPCMM18_28 sample.



**(a)**                                                              **(b)**
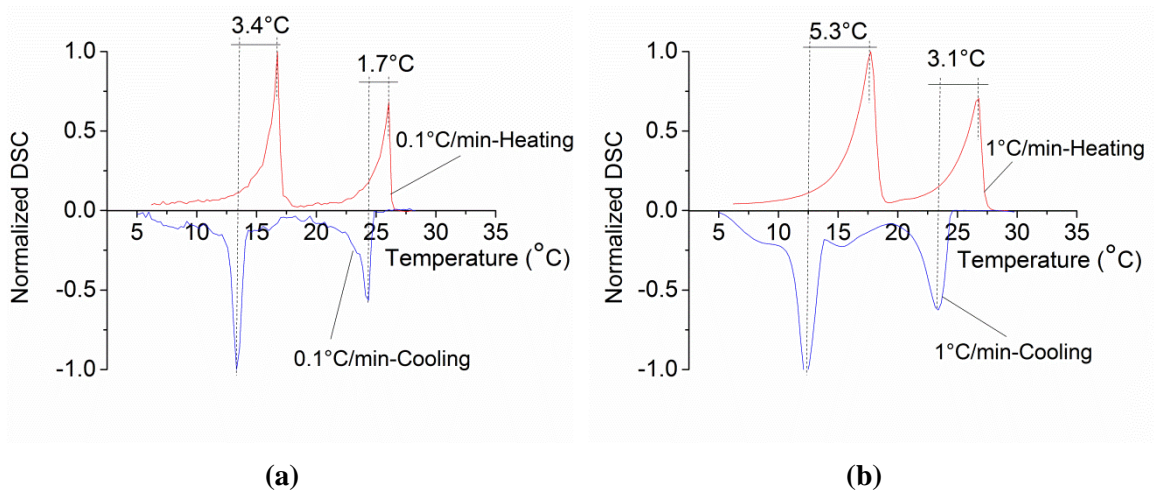
Figure 4-14: Comparison between normalized DSC curves of HPCMM18_28 with rates of: (a) 0.1ºC/min and (b) 1ºC/min.

--------------------------------------------------------------------------------------------------------------------

The normalized DSC curves that allow evaluating the overall hysteretic behaviour in HPCMM18_28 for the heating/cooling rates of 0.1ºC/min and 1ºC/min can be seen in Figure 4-14. It is once again clear that the observed apparent hysteresis is much smaller at lower rates of testing. However, unlike the observation made for SPCMM, a slight hysteretic behaviour is still seen for the heating/cooling rate of 0.1ºC/min.

*Specific enthalpy of specimens*

The specific enthalpy assessment for the three mortars is discussed hereafter. From the DSC output, the specific enthalpy is calculated for each phase transition based on methodology that was detailed for pure PCM samples (presented in Chapter 2). This was employed for specific enthalpy calculation of specimens. The results of the calculation of specific enthalpy evolution along temperature for SPCMM24 are shown in Figure 4-15a,c for both heating and cooling processes, whereas the corresponding systematization of the total enthalpy versus temperature is shown in Figure 4-15b,d.



(a)



(b)



(c)



(d)
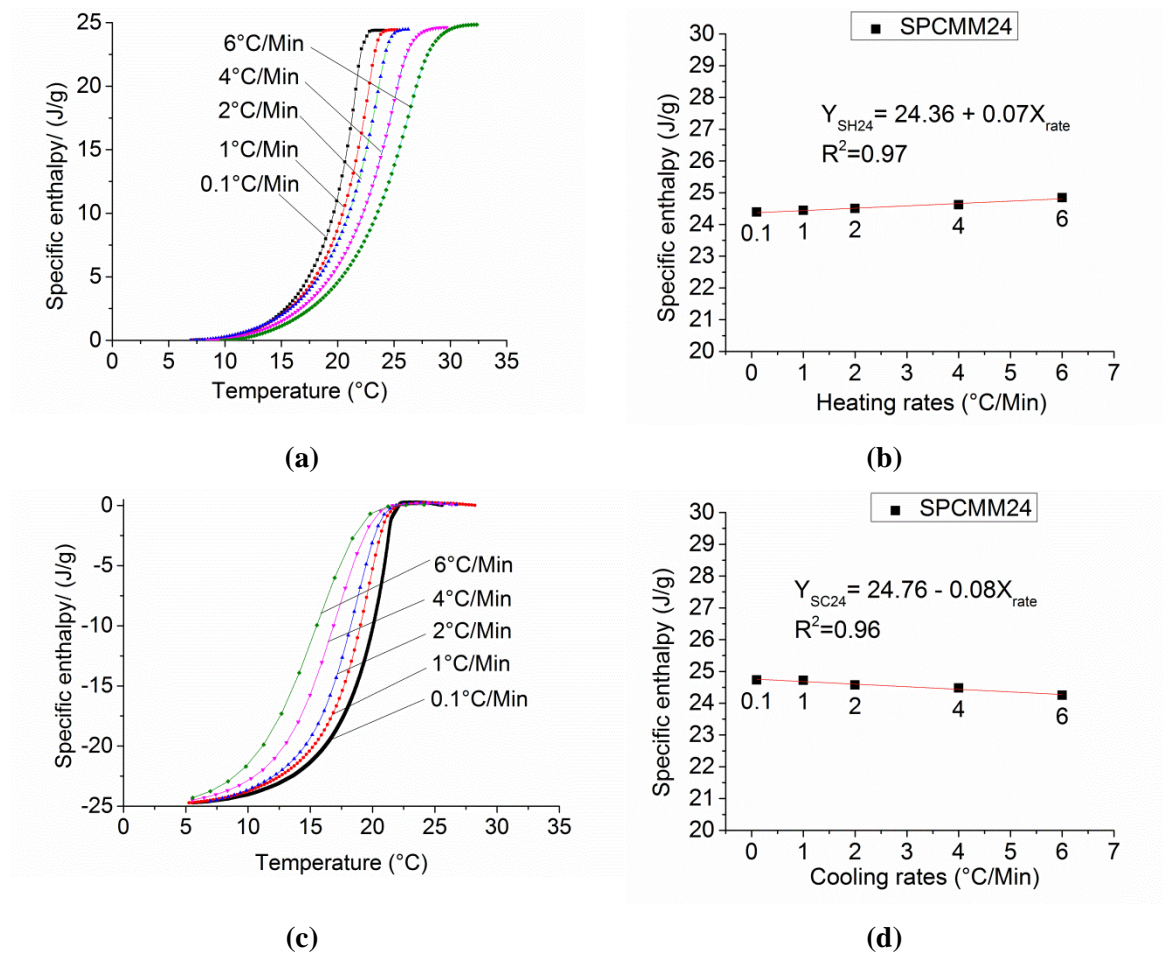
Figure 4-15: Specific enthalpy for SPCMM24 mortar with different heating/cooling rates: (a) specific enthalpy curves for heating; (b) variation of specific enthalpy for heating; (c) specific enthalpy curves for cooling; (d) variation of specific enthalpy for cooling.

---------------------------------------------------------------------------------------------------------------------

It can be observed that the accumulated specific enthalpy is almost constant regardless of the heating/cooling rate, even though slight linear variations exist (see Figure 4-15b,d): increasing heating rate leads to increased specific enthalpy, whereas increased cooling rate leads to decreased specific enthalpy.

Figure 4-16 is homologous to Figure 4-15, except for the fact that it deals with HPCMM18_28. The observations are also analogous to those already made for SPCMM24. An added analysis is made in regard to the summation of total enthalpy corresponding to the transition of embedded MC18 and MC28 (see Figure 4-16b,d), allowing again observing that, as expected, the total accumulated enthalpy is almost independent of the heating/cooling rate.
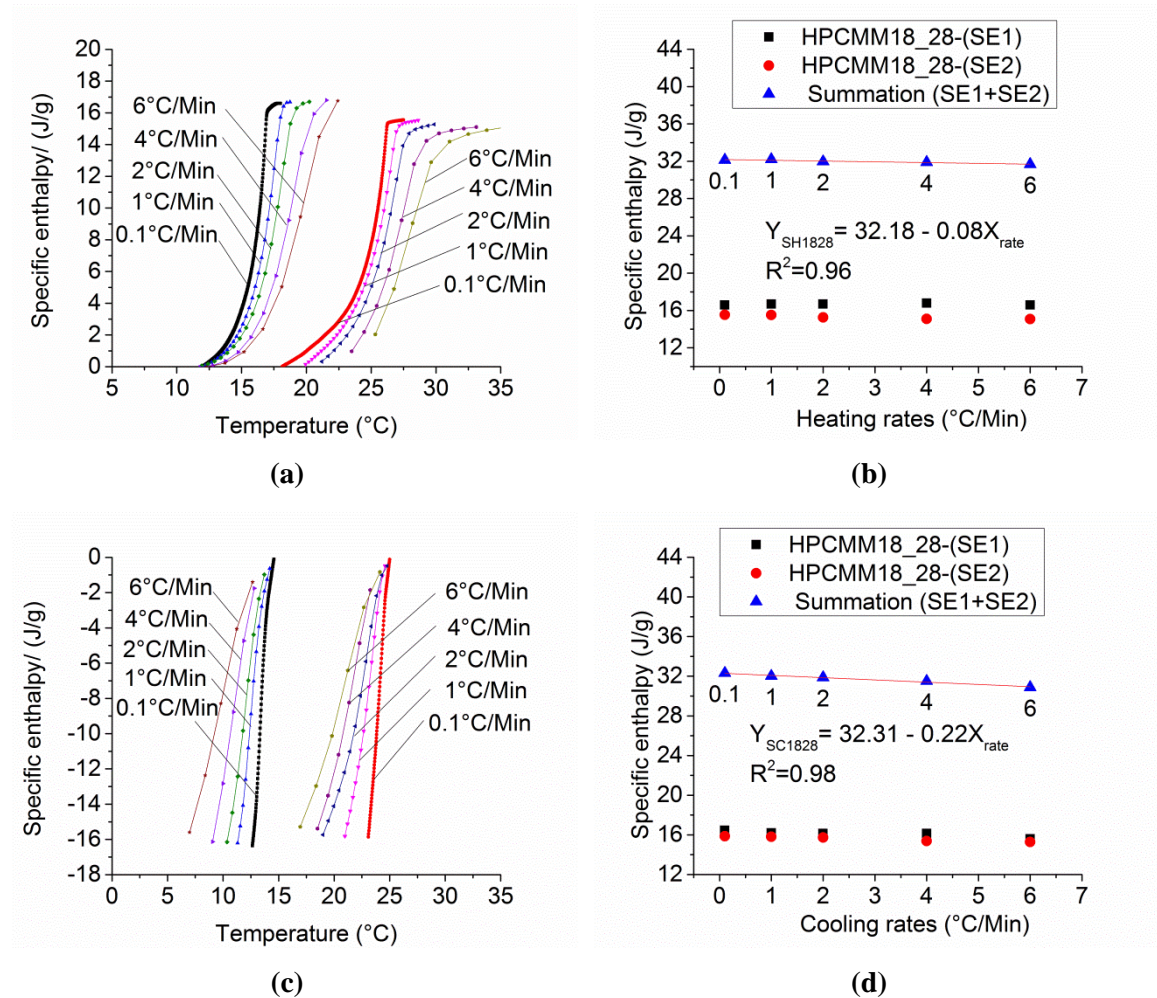


Figure 4-16: Specific enthalpy for HPCMM18_24 mortar with different heating/cooling rates: (a) specific enthalpy curves for heating; (b) accumulated specific enthalpy for heating; (c) specific enthalpy curves for cooling; (d) accumulated specific enthalpy for cooling.

----------------------------------------------------------------------------------------------------

### 4.2.5 Elemental investigation of specimens with SEM/EDS technique

The chemical analyses of the different mortars were investigated with technique of EDS and described in this section. The results here reported deal with determination of elements of investigated surface of the mortar containing one or more types of microencapsulated PCM or without microencapsulated PCM. REFM, SPCMM24 and HPCMM18_28 specimens after being polished according to the method mentioned before, each sample was conducted to an energy dispersive X- 20 ray spectrometer (EDS) attached to the SEM for elemental analysis.

### 4.2.6 SEM/EDS analysis

*Effect of polishing technique on the SEM image of mortars*

Based on the experience achieved on the surface preparation of the specimen to improve quality and accuracy of the SEM/EDS testing, such a procedure leads to a clear surface, which could be observed by visual inspection.

However, the surface quality was observed using a SEM. Figure 4-17 shows a sample of the SEM micrograph of the studied mortars, REFM (case without PCM) and SPCMM24 (case with PCM). As it can be seen, in Figure 4-17a and Figure 4-17c, the polishing and major flattening of the surface is visible when compared with the case of without polishing procedure (see Figure 4-17b and Figure 4-17d) which are the rough ground sample surfaces. Moreover, the surface topographic data were then collected over several images of 1×1 mm and smaller for all the mortars.

*Microstructure assessment of the composites*

The general view of the microstructure of the investigated mortars is presented in Figure 4-18. In a reference plain mortar and PCM enriched mortar the sand particles tend to be distributed uniformly on the surface of the investigated material (see example for REFM Figure 4-18a). No signs of agglomeration were observed, suggesting spatially homogeneous microstructures in both cases. The aggregate inclusions of quartz are hosted by the cementitious matrix composed predominantly of calcium-silica-hydrates (C-S-H) and portlandite (CH).

These two phases are known to be the main products of cement hydration (Taylor H.F.W 1990). The interstitial transition zone (ITZ) shows no signs of fractures or

--------------------------------------------------------------------------------------------------------

damage at the aggregate perimeter, and this is typical attribute of the plastering mortar with good integrity between cement paste and aggregate inclusions.



(a)              (b)

(c)              (d)
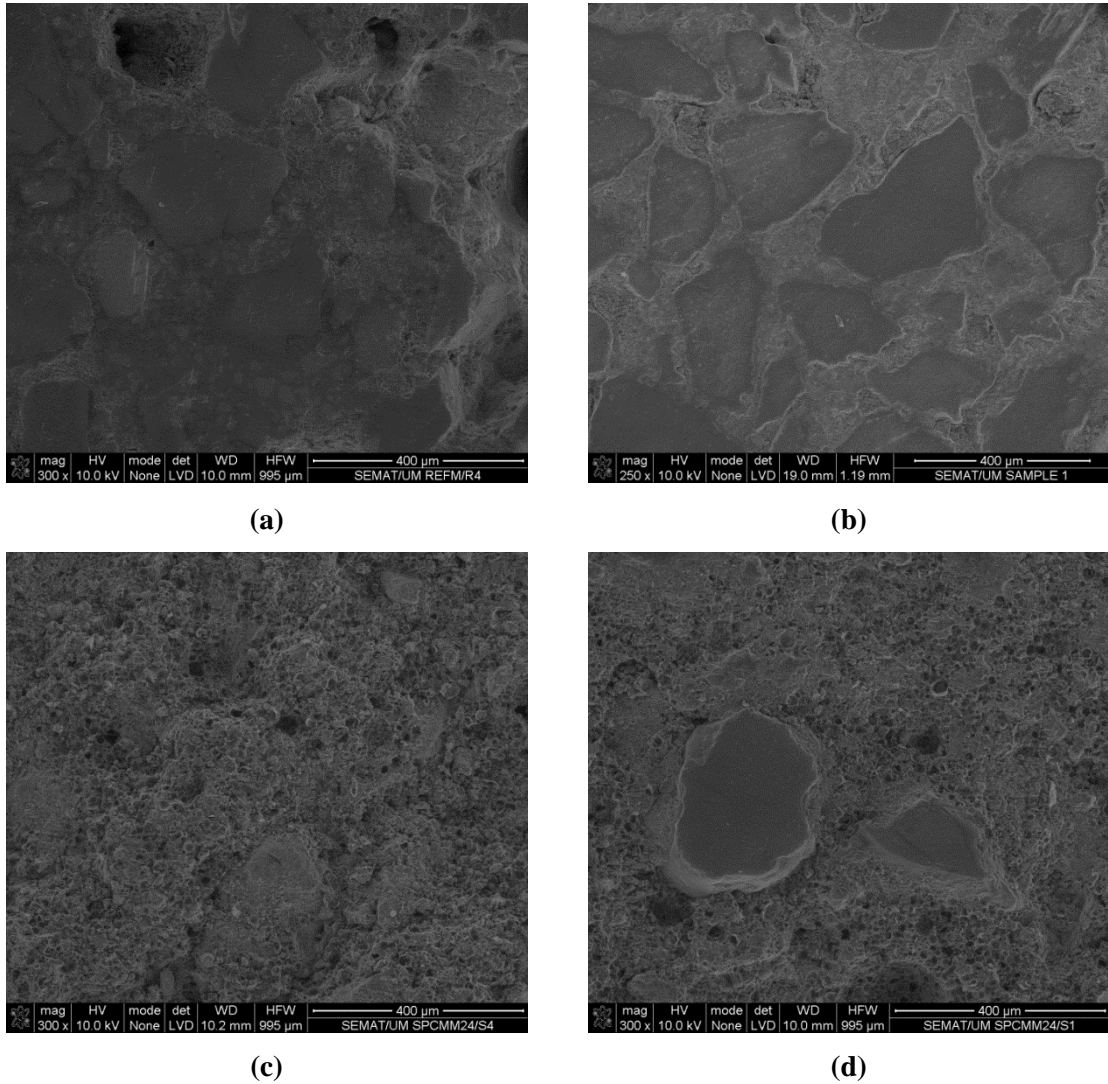
Figure 4-17: SEM image of the mortars before and after polishing surfaces: (a) REFM mortar before polishing surface; (b) REFM mortar after polishing surface; (c) SPCMM24 mortar before polishing surface; (d) SPCMM24 mortar after polishing surface.

The microencapsulated paraffin wax particles are incorporated in the microstructure of SPCMM24 mortar Figure 4-18b). Together with products of cement hydration they form a host matrix for the hard sand inclusions. It is observed, despite the different nature of the PCM particles (organic) and cement hydration products (inorganic), their microstructural assembly tends to be sound and continuous, with hydration products tightly encompassing the PCM external boundary.

(a)                                                     (b)
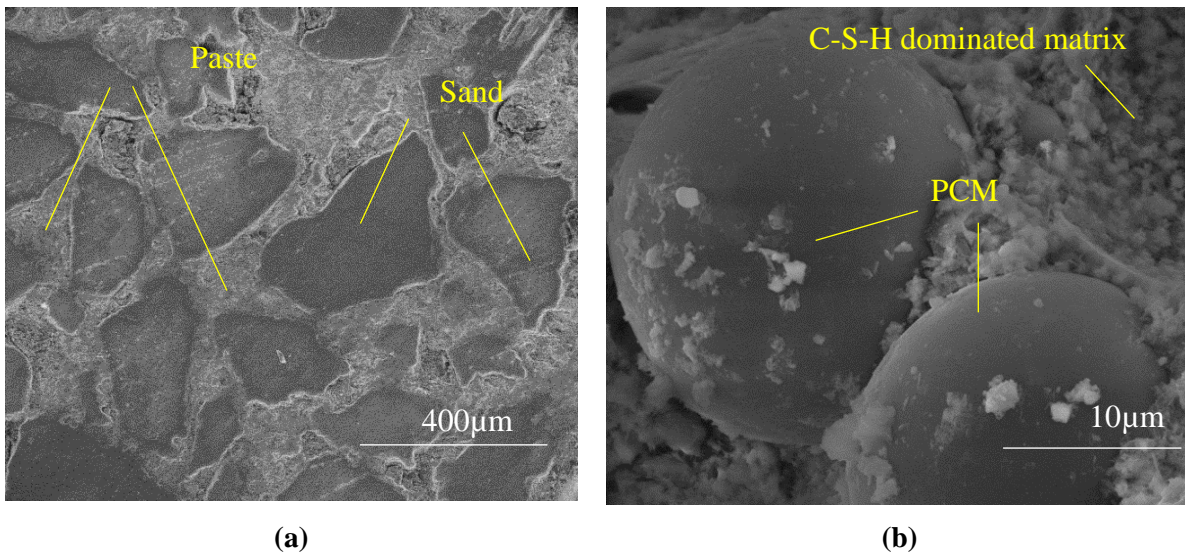
Figure 4-18: SEM images of polished surface of the specimens: (a) SEM micrograph of the reference specimen with formulation of REFM; (b) SEM micrograph of the plastering mortar sample with formulation of SPCMM24.

This observation is also in line with the previous studies focused on the microstructure and mechanical properties of the PCM mortars (Biwan *et al.* 2013, Li M *et al.* 2013, Lucas *et al.* 2013). According to these studies, the PCM microcapsules contribute to reduce the amount of the biggest pores and the mean pore size present in the mortar. This tends to result in more cohesive internal structure of PCM mortars as compared to standard plain mortars. The current SEM investigation did not reveal any damage or fracture in the boundary zone between these two components at the micrometre scale.

Additionally, the majority of microencapsulated PCM particles retain their spherical shape upon processing of both mortars: slurry mixing, moulding and mortar curing. In summary, SEM results tend to suggest adequate compatibility and spatial homogeneity of the PCM materials, which is important factor in the selection, analysis and understanding of the microstructure of the mortars.

*Elemental investigation of composites*

The energy spectrum of different zones (was shown before in Figure 4-3) for different mortar specimens as well as for the pure PCM sample (MC24) were performed. Figure 4-19 presents, the counts versus energy as well as zoomed region of interests for surface analyses.
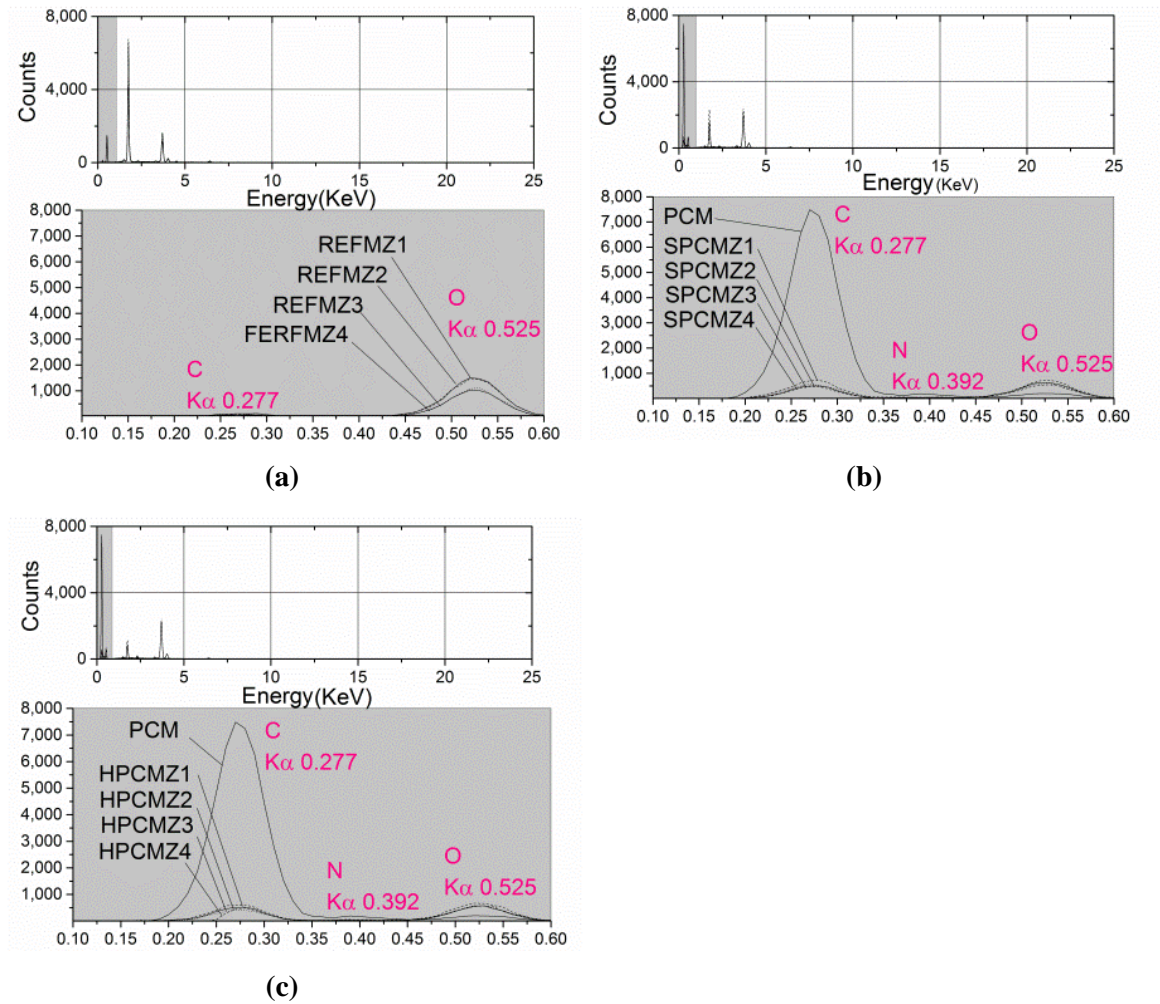
Figure 4-19: The surface analysis SEM/EDS for different zones of each formulation: (a) REFM; (b) SPCMM24 (b) HPCMM18_28.

As it can be seen in Figure 4-19a, the carbon C element is identifiable with slight peaks for all studied zones of REFM samples. These carbon elements may come from abrasive in the polishing process. Therefore, it can be conclude that, the REFM specimen have no sign of carbon C element. From the EDS result of SPCMM24 and HPCMM18_28 specimens, the most abundant elements are O, C and N in the interested region (see Figure 4-19b, c).

Bear in mind, the pure PCM (was shown in chapter 3) that has a strong peak of C element; it was expected to appears such a peak in the mortars with PCM. It is obvious that a strong peak of carbon C element and consequently the spectrum of both samples, SPCMM24 and HPCMM18_28 have higher intensity of carbon C element peaks when compared with REFM. These increase behaviours were expected as carbon C element is

-----------------------------------------------------------------------------------------------------------------

the principal elements for the PCM's material. However, these intensities of the carbon C element for different zones of PCM mortar samples appeared with slightly differences (see Figure 4-19).

This simple criterion has been used to establish the homogeneity of the sample for the elements of interest (Goldstein J *et al.* 1992).These analysis results shown that, the PCMs in both, single PCM and hybrid PCM mortars appeared on the surfaces of SPCMM24 and HPCMM18_28 samples.

Mean value of integrated intensity of element for different mortars was calculated with accounting of errors for the measurement and the results are presented in Figure 4-20. For example, in the Figure 4-20a, C element content of the mortars are shown and the results revealed that the C element is as high as about 32.25%, which is from the paraffin PCM in the mortars with PCM.

It can be inferred that the regular particles are the composite PCM. However, the mean value of integrated intensity of the Si element for PCM mortars reaches to less than half when compared with reference mortar due to the fact that, the PCM has been replaced with amount of sand in the mixtures (see Figure 4-20b).

Regarding the Ca element, it can be observed that, in both cases, with and without PCM, there is in the mean value of integrated intensity values. However, a slightly reduction can be seen in the case of reference mortar (see Figure 4-20c).
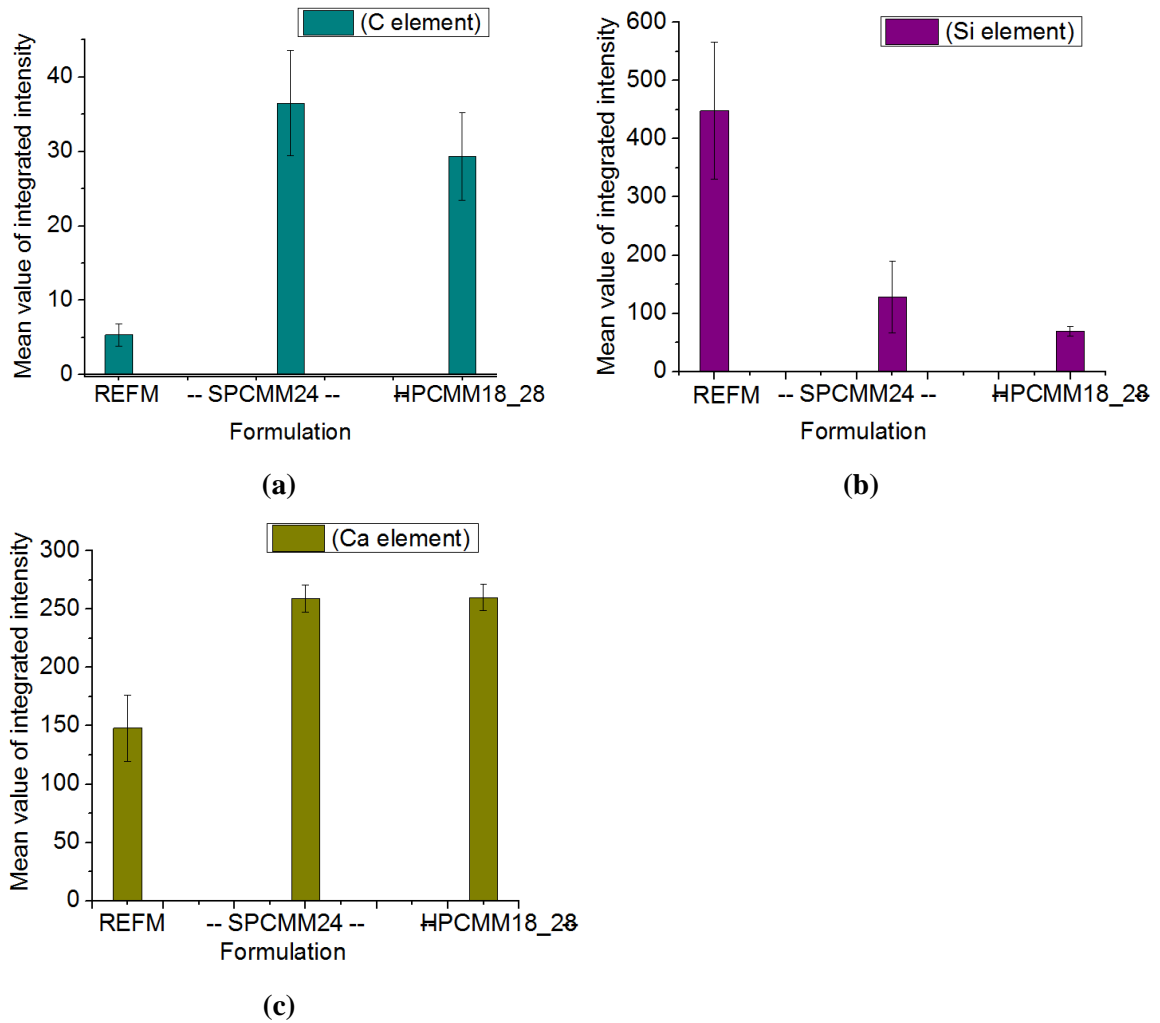
Figure 4-20: Mean value of integrated intensity of element and corresponding errors for different mortars: (a) C element; (b) Si element; (c) Ca element.

## 4.3 Study of delayed freezing mortars

In this section, different thermal energy storage systems were evaluated in regard to the presence of paraffin PCMs into LWAs, as PCMs are latent thermal storage materials possessing a large amount of heat energy stored during its phase change stage. In the previous chapter, the feasibility of impregnation/encasement of paraffin PCMs in LWAs was described. In fact, experimental studies on the impregnation method led to conclude that the impregnation method is simple. This research work requires further confirmation that the embedded PCMs may provide the mortars with a large thermal energy storage capacity due to the quantities of PCM that can actually be incorporated. This technique may help to extend the service life of pavement structures, by reducing freezing damage through the incorporation of phase change materials (PCMs).

However, it should be stressed that the development of PCM composites for this purpose is still in its infancy, and there are many questions that will need to be answered in the future before such composites are ready for real applications. This research will help to serve as part of a foundation for such studies. For the purpose of illustration, a type of LWAs (Expanded Clay) with one type of PCM (R5) was considered for incorporation into the cement based materials. Some mechanical tests on such mortar systems were performed.

## 4.3.1 Materials and formulations

For the preparation of the mortars, a commercially available Portland cement CEMII-32.5N was used. The natural aggregate was composed of fine grain size and mean grain size portion, which had been used in the previous studies (Barreneche *et al.* 2016) and characterized in the previous chapter. A single LWA was selected for this study: Expanded Clay supplied by ARGEX- SA (Portugal) (ARGEX 2013) also characterized in the previous chapter. Such aggregate has been considered suitable for impregnation in previous works (Nóvoa *et al.* 2004, Karaipekli *et al.* 2009, Lu *et al.* 2014, Barreneche *et al.* 2016). The particle size distributions of all aggregates were assessed in the previous chapter.

A type of organic PCM paraffin was used: R5 Rubitherm RT series (melting temperature of 5°C) (Rubitherm GmbH 2012). The latent heat fusion of the selected PCM was characterized and mentioned in the previous chapter was of 180 kJ/kg. Selection of melting temperatures of the PCMs under study was based on the target application of de-icing delaying in pavements. Therefore, the melting temperature was selected to be slightly above 0°C, in order to attenuate the enduring of such temperature within the mortars into which the PCMs were applied. Furthermore, chemical compatibility with the porous materials (Sakulich *et al.* 2012, Kheradmand *et al.* 2015) was taken into account, as well as the range of available PCMs products in the market. Bear in mind, to avoid possible leakages of PCM from the soaked LWA, a coating solution named Weber Dry Lastic (a liquid membrane used for waterproofing roofs) (Weber 2009) was trialled to envelope the impregnated LWA.

The composition of each mortar mixture under study can be found in Table 4-3. Three mortars were produced: a mortar containing only river sand aggregates, and two mortars, each containing both the light weight expanded clay and river sand aggregate at

distinct proportions. During the production, adjustments were made to the water dosage, so as to ensure a consistency between 160mm and 180mm in the flow table testing.

Table 4-3: Mixture proportions by mass, in grams.

| Mixture | REFM0* | PCMM10* | PCMM20* |
|---|---|---|---|
| Cement (g) | 1286.1 | 1286.1 | 1286.1 |
| Water (g) | 707.4 | 603 | 573 |
| Sand (g) | 3649.7 | 1607.6 | 1205.6 |
| PCM impregnated LWAs (g) | - | 401.9 | 803.8 |
| Superplasticizer (g) | 38.5 | 38.5 | 38.5 |

*Abbreviations: REFM0= reference mortar without PCM; PCMM10=mortar with incorporation of ≈10% PCM impregnated LWAs of total weight of mortar; and PCMM20=mortar with incorporation of ≈20% PCM impregnated LWAs of total weight of mortar.

## 4.3.2 Specimen preparation

The mortar mixtures were made in a conventional mortar mixer. First, all the solid components were placed into the mixer, operating for 30 s at normal speed. Then, the mixer was stopped and the superplasticizer was added, together with 50% of the water. The mixer was then turned on again at normal speed for 3 min. After 1 min., the remaining 50% of water was added to the mixture, while the mixer was in operation. Afterward, the mixer was stopped for 1 min, and then started again for more 3 min at normal speed, while all the components are already added to the mixture.

After the mixing procedure, the consistency of the mortar was evaluated through flow table testing in accordance with EN 1015-11 (1999). For each mortar, six prisms of $40{\times}40{\times}160mm^3$ were prepared for the tests of flexural strength, compressive strength and density. For the thermal performance tests, from each of the mortars, a small plate of $150{\times}150{\times}25mm^3$ was created. The fresh mortars were moulded and vibrated by a standard mechanical vibrator. Afterward, the moulded specimens were protected by plastic paper in order to prevent premature loss of water and were placed in a standard curing room (three prisms for 7 days age and three prisms for 28 days age, for each mortar composition).

### 4.3.3  Methodology

The flexural and compressive tests were conducted at the ages of 7 days and 28 days, according to the EN 1015-11 (1999). A total of 3 specimens were used for flexural tests at each age of testing. In regard to compressive strength testing, 6 specimens were tested at each age (they resulted from the specimens after flexural testing). The density of mortars was determined based on recommendation of EN 1015-10 (1999).

### 4.3.4  Results of flexural and compressive strengths, and density of mortars

The results of flexural strength, compressive strength and density of hardened mortars (SDM) are shown in Figure 4-21.



(a)                                                     (b)



(c)
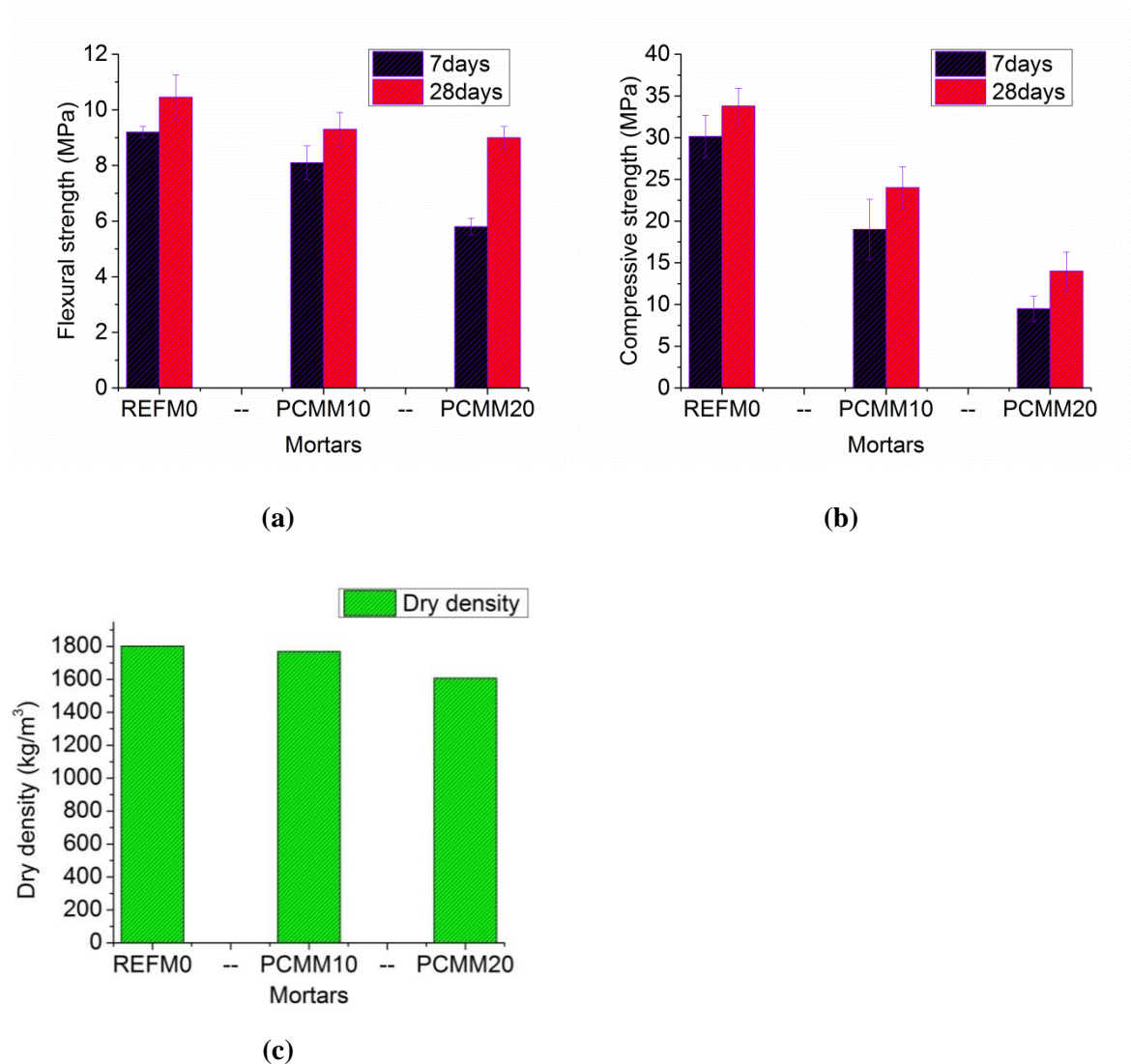
Figure 4-21: (a) Flexural strength of mortars (SDFM) at 7 and 28 days; (b) Compressive strength of mortars (SDFM) at 7 days  and 28 days;(c) Dry density of mortars (SDFM) at 28 days.

Following, Figure 4-21(a), shows the results of the flexural strength of mortars at 7 days and 28 days. As expectable, the results indicate that the reference mortar (REFM0) with natural aggregates, had higher flexural strength in comparison to the mixes that contained impregnated LWAs. By comparing between mortars with LWAs, the increase in LWA content led to a decrease of compressive strength, which is also coherent with findings for other mixes containing LWA (Barreneche *et al.* 2016). The compressive strength test results at 7 days and 28 days are shown in Figure 4-21(b). Similar trends to those reported for the flexural strength are observed.

The values of dry density of mortars are presented in Figure 4-21(c). The densities of the REFM0 were the highest, due to the fact that, the REFM0 has incorporated only natural aggregates. For the LWAs mortars, the density reduces as the weight percentage of the LWAs increase.

Generally, comparing a mortar of natural aggregates with W/C ratio of 0.55 (REFM0), with the mortar with lower W/C ratios of 0.46 and 0.43 for PCMM10 and PCMM20 respectively, has reduced the flexural strength from 10.5MPa to 9.1MPa and 8.5MPa for PCMM10 (9%) and PCMM20 (19%), respectively, has reduced the compressive strength from 34MPa to 24MPa and 15MPa for PCMM10 (29%) and PCMM20 (55%), respectively, has reduced the dried density from 1803.1kg/m$^3$ to 1770 kg/m$^3$ 1607kg/m$^3$ for PCMM10 (2%) and PCMM20 (10%), respectively. The decrease in compressive strength in mixes with LWA (with and without PCM) can be related to the porous nature of the LWA that resulting it weaker in compression.

## 4.4  Comparison between mortars in terms of PCM incorporation

The results of DFM system showed that the total amount of PCM absorbed in each LWA is very high. It is interesting to have a comparison between the global quantities of PCMs that can be introduced in the mix by impregnation technique and classical way of incorporating commercially microencapsulated PCM.

Considering cement based mortar incorporated with microencapsulated PCM (plastering mortar) that has been developed earlier. Giving one example, a mortar with name of SPCMM24 contains 293 kg of microencapsulated PCM per cubic meter, whereas, the impregnation technique let to a maximum per cubic meter PCM of about 213 kg/m$^3$ for EV case. This is not higher, but it is not necessarily a problem because it is approximately within the same order of magnitude, but at a fraction of the cost of the microencapsulated PCM. Even thought, the effectiveness of LWA impregnation is not higher than that of microencapsulation. Also, impregnation technique let to a maximum per cubic meter PCM of about 49 kg/m$^3$, 109 kg/m$^3$, and 171 kg/m$^3$ for IC, GC, and AP respectively.

## 4.5   General remarks

This chapter provides an understanding of the thermal mortars in relevant aspects. In the study of plastering mortar, the influence of different heating/cooling rates on the thermal behaviour of the plastering mortars has been analysed, namely in regard to the peak temperatures on the DSC thermogram, as well as on the calculated specific enthalpy. Moreover, the impact of the heating/cooling rate on the hysteretic behaviour of the thermal response of mortars with PCM was analysed. Thermal behaviour of the plastering mortar by use of more than one type of PCM in the mortar has revealed, being consistent with the predictable outcome of the two incorporated PCMs used individually at the same proportions. Thus, it is considered that the DSC testing allowed further confirming the feasibility of hybrid PCMs in mortars. The SEM/EDS analysis assist to evaluate the microencapsulated PCM particles incorporated in the microstructure of both SPCMM24 and HPCMM18_28 mortars. Experimental investigation on DFM system comprised PCM (R5) embedded into lightweight aggregates (expanded clay) with the goal of highlighting behavioural differences in regard to the reference mortars that do not include PCMs.

# Chapter 5  Laboratory Scale Prototypes

## 5.1  General overview

This chapter involves two parts. The first part deals with assessing thermal performance of the plastering mortars through laboratory scale testing which is in the scope of the thesis and also additionally, the second part reveals the study of delayed freezing mortars that involved paraffin PCMs impregnated into LWAs. The aim of the first part of the experimental work is to reveal that mortar with hybrid PCM has potential as a passive solution as well as active solution by decreasing the internal temperatures variations and the internal temperature peak, and increasing the time delay between the external and the internal conditions. These types of results are clearly a synonymous of thermal efficiency of buildings, by contributing to the reduction of the energy consumption associated to active systems using more efficiently the available energy sources. Considering the real climatic data available for Portugal (were taken from whether station at the University of Minho), the imposed conditions were defined for the experimental campaign. In order to assess thermal performance of the mortars, it was necessary to design laboratory scale prototypes. Afterwards, the mortar specimens were coated into the built prototypes and tested with the selected climatic conditions.

Regarding the second part of the experimental work, it aimed the experimental investigation of mortars, comprising PCM embedded into lightweight aggregates, with the goal of highlighting behavioural differences in regard to the reference mortar that do not include PCMs. In fact, the presences of PCMs in the cementitious mix, with solidification temperatures that are near the freezing point of water, are bound to

-----------------------------------------------------------------------------------------------------

contribute for the minimization of potential freeze-thaw effects upon application in pavements.

The work methodology is structured into two main steps: (i) climatic conditions, definition of material properties; and (ii) mortar specimen's construction and experimental testing. The work developed follows the flowchart shown in Figure 5-1.
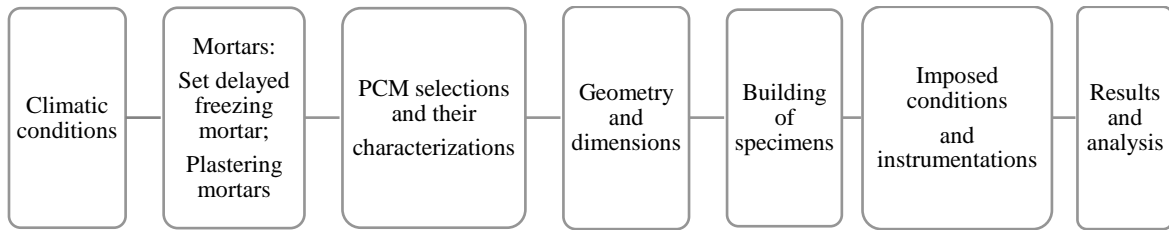


Figure 5-1: Flow diagram of the work methodology.

## 5.2 Study of plastering mortars

The previous chapters have been focused on the possibility of using more than one type of PCM (with distinct melting ranges and specific enthalpies) in the same plastering mortar for improvement of the effectiveness of the PCM-based system. However, such possibility (here termed as hybrid PCM), was solely assessed at the material level in what concerns to homogeneity distribution at different matrices within plastering mortar and the behaviour of hybrid PCMs under DSC testing. Based on the promising results of such previous works, the present chapter focuses on experimental testing of the hybrid PCM concept applied to mortars. Small scale prototypes have been tested under realistic daily temperature histories. In order to provide deeper knowledge about the advantages of using more than one type of PCM in the same plastering mortar, and relate the resulting behaviour to that of control mortars (without PCM), the experimental focused on both types of mortar formulation. The experiments were preceded by a detailed material characterization of the mortars involved, namely the thermal conductivity and the thermal behaviour by DSC. The hybrid PCM was incorporated into plastering mortar coated as a render on the extruded polystyrene (XPS) surfaces (prototypes shaped as a hollow cubes). The closed cubes were placed into a climatic chamber and

-----------------------------------------------------------------------------------------------------------------

subjected to simulated real temperature variations, thus allow evaluating the differences in thermal performance of the two types of tested mortars.

## 5.2.1 Materials and formulations

*Choice of PCMs for incorporation*

Usually in Southern European countries (such as Portugal), in a typical summer day the maximum equivalent temperature reaches to 44ºC while, the minimum equivalent temperature reaches to 5ºC during winter season. Since the study in question aims at selecting the best material for regulating temperature within human comfort limits, phase change temperature becomes the single most important screening criterion. Generally, it is advisable, the use of single PCM with melting temperature around 24ºC consider as a suitable PCM for thermal comfort application for buildings during summer period. In fact, the act of phase change in PCMs is broader than what is known as a melting temperature point. Bear in mind, such behaviours have been observed through DSC testing of the PCMs (see previous chapters 3 and 4). Hence, our initial selection of materials was limited to those exhibiting phase change in the temperature range of 10–30°C.

This selection range may cover sol-air temperature variations mentioned above. Furthermore, chemical compatibility with inorganic materials and the range of available PCM products in the market was also taken into account (Zhang *et al.* 2005, Tyagi *et al.* 2007, Sakulich *et al.* 2012, Pires *et al.* 2013). Four types of organic PCMs were considered: RT10 with melting temperature of 10°C (from Rubitherm paraffin RT series (Rubitherm GmbH 2012)), MC28 with melting temperature of 28°C, MC24 with melting temperature of 24°C (from DEVAN microencapsulated MC series (Microthermic 2012)) and BSF26 with melting temperature of 26°C (from BASF microencapsulated Micronal series (Bentz *et al.* 2007)).

The properties of the selected PCMs for this study, as provided by their manufacturers, are presented in Table 5-1. It should be mentioned that, incorporation of the RT10 as paraffin PCM, was also considered advisable to be incorporated in the mixture in the same manner of microencapsulated PCMs.

Table 5-1: Properties of PCMs, provided by suppliers.

| Properties | Operating temperature ranges (°C) | Latent heat of fusion (kJ/kg) | Melting point(°C) | Apparent density at solid stage (kg/m$^3$) |
|---|---|---|---|---|
| RT10 | 2–12 | 150 | 10 | 880 |
| MC24 | 12–25 | 162.4 | 24 | * |
| BSF26 | 10–30 | 110 | 26 | 350 |
| MC28 | 22–32 | 170.1 | 28 | * |

* No information available on behalf of the suppliers.

*Mortar formulations*

According to previous developments of this research team that were mentioned in the previous Chapter, the formulation of mortars with incorporation of microencapsulated PCM allowed the mass fraction of PCM to reach nearly 20% of the global mass of the mortar. In spite of such high incorporation level, the performance in terms of several properties was maintained satisfactory, namely in regard to: workability, compressive strength, flexural strength and adhesion (Cunha *et al.* 2015). The mix designs of the two mortars studied herein, together with their adopted designations (REFM for the reference mortar and HPCMM for the hybrid PCM mortar) are presented in Table 5-2.

Table 5-2: Mix proportions of formulations REFM and HPCMM.

| Materials | Formulations (percentage of the total weight of mortar) | |
|---|---|---|
| | REFM | HPCMM |
| Cement type I-42.5R | 22.64 | 31.32 |
| Sand | 64.23 | 30.59 |
| Water | 12.45 | 18.79 |
| Super plasticizer | 0.63 | 0.94 |
| RT10 | - | 6.12 |
| BSF26 | - | 6.12 |
| MC28 | - | 6.12 |

It should be noted that, the formulation of mortars HPCMM had not been used in the previous works, as HPCMM incorporates a combination of three PCMs with melting temperatures of 10°C, 26°C and 28°C. However, all these three PCMs are placed in equal mass quantity, thus globally reaching 18.34% of weight of PCM in the mortar. The binder adopted to be used for the production of plastering mortars, is Portland cement type I class 42.5R provided by Companhia Geral de Cal e Cimento S.A. (Secil)

in Outão, Portugal (detailed in chapter 3). Industrial sand with mean particle size around 440 μm was used as filler. The detailed grain size distribution of the sand can be found in chapter 3. It should be remarked that, experimental limitations led to the impossibility of testing a mortar containing a single PCM in the scope of this research work. Even though this was an undesirable situation, it is not seen as truly problematic, as the single PCM concept is not a new concept and therefore, only accounted through numerical simulation of single PCM mortars that will be detailed in the next chapter.

### 5.2.2 Characterization and classification of the materials

The main thermo-physical properties of the materials used in both prototypes, REFM and HPCMM, are detailed next.

***Dry density***, in order to determine dry densities of the mortars, a total number of 8 specimens were deployed. This includes four representative specimens of each mortar system for the dry density measurements following recommendation of European Standard EN 1015-10 (1999).

Firstly, the specimens had the dimensions of $50 \, \text{mm} \times 50 \, \text{mm} \times 50 \, \text{mm}$, using the standard mould. After being kept at laboratory environment for about 24 h, all the cubes were maintained under water at $20 \pm 1°C$ for 7 days. Then, the cubes were dried at 70°C until their weight did not change. The accurate dimensions of the cubes were measured using a digital caliper with a precision of 0.02 mm, and their weights were measured using an analytical balance with a precision of 0.001 g, respectively.

The densities ($\rho$) of the cubes were calculated by the following formula:

$$\rho = m / V_1 \tag{5.1}$$

Where $m$ is the mass of the cubes (g) and $V_1$ is the volumes of the cubes (cm$^3$). The results are presented in Figure 5-2.
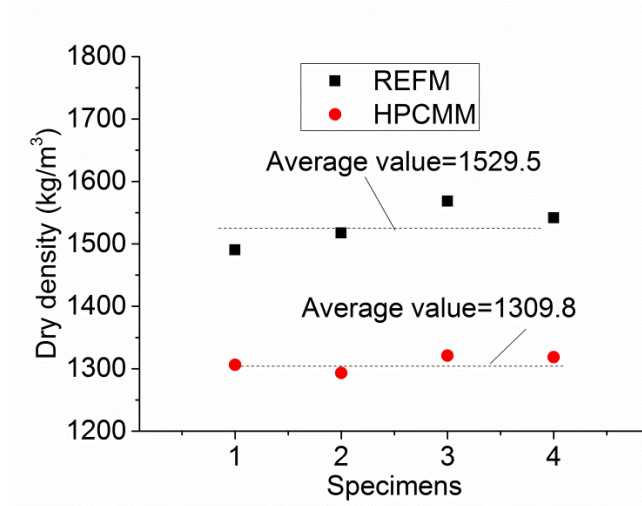
Figure 5-2: Dry densities measurements of the REFM and HPCMM mortars.

***Thermal conductivity***, four representative specimens of each mortar system were used to thermal conductivity measurements through a steady state heat flow meter apparatus (ALAMABETA, model Sensora) according to ISO:8301 (1991) using hot plates. Mortars were casted in the home-made cylinder moulds with diameter of 0.1 m and thickness of 0.01 m respectively, which were cured for 28days (production of mortars are analogous to those mortars already made in the previous chapter). The results of thermal conductivity measurements are presented in Figure 5-3.
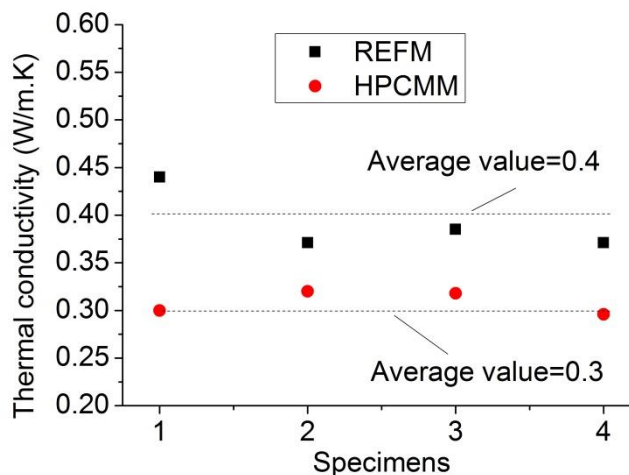


Figure 5-3: Thermal conductivities measurements for REFM and HPCMM mortars.

It should be noted that, the thermal conductivities decrease with presence of PCMs in the mortar. These results are in agreement with the theoretical predictions and are due to

the low thermal conductivities of PCM microencapsulated paraffin (Lecompte *et al.* 2015). This difference in the thermal conductivities can influence the results of thermal behaviour tests because the lower thermal conductivity turns the mortars less sensitive to outside temperature variation (less heat transfer). Thermal conductivity results may also have influenced of room temperature of 20˚C in which, pertains to the vicinity of phase change transition of the PCMs.

*Specific heat capacity,* determination of specific heat capacities of the mortar specimens were performed through DSC testing with recourse to a NETZSCH 200 F3 Maia following the methodology recommended by EN ISO 11357-1 (1997). One specimen was prepared for each type of mortar: REFM and HPCMM. The specimen preparation for DSC testing followed the methodology detailed in chapter 4. The weight of the prepared specimens was 24 mg and 37.88 mg, for REFM and HPCMM, respectively. A low heating rate of 1°Cmin$^{-1}$ was considered for all experiments (Biswas *et al.* 2014). The applied program steps for the test procedure of specimens were the following: (i) initial isothermal period at 0°C for 5 minutes; (ii) dynamic heating up to 40°C according to the proposed rate (1°C min$^{-1}$).

Figure 5-4 presents the specific heat capacity curves obtained for the mortar specimens of REFM and HPCMM.
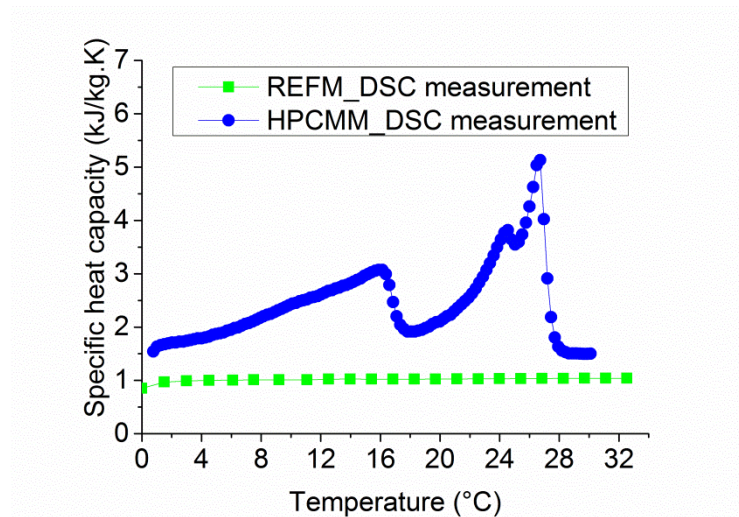


Figure 5-4: Specific heat capacities calculated with the DSC outputs of mortars (REFM and HPCMM).

The graph of Figure 5-4 shows that the PCMs held its characteristics when incorporated into mortar mixture as the DSC for the case of HPCMM reveals three peaks corresponding to three PCMs in the range of their phase change temperatures started from 2ºC to 29ºC, approximately. However, it can be observed that the peak temperature of the RT10 in HPCMM shifted about 6ºC, while, the peak temperatures of the BSF26 and MC28 in HPCMM delayed nearly 2ºC. The reason can be related to the fact that, in DSC testing, the temperature sensor monitors the surface temperature of the specimen regardless of specimen container (crucible). In fact, during the heating process, although the surface temperature of the specimen increased, the inner temperature of the specimen was still lower than the surface temperature because of the specimen thermal resistance (Jin *et al.* 2014), which revealed that the peaks would delay for the lower temperature. It should be remarked that, the insulation material was placed on the outer wall next to the mortar. It consisted of ready to used plates of XPS (extruded polystyrene) from FIBRAN Corporation (FIBRANs 2011).

### 5.2.3 Design and fabrication of the prototypes

In order to assess the effect of the hybrid PCM concept into plastering mortars used as internal coatings for buildings, two closed prototypes were built with laboratory scale dimensions. The materials used for the construction of the prototypes were from inside to outside: a 0.02m thick layer of REFM or HPCMM, and a 0.03m thick of extruded polystyrene (XPS). The schematic diagram of the physical models and cross-section of the model are shown in Figure 5-5.



**(a)** Plan view C–C.     **(b)** Cross section B–B.     **(c)** Corner detail (Zoom-section-A).
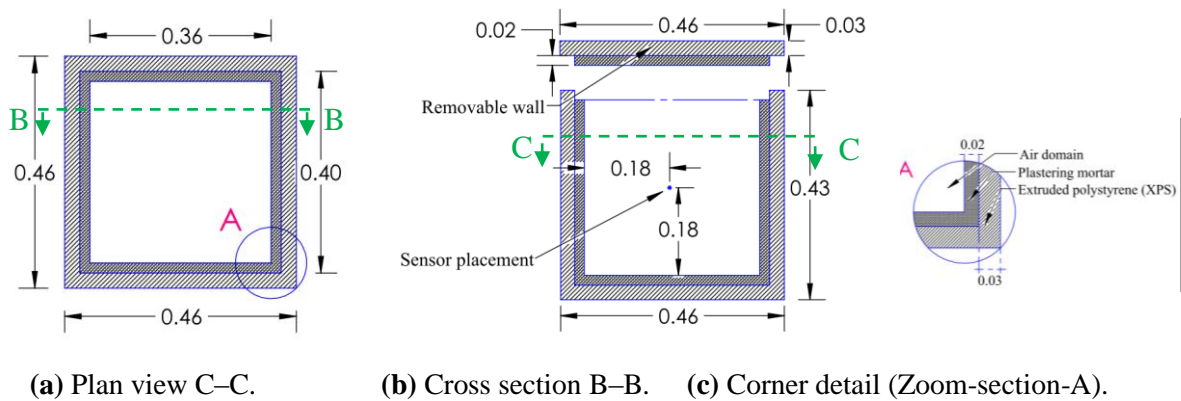
Figure 5-5: Schematic representation and sensor placement of the prototypes. Units: [m].

In regard to temperature monitoring, PT100 sensors, with 0.1°C accuracy, were positioned at the geometrical centre of the internal hollow region, with the final intention of monitoring internal temperature variations within the prototypes (Figure 5-5).

The composition of the walls of the test cell is not a typical one in building envelopes. In fact, the target in this case was to have a small-sized prototype, with relatively thin walls, which would however have a thermal transmittance ($U \approx 0.89$ W/m$^2$ K) lower than the maximum limit according to Portuguese regulations for vertical elements (of $U = 1.45$ W/m$^2$ K) (RCCTE 2006), thus having a reasonably similar thermal behaviour to actual building envelopes.

## 5.2.4 Thermal performance of prototypes

Each prototype was placed inside a controlled climatic chamber with inner dimensions of 1.04 m×1.2 m×0.6 m. The temperature cycles through the exterior surfaces of the model were programmed to match the sol–air temperature corresponding to the surface temperature of a vertical wall facing south, which is considered for summer and winter time in Portugal.

Sol-air temperature ($T_{Sol-Air}$) was predicted according to the following Eq. (5.2) (Vaz Sá *et al.* 2012):

$$T_{Sol-Air} = T_{Air} + \alpha I_g R_{se} \tag{5.2}$$

$T_{Air}$ is the exterior temperature (°C); $\alpha$ is the absorption coefficient of the surface; $I_g$ is the global solar radiation (W/m$^2$); and $R_{se}$ is the external surface resistance ((m$^2$ K)/W). The values of exterior temperature ($T_{Air}$) and global solar radiation ($I_g$) were considered regarding average hourly values recorded for a typical summer and winter days in northern Portugal (Guimarães), as shown in Figure 5-6. An absorption coefficient $\alpha = 0.6$ was considered (Vaz Sá *et al.* 2012).

The value of external surface resistance was adopted as $R_{se} = 0.04$ m$^2$ K/W in accordance to the recommendations of ISO6946 (2007). As a result of the application of the sol–air temperature model, the 24h cycles shown in Figure 5-6 were obtained for summer and winter. A total of four experiments were conducted by submitting the two

prototypes (REFM and HPCMM) to the two environmental conditions (summer and winter), with each experiment lasting 72h.



**(a)**                                                **(b)**
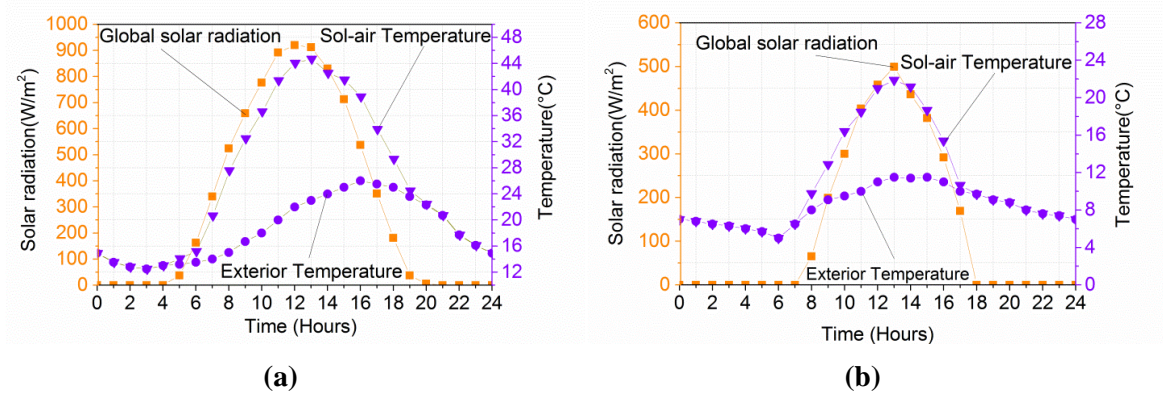
Figure 5-6: Exterior temperature, solar radiation and sol–air temperature of: (a) a summer day and (b) a winter day in Guimarães, Portugal.

The climatic chamber in which the test was conducted also allowed the control of internal relative humidity, which was set to the constant value of RH = 50% throughout all the performed experiments. The physical arrangement of this setup can be observed at the pictures of the prototype and monitoring system showed in Figure 5-7. The readings of temperature sensors were collected through a computer-based data acquisition system (AGILENT 34970A) with a rate of one measurement per minute during whole period of experiment.



**(a)**                                                **(b)**
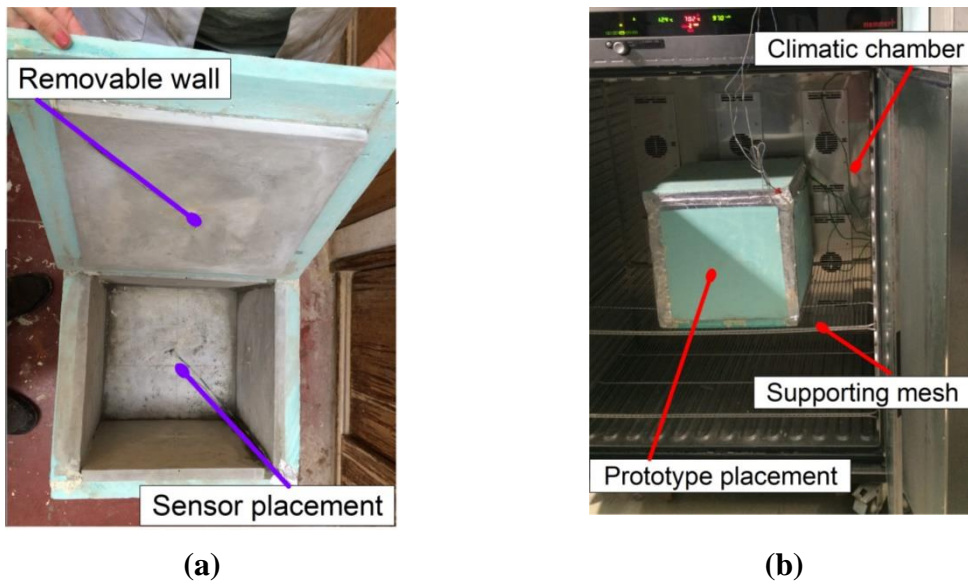
Figure 5-7: (a) Picture of sensor arrangement at geometrical centre inside prototype; (b) Picture of the test setup configuration.

### 5.2.5  Temperature monitoring results

Regarding the monitored results registered for both prototypes under summer day conditions, shown in Figure 5-8, it can be observed that the maximum and minimum internal temperature inside REFM prototype were 33ºC and 20ºC, whereas the corresponding maximum and minimum temperature in HPCMM prototype were 31.5ºC and 22.6ºC respectively. The minimum peak temperature differences of 2.6 K are reasonably consistent with the observations of (Vaz Sá *et al.* 2012), who observed similar magnitude peak temperature differences of 2–3 K in prototypes containing mortar with a single PCM and without PCM. However, the maximum internal temperatures inside the prototypes are also different. In fact, 1.5 K difference between REFM and HPCMM prototypes confirming that HPCMM can also assist temperature regulation in this range. The delay between the maximum temperatures registered inside climatic chamber and inside the HPCMM prototype was of nearly 4.5 h. Also, the difference in such delay between the REFM and HPCMM prototypes was of approximately 1.5 h., with advantage for HPCMM.
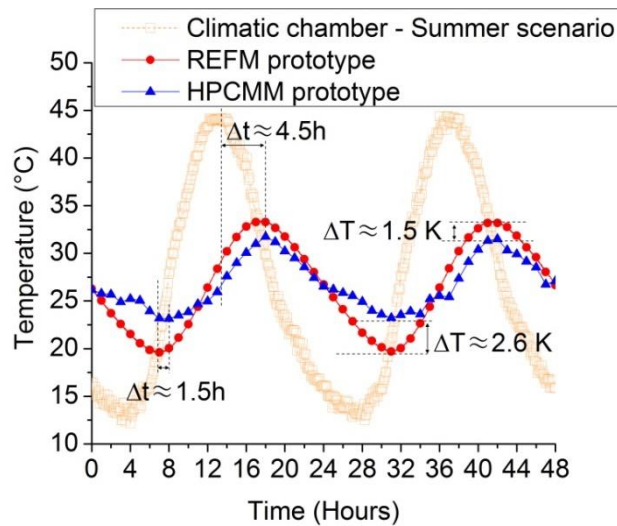


Figure 5-8: Monitored temperatures of the prototypes with inner coatings made of HPCMM and REFM under summer scenario.

It is interesting to note that, the minimum temperature achieved on the HPCMM prototype is mostly close to the phase transition of BSF26 and MC28 (see the DSC measurements in Figure 5-4). The collected result for summer scenario revealed that hybrid PCM acts by reducing inside temperature amplitudes during the day, levelling

91

-----------------------------------------------------------------------------------------------------------------

them and turning them closer to comfort temperature levels (around 24ºC). All this has occurred in spite of the fact that the RT10 PCM embedded in HPCMM was never activated within this summer scenario. Also it should be remarked that, such decreased temperature variations behaviour is associated with conduction of heat from environmental chamber to inside of the prototypes, with the beneficial influence of lower thermal conductivity of the HPCMM case rather than REFM case.

The monitored values registered during the experimental program for a winter scenario are shown in Figure 5-9.
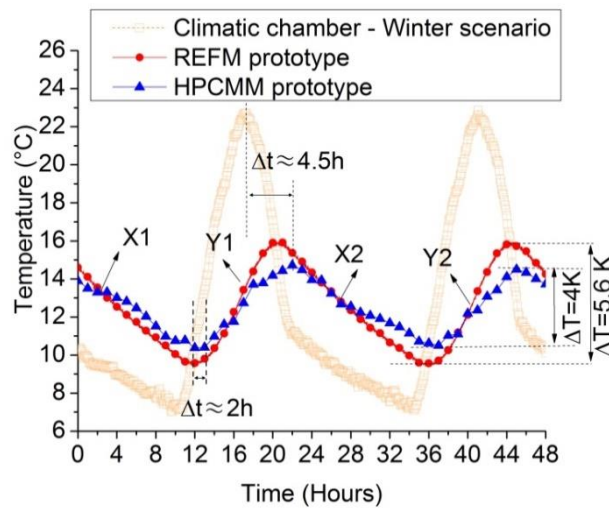


Figure 5-9: Monitored temperatures of the prototypes with inner coatings made of HPCMM and REFM under winter scenario.

It can be observed that the thermal amplitudes inside the prototype were lower for the case of HPCMM as compared to REFM. It is interesting to note that, the exhibition of phase change transition reasonably due to presence of PCM with melting temperature around 10ºC (RT10). In fact, the heat was released at phase change temperature of the RT10 (labelled as X1 and X2 in Figure 5-9) and therefore, the minimum interior temperature of the HPCMM prototype increased by 0.7ºC. In accordance, at phase change transition (labelled as Y1 and Y2 in Figure 5-9), heat was absorbed by RT10 and corresponding maximum interior temperature of HPCMM prototype was decreased by 1ºC. However, it should be stressed that, neither REFM nor HPCMM prototypes meet the thermal comfort level.

This situation would not be acceptable in a real case-scenario, where a heating element would be added to the system. Even though such heating element was not included in this research, the increased capacity of HPCMM in attenuating thermal amplitudes as compared to REFM was demonstrated as intended. Further research works was specifically focus on integrating a heating element within the studied prototype and evaluate energy savings associated to the inclusion of hybrid PCM mortars detailed in the next section. The overall observations for this winter scenario are similar to those already reported above for summer scenario: the incorporation of PCM leads to a reduction of peak temperatures and an increase in minimum temperatures.

## 5.2.6 Thermal performance of prototypes in active system mode

In this section, the same boxes studied in pervious section, without PCM and with hybrid PCM, were taken. The target is to assess the energy efficiency gains for space heating using hybrid PCMs into plastering mortars used as internal coatings for buildings. The heating system was placed inside the box (centre of the heater coinciding with the geometrical centre of the cube) as shown in Figure 5-10. The heater (ROTFIL-air heater series) had dimensions of 0.02m×0.02m×0.1m, with a power rating of 300 W. The heater was connected to a multifunctional electricity source with alternative parameters (ampere and voltage for the output) and a temperature controller (OMRON-E5CSV) in order to control internal temperature sets of the ambient temperature of the prototype. The control of the heating system was made in order to maintain a temperature of comfort level. The standard (ASHRAE55 2004) recommends that air temperature inside the building should be minimum 20°C and maximum 25°C during winter season.



**(a)** Plan view C–C.         **(b)** Cross section B–B.         **(c)** Sensor placements cross section A–A.
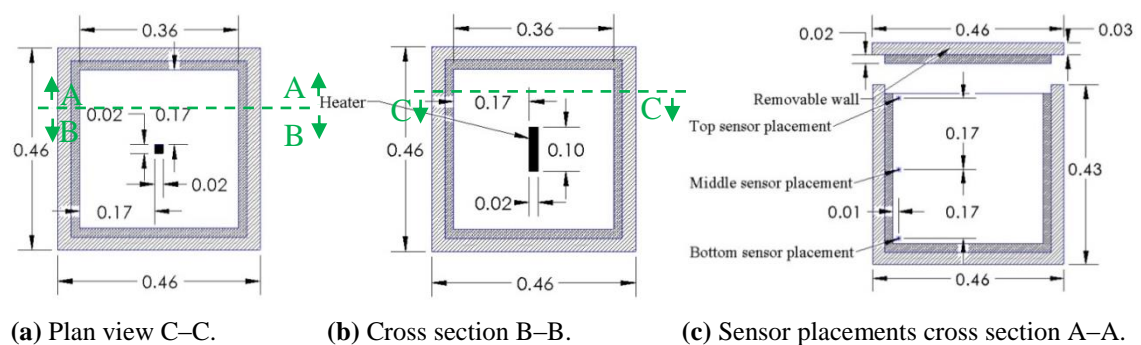
Figure 5-10: Schematic representation of the prototype placed inside the climatic chamber. Units: [m].

### 5.2.7 Data acquisition and control

The same boxes as previous section in addition with a heating system (discussed above) were deployed for this section. The test setup for total number of 2 experiments was repeated according to section 5.2.4. Only, the winter scenario was imposed as climate condition inside the climatic chamber room. The experimental point's sensors arrangement of the prototypes was changed and the temperatures were monitored at the three different height levels at the corner of the prototypes as top, middle and bottom sensors of the prototype (presented in Figure 5-10). It should be mentioned that, the heater system sensor was attached to the sensor of bottom of the prototype as this would be the coldest region within the prototype. Thus, the number of environment that was tested is 1 (a winter scenario) and the number of prototypes is 2 (without PCM and with PCM). The evaluation parameter of the performance of the several studied plastering mortars (without and with PCM) for the heating season was the energy demand of the heater in order to maintain adequate internal comfort levels.

It is assumed that, in the cooling season it is assumed that the PCM can handle the adequate internal thermal comfort levels. Therefore, the energy analysis was performed only for the heating season testing.

The heater was connected to a multifunctional electricity source with alternative parameters (ampere and voltage for the output) and a temperature controller (OMRON-E5CSV) in order to control internal temperature sets of the ambient temperature of the prototype. The control of the heating system was made in order to maintain a temperature of comfort level. Specification of the temperature controller is given in Table 5-3.

Table 5-3: Specification of E5CSV temperature controller.

| Quantity | Value |
|---|---|
| Sensor input | Platinum resistance thermometer: Pt100, Thermocouple: K, J, T, R, or S |
| Power supply voltage | 100 to 240 VAC 50/60 Hz, 24 VAC 50/60 Hz, or 24 VDC |
| Operating voltage range | 85% to 110% of rated supply voltage |
| Control output | Output voltage: 12 VDC +25%/−15% (PNP), max. load current: 21 mA, with short-circuit protection circuit |
| Indication accuracy | (±0.5% of indicated value or ±1°C, whichever is greater) ±1 digit max. |
| Relay output | 250 VAC, 3 A (resistive load), minimum applicable load: 5 V, 10 mA |

The scheme illustrated in Figure 5-11a shows, the temperature controller and the energy meter units were programmed to receive interior temperature of the prototype which is attached to the placement of corner bottom sensor (here termed IT), exterior temperature (placed at climatic chamber ambient), and power consumption of the heating element unit.



| (a) | (b) |
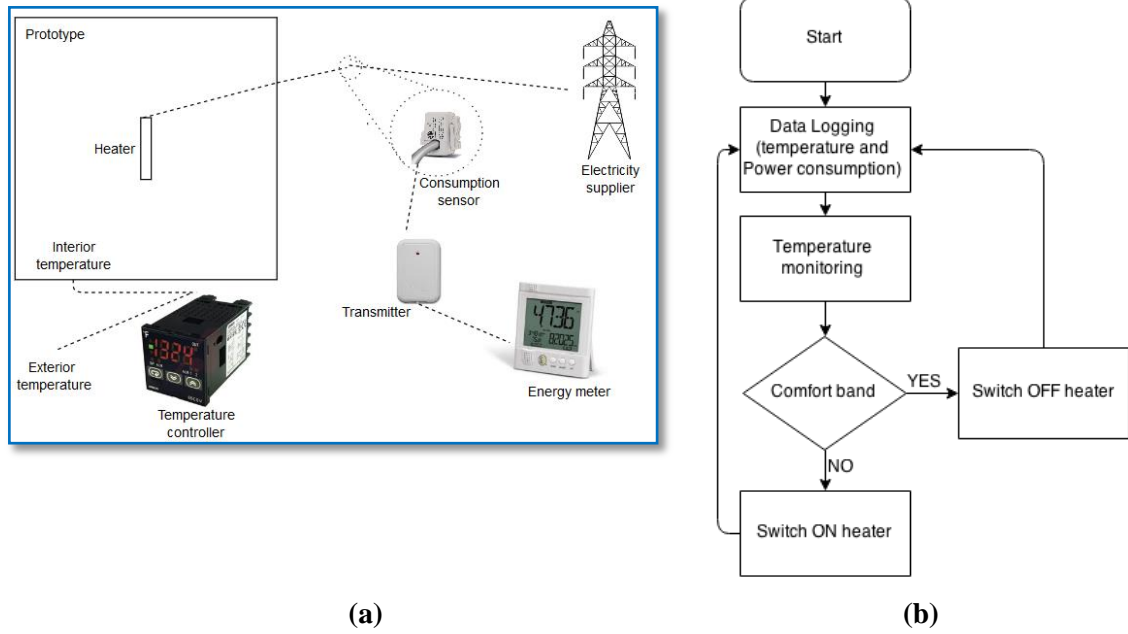
Figure 5-11: (a) Monitoring and control arrangement system scheme; (b) Experimental procedure for the heater element.

According to the standard ASHRAE55 (2004) recommends that air temperature inside building should be minimum 21°C and maximum 25°C during winter season. The operating principle of the devised system is presented in Figure 5-11b. The heater is ON when the temperature inside the box goes below the 21˚C and it is turned OFF when the temperature reaches 21ºC again (see Figure 5-11b). On the other hands, the control mode used was dependent on the interior temperature (IT) of the prototype. If IT is smaller than 21ºC, the controller proceeds to ''ON mode'' and interior air temperature of the prototypes is kept within the ''low peak temperature'' range of 21 and 25ºC. As mentioned before, hybrid PCM mortar has three peak melting points within the range of 4ºC to 29ºC. Maintaining the interior temperature of the prototype within the low peak temperature range enables reduces energy consumption of the heater to maintain the interior temperature ambient at minimum 21ºC. In the next step, the temperature controller unit receives data from temperature sensor attached to the bottom sensor of

the prototype and uses the heating unit to keep the IT within the range of 21–25ºC. As soon as IT rises above 21ºC, the controller switches to ''OFF mode''. This implies a lower temperature range, in order to use less energy and capture the stored energy in the hybrid PCM case during this period. It should be mentioned that, IT was measured using PT100 sensor connected to data acquisition system (AGILENT 34970A). The specification of the used PT100 sensor is as given in Table 5-4. Electrical consumption of the heating units was measured using Energy Meter (The OWL_USB). The specification of the used data acquisition system (AGILENT 34970A) and Energy Meter (The OWL_USB) are given in Table 5-5and Table 5-6 respectively.

Table 5-4: Specification of platinum temperature sensor type PT100 (100 Ohms @ 0ºC).

| Quantity | Value |
|---|---|
| Temperature range | −50 to +500 °C |
| Fundamental interval  (0ºC to 100ºC) | 38.5Ω (nominal) |
| Stability | ±0.05% |
| Self heating | <0.5ºC/m W |

Table 5-5: Specification of AGILENT 34970A data logger.

| Quantity | Value |
|---|---|
| Number of channels | 20 |
| Temperature accuracy | 0.06 °C |
| Thermocouple types supported | Platinum resistance thermometer: Pt100, Thermocouple: B, E, J, K, N, R, S, T |

Table 5-6: Specification of OWL_USB energy meter.

| Quantity | Value |
|---|---|
| Operating frequency | 433MHz |
| Operating range | up to 30m |
| Number phases | 3 |
| Standard Sensor clamp | < 10mm cable, < 71A |
| Accuracy | ±10% |
| Supply | 240 V AC |
| Measuring quantity | Kw h |

## 5.2.8 Physical test configuration

A total of two experiments were conducted by submitting the two prototypes (REFM and HPCMM) to the two environmental conditions (winter scenario testing), with each experiment lasting three full cycles (72 h). The climatic chamber in which the test was conducted also allowed the control of internal relative humidity, which was set to the constant value of RH = 50% throughout all the performed experiments. The physical arrangement of this setup can be observed at the pictures of the prototype/monitoring shown in Figure 5-12.
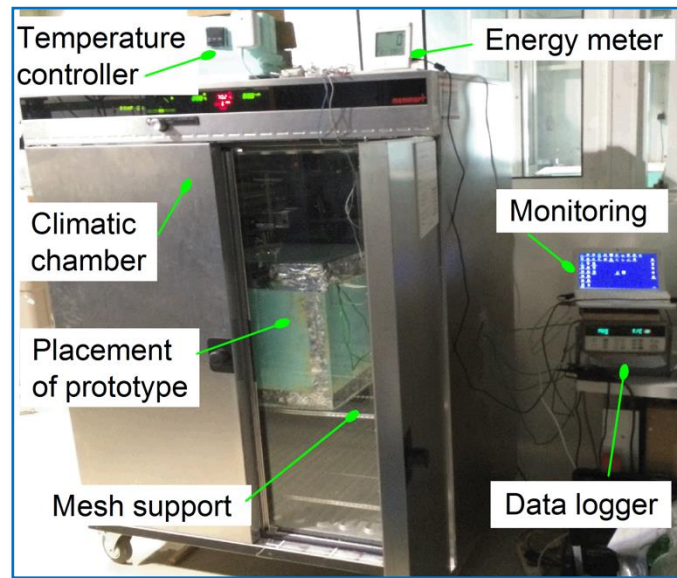


Figure 5-12: Photo of the prototype ready for testing, highlighting the location of the prototype within the climatic chamber.

## 5.2.9 Temperature monitoring results of active system

Figure 5-13 shows the air temperature variations of the REFM prototype over a 48h period with respect to the heater system. As shown, during a cycle of 24h, interior air temperature was kept at the minimum comfort temperature of 21ºC according to the predefined set point temperature for the heater.

During the first 3h period, when the ambient temperature drops to the 10ºC, the interior temperature of the prototype reaches to the limit temperature of 21ºC. Almost similar temperature was recorded for all sensors within prototype which were positioned at: top,

----------------------------------------------------------------------------------------------------------------------

middle and bottom, confirming insignificant temperature variation inside the prototype and accordingly negligible natural convection. At this time, the heater system starts to work in order to sustain the temperature above the set point of 21°C.
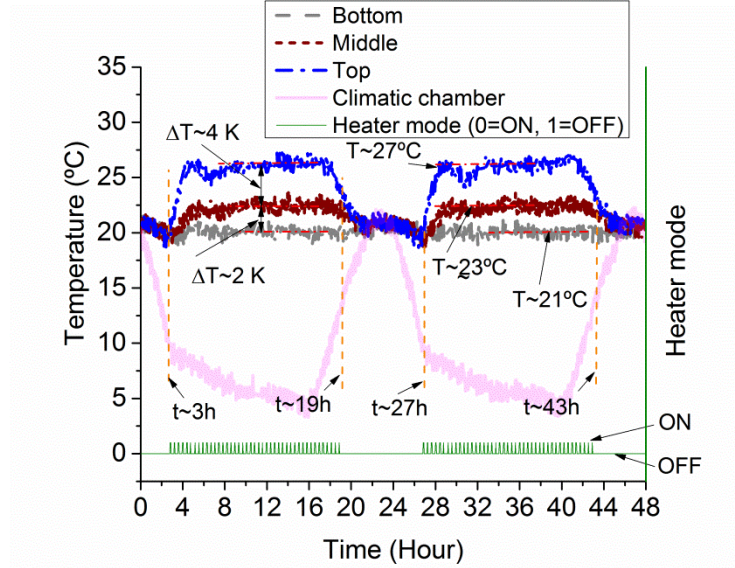


Figure 5-13: Monitoring temperature variations at different positions inside the REFM prototype under tested controlled environment accounting heater modes.

In fact, at the time of t≈3h, the temperature controller started supplying electricity to the heater and, as a consequence, the interior temperatures of the prototype increased sharply from 21°C to 21.5°C, 23°C and 27°C for bottom, middle and top sensors and remained relatively constant for almost 16h until the ambient temperature increased (see t≈19h in the Figure 5-13). At the time of t≈19h to t≈27h, the heater system was in the "OFF mode" and therefore, the monitored interior temperatures within the prototypes getting narrows to it is set point temperature of 21°C again. On the other hand, at the both times of t≈3h and t≈27h, the interior air temperature reached 21°C and the temperature controller turned on the heater element in order to prevent further temperature drop in the prototype. During the heating process, differences in the monitored temperatures can be observed as a gradient change by 2K and 6K for middle and top sensors respectively. These temperature differences between the measured points is caused by the action of temperature gradients in conjunction with a gravitational field (so called Natural or Buoyant or Free convection). In fact, in this experiment, the basic scenario in the context of natural convection can be explained by

------------------------------------------------------------------------------------------------------

existence of density gradient in the fluid in a direction that is parallel to the gravity vector. Such situations can lead to unstable temperature stratification of the fluid (here is the air). In a stable stratification (at the time when the heater is in OFF mode), less dense fluid is at the top and more dense fluid is at the bottom. While, in second scenario, unstable stratification (at the time when the heater is in ON mode), less dense fluid is at the bottom, and more dense fluid at the top, provided the density gradient is sufficiently large, convection was started spontaneously and significant mixing of the fluid was occurred.

The results of thermal behaviour in the hybrid PCM prototype (HPCMM) are shown in Figure 5-14. In fact, Figure 5-14 is analogous to Figure 5-13, except for the fact that it deals with HPCMM. The observations are also analogous to those already made for REFM. In brief, Figure 5-14 shows the interior air temperatures of HPCMM when it was conducted into the climatic chamber and heated during the cold hours (when it reaches to the set temperature point of 21ºC) using a heater element.
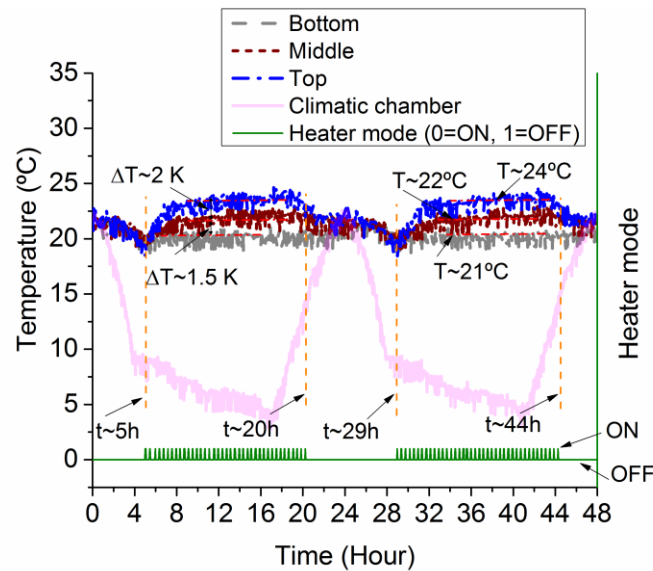


Figure 5-14: Monitoring temperature variations at different positions inside the HPCMM prototype under tested controlled environment accounting heater modes.

It is interesting to note that, in the case of HPCMM there is a possibility of taking advantages of PCMs due to the fact that they can absorb or release the heat during their phase change temperatures. Comparing Figure 5-14 with Figure 5-13, it can be seen that

in the case that PCM is employed, the temperature distribution inside the prototype is more uniform than the case without PCM incorporation. This shows that, in the case without PCM, some portion of energy was not used in an efficient way (see the highest temperature of measured at top location in Figure 5-13 reached to nearly 27ºC) which is upper than ultimate temperature required for winter season which is 25ºC.

The controller stops supplying heat to the heater during the early hours (first 5hrs), and, as a consequence, the interior air temperatures of HPCMM drops sharply and reaches the minimum temperature constraint at t≈5h. The air temperature for HPCMM remains above the temperature constraint until the prototype is heated as a result of heating element as well as phase change transition of PCM within mortar. This shows clearly that the PCM can successfully be used for t≈5h to t≈20h and t≈29h to t≈44h.

Comparing both figures Figure 5-14 and Figure 5-13, despite the good performance of the HPCMM in compare with REFM in the early hours of cycle, which allows 2h delaying in the time to reaches to the 21ºC as the temperature drops in REFM by t≈0–3h and in HPCMM by t≈0–5h. This is because there is usually no need for heating during the first 5hours and, as a consequence, the stored energy in the HPCMM is discharged. This can be clearly observed in Figure 5-14, which shows that the HPCMM case was turned on the heater and, suggesting that the PCM is discharged and can contribute to the heating of the HPCMM prototype.

For further evaluating the impact of the PCM on thermal efficiency of the system, the accumulative energy consumption by the heater equivalent to the both cases of REFM and HPCMM were calculated for a period of 24h and are demonstrated in Figure 5-15. It is interesting to note that, the variation in the impact of the PCM on the multi-layered heat transfer is based on configuration and weather conditions.

Highest reductions in the calculated wall heat gains with PCM were observed during a winter day. In fact, during demonstrated tested 24h, the configuration with PCM allowed approximately 20% reduction in energy demands for maintaining the

100

---------------------------------------------------------------------------------------------------------------

temperature inside the prototypes within the comfort temperature. This shows that the electricity saving achieved in each day comes from PCMs and is affected by outdoor temperature.
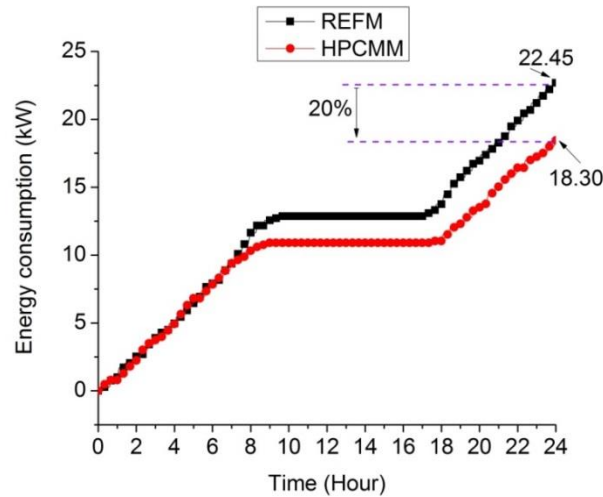


Figure 5-15: Accumulative energy consumption versus time.

This method can benefit from the PCMs and variable electricity prices during the winter period to reduce electricity consumption while performing peak load shifting. The proposed method in this research can be applied in any locality which offers a variable electricity price. It should be noted that the melting point of the PCM needs to be selected according to the thermal comfort requirements.

## 5.3   Study of delayed freezing mortars

In this section, the experimental investigation of delayed freezing mortars (here termed as DFM) comprising mortars incorporating PCM, targeted behavioural differences in regard to the reference mortars that do not include PCMs. In fact, the presence of PCM in the cementitious mix, with freezing temperatures that are near the solidification point of water, are bound to contribute for the minimization of potential freeze-thaw effects upon application in pavements. However, in this thesis, the application on the pavement structure has not been attempt; instead, an experimental test setup was established to evaluate the performance of these mortars. Three mortars were prepared and tested under controlled environmental conditions: one conventional mortar and two with PCM.

All samples were monitored when subjected to freezing temperature profile, in order to understand the effect of the PCM incorporation.

Bear in mind, in the previous chapter the experimental studies on the impregnation method and thermal performance of the composites led to conclude that the impregnation method is simple but the question if it is effective in term of embedding PCMs into porous materials such as mortar or concrete need to be addressed. In continues, this research work has further confirmed that the embedded PCMs provide the mortars with a large thermal energy storage capacity due to the quantities of PCM that can actually be incorporated. The results indicate that additionally PCM mortars improve the thermal inertia as well as delayed freezing in the sub layer. This technique may help to extend the service life of pavement structures, by reducing freezing damage through the incorporation of PCMs. However, it should be stressed that the development of PCM composites for this purpose is still in its infancy, and there are many questions that will need to be answered in the future before such composites are ready for real-world applications. This research will help to serve as part of a foundation for such studies.

### 5.3.1 Materials and rationales

The composition of each mortar mixture under study can be found in Table 5-7.

Table 5-7: Mixture proportions by mass, in grams.

| Mixture | REFM0* | PCMM10* | PCMM20* |
|---|---|---|---|
| **Cement (g)** | 1286.1 | 1286.1 | 1286.1 |
| **Water (g)** | 707.4 | 603 | 573 |
| **Sand (g)** | 3649.7 | 1607.6 | 1205.6 |
| **PCM impregnated LWAs (g)** | - | 401.9 | 803.8 |
| **Superplasticizer (g)** | 38.5 | 38.5 | 38.5 |

*Abbreviations: REFM0= reference mortar without PCM; PCMM10=mortar with incorporation of ≈10% PCM impregnated LWAs of total weight of mortar; and PCMM20=mortar with incorporation of ≈20% PCM impregnated LWAs of total weight of mortar.

It should be mentioned that, the formulation of the mortars are similar to those already used in chapter 4 for the study of DFM. In this way, three mortars were produced: a mortar containing only river sand aggregates, and two mortars, each containing both the

light weight expanded clay and river sand aggregate at distinct proportions. During the production, adjustments were made to the water dosage, so as to ensure a consistency between 160mm and 180mm in the flow table test.

### 5.3.2 Testing program

*Specimen mortar preparations*

For the thermal performance tests, from each of the mortars, a small plate of $150\times150\times25mm^3$ was created. The fresh mortars were moulded and vibrated by a standard mechanical vibrator. Afterward, the moulded specimens were protected by plastic paper in order to prevent premature loss of water and were placed in a standard curing room for 28 days.

*Thermal performance test of the mortars*

The temperature of the pavement surface is affected by various weather variables such as radiation, atmosphere temperature, wind speed and so on. It is also related to the surface characteristics of the pavement materials. Principle of the test can be expressed as: to delay freezing of surface layer of pavement, use of such mortar with incorporation of PCM may bring some benefits in the scope of geothermal heating applications. In fact, use of mortar on above surface of the pavement to delay or prevent freezing at the pavement structure.

The measurement temperature of the below surface of mortar layer will reflect whether the consideration of weather variables (emulating of snow or ice) in the experiment is reasonable. Within the composite material itself, energy is transferred through conduction from the interface with ice layer, into the surrounding mortar layer, and eventually to the below surface of the composite mortar, where it is air bound. In fact, this test helped to understand the effectiveness of the PCM on the mortar, it was particularly important to consider in detail the heat releasing process, since this freezing process enabling to detect the potential of the stored energy within mortar with PCM. For the purposes of simulation of snow or ice, models began with a layer of ice at the top of the mortars. This allows comparing three system mortars: REFM0, PCMM10 and PCMM20.

----------------------------------------------------------------------------------------------------

The test box has been placed inside a controlled climatic chamber room with constant temperature of 0ºC in order to avoid melting of the ice material.

The measured quantified were the upper and lower surface temperatures of the mortars. The experimental test setup and sensors placement are shown in Figure 5-16(a). The test box was a hollow cube, with internal hollow volume of $200\times200\times250mm^3$, depicted in Figure 5-16(b), and whose walls are made with a 50mm thick layer of thermal insulation, extruded polystyrene (XPS). The top of the cube was composed of (from the outside to the inside, at the centre of the top); a layer of ice material with dimensions of $150\times150\times25mm^3$ and a layer of mortar (REFM0, PCMM10 or PCMM20) with dimensions of $150\times150\times25mm^3$. The sensors (thermocouple type K) were connected to a data logger in order to record the measured temperatures with time step of 1 min.



|        (a)        |        (b)        |
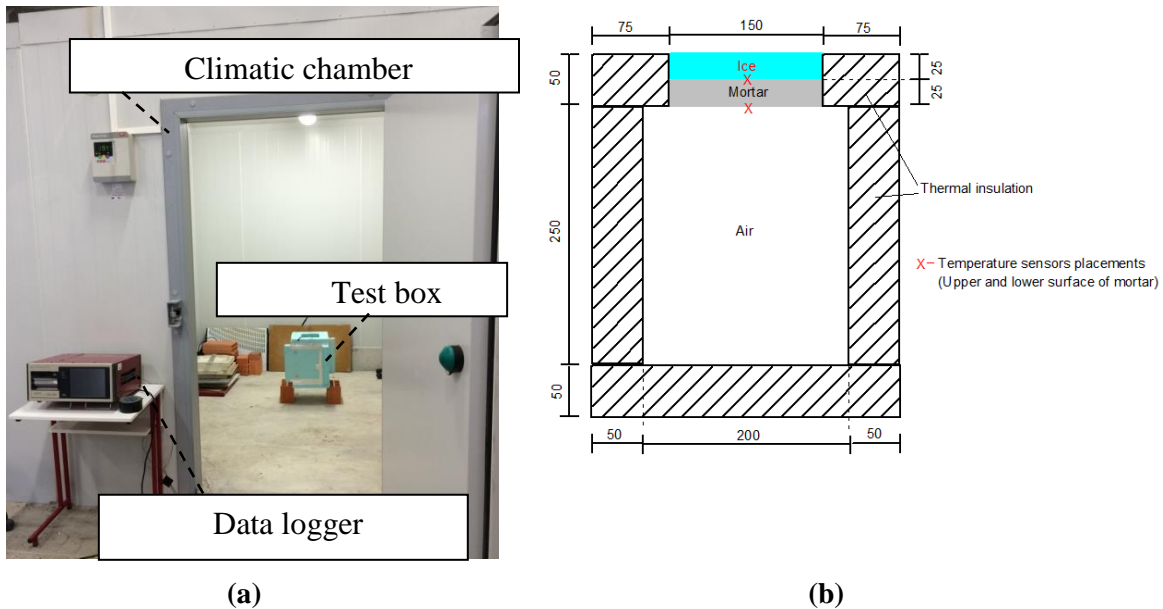
Figure 5-16: (a) The experimental test setup designed for the evaluation of the thermal performance of REFM0, PCMM10 and PCMM20; (b) Test box section view, units: [mm].

## 5.3.3   Results of thermal performance testing

Figure 5-17 presents the results of thermal test for REFM0 (a), PCMM10 (b) and for PCMM20 (c). The plots presented in Figure 5-17, show the time to reach a freezing

temperature at the mortar surfaces (both upper surface of mortar that is interconnected with ice and lower surface of the mortar).
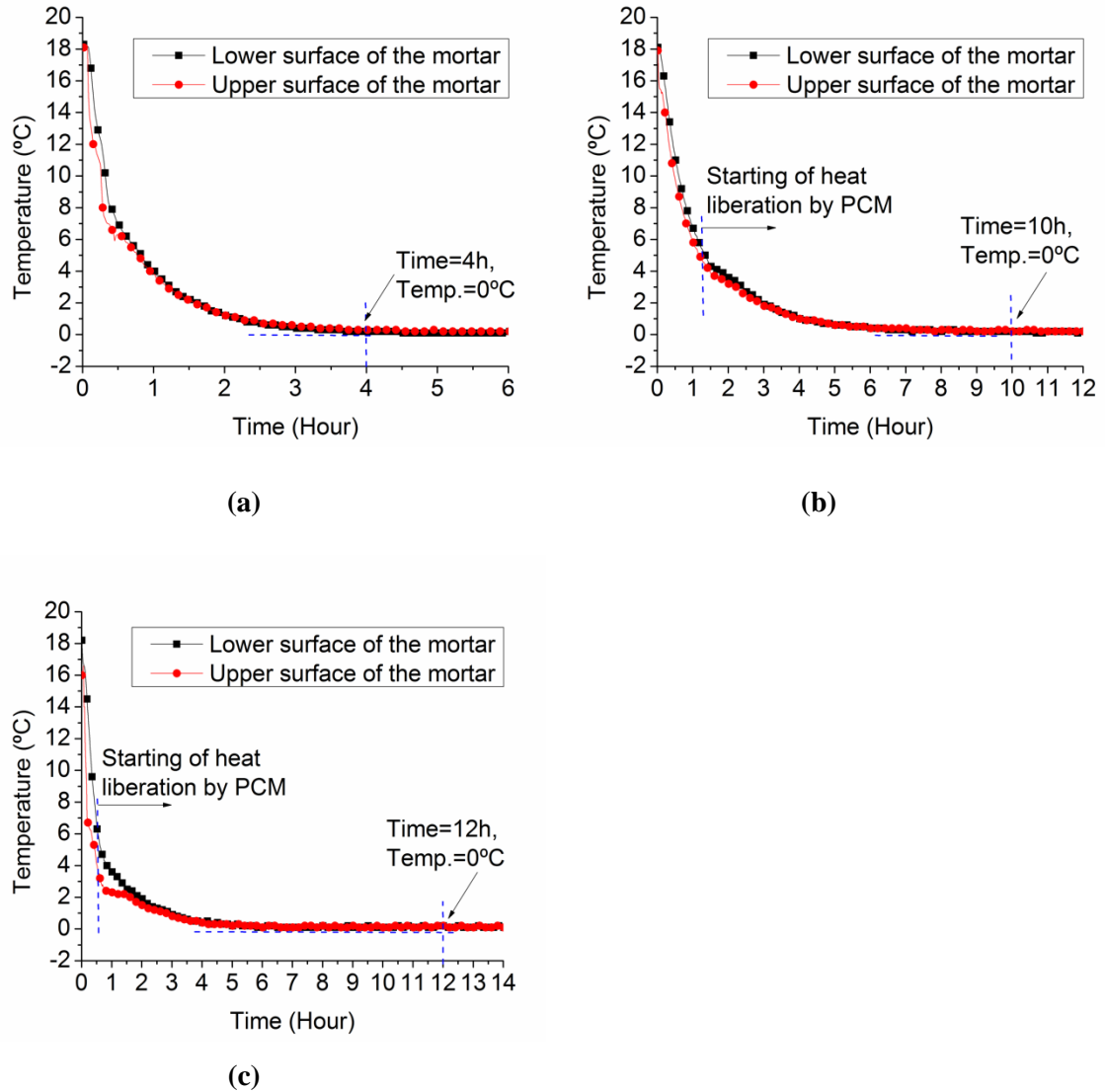


Figure 5-17: Behaviour of mortars under ice loading: (a) REFM0 case; (b) PCMM10 case; and (c) PCMM20 case.

The scenario is explained by the case that the system was continually running and could provide significant heat energy to prevent/delay the freezing at sub layer. The scenario for non-freezing time is when the entire lower surface of the mortar is above 0ºC. It should be noted that, the melting of the ice has not been occurred when placed at the upper surface of the mortar since all the system is settled inside a climatic chamber that

is programmed with fix temperature of 0⁰C. From the plots of Figure 5-17, the following observation can be made:

- o As the PCM incorporation increases, the time for the sub layer to reach a freezing temperature increases. In fact, when the upper surface temperature (interface bound ice and mortar) dips to 0⁰C, the PCMM20 system showed delay of icing of 12hours, which show that the delay time significantly varies with the PCM incorporation.

- o The phase change behaviour of the PCM occurred according with the phase transition temperature of 5⁰C for the cases with PCM (both PCMM10 and PCMM20). The PCMM10 offers similar trends in behaviour to PCMM20, with respect to the effects of upper surface temperatures and PCM incorporation on system behaviour. However, PCMM20 offers better overall system performance than PCMM10 in terms of their times to freezing lower layer temperatures, due to their increase thermal energy storage potential.

## 5.4   General remarks

The thermal performance of hybrid PCM plastering mortars was experimentally evaluated using prototypes subjected to realistic daily temperature profiles in comparison to the performance of normal plastering mortars (without PCM) under the same conditions. Further experiments were performed to evaluate the thermal performance of mortars with hybrid PCM, as well as to understand the contribution of hybrid PCM to energy efficiency. Incorporation of hybrid PCM into plastering mortar was assessed to highlight the potential reduction in term of heating/cooling temperature demands for maintaining the interior temperature within comfort level when compared with normal mortar. Comparing thermal performance of delayed freezing mortars was also evaluated through small scale testing for both cases with and without PCM incorporation. It was remarked that the use of PCMs incorporated in LWAs revealed adequate thermal behaviour, as desirable outcome to delay the freezing of the lower layer under ice load conditions for pavement applications. However, this investigation carried on at material level and the feasibility of the proposed method for PCMs incorporation in LWAs and the pavement structure has not been tested.

# Chapter 6  Numerical Simulations

## 6.1   General overview

This chapter deals with the numerical simulation of the thermal behaviour of construction elements that comprise mortars with embedded PCMs.

The numerical simulations are begun in the context of the small scale prototypes that were experimentally tested in the scope of Chapter 5. This initial stage of simulation has the main objective of validating the numerical simulation approaches.

After the initial validation, the thermal simulation framework is deployed for simulation of a real-scale situation (residential building) as to evaluate the actual benefits that can be harvested by using plastering mortars with incorporated PCMs (single or hybrid). The performance of the system in terms of thermal behaviour and energy saving are compared to the case without PCM incorporation.

## 6.2   Numerical simulation of heat transfer in the context of building physics

Numerical models target in the description of a physical system through mathematical terms, and therefore rely on several basic assumptions.

Usually, it is important to validate the numerical simulations by mean of experimental results that may reflect the physic of the model. On the other hands, validation refers to an iterative procedure where the model outputs are compared to experimental data, until the errors are justified within the limits of confidence. Even though, a suitable validation

---------------------------------------------------------------------------------------------------------------

should be provided by measuring of the models accuracy. Once a model is validated, it can be used in sensitivity and parametric analyses, where specific model parameters are varied and their respective impacts on the main variables investigated.

### 6.2.1 Finite Element Method (FEM)

The finite element method has been used by several authors in the context of incorporation of PCM in mortars for building envelopes (Lamberg *et al.* 2004, Ravikumar *et al.* 2008, Kheradmand 2012, Vaz Sá *et al.* 2012). All of these studies report that the finite element method can simulate the transient behaviour of phase change materials in the context of building physics. The key challenge in the modelling pertains to the modelling of the phase change of the PCM itself, for which specific methods will be discussed in Section 6.3. There is a wide choice of commercial FEM software, suited for implementing the PCM behaviour in the calculations, such as DIANA (Manie J 2010), ANSYS-APDL (Madenci *et al.* 2015), COMSOL (Robynne *et al.* 2011). The most important shortcoming in standard FEM simulations of thermal fields in building physics regards the simulation of the air behaviour itself in the sense that it flows and follows convective patterns. Such types of phenomena cannot be simulated with standard FEM. However, natural convection and even ventilation can play a relevant role in many practical applications, thus potentially demanding for more sophisticated approaches.

### 6.2.2 Computational Fluid Dynamic (CFD)

Computational Fluid Dynamics (CFD) models applied to building physics numerically solve a set of partial differential equations for the conservation of mass, momentum (Navier-Stokes equations), energy, chemical-species concentrations, and turbulence quantities. The solution provides the field distributions of air temperature for both indoor and outdoor spaces (Chen Q 2009). The CFD models have been widely used to study indoor air quality and thermal comfort in buildings (Chen Q 2009, Gómez *et al.* 2012, Gowreesunker *et al.* 2013). The accuracy of simulation depends on the grid resolution. Therefore, CFD models usually require much more computing time for calculations when compared with standard FEM approaches for temperature simulation. The available CFD models for predicting air temperature and distribution of air flow in buildings still bring uncertainties in predictions because of the complex air flow types such as laminar and turbulence. For example, Zhai *et al.* (2007) evaluated eight

turbulence models, that could be used for indoor environment modelling. They identified four indoor geometries, under forced, natural and mixed forced/natural ventilation and compared the numerical results with experimental data. They concluded that CFD models offer accurate results, but require much higher computing time and storage space. One of the difficulties in the modelling effort is to reproduce the programming of user defined functions (UDF) such as: the PCM effect, heat source according to the frame of the problem. Such optimization requires advanced simulation techniques that involve complex thermal exchange phenomena, leading many of currently existing simplified simulation approaches to provide results that deviate from experimental evidences (Cabeza *et al.* 2011). This method is important from the aspect of building physic modelling. Generally, for engineering problems, it is more important to obtain a solution where the general numerical solution accuracy is within the real–life uncertainties of the adequate sensors (Gowreesunker *et al.* 2013) as opposed to having a solution with very small–scale details. This allows for a quicker and more efficient use of the CFD tool for engineering purposes.

Gowreesunker *et al.* (2013) investigated the performance of PCM boards in a test cell equipped with a heating/cooling device. They modelled interior air and temperatures and then compared with experimental results. They concluded that the model was accurate enough in the air temperature values with acceptable range of errors (less than 1ºC). They also, validated a numerical model to investigate PCM building boards in a test cell. Using the model, they studied the effect of ventilation flow rates on the charging performance of the PCM boards. Employing numerical models can therefore prevent the construction of expensive experimental setups for parametric studies, as well as save considerable amount of time and resources.

In the models with large indoor spaces, the International Energy Agency (IEA) suggests that the air flow inside the space is crucial, and recommends the use of CFD for performance evaluations (Jeong *et al.* 2013).

### 6.2.3 Governing Equations

In order to predict air flow and temperature fields in indoor environments, CFD can be used by numerically solving the Navier-Stokes set of partial differential equations for mass, energy and momentum. These equations are linearized, discretized, and applied to finite volumes in the solvers to obtain a detailed solution, including velocity and

-----------------------------------------------------------------------------------------------------

temperature fields. In this thesis, the general transient heat balance equation (Incopera *et al.* 2007) was applied for the numerical treatment of the heat transfer processes in the studied models. All involved materials are considered homogeneous and isotropic. The effect of natural convection due to potential convective flows inside/outside the prototypes was considered through computational fluid dynamics(Gowreesunker *et al.* 2013):

Continuity Equation:

$$\frac{\partial u}{\partial x}+\frac{\partial v}{\partial y}+\frac{\partial w}{\partial z}=S_m \tag{6.1}$$

Where $S$ is the source term; $u$ is the velocity component along x-axes; $v$ is the velocity component along y-axes; and $w$ is the velocity component along z-axes.

Momentum Equations:

$$\frac{\partial u}{\partial t}+u\frac{\partial u}{\partial x}+v\frac{\partial u}{\partial y}+w\frac{\partial u}{\partial z}=\frac{1}{\rho_{Air}}\left(-\frac{\partial P}{\partial x}+\mu_{Air}\nabla^2 u\right)+S_x \tag{6.2}$$

$$\frac{\partial v}{\partial t}+u\frac{\partial v}{\partial x}+v\frac{\partial v}{\partial y}+w\frac{\partial v}{\partial z}=\frac{1}{\rho_{Air}}\left(-\frac{\partial P}{\partial y}+\mu_{Air}\nabla^2 v+(\rho\eta)_{Air}\,g(T-T_{ref})\right)+S_y \tag{6.3}$$

$$\frac{\partial w}{\partial t}+u\frac{\partial w}{\partial x}+v\frac{\partial w}{\partial y}+w\frac{\partial w}{\partial z}=\frac{1}{\rho_{Air}}\left(-\frac{\partial P}{\partial z}+\mu_{Air}\nabla^2 w\right)+S_z \tag{6.4}$$

Where $\eta$ is the thermal expansion coefficient; $g$ is the gravitational acceleration; $P$ is the pressure; $t$ is the time; $\mu_{Air}$ is the dynamic viscosity for the air; $\rho_{Air}$ is the density for the air; and the temperature $T$ will be computed from the energy equation.

Energy equation:

$$\frac{\partial(h)}{\partial t}+u\frac{\partial(h)}{\partial x}+v\frac{\partial(h)}{\partial y}+w\frac{\partial(h)}{\partial z}=\frac{k}{(\rho C_p)_{Air}}\left(\left[\frac{\partial^2 T}{\partial x\partial y}\right]+\left[\frac{\partial^2 T}{\partial z\partial y}\right]+\left[\frac{\partial^2 T}{\partial x\partial z}\right]\right)-S_E \tag{6.5}$$

The density of the air is calculated based on the compressible ideal gas flow law as follows:

$$\rho_{Air} = \frac{P}{RT}$$

(6.6)

Where $R$ is the universal gas constant.

In regard to boundary conditions applied to the temperature field computation, interaction with an 'infinite' surrounding air medium can be expressed through convective/radiative boundary fluxes, as shown in Eq. (6.7), where $T$ is the temperature (ºC), $T_s$ is the surface temperature (ºC) and $h_{eq}$ is a convection/radiation coefficient that depends on air speed (W/m K):

$$q = h_{eq}(T - T_s)$$

(6.7)

Discretisation is a way to the process of breaking down the terms of the governing Equations (mentioned above) into simpler discrete algebraic forms in order to be solved. It can also refer to the breaking down of the flow domain into separate control volumes. For the purpose of illustration, Figure 6-1 shows schematic of mesh discretization, which allows the production of localised solution fields for a particular domain. In this figure, the cell centre values are labelled as 1, 2, 3, 4 and 5, while the face values are labelled as a, b, c and d. The approximate form of the governing equations is applied to each control volume and the face values are required to obtain a solution.
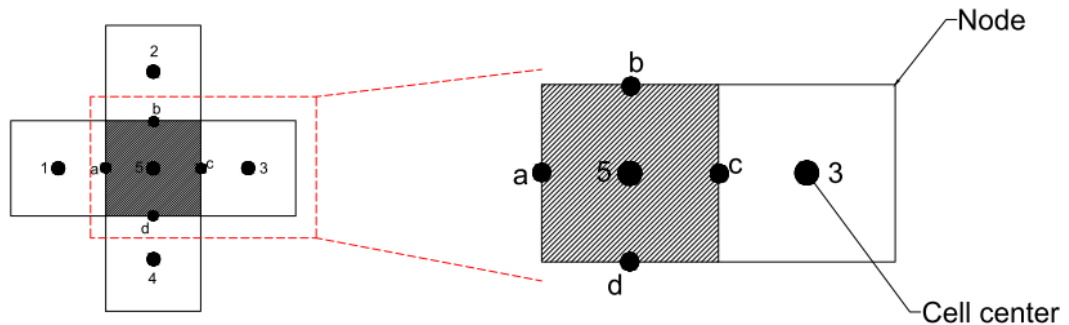


Figure 6-1: schematic of the mesh discretization.

111

## 6.3 Thermal modelling of phase change

The phase change mechanism occurs in several natural and industrial processes which have significant environmental and financial impact (Hassan A 2010). As the variety of processes involving phase change is increasing, so is the scope and complexity of modelling. The present section aims to provide an insight on the numerical simulation of phase change processes and the typical methods to consider the latent energy storage/release by PCMs.

### 6.3.1 The Enthalpy-Porosity Method

Theoretically, PCM is treated with three separate states during the phase change procedure which called: solid, liquid, and phase change state. The phase change state is a transient stage between solid and liquid. In this stage PCM exists within the material in both the solid and liquid phase simultaneously. The governing equation for this model is re-configured to consider enthalpy as the variable. This equation is identical for both phases; the single interface is replaced and treated as the phase change state between the two phases. The creation of the phase change state and the rate of change of its volume and thickness are governed by the rate of absorption/release of the latent heat.

In fact, in this method, relationship between enthalpy-temperature is defined as $\Delta H = f(T)$ to model the effect of phase change.
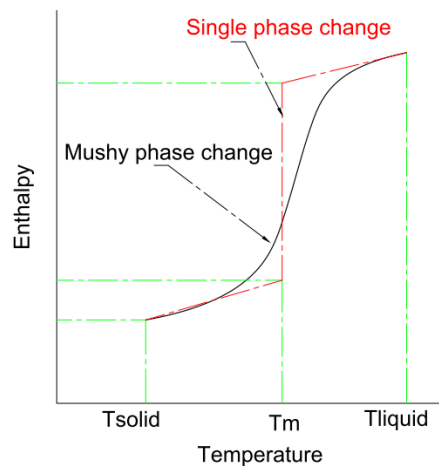


Figure 6-2: Enthalpy-Temperature relationship.

Research by Hong *et al.* (2004) was focused on materials with discrete phase change temperatures, where the enthalpy-temperature relationship was a step function. However, as most materials possess a phase change temperature range (i.e. a mushy region), with the enthalpy changing with different temperatures within the mushy region (Figure 6-2), the problem becomes more complex.

The effects of the mushy zone are modelled through a parameter known as the liquid fraction ($\beta$), which has been adopted by various commercial packages, such as ANSYS–FLUENT. The liquid fraction is defined as Eq.(6.8):

$$\begin{cases} \beta = 0; & if \quad T < T_{Solidus} \\ \quad \beta = \dfrac{T - T_{Solidus}}{T_{Liquidus} - T_{Solidus}} & if \quad T_{Solidus} < T < T_{Liquidus} \\ \beta = 1; & if \quad T > T_{Liquidus} \end{cases} \tag{6.8}$$

From Eq. (6.8), $\beta$ is obtained by the lever rule and the latent heat content of the material can be expressed as $\Delta H = \beta L_f$ (where $L_f$ is the total latent heat). In fact, the lever rule assumes linear relation between enthalpy-temperature, while it may not be entirely true.

The latent heat can therefore be incorporated into the governing energy Eq.(6.5) and the total energy in the control volume with phase change given by Eq.(6.9).

$$H = h_{ref} + \int_{T_{ref}}^{T} C_p dT + \beta L_f \tag{6.9}$$

In which $h_{ref}$ is reference enthalpy; $T_{ref}$ is reference temperature and $C_p$ is specific heat at constant pressure. Hence by replacing Eq.(6.9) into the governing energy equation (Eq.(6.5)), the effect of phase change can be modelled as follows (Eq.(6.10)):

$$\frac{\partial}{\partial t}(\rho H) + \nabla(\rho u_j H) = \nabla(k \nabla T) \pm S_E \tag{6.10}$$

Vaz Sá *et al.* (2012), applied this method to numerically simulate transient thermal behaviour of the PCM plastering mortar. They conclude that the numerical results match quite closely to those recorded in the experimental results.

However, one drawback of this method is the procedure to quantify the rate of change of liquid fraction that may have a negative impact on the accuracy of the method.

### 6.3.2 The Effective Heat Capacity Method

The basis of the effective heat capacity method is similar to the enthalpy-porosity method, but instead of directly influencing the enthalpy of the PCM as in Eq. (6.5), it models phase change as a sensible process with an increased (effective) heat capacity. (Zhang *et al.* 2014). This can be visualised in Figure 6-3.
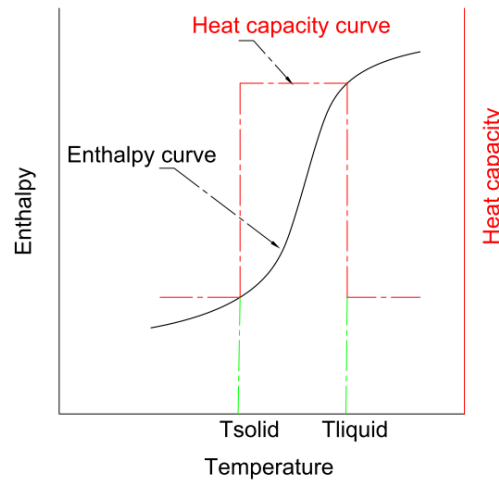


Figure 6-3: Effective heat capacity curve compared with enthalpy curve.

In the effective heat capacity method, a new parameter known as the effective heat capacity ( $Cp_{eff}$ ) defines as follows Eq.(6.11) (Al-Saadi *et al.* 2013):

$$
\begin{cases}
Cp_{eff} = Cp_{solid}; & if \quad \text{T} < T_{Solidus} \\
Cp_{eff} = \left[(1-\beta)Cp_{solid} + Cp_{liquid}\right] + \left[\dfrac{L_f}{T_{Liquidus} - T_{Solidus}}\right] & if \quad T_{Solidus} < T < T_{Liquidus} \\
Cp_{eff} = Cp_{liquid}; & if \quad \text{T} > T_{Liquidus}
\end{cases}
\tag{6.11}
$$

Where $\beta$ is the liquid fraction defined by Eq.(6.8). Consequently, without explicitly tracking the phase change a numerical phase change can be obtained by iterating between Eqs.(6.8), (6.11) and (6.12) as following expression:

$$\frac{\partial}{\partial t}(\rho Cp_{eff}T) + \nabla(\rho Cp_{eff}u_jT) = \nabla(k\nabla T) \pm S_E \qquad (6.12)$$

One of the limitations of the effective heat capacity method is that, small time steps required for the analysis with this method due to the fact that, in the case that the total phase change happens in one time step, with the large time steps its effect will not be captured. Thus, small time steps are required, consequently increasing the computational time.

## 6.4  Numerical simulation approaches adopted in this research

The general set up for a CFD simulation consists of a model generator, a CFD solver and a post–processor. In this study, ANSYS–FLUENT was used as the CFD solver.

Discretization of the terms of the governing equations into algebraic forms in the ANSYS–FLUENT handles using a control-volume-based technique to convert the governing equations to algebraic equations that can be solved numerically. The control volume technique consists of integrating the governing equations for each of cell (control volume), discrete equation that conserve each quantity on a control–volume basis (ANSYS FLUENT 2015). In the other hand, ANSYS-FLUENT uses a control volume approach (also referred to as a finite volume approach) to calculate the dependent variables (e.g. $T$, $v$) at the centre of each cell; however, these variables are needed at cell faces to compute fluxes. A second order upwind discretization scheme is employed to compute variables at the momentum, density and energy. The second order upwind scheme uses a Taylor series expansion of the variable about the cell face to compute flux values. The SIMPLE algorithm was used for the pressure–velocity coupling (ANSYS FLUENT 2015). The SIMPLE algorithm initially solves for a velocity field using a given pressure field, and velocity field. This will give an intermediate velocity field. The final solution for the velocity field must satisfy the continuity equation. Once the pressure correction is found, a velocity correction is

calculated. Finally, all other equations are solved using the updated pressure and velocity fields.

### 6.4.1 Phase change modelling strategy

Two typical methods have been introduced to simulate the latent heat energy release/absorption during phase change processes. In this study, the effective heat capacity method was used to simulate PCM effect. In this way, the effective heat capacity of the PCM as a function of temperature, which was obtained from the DSC measurement, was used in the calculations.

In fact, phase changes were modelled through a simplified approach by which the energy release/absorption associated to the phase change process is considered through artefacts applied to the specific heat capacity term.

The computation of the specific heat capacity of the specimen along the tested temperatures $C(T)$ (J/g K) is made according to Eq.(6.13):

$$C(T) = \frac{\left( DSC(T)_{sample} \right)}{\varphi} \tag{6.13}$$

Where $DSC(T)_{sample}$ the heat flow across the specimen at temperature $T$ from the thermogram (mW/mg), and $\varphi$ is the heating rate (°C/s). This method allows to implement directly of specific heat capacity curve into the software which is useful since the sensible heat and latent heat are not distinguishable in the DSC output curve (particularly in the hybrid PCM case); therefore, the state of the PCM is not necessary to be defined as all the entire curve is given to the model.

### 6.4.2 Simulation parameter estimation

Even though the experimental program did not encompass testing of a prototype containing a single type of PCM embedded, such situation was tackled in the numerical simulation, as to illustrate the performance advantages of the hybrid PCM concept (HPCMM). Therefore, a single PCM mortar, termed as SPCMM was added to the process of numerical simulations. The single PCM mortar selected for such comparison

corresponds to a mix that has been performed and tested in the previous chapter, which contains 18.34 % weight of PCM with melting temperature of 24°C. It is worth to mention that, such a melting temperature (around 24°C) is usually used for human thermal comfort purposes (Vaz Sá *et al.* 2012, Evola *et al.* 2014, Jaworski 2014, Cunha *et al.* 2015). Furthermore, three fictitious single PCM mortars made of 18.34% of RT10 (here termed as SPCMM10), BSF26 (here termed as SPCMM26) and MC28 (here termed as SPCMM28) distinctly were also considered.

As the experimental program did not include the thermal characterization of single PCM mortars, their properties had to be estimated for the numerical simulations.

In order to support such estimates, specific DSC experiments were conducted on the relevant PCMs: RT10, MC24, BSF26 and MC28. One specimen per each type of PCM was considered and the weight of the prepared specimens was of 4.185 mg, 5.76 mg, 5.271 mg and 5.126 mg for RT10, MC24, BSF26 and MC28 respectively. The applied program for DSC testing was analogous to those already made for mortars (detailed in chapter 4). The graph of Figure 6-4a shows that obtained results are in accordance with the characteristics given by the manufacturers (Microthermic 2012, Rubitherm GmbH 2012).

In order to estimate the specific heat capacity curve of single PCM mortars (to be used in the numerical simulations), the method forwarded by (Tittelein *et al.* 2015) was utilized. It consists in a proportional mixing law for the specific heat, based on the constituents of the mortar, their weight proportions and their individual specific heat capacities. Therefore, the specific heat capacity of the mortar can be estimated through Eq.(6.14):

$$C_{specimen} = C_{PCM} \times W_{PCM} + C_{mortar} \times W_{mortar} \qquad (6.14)$$

Where $C_{specimen}$ is the specific heat capacity of the specimen (J/kg K); $C_{PCM}$ is the specific heat capacity of the PCM (J/kg K); $W_{PCM}$ weight ratio of the PCM to the specimen; $W_{mortar}$ mass fraction of the plain mortar and $C_{mortar}$ is the specific heat capacity of the plain mortar (J/kg K). Therefore, the specific heat capacities that were considered for the mortars are presented in the Figure 6-4b.

For the particular case of SPCMM, values of relevant properties were obtained from a chapter4 with this mortar: density of 1360.9 kg/m$^3$ and thermal conductivity of 0.3 W/m K. And also these values were considered with same quantities for other single PCM mortars with RT10, BSF26 and MC28.



**(a)**          **(b)**
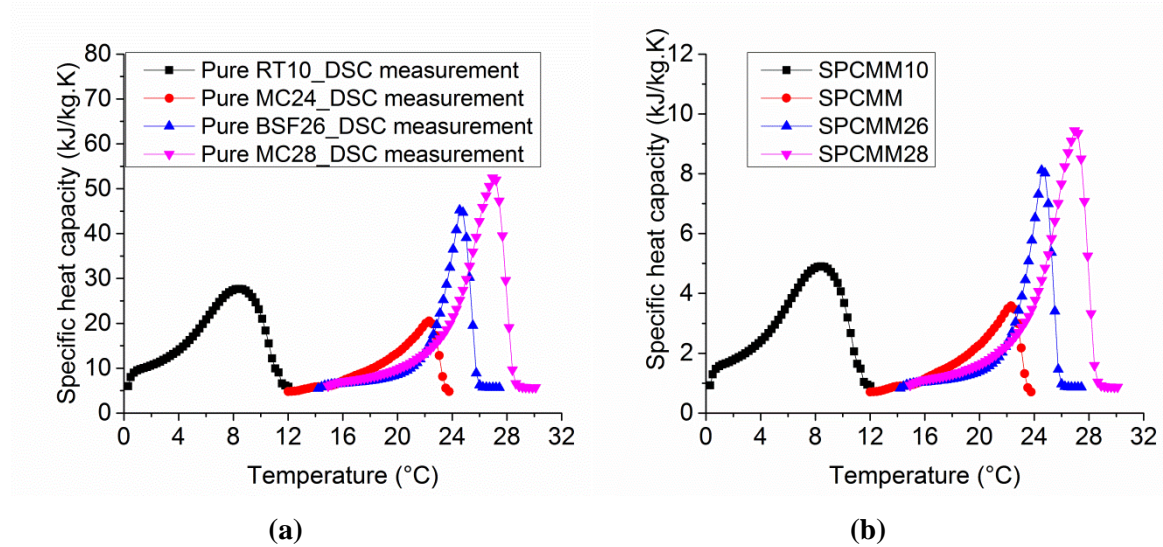
Figure 6-4: (a) Specific heat capacities calculated with the DSC outputs for the pure PCM specimens (RT10, MC24, BSF26 and MC28); (b) Estimated specific heat capacity curves of the single PCM mortars.

## 6.5   Numerical simulation of small scale prototype

In this section, a numerical simulation model was employed to validate the capacity of simulating temperature evolution within the prototypes tested in the scope of this section. This section contains two sub sections in which the first sub section deals with the numerical simulation of the small scale prototype without considering natural convection effect. In the second sub section, all the simulations accounted for natural convection effects as to demonstrate its influence on the prediction of numerical simulations.

### 6.5.1   Numerical consideration: without natural convection effect

In specific regard to the simulation model of the 0.46 m× 0.46 m× 0.46 m prototype, two vertical symmetry planes were considered, leading to the necessity of solely modelling one fourth of the prototype (0.23 m× 0.23 m× 0.46 m), according to the geometry shown in Figure 6-5. The computational mesh was built by using hexahedral cells (8 nodes) with typical size of 10$^{-6}$ m$^3$. A constant time step ($\Delta t$) of 300 s was also

considered. The grid size and the time step were chosen after careful examination of the independency of the results to these parameters. Taking into account the nonlinearities of the solution process associated to the phase change processes, which induced temperature dependency on the specific heat, specific attention was given to the accuracy of results in such concern. In this way, the energy–based convergence criterion was checked at each time step, with relative variation under $10^{-7}$. The generated finite volume mesh resulted in 25944 cells, depicted in Figure 6-5. The exterior top, bottom and lateral surfaces (except for the symmetry planes), were assigned with convective thermal boundary conditions, taking into account the varying temperature imposed in the climatic chamber (recorded values) as shown in Figure 5-6. As the prototypes were placed inside an indoor climatic chamber, a value of $h_{eq}$ = 5 W/m K (Azenha  M 2009) was considered for the surface convection coefficient, in correspondence to near stagnant air conditions. The material properties of the prototypes are given in Table 6-1.
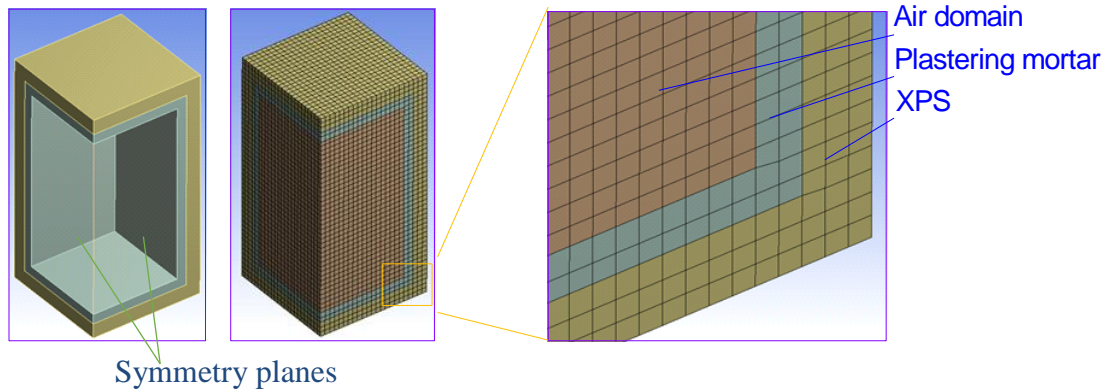


Figure 6-5: The 3D geometric model, model mesh and zoomed mesh.

Table 6-1: Thermo-physical properties of the materials used in REFM and HPCMM prototypes.

| Thermo-physical Properties | Ab. | Units | REFM (internal coating) | HPCMM (internal coating) | XPS [a] (external coating) |
|---|---|---|---|---|---|
| Density | $\rho$ | [kg/m$^3$] | 1529.5 | 1309.8 | 32 |
| Thermal conductivity | $k$ | [W/m K] | 0.4 | 0.3 | 0.034 |
| Specific heat capacity | $C_p$ | [kJ/kg K] | Figure 5-4 | Figure 5-4 | 1400 |

a Thermo-physical properties of XPS was provided by the supplier (Fibran 2013).

-----------------------------------------------------------------------------------------------------------

In the symmetry planes, adiabatic boundaries were considered. It should be mentioned that, the characteristics of the air materials used in the simulation are in correspondence to the air temperature of 24ºC as forwarded: density of 1.225 kg/m$^3$, specific heat capacity of 1006.43 J/kg K and thermal conductivity of 0.0242 W/m K.

### 6.5.2 Results of the numerical simulations

The numerical algorithm was initially validated by comparing its predictions with experimental results available in the literature. The available experimental work by (Vaz Sá *et al.* 2012) has been considered to validate the model. Such experimental work encompassed similar small-scale prototypes, which contained a single-PCM mortar. The simulation framework adopted herein is fairly similar, and its validation was achieved by simulating the experiments of, with differences of predicted temperatures below 0.1ºC in comparison to their experimental results (Vaz Sá *et al.* 2012). Such confidence in the numerical simulation framework was a cornerstone to the remaining numerical simulations presented in this chapter.

The comparison of experimental and simulation results for prototypes with REFM and with HPCMM are shown in Figure 6-6 for the summer scenario, and in Figure 6-7 for the winter scenario.
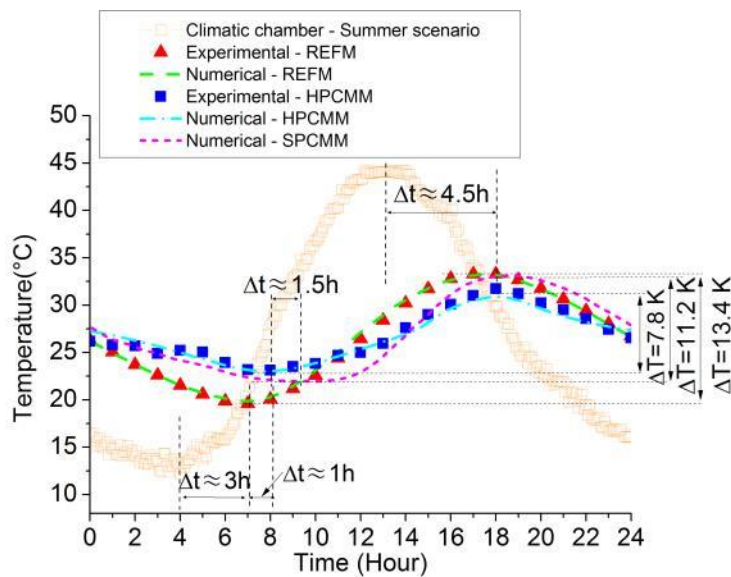


Figure 6-6: Experimental versus numerical values for test cells REFM and HPCMM (summer scenario).

--------------------------------------------------------------------------------------------------------------
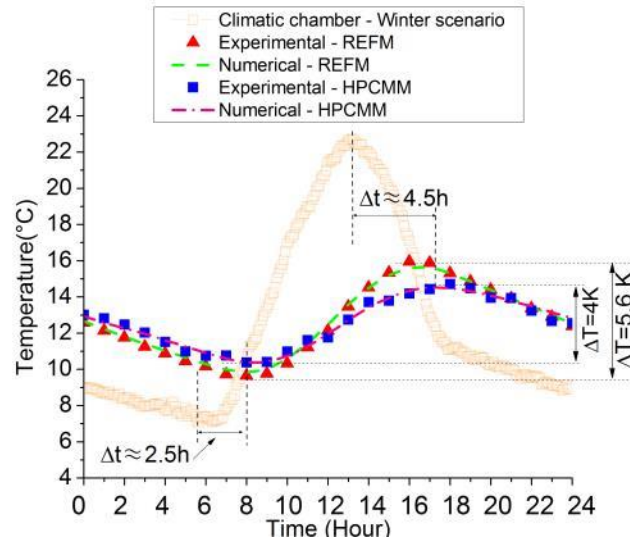


Figure 6-7: Experimental versus numerical values for test cells REFM and HPCMM (winter scenario).

From observation of both figures, it can be confirmed that the numerical predictions for the T–t evolutions match quite closely the ones measured by the temperature sensor (PT100), within error margins below 0.1ºC upon validation criteria of RSME.

Even though the simulation of the winter scenario was successful, thus adding value to the validation of the simulation framework, no further discussions will be made on such scenario due to the reasons highlighted before, according to which the prototype for winter would need to take into account the existence of heating devices to bring temperatures nearer to comfort levels. Based on the high confidence level provided by the validations mentioned above, a further simulation was carried out for the summer scenario, in which the mortar of the prototype encompassed a single type of PCM with melting temperature of 24ºC (termed SPCMM), with the composition mentioned in earlier. The results of such simulation can better assist evaluating the potential benefits that the hybrid PCM concept can bring about. The results of the simulation for SPCMM are included in Figure 6-6 for direct comparison of performance with REFM and HPCMM. As it can be seen in Figure 6-6, the maximum peak temperatures are reached with about 4.5 h delay in comparison to the maximum peak in the climatic chamber, regardless of the fact that the mortar has PCM or not. Furthermore, the minimum temperatures are reached with delays of nearly 3 h, 4 h and 5.5 h for the cases of REFM, HPCMM and SPCMM compared with the minimum environmental temperature respectively. Minimum temperatures in the SPCMM and HPCMM are nearly 2°C and

2.5°C higher than in the REFM case. Smoother heating/cooling processes are exhibited for the cases in which PCM-based mortars are used (both HPCMM and SPCMM) in comparison to the reference mortar.

It is interesting to note that, heating and cooling processes are smoother for HPCMM prototype than for the simulated SPCMM prototype. The reason might be due to the existence of a wider phase change domain in the case of HPCMM (between 2ºC to 29ºC as shown in Figure 6-4), as compared to the narrow domain of actuation of MC24 seen in Figure 6-4 (approximately ranging from 12ºC to 24ºC). The surface temperature of internal walls is one of the most important thermal comfort parameters in a room (Catalina *et al.* 2009). The following analysis shows the effects of latent heat storage on the thermal behaviour of the internal plastering mortar.

To better understand the PCM action, Figure 6-8 compares the simulated temperature evolution at mid-depth of the mortar layer for both the HPCMM and REFM prototypes under summer and winter scenarios with the corresponding external environmental temperature. In this figure, the relevant phase change domain temperatures of the PCMs present in HPCMM are signalled with a shaded region: (i) for the summer scenario, the shaded region ranges 20.5ºC–27.5ºC corresponding respectively to the onset temperature of BSF26 and the end temperature of the MC28; (ii) for the winter scenario, the shaded region ranges 9ºC-16ºC, corresponding to the onset and end temperatures of RT10.



**(a)**                                         **(b)**
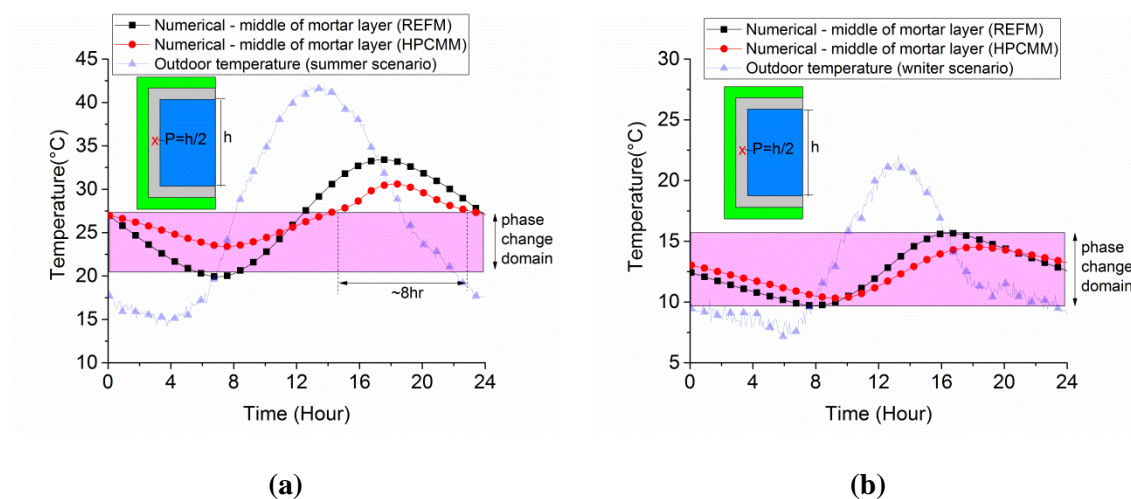
Figure 6-8: Simulation of evolution of temperature at mid-depth of the mortar layer (labelled as P) for both REFM and HPCMM prototypes: (a) summer scenario; (b) winter scenario.

--------------------------------------------------------------------------------

Figure 6-8a, b shows that the internal mortar temperature (labelled as P) for HPCMM keeps within its phase change domain for about 67% and 100% of the time of each daily cycle, respectively. This is a clear indication that the capacity to store/release energy of the PCMs present in the mortar is being constantly or almost constantly deployed, in correspondence to an adequate design of the hybrid PCM blend.

For further illustration of the effect of PCM in the mortar, Figure 6-9 shows the calculated temperature profile in the wall layer of the HPCMM prototype at several instants within a given daily cycle (summer scenario).
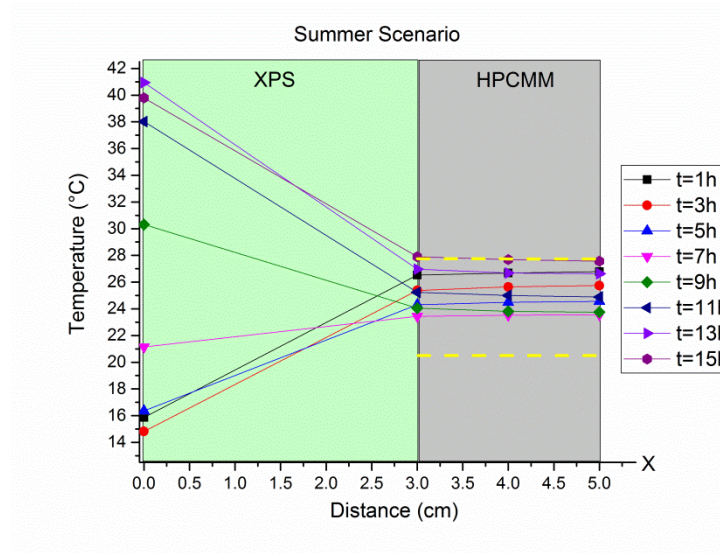


Figure 6-9: Temperature variations along the thickness of the wall of HPCMM prototype at different hours in summer scenario.

The selected instants that range 1h to 15h show that the HPCMM layer is enduring a quasi-isothermal state at such stage (attained by latent heat storage/release), while the temperatures in the outer XPS layer keep oscillating with significant gradients, according to the outer environmental temperature (Vicente *et al.* 2014). Naturally, this capacity is manifested within the relevant melting ranges of the PCMs present in the mortar, as identified by horizontal dashed lines in Figure 6-9: onset temperature of 20.5ºC for BSF26 and end temperature of 27.5ºC for MC28. Similar findings/conclusions can be attained by analysis of the winter situation.

The potential to save energy induced by the presence of hybrid PCM materials may be discussed with basis on the observation of the various temperature evolutions. Usually, the calculation of accumulated energy is performed with basis on heat flux

measurements (Sayyar *et al.* 2014). However, in the absence of heat flux measurements, this work relies on a simplified approach that can provide indirect information about energy savings for cooling. For the purpose of comparison, a set of transient thermal analysis was performed for single PCM mortars (those were estimated and mentioned in section 6.4). However, for the sake of brevity/coherency, the results of thermal behaviour of single PCM mortars are avoided and not further discussed as the target is to have a comparison between all the studied cases in term of energy saving potential hereafter. The process is quite simple and it is illustrated in Figure 6-10. First, a maximum threshold temperature for comfort was established as 26ºC for the summer scenario.

When the temperature within the studied prototype overcomes this threshold, the internal environment is considered to be within a discomfort period, and a penalty function is calculated by integrating the time-temperature diagram with the baseline of the threshold temperature (shaded Region A in Figure 6-10). The global value of such penalty function for a full daily cycle is expressed as the TT index (units: ºCh). This TT index can be used as a comparative performance indicator in terms of cooling needs: the higher the index, the higher the cooling energy demands are. The results of the calculated TT index are shown in Figure 6-11.
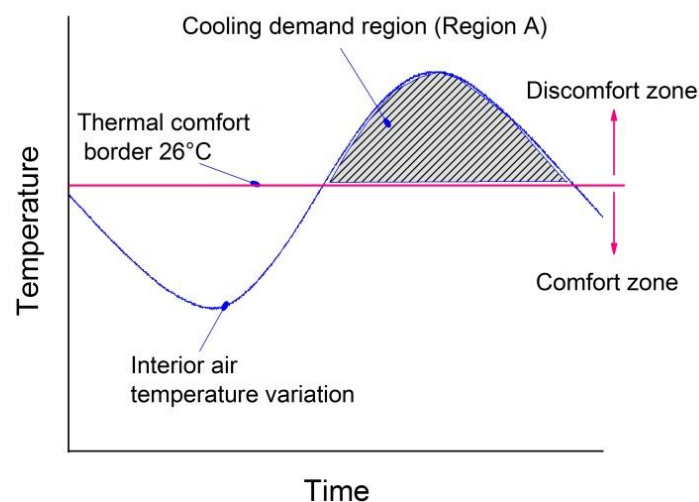


Figure 6-10: Theoretical bases of temperature along time strategy with respect to the thermal comfort level during a cycle (includes a day and a night).

These results reveal that, in the tested summer day, the HPCMM mortar is clearly the best-performing material in terms of thermal comfort and potential energy savings.

-------------------------------------------------------------------------------------------

Indeed, it outperforms any of the other alternatives by more of 50% reduction in TT. It is also interesting to note that inadequate selection of PCM can bring even worse behaviour as compared to REFM. This is the case of SPCMM10 and SPCMM (includes MC24). The reason for this decreased behaviour is that the phase change of both these PCMs (ranges of operation identified in Figure 6-4) is never mobilized with the sol-air temperature that is being imposed to the prototype, and also because the volumetric specific heat of SPCMM10 and SPCMM is smaller than that of REFM.
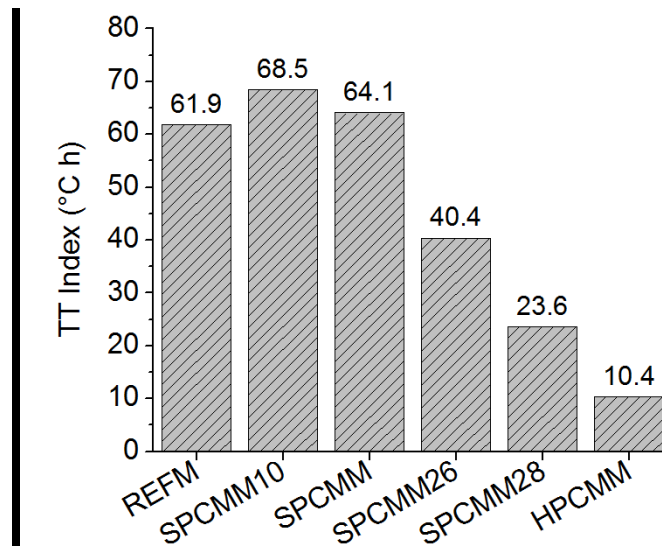


Figure 6-11: Comparison between different cases on the total required cooling temperature through time (based on calculation of region A) in order to turn the temperature at comfort level.

## 6.5.3  Numerical consideration: with natural convection effect

A set of simulations was performed to compare the modelling strategies of disregarding or considering the effect of natural convection in the temperature simulations. The exact same summer scenario as reported in the previous section was used, but in this case, the simulation of air movement was explicitly considered.

Figure 6-12, presents the mesh of the model considered in the present simulation, and zoomed mesh distribution in walls and air boundary layer. The mesh was designed using the Pointwise meshing software (Pointwise Inc. 2015), and the resulting mesh comprised of hexahedral cells in the near-wall inflated layers and wall domains as well as in the air domain. A fine mesh size was considered, composed by cells with

--------------------------------------------------------------------------------------------------------------------

minimum volume $9.9\text{x}10^{-10}$ m$^3$ and maximum volume $2.43\text{x}10^{-2}$ m$^3$. Time stepping was fixed at both 50s and 300s in two separate analyses, as to verify the independency of results in regard to time discretization. Air was considered as an ideal gas.
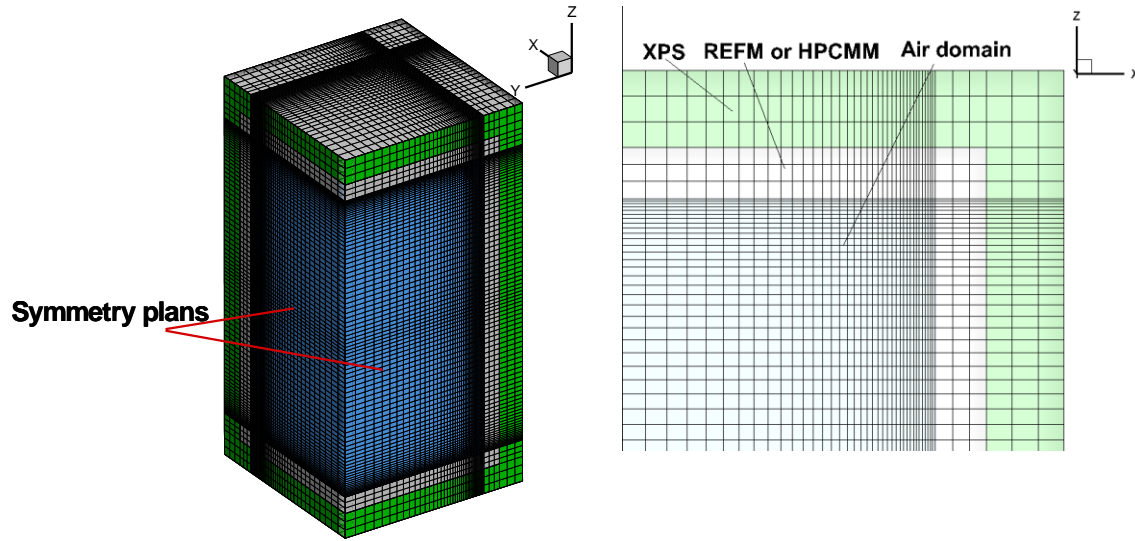


Figure 6-12: Mesh of one-fourth of the numerical thermal model and zoomed mesh distribution in walls and air boundary layer.

## 6.5.4   Results of the numerical simulation

Figure 6-13 shows the results for the summer scenario model, comprising both the case in which natural convection is considered, and the case in which natural convection is neglected for both REFM and HPCMM. It can be observed that the similitude of the simulation results in both simulation approaches is quite remarkable, with relative temperature differences below 0.2ºC (for both REFM and HPCMM).

Even though the results simulation approach that considers natural convection allowed a better coherence with the experimental results, the margin of error of the simplified analysis without convection is small enough to be considered acceptable for the aims envisaged in this thesis.

**(a)**                                        **(b)**
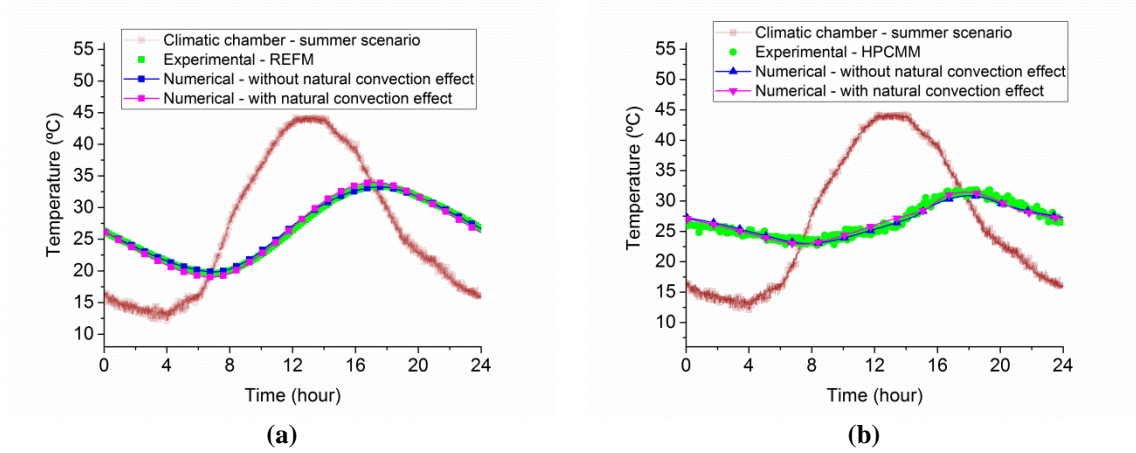
Figure 6-13: Temperature-Time variation and corresponding errors in compare with experimental results of the studied cases with and without natural convection effect under summer scenario: (a) REFM case; (b) HPCMM case.

It is further remarked that the homogeneity of temperature within the air inside the test box was also checked among three levels inside the model as exemplified in Figure 6-14. It is seen that the differences in temperature between top, centre and bottom of the air inside the box tend to remain within less than 0.1ºC, thus further highlighting the small relevance of natural convection effects.



**(a)**                                        **(b)**
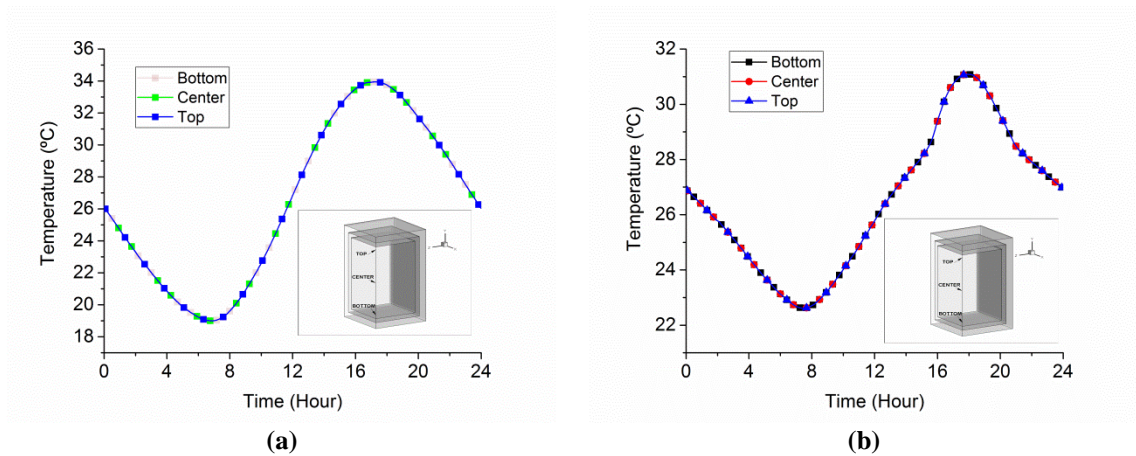
Figure 6-14: Simulated temperature-time variation at three different points inside the prototypes: (a) REFM case and (b) HPCMM case.

Based on the analyses and illustrations mentioned above, it can be concluded that the assumption of negligible natural convection for the cases under study is plausible.

## 6.6   Numerical simulation of small scale prototype with heater unit

This section presents the simulation of the experiments in the small scale prototype in which the heater unit was included. This experiment and its results have been thoroughly described and discussed in Section 5.2.6. In the following section, the accuracy of the current model, which explicitly considered the effects of air convection (due to the expectable importance of convection induced by the heater), was assessed for both cases of REFM and HPCMM. The control of the heater was implemented in ANSYS–FLUENT as User Defined Functions (UDF), which allow programming extensions to the capacities of the program through small scripts in C language.

### 6.6.1   Model consideration and User Defined Function

The external surfaces of the prototypes are bounded by convective heat transfer conditions as shown in Figure 5-10.

A simplified approach was employed to simulate the behaviour of the heater. In fact, the heater was controlled by a PID (proportional- integrative-derivative) temperature controller, whose PID parameters were unknown. The simulation performed herein considered the simplification of a simple ON-OFF controller on a heater with dimensions of 0.02m×0.02m×0.1m, with power of 300 W. Since the ANSYS-FLUENT requires such values in the unit of W/m$^2$, a heat generation rate of 34129.7 W/m$^2$ was considered in the model.

The location of and size of the heater in the simulation model, shown in Figure 5-10, match the actual situation of the experiment. The mechanism of the heater is illustrated in Figure 6-15. In fact, the sensor of the heater is controlled through bottom sensor within the prototype. The UDF code is also presented in Appendix A.

Since the presence of air movement inside the prototype predominated with heater element, the presence of convection effect for the air might be important to be considered in which pertains the flow equations.
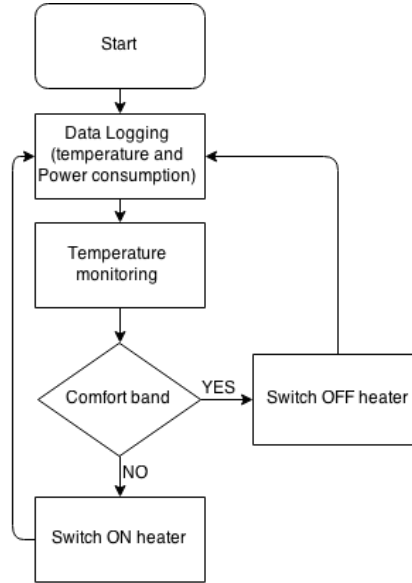
Figure 6-15: Mechanism of the system with heater implemented into the simulation model.

In this way, two types of solutions were studied: with consideration of convection effect in the air and the second round, no convection effect in the air. In this way, for the solutions were the flow equations are being solved, the air was considered as an ideal gas. The material properties of the wall are given in Table 6-1.

A constant time step size ($\Delta t$) of 60 s was considered. The convergence criterion at each time step was checked under $10^{-3}$ for momentum equation, $10^{-3}$ continuity equation and $10^{-5}$ for energy equations (Wang *et al.* 2011). In specific regard to the simulation model of the $0.23$ m$\times 0.23$ m$\times 0.46$ m prototype, one-fourth of the model was considered, according to the geometry shown in Figure 6-16.

The employed mesh is shown in Figure 6-16.The resulting mesh comprised of hexahedral cells in the air and wall domains. The mortar layer contains 2 mesh intervals along the thickness. The mesh minimum cell size of 6.6 x $10^{-9}$ m$^3$ and maximum cell size of 2.2 x $10^{-6}$ m$^3$ was obtained.

**(a)**        **(b)**
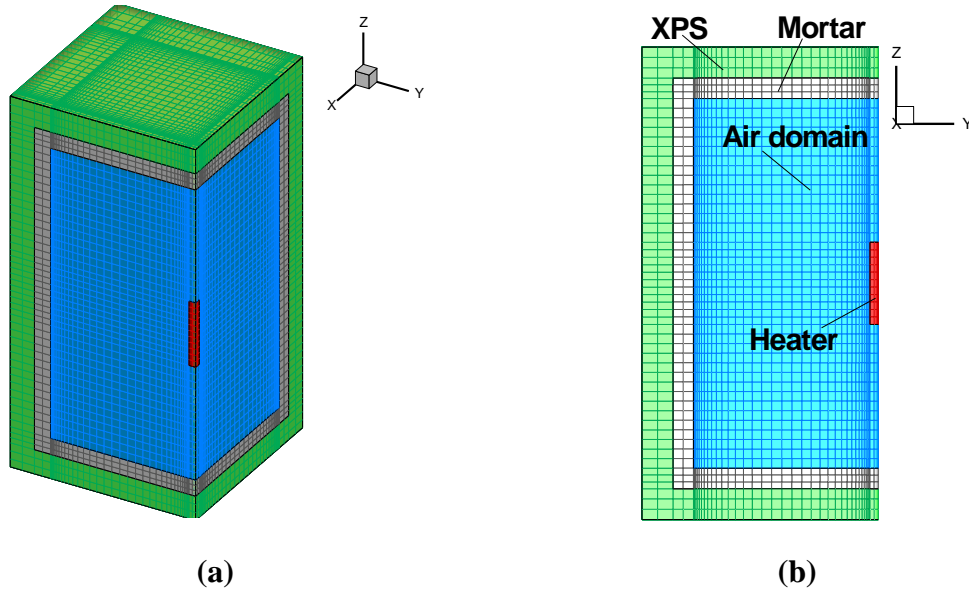
Figure 6-16: (a) One-fourh 3D mesh of the model; (b) Cross section of mesh distribution in walls and air boundary layer.

The exterior surfaces were assigned with convective thermal boundary conditions, taking into account the varying temperature imposed in the climatic chamber. A value of $h_{eq}$ = 5 W/m K was adopted for the same reasoned mentioned in the section 6.5.1.

In both cases, the model was initialized from 27ºC, with the external air temperature increasing with the 300 W heater turned on to maintain the ambient temperature of the prototype at comfort level (20ºC) during tested period.

### 6.6.2   Results of the numerical simulations

The results of numerical simulation of prototypes equipped with heater unit for both cases of REFM and HPCMM are presented in Figure 6-17 and Figure 6-18 respectively. As it can be seen in these figures, The controller function for the heater is working properly and sets the temperature at 21ºC to be matched with experimental results in both cases of REFM and HPCMM. However, the predictions of the air temperatures within small scale prototypes are not adequately achieved for the middle and top monitored points. These temperature miss predictions might be related with problem in airflow simulation.

---------------------------------------------------------------------------------------------



**(a)**                                        **(b)**



**(c)**
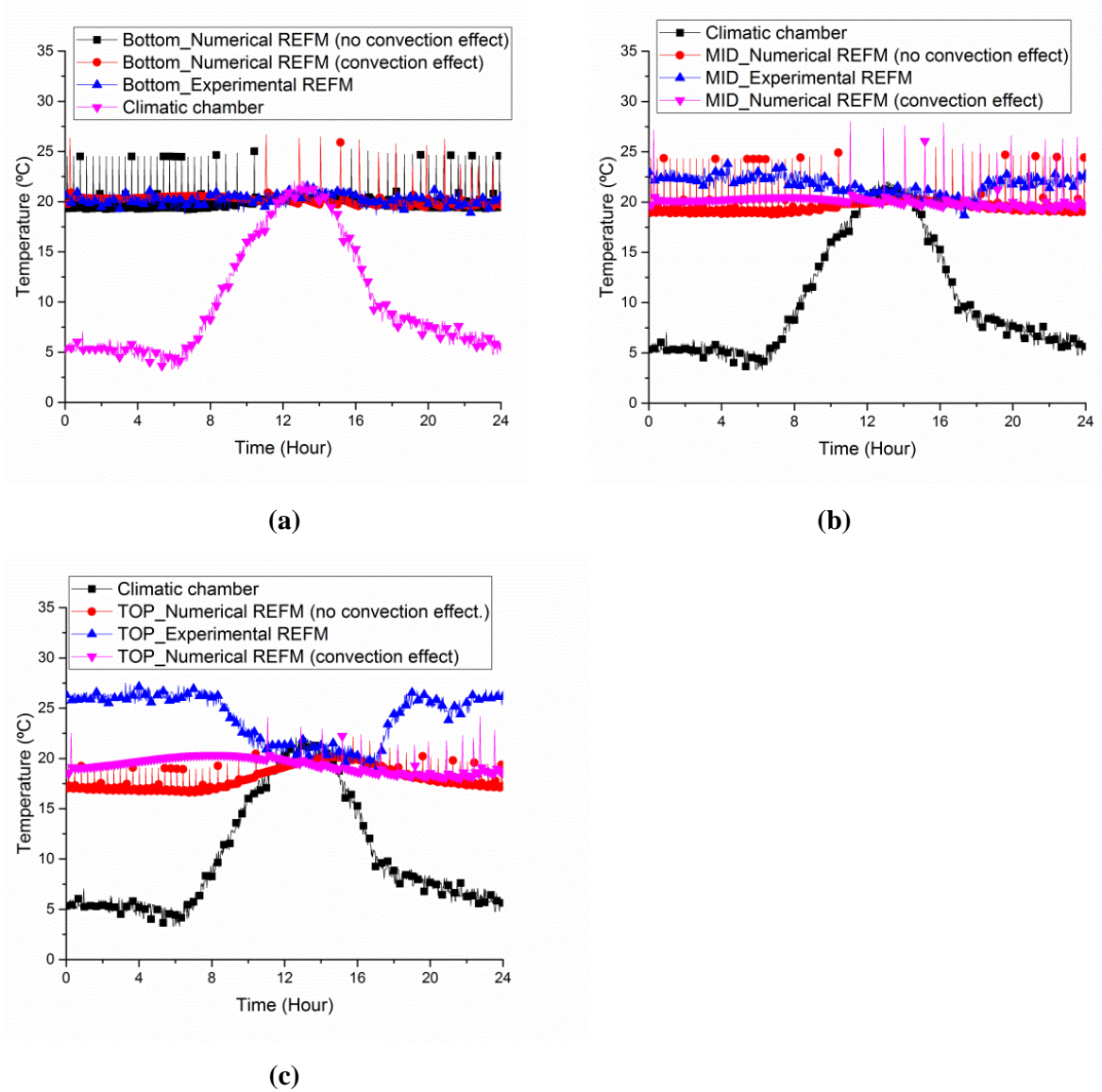
Figure 6-17: Comparison of monitored temperature variations between experimental and numerical simulation of REFM case: (a) bottom point; (b) middle point; and (c) top point.

It should be mentioned that, in the experimental work, the temperature controller was handled by PID controller in order to use the heater in a more efficient manner and turn as much as faster to the predefined set point temperature. This usually brings a complexity to the numerical simulation due to the fact that, three parameters of P, I and D, need to be given to the model. Since these parameters of P, I and D were not known, it was considered advisable to make the numerical simulation regardless to these parameters. In fact, the heater would produce different air pattern when the PID is used in the numerical simulation. As it can be seen in these figures, neither of numerical predictions with or without convection effect was not able to directly match the experimental results (particularly the temperatures at middle and top points) by

131

--------------------------------------------------------------------------------------------

differences of ~5ºC. One possibility of such differences can be related to the numerical simulation that does not account for effect of PID controller algorithm. Therefore, in all the cases, several disturbs in the temperature variations along time can be observed. However, the results with consideration of both with convection effect are better than that of cases were accounted for no convection effect as the effect of convection due to the air movement inside the prototypes which is actually modelled.



**(a)**                                                                          **(b)**



**(c)**
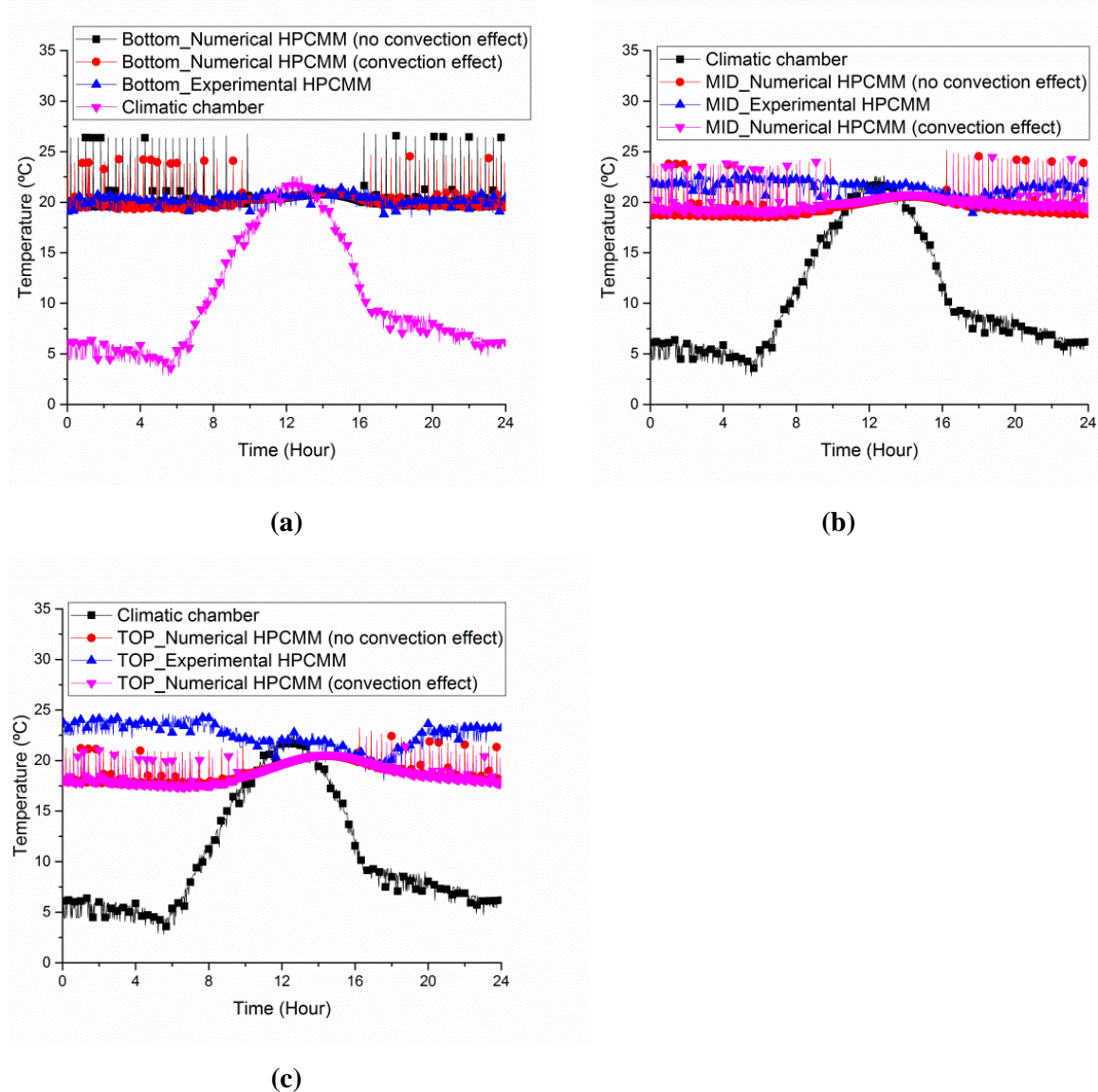
Figure 6-18: Comparison of monitored temperature variations between experimental and numerical simulation of HPCMM case: (a) bottom point; (b) middle point; and (c) top point.

Solely attention to the both cases of REFM (Figure 6-17a) and HPCMM (Figure 6-18a), the bottom points are following the same trend as the experimental results for both studied cases: with convection effect and without convection effect. It can be seen in

these figures, there are peak temperatures that illustrate the status of the heater in which it is ON or OFF mode. The sensitivity analysis indicated the influence of the convection effect on the temperature predictions within the prototypes and is compared with the case when no convection effect was considered rather than experimental results. In this basis, the model is valid for set temperature of the heater regardless of PID effect. The result further suggests considering the convection effect in the numerical simulation with the heater unit as the results are slightly better than of the experimental results. Therefore, from now on, the numerical simulations are accounted for the convection effect as to predict the result with better accuracy.

## 6.7   Case study of a simulated building

Based on the confidence gained in the simulation models and their validations that were presented in the preceding sections, the modelling framework was applied to a real-scale building, as to infer potential savings that can be obtained through application of microencapsulated PCMs in the internal coatings of façades.

Three test cases of an hypothetical test building were considered in regard to the composition of the interior coating mortar of external walls: (i) one in which a hybrid PCM mortar is used (here termed as HPCMM); (ii) another in which a single PCM mortar is used (here termed as SPCMM) (iii); a third case in which a regular mortar is used (here termed as REFM). The three cases were subjected to realistic outdoors temperature variations. A set of cost analyses is illustrated at the end of the chapter.

### 6.7.1   Materials and features of the wall system

In the cases with PCM, both SPCMM and HPCMM were considered with nearly 20% of PCM related to the global mass of the mortar. The formulation of SPCMM adopted herein contains one type of PCM with melting temperature of 24ºC with quantity reaching 18.34% of weight within the mortar.

The formulation of mortar HPCMM adopted herein contains three distinct PCMs, as in the line with previous consideration of small scale prototypes as mentioned earlier in this chapter. The main thermo-physical properties of the mortar cases, REFM, SPCMM and HPCMM, are synthetized on Table 6-2, obtained with basis on pervious experimental works mentioned in chapter 5.

It is noted that the specific heat capacity of HPCMM was obtained experimentally and was adopted from Figure 5-4 in chapter 5 which had PCM melting temperatures of 10ºC, 26ºC and 28ºC.

The specific heat capacity of SPCMM was adopted from Figure 6-4 in the present chapter for a mortar which had PCM with melting temperature of 24ºC. Table 6-2 also contains information about the XPS (extruded polystyrene), brick (Vicente *et al.* 2014) and air (Incopera *et al.* 2007) that were part of the considered wall system.

Air material considered as ideal-gas with thermal conductivity of 0.0242 W/m K and specific heat capacity of 1.00643 kJ/kg K.

Table 6-2: Thermo–physical properties of the materials used in the numerical simulations.

| Thermo-physical properties | Ab. | Units | REFM | HPCMM | XPS | Brick | SPCMM |
|---|---|---|---|---|---|---|---|
| Density | $\rho$ | [kg/m$^3$] | 1529.5 | 1309.8 | 32 | 1976 | 1360.9 |
| Thermal conductivity | $k$ | [W/mK] | 0.4 | 0.3 | 0.034 | 0.77 | 0.3 |
| Specific heat capacity | $C_p$ | [J/kgK] | Figure 5-4 | Figure 5-4 | 1400 | 835 | Figure 6-4 |

The composition of the walls of the model is a typical one in Portuguese building envelopes. In fact, the target in this case was to have a real-sized dimension, which would however have a thermal transmittance ($U \approx 0.7$ W/m$^2$ K) lower than the maximum limit according to Portuguese regulations for vertical elements (of $U = 1.45$ W/m$^2$ K) (RCCTE 2006).

The exterior walls, schematically represented in Figure 6-19, have a typical layout characterized by (from outside to inside): a 0.02m thick of plastering mortar (REFM), 0.1m of brick, a 0.03m of extruded polystyrene (XPS), another 0.1m thick of brick and a 0.02m of plastering mortar (REFM, SPCMM or HPCMM) as inner lining.
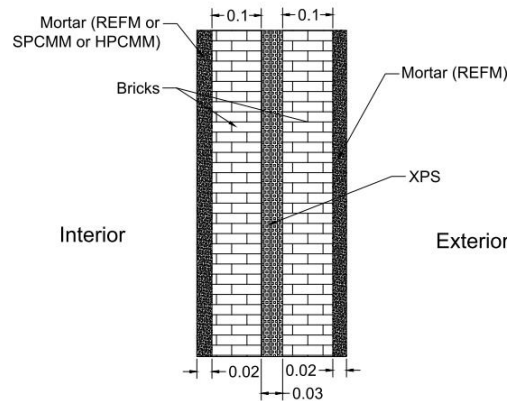
Figure 6-19: Details of the walls from exterior to the interior (REFM; brick; extruded polystyrene (XPS); brick; REFM, SPCMM or HPCMM). Units: [m].

## 6.7.2   Simulation model

A 5 storey building located in Portugal is considered for the simulation − see Figure 6-20a. Usually, a real situation building includes several objects such as: windows, internal partitions and furniture. These features can bring complexity in the geometry of the model as well as meshing complexity. In order to have tackled the mentioned issues, the following assumptions/simplifications were considered for the simulated plan: choice of plan disregard to the windows, internal partitions and furniture. Effective of these objects considered negligible, however, they can store sensible heat and this may give an added inertia to the building.

The entire 3$^{rd}$ floor is analysed, as the distance of this intermediate floor to the roof and foundation is enough to assuming that no thermal exchanges occur on both bottom and upper slabs (i.e. adiabatic conditions). I.e. the temperature in the 2$^{nd}$ and 4$^{th}$ floor are assumed to behave equally to the 3$^{rd}$ floor and  shown in Figure 6-20b,c, the volume of study is the 3$^{rd}$ floor with inner dimensions of 9.71m (length) $\times$ 9.71m (width) $\times$ 3m (height). The simulated model equipped with a heater unit that has a heated or cooled area of 3.29m$^2$ with a power of 1500 W placed at the geometrical centre of the model. The point labelled as "monitoring point" in Figure 6-20b,c was used as the reference control point for the thermostat of the heating/cooling system and for the temperature analyses presented in this study. The monitoring point placement was considered to be the unfavourable temperature condition inside the plan for human thermal comfort as it is placed adequately far away from the heating/cooling system. The heating/cooling

system was turn on the heating or cooling modes in order to maintain the internal temperature at the desirable comfort temperature of 20°C during winter scenario testing, and 24°C during summer scenario testing according to the recommendations of ASHRAE55 (2004). The operating principle of the thermostat of the heating/cooling system is a simple ON/OFF algorithm the same model as the previous section was used.
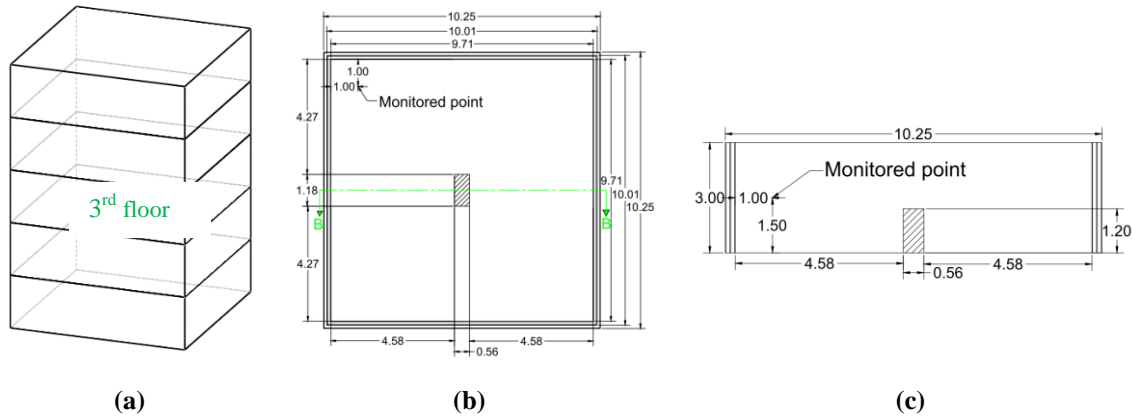


Figure 6-20: Schematic representations of the simulated model: (a) location of the studied floor in the building; (b) Plan view; (c) Section view B-B. Units: [m].

A winter scenario and a summer scenario were studied in this research, corresponding to the location of Guimarães in the North of Portugal. Solar radiation effects were considered in a simplified manner through a sol-air temperature algorithm, according to methodology detailed in section 5.2.4. As a result of the application of the sol–air temperature algorithm, the 24h cycles shown in Figure 6-21were obtained for both summer and winter scenarios.

The external surfaces of the flat are bounded by convective heat transfer conditions. A value of 20 W /m K (Azenha  M 2009) was considered for the surface convection coefficient. In the top and bottom planes, adiabatic boundaries were considered. A boundary condition heat flux of ±454 W/m$^2$ is applied to the model heating/cooling system, together with the ON/OFF algorithm for its operation. For instance, during the summer scenario, with the setpoint of 24ºC: the cooling system is turned ON when the temperature inside becomes lower than 24˚C and it is turned OFF when the temperature reaches 24ºC again. The UDF code was written as to control the heating/cooling system presented in Appendix B (for heating) and Appendix C (for cooling).

**(a)**                                             **(b)**
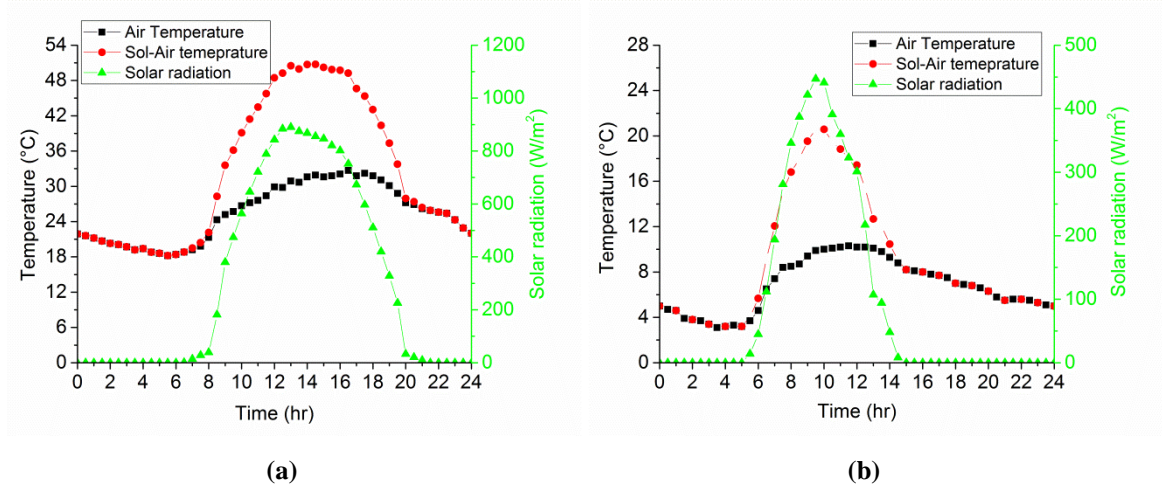
Figure 6-21: Exterior temperature, solar radiation and sol–air temperature (south-oriented wall) for: (a) A summer day and (b) A winter day in Guimarães, Portugal.

The exterior lateral surfaces of the walls (except for the top and bottom plans), were assigned with convective thermal boundary conditions, taking into account the varying temperature imposed in the model. In both the cases, the model was initialized from 20ºC for winter scenario and 24ºC for summer scenario. A total of three simulations was conducted by submitting the each case to summer scenario and winter scenario testing, with each simulating lasting six full day cycles (144 h), with the analysis of this section incident on the 4$^{nd}$ stabilized cycle. A constant time step size ($\Delta t$) of 300 s was considered. The convergence criterion at each time step was checked under $10^{-3}$ for momentum equation, $10^{-2}$ continuity equation and $10^{-5}$ for and energy equations (Wang *et al.* 2011). Air was considered as an ideal gas. The mesh of the model is structured, being comprised of hexahedral cells as shown in Figure 6-22.
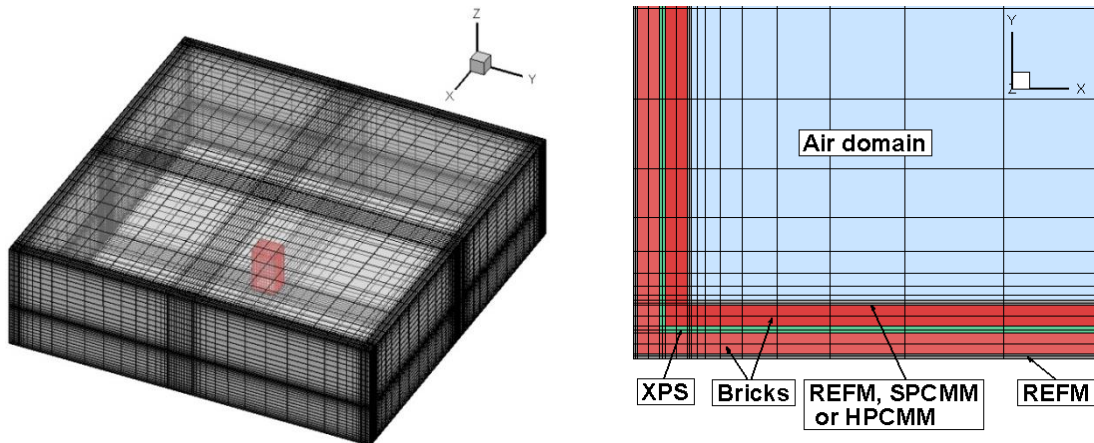


Figure 6-22: 3D mesh of the simulated model and mesh distribution in walls and air boundary layer.

### 6.7.3   Results of thermal behaviour and energy saving

Figure 6-23 shows the temperature variation of the "monitored point" for winter scenario for the SPCMM, HPCMM and REFM cases. In the winter scenario, the heater is turned on for a total of 6.7h per day for the REFM scenario, whereas the SPCMM and HPCMM scenario allowed a reduction of the heating time to 5.5h and 6.4h, which by itself represents a 17.5% and 4% saving respectively.

Temperature distribution in the interior environment of the buildings becomes important as the building geometries are usually large and complex. In such situations, thermal stratification may become an effective parameter in the enhanced energy design of buildings. In this way, an example of the studied flat when it is under winter scenario is assessed to indicate the importance of thermal stratification in the interior air environments. The interior air temperature of studied flat is set to maintain at comfort temperature (20ºC) during winter scenario.
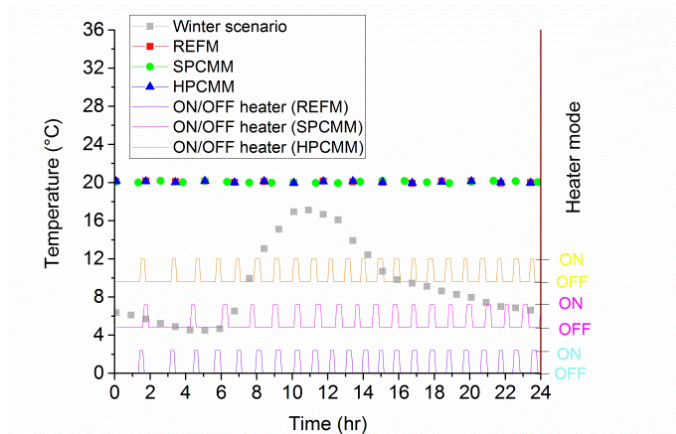


Figure 6-23: Interior temperature of the flats with and PCM controlled with heating system under winter scenario.

During the heating period, the buoyancy, due to the heater is the dominant force in the air flow, as shown in the temperature contours of Figure 6-24. It should be mentioned that the three points are monitored labelled as 1, 2 and 3, which have similar positions at XY direction (X=5m and Y=0.1m), while, they are distributed at several height in Z direction by Z=0.1m, 1.5m and 2.9m for 1, 2 and 3 points, respectively. The experimental work (Gowreesunker *et al.* 2013) suggests that an aspect ratio (height/width)<1 causes stable stratification, due to the tendency for turbulent mixing at the top of the air domain is lower. In the studied flat, the aspect ratio of the flat with

respect to the Z direction is 0.3, while the aspect ratio with respect to the X direction is 1. The results from Figure 6-24 abide by the observations made in Ref. (Gowreesunker *et al.* 2013), as although the aspect rations of the flat are 0.3 and 1, they are not high enough to destroy stratification. Thus stratification near the walls is observed in this simulation. It can be observed from the contour plots that the air flow is dominated by the buoyancy generated by the heater unit. Vertical temperature stratification in the air domain of the HPCMM is about 0.4 K/m compared to 0.6 K/m in the REFM, and stratification in the HPCMM is more uniform compared to the REFM. In fact, a more uniform and less stratified environment in the occupied zone provides better thermal comfort (Gowreesunker et al. 2013).
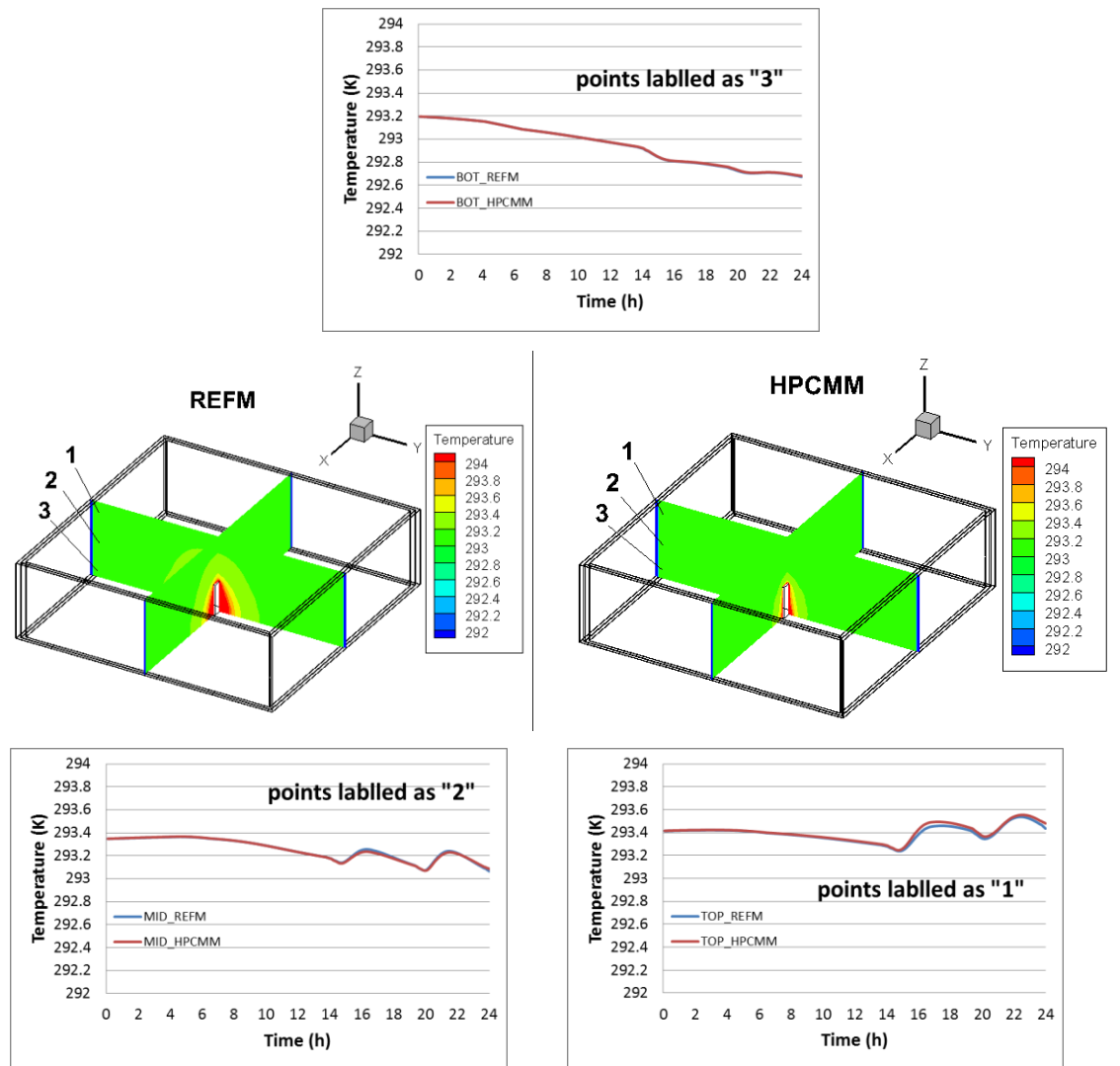


Figure 6-24: Comparison of temperature evolutions at 3 points (bottom, middle and top positions) in the flats, and temperature contours (K) at the heating period with HPCMM and REFM on the walls.

-----------------------------------------------------------------------------------------------------------

Figure 6-25 shows the interior temperature of the flat in the summer scenario, the cooler mode was active for a total of 4.7h per day for REFM case, while the SPCMM and HPCMM cases reached reduction of the cooling time to 4.3h and 3.5h, which showed energy savings of 9% and 23.5% respectively.

In this basis, the total amount of energy that can be saved by PCM cases indicates significate in which for the HPCMM case reaches to 27.5% while, for the SPCMM reduction value of 26.5% obtained. Further confirmation on the better performance of the HPCMM, as illustrated even 1% rather SPCMM in the reduction of the energy consumption through the heating/cooling seasons.
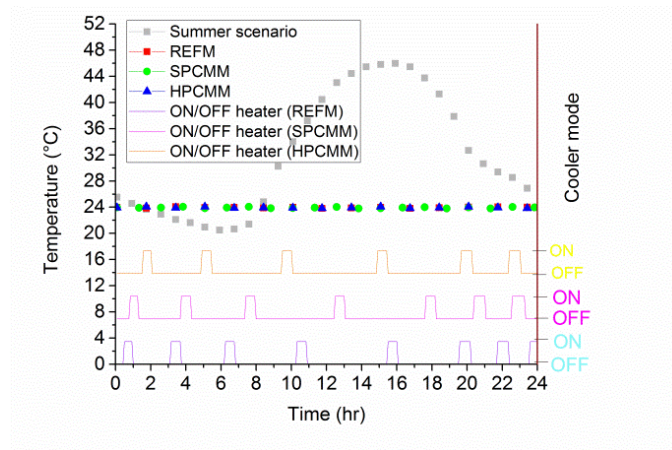


Figure 6-25: Interior temperature of the flats with and PCM controlled with cooling system under summer scenario.

## 6.7.4   Global performance of a building systems with hybrid PCM

The present section deals with the global performance of the system when it is more close to the realistic situations. In fact, the building usually, equipped wit: TV, washing machine, refrigerator, water heater, battery and etc. Therefore, it is advisable to evaluate the performance of the overall system when the hybrid PCM incorporated. In this way, a study was considered and analysed base on household energy management model (HEM). Two cases with hybrid PCM (HPCMM) and without PCM (REFM) were studied. In brief, conceptually, smart grid is the idea to improve the efficiency of the system from producer to the consumer (Gellings 2009). Buildings may be considered as

a smart grid object. Smart buildings can take the advantages of smart grids concept in which, they can minimize the demanded electricity costs.

The target is to minimize the electricity costs for the household when different tariffs are deployed. Demand response programs (DRPs) can play an important role in the future buildings. Because, they can usually shift the peak loads to the off peak load hours. Additionally, PCMs enable to shift the load from peak to off peak electricity consumption period. The combination of PCM into the DRPs can enhance the performance of the system. The aims of DRPs are to assess the sensitivity of variations of electricity prices in different hours.

The importance of the PCM accounted in the DRPs that is given through an example. Figure 6-26 represents an example of smart building with group of equipment as a critical loads and controllable loads. The concept of the proposed model can be explained by: during the winter time, the householders use the heating systems during the coldest hours of the day, while, this can increase the demand peak. The detailed discussion on the proposed model can be found in the Ref. (Shafie-khah M *et al.* 2015).
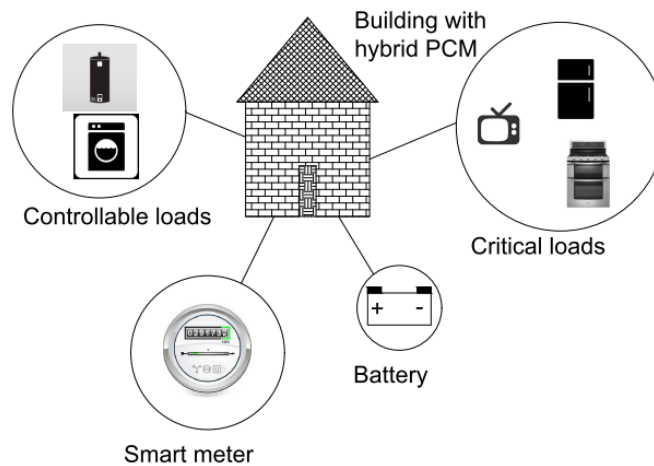


Figure 6-26: Example of a smart building system.

Figure 6-27 gives residential electricity costs for different tariffs based on the available price list provided by a typical manufacturer company in Portugal called EDP (Energias de Portugal). As it can be seen, there is different energy prices at each hours of the day except for flat rate tariff which presents only one value through the entire day. In the following analysis, the study was based estimates of the energy saved by employing PCM mortar into the buildings based on the unit electricity costs for each selected tariff.

-------------------------------------------------------------------------------------------------------------

In fact, electricity prices are different in different hours. Each tariff, encourage the electricity use in response to fluctuations for price over the time, or to offer incentives, or to charge penalties that are considered to provide lower use during high electricity prices. Time of Use (TOU), Real Time Pricing (RTP) and Critical Peak Pricing (CPP) are categorizes as classification of demand response programs.
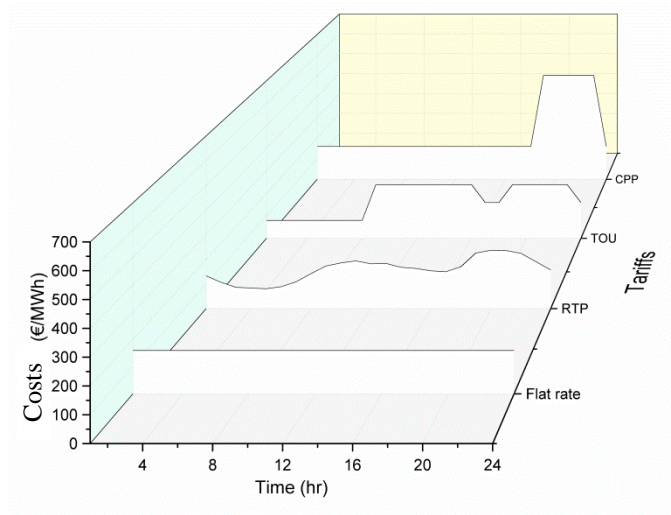


Figure 6-27: Hourly prices of the energy for residential customers.

Figure 6-28 illustrates the critical load data that were taken from consumption of a typical 100m$^2$ house is Portugal in winter season. It should be remarked that, HPCMM and REFM are tested in previous section and the results confirmed that the energy consumption for heating the interior in the case with HPCMM reduced when compared with the REFM. Furthermore, the HPCMM dedicates the shifting of the electricity consumption during entire tested day when compared with REFM as previously shown in Figure 6-23 and Figure 6-25.
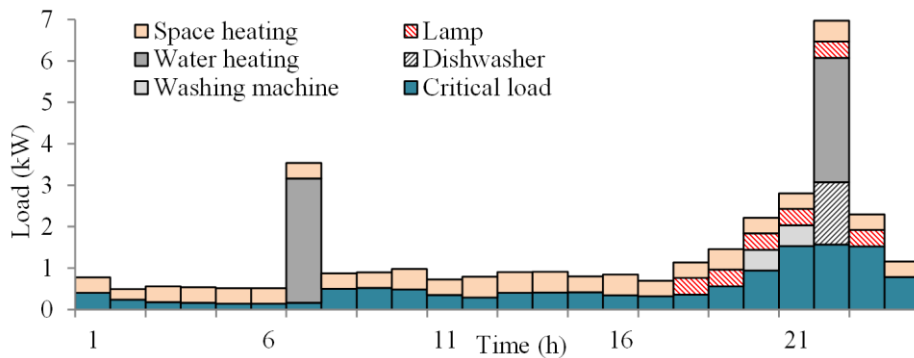


Figure 6-28: Initial household electricity demand.

The household's cost in tested one day considering different DRPs is compared in Figure 6-29. It can be seen, the CPP brings significantly higher cost to the household, and however, the proposed model with HPCMM can reduce it by nearly 40%. Different case studies indicated that implementation of HPCMM in the buildings can meaningfully affect the costs of householders in different DRPs.
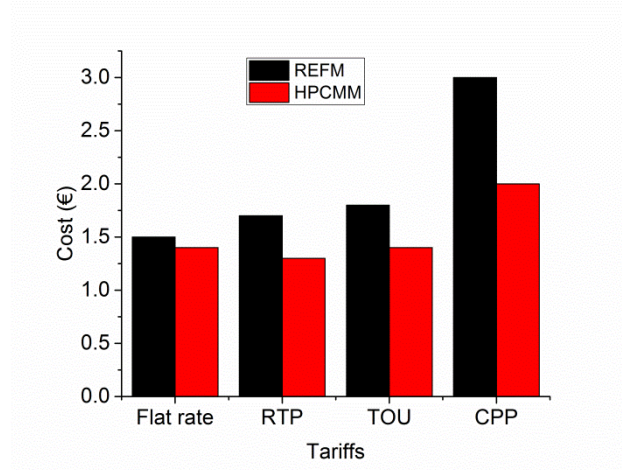


Figure 6-29: Customer's cost in different DRPs during a 24hr.

## 6.8 General remarks

This chapter initially, was described general understanding of the thermal modelling in the context of building physics as well as phase change model. This chapter also describes a brief on the introduction of CFD their utilization in the simulation of indoor environments.

This chapter was also demonstrated the numerical simulations of small scale prototypes and real scale model under realistic weather climate conditions. The experimental data from previous chapter were used to validate CFD models of the small scale prototypes. The simulation results of the both REFM and HPCMM were in excellent agreement with measurements when the system was not include the heater unit. In the numerical simulations of small scale prototypes including the heater unit, the obtained results had differences when compared with experimental results due to the fact that the model was not accounted for PID controller effect. However, in such way provided ground confidence on the accurate set point temperature of the UDF code. Next, the numerical models were used to evaluate the HPCMM and REFM under heating/cooling loads considering a heating/cooling system in the model. In fact, a summer day and a winter

day simulations were performed using practical wall system according to the Portuguese standard and air sol temperature imposed into the model. Thermal comfort set points of 20ºC and 24ºC were used in the simulation to evaluate their impact on the performance of the PCM mortar. Overall, based on the tested period of simulations, the PCM mortars did show the potential for reducing electricity consumption for space conditioning. Finally, a global performance of a residential building incorporated with hybrid PCM has assessed with consideration of different tariff rates based on the electricity prices in the Portuguese market.

# Chapter 7 Conclusions and Future Works

The development of enhanced and innovative thermal energy storage systems such as cement based mortar should motivate continuing research. This includes novel developments in the field of materials science of basic combinations of phase change materials into the cement based mortars. In particular, the study of the material characterization is relevant for the reliable prediction of the engineering purposes. This thesis has contributed to the understanding of the complex thermal behaviour of pure PCMs and PCM mortars at different material level investigations. Thermal performance of the regular mortars and PCM mortars were assessed at small scale design testing as well as real scale dimensions through experimental and numerical simulation approaches.

## 7.1 Concluding remarks

The experimental approach followed in this thesis provides a detailed study of the PCM itself and mortar with PCM that can be used for thermal comfort purposes. A series of testing has been proved, in order to understand the influence of such mortars to increase the energy efficiency in buildings. Such mortars are linked to the composition of the wall systems in the building envelopes to provide a significant energy saving by the processing technology.

In regard to the thesis work as a whole. a set of 5 main conclusion sets is shown in the following paragraphs.

*Conclusions 1*: This study focused on specific enthalpy estimation and phase change temperature for PCM mortars and pure PCM samples as important parameters of

------------------------------------------------------------------------------------------------------------------

thermal characterization. The results showed that the mix of two PCMs has a similar behaviour to the superposition of effects of independent PCMs. Therefore, it can be inferred that the two PCMs did not have thermal interaction with each other. Also, DSC tests of different samples showed that both plain microencapsulated paraffin samples (PCM) and plaster mortars containing microencapsulated PCM exhibit hysteretic behaviour of the phase change temperature in regard to heating/cooling cycles. Furthermore, it was observed that the specific enthalpy is linearly proportional to the mass fraction of PCM in the mortar sample as compared to the behaviour of plain PCM samples. The numerically extrapolated enthalpy values for PCM mortars matched the measured values quite closely in both heating and cooling processes, indicating an adequate incorporation of PCM and the feasibility of the extrapolation procedure (principle of superposition). Using this superposition method, the necessity of testing hybrid PCM mortars for specific enthalpy can be avoided, as long as basic information about the thermal behaviour of each microencapsulated PCM is available. The use of this method can therefore be clearly advantageous when attempting to estimate latent heat properties of hybrid PCM mortars for numerical simulations targeted to optimize the types and temperatures of PCMs to incorporate in the plastering mortar.

***Conclusion 2***: This thesis presents the microstructure assessment by mean of SEM/EDS and thermal characterization through DSC for mortars containing phase change materials targeted for thermal comfort in buildings. The study encompasses a reference mortar termed REFM, as well as two mortars containing distinct PCMs: (i) one mortar called SPCMM24, containing a mass fraction of 18.34% of microencapsulated paraphin PCM with melting temperature of 24 °C; (ii) another mortar called HPCMM18_28 with mass fraction of 9.17% of PCM with melting temperature of 18 °C and 9.17% of PCM with melting temperature of 28 °C. The hybrid blend of two distinct types of PCM may prove advantageous for improved thermal comfort assurance in buildings (reducing energy consumption for heating/cooling seasons), and their feasibility at material/thermal level was evaluated in this work. From the observation of SEM analysis it was concluded that, the microencapsulated PCM particles were well incorporated in the microstructure of both SPCMM24 and HPCMM18_28 mortars. Together with products of cement hydration they form a host matrix for the hard sand inclusions. The SEM investigation did not reveal any damage or fracture in the boundary zone between these two components at the micrometre scale.

146

The observation of DSC thermograms pertaining to three consecutive heating/cooling cycles of testing on each mortar suggest that maximum accuracy and homogeneity of results can be achieved by always performing at least two cycles, and the analysis can operate on the results of the second cycle.

The influence of different heating/cooling rates on the thermal behaviour of the mortars has been analysed, namely in regard to the peak temperatures on the DSC thermogram, as well as on the calculated specific enthalpy. It was found that tests with higher heating/cooling rates intensify the differences between the thermograms of the heating and cooling processes, both in terms of the peak temperatures and the overall shape of the curve. However, the calculated specific enthalpy for each phase transition seems to be independent of the heating/cooling rate. Moreover, the impact of the heating/cooling rate on the hysteretic behaviour of the thermal response of mortars with PCM was analysed. It was concluded that the hysteretic DSC response is intensified as the heating/cooling rates are increased, and that the lowest testing speeds exhibited minimum to no apparent hysteresis.

When the purpose of DSC testing is to assist numerical simulation of PCM performance in building façades, it becomes apparent that the slowest heating/cooling rate studied (0.1 °C/min) is the one that mostly resembles real scenarios of daily temperature variations. However, it must also be borne in mind that these low heating cooling rates for testing strongly increase the testing time, thus the occupation of the DSC device.

It is remarked that the use of more than one type of PCM in the mortar has revealed adequate thermal behaviour, being consistent with the predictable outcome of the two incorporated PCMs used individually at the same proportions. Thus, it is considered that the DSC testing allowed further confirming the feasibility of hybrid PCMs in mortars.

***Conclusion 3:*** This thesis assessed the thermal and physical aspects of lightweight aggregates (LWAs) incorporating phase change materials (PCMs), with the objective of improving freeze/thaw resistance of the studied composites, at material level. The study presents results from two different impregnated/encased PCMs in several LWA composites, namely: (i) a series containing paraffin PCM with melting temperature of 3 °C (R3); (ii) a series containing paraffin PCM with melting temperature of 5 °C (R5). These composites may prove advantageous for improving thermal resistance in

pavements (reducing freeze/thaw cycles), and their feasibility at material/thermal/physical level was evaluated in this thesis. The experimental works included: comprising a detailed analysis of the LWAs (particle density, absorption capacity of water and waterproofing material), as well as the performance of coated/impregnated LWAs under freeze/thaw cycles and exposure to high temperature. From the observation of particle density analysis, it was concluded that, expanded vermiculite (EV) has the greatest variation between the dry and saturated states among other types of LWAs. EV's pore structure analysis also revealed it has a highly porous matrix suitable for PCM impregnation when compared with other types of studied LWAs.

The observations of DSC thermograms pertaining to a consecutive heating load of testing on each PCM suggest that maximum specific enthalpy result was achieved for the R5. Therefore, R5 with specific enthalpy value nearly 180 J/g has better potential of thermal energy storage than the other type of studied PCM (R3). Furthermore, it was found that tests with higher heating/cooling rates intensify the differences between the thermograms of the heating and cooling processes, both in terms of the peak temperatures and the overall shape of the curve. However, the calculated specific enthalpy for each phase transition seems to be independent of the heating/cooling rate.

From SEM analysis of the composite mortar it was concluded that, the IC particles were well coated with the waterproofing material. The SEM investigation also revealed non-homogeneity of the waterproofing's thickness around the IC particles.

The influence of different waterproofing solutions on the weight loss of the composites under freeze/thaw cycles was analysed, namely in terms of the weight drop percentage by mass as well as the amount of leaked PCM from the studied composites. Weight loss was found to be dependent on the used type of waterproofing materials. Since the waterproofing has potential of losing water content, thus, the issue related to the higher mass loss in the composites can be justified by the fact that, these composites might had had thicker layers of waterproofing. Nevertheless, the amount of leaked PCM from different composites under freeze/thaw cycles was always under 0.5%, which indicated very small to negligible leakage of PCM from LWAs. Furthermore, visual observation confirmed that no leakage of the PCM seems to have occurred.

The observations from drying tests of the composites were also analogous to those already made for freeze/thaw test, confirming that, as expected, variation of weight loss percentages of the composites with and without waterproofing. However, an added analysis was made in regard to the waterproofing properties corresponding to the minimized PCM leakage. The influence of drying test has confirmed that, the waterproofing keeps its properties when drying temperature is 40 °C. However, there is a slightly higher weight drop percentage mass occurred when compared with the results from the freeze/thawing test.

The results from comparision between the case of a cement based mortar incorporating with commercial microencapsulated PCM and impregnation technique that were formulated in the scope of thsis thesis. A mortar contained 293 kg of microencapsulated PCM per cubic meter, whereas, the impregnation technique used in this investigation allows for up to a maximum PCM content of about 213 kg/m$^3$ when using the EV aggregate (a reduction of about 27%). This is not a significantly lower PCM content, and is therefore, not necessarily a problem as it is approximately within the same order of magnitude, but at a fraction of the cost of the microencapsulated PCM. With respect to LWA types IC, GC and AP, the impregnation technique used in this investigation allows for a maximum PCM content of about 49 kg/m$^3$, 109 kg/m$^3$, and 171 kg/m$^3$ respectively.

It is remarked that the use of PCMs incorporated/encased in LWAs revealed adequate thermal behaviour, as desirable outcome to reduce the freeze/thaw cycles effects under real climate conditions in pavement applications. Thus, this investigation carried out at material level confirms the feasibility of the proposed method for PCMs incorporation/encasement in LWAs. Furthermore, this methodology can be extended to building applications to increase thermal comfort. It may bring economic benefits due to the fact that some LWAs have the potential of high PCM absorption when compared with commercially available microencapsulated PCM products.

*Conclusion 4:* In this thesis, a set of experiments and numerical simulations were performed in order to demonstrate the transient thermal behaviour of plastering mortars containing hybrid PCM blends, as compared to the behaviour of regular mortars, or those containing a single type of PCM. After an initial round of characterization of the materials involved in the experimental program, laboratory scale prototypes that

consisted in hollow boxes rendered with the mortars under test, were deployed as to evaluate the capacity of the tested mortars in effecting inner temperatures of the prototypes themselves. Two prototypes, containing respectively a reference mortar (REFM) and a mortar containing and hybrid blend of embedded PCMs (HPCMM), where submitted to realistic daily temperature cycles and inner temperatures were recorded. Finally, a set of numerical simulations of the thermal behaviour of the prototypes was performed through a Computational Fluid Dynamics framework, aiming validation of simulation capacity, but also for further sensitivity analysis of test situations that were not experimentally assessed. From the conducted research the following main conclusions were obtained: (i) the prototype rendered with HPCMM allowed a much stronger attenuation of the external thermal amplitudes on its interior, as compared to the situation of the REFM prototype. This situation was observed in both summer and winter scenarios; (ii) the adopted framework for numerical simulation has shown adequate predictive capacity by reproducing the experimental results of all experiments with an error margin that was always below 0.1ºC. This validation of simulation capabilities provided grounds for the conduction of further simulations for sensitivity analyses; (iii) based on the set of experiments and simulations, it was also inferred that the utilization of hybrid PCM blends has revealed the capacity to better attenuate daily environmental thermal amplitudes within the test cells for both summer and winter scenarios as compared to any of the other studied alternatives (reference mortars or single PCM mortars). Indeed the combination of several PCMs with melting points that cover a large range of temperatures allow this solution to be advantageous in a much broader sense than classical single PCM approaches that tend to have a more limited scope of activation and usefulness. It could even be demonstrated that a bad choice of PCM melting points in a given blend can even induce worse behaviour than that which would be expectable in a traditional mortar; and (iv) even though direct conclusions could be obtained in regard to the potential of cooling energy saving harvested by the use of hybrid PCM blends in the summer scenario (using the TT index), no direct conclusions can be taken for the winter scenario. Indeed the winter experiments/simulations just allowed demonstrating that the hybrid PCM mortar still outperforms the reference mortar in reducing internal thermal amplitudes inside the prototype. However, the range of internal temperatures in the prototype was unrealistically low as compared to the desirable thermal comfort ranges. Therefore, in order to obtain more definite conclusions in this concern, new further experiments are

---------------------------------------------------------------------------------------------------------

being deployed, in which an internal heater is placed in the prototypes, and the performance assessment in winter scenarios is made directly through the energy savings in heating as to maintain internal temperature within acceptable comfort limits.

The experimental testing of the two layered wall prototypes that were designed and equipped with heater unit have been assessed to complement high latent heat storage capacity and energy saving potential of hybrid PCM through laboratory scale testing. Prototype incorporated with hybrid PCM mortar produced smaller indoor temperature variations (21°C-24°C) than those of reference mortar (21°C-27°C). These results confirmed the important benefits of hybrid PCM mortar in terms of energy efficiency, thermal comfort and energy cost saving. The energy saving results indicated a reduction of 20% in energy demand to maintain the interior within the thermal comfort range by application of the hybrid PCM mortar. It is also remarked that the use of hybrid PCMs in mortar revealed adequate thermal behaviour, as desirable outcome to reduce the energy demand under real climate condition in building applications. This method can benefit from the PCMs and variable electricity prices during the winter period to reduce electricity consumption while performing peak load shifting. The proposed method in this research can be applied in any locality which offers a variable electricity price. However, it should be noted that the melting point of the PCM needs to be selected according to the thermal comfort requirements.

Numerical simulation of the prototype with heater unit was performed (with and without convection effect) throughout the CFD simulations. The results indicated that, neither of numerical predictions with or without convection effect was not able to directly match the experimental results by differences of ~5ºC. However, the results of interior temperature monitoring, including the convection effect of the air inside the prototype, improves the simulation accuracy compared to the without convection approach employed in commercial CFD codes by about 4% (0.5 K).

The average error in the simulations compared to the experimental results was found to be 5ºC. These errors maybe acceptable judged uncertainties in the measurements, but can be important in applications where the temperature ranges encountered are small.

As an important note, it is pointed that the concept of blending more than one type of PCM into plastering mortars has revealed promising performance capacity. The up scaling of this concept is bound to bring added value to thermal performance of buildings. Indeed, by being able adequately predict the behaviour of such blends of PCMs in the scope of real buildings; it will be possible to tailor the optimum blends for

specific needs, both in terms of façade orientation, but also regarding the building location as a whole.

***Conclusion 5:*** case study of a simulated building was conducted in order to assess the hybrid PCM at real scale dimensions. The results of the interior air temperature variation under winter scenario for the SPCMM, HPCMM and REFM cases when a heater is implemented in which, the heater is turned on for a total of 6.7h per day for the REFM scenario, whereas the SPCMM and HPCMM scenario allowed a reduction of the heating time to 5.5h and 6.4h, which represents a 17.5% and 4% saving respectively.

Also, the interior temperature of the real scale model in the summer scenario indicated the cooler needed to be in active model for a total of 4.7h per day for REFM case, while the SPCMM and HPCMM cases reached reduction of the cooling time to 4.3h and 3.5h, which showed energy savings of 9% and 23.5% respectively.

Thus, the total amount of energy that can be saved by PCM cases indicates significate in which for the HPCMM case reaches to 27.5% while, for the SPCMM reduction value of 26.5% obtained. Further confirmation on the better performance of the HPCMM, as illustrated even 1% rather SPCMM in the reduction of the energy consumption through the heating/cooling seasons.

Temperature distribution in the interior environment of the buildings becomes important as the building geometries are usually large and complex. In such situations, thermal stratification may become an effective parameter in the enhanced energy design of buildings. The qualitative results show that the temperature stratification effects can be adequately predicted with the CFD modelling and together with phase change model, can enable more efficient building design using PCM mortars for cases with or without convection scenarios. In buildings, the impact of PCM mortars under real climatic condition can be evaluated and appropriate mass fraction of the PCMs and their melting temperatures configurations can be investigated to ensure complete activation of the PCMs.

In addition, incorporation of hybrid PCM mortar had a complementary effect on the proposed HEM system. The results revealed that by utilizing the proposed model, the customer's cost could be reduced up to 40%, which is significant.

## 7.2 Recommendations for future work

The study presented here aims at the incorporation of the PCM into cement based mortar for increased energy efficiency of buildings which started with material level investigations to application of real scale dimensions. The chosen approach provided the necessary results to achieve the objectives were considered on the beginning of the thesis.

The small scale prototypes conducted into the climatic chamber room developed as part of this study in order to pave the ground for validating different numerical simulation scenarios. The performance of the PCM systems can however be further investigated at real scale dimension of the buildings for various scenarios, includes: different heating/cooling set points; different comfort temperature ranges; different controlling strategies applicable to commercial buildings; different hybrid PCMs with desirable melting temperature upon target climatic conditions; and different PCM configurations as exterior coatings or precast fabricated panel systems. Furthermore, the following recommendations also highlighted in the scope of the building physic:

- The study of the combination of hybrid PCM-based strategies in both residential and commercial buildings.
- The additional possibilities of blends of hybrid PCMs to be studied systematically.
- Extension of the numerical simulation including: explicitly the solar radiation effect, internal masses that exist inside the building and clearly attenuate things through their specific heat capacity.
- Development at the level of a better and more consubstantiated "air movement modeling".

# Appendix

# Appendix A

```
#include "udf.h"
real thermosensor_temperature1;
thermosensor_temperature1=293.15;
DEFINE_EXECUTE_AT_END(tsensor)
{
 real thermosensor_coordinate[ND_ND];
 real thermosensor_temperature;
 real xmin;
 real xmax;
 real ymin;
 real ymax;
 real zmin;
 real zmax;
 real x,y,z,nt;

 cell_t c;
 Domain *d;
 Thread *t;
 d = Get_Domain(1);
 xmin=0.055;
 xmax=0.056;
 ymin=0.055;
 ymax=0.056;
 zmin=0.055;
 zmax=0.056;
 thermosensor_temperature=0.0;
 nt=0.0;
 thread_loop_c(t,d)
 {
 begin_c_loop(c,t)
 {
 C_CENTROID(thermosensor_coordinate,c,t);

 x=thermosensor_coordinate[0];
 y=thermosensor_coordinate[1];
 z=thermosensor_coordinate[2];

 if ((x >= xmin) && (x <= xmax))
```

```
   {
   if ((y >= ymin) && (y <= ymax))
    {
    if ((z >= zmin) && (z <= zmax))
     {
     thermosensor_temperature=thermosensor_temperature + C_T(c,t);
     nt=nt+1.0;      /* count number */
     }
    }
   }
  }
  end_c_loop(c,t)
  }
  thermosensor_temperature=thermosensor_temperature/nt;
  thermosensor_temperature1=thermosensor_temperature;
 }
DEFINE_PROFILE(heater_bc,t,i)
{
 real cutoff_temperature;
 real heater_on;
 real heater_off;

 face_t f;
 cutoff_temperature=293.15;

 heater_off = 0.0;
 heater_on = 34129.7;  /* heater 300W, area of the heater boundary condition 0.00879m2,*/

 if (thermosensor_temperature1<=cutoff_temperature)
 {
 begin_f_loop(f,t)
 {
 F_PROFILE(f,t,i) = heater_on;
 }
 end_f_loop(f,t)
 }
 else
 {
 begin_f_loop(f,t)
 {
```

```
  F_PROFILE(f,t,i) = heater_off;
 }
 end_f_loop(f,t)
 }


 }
```

## Appendix B

```
#include "udf.h"
real thermosensor_temperature1;
thermosensor_temperature1=293.15;
DEFINE_EXECUTE_AT_END(tsensor)
{
 real thermosensor_coordinate[ND_ND];
 real thermosensor_temperature;
 real xmin;
 real xmax;
 real ymin;
 real ymax;
 real zmin;
 real zmax;
 real x,y,z,nt;

 cell_t c;
 Domain *d;
 Thread *t;
 d = Get_Domain(1);
 xmin=0.90;
 xmax=1.1;
 ymin=0.90;
 ymax=1.1;
 zmin=1.4;
 zmax=1.6;
 thermosensor_temperature=0.0;
 nt=0.0;
 thread_loop_c(t,d)
 {
```

```
begin_c_loop(c,t)
{
C_CENTROID(thermosensor_coordinate,c,t);


x=thermosensor_coordinate[0];
y=thermosensor_coordinate[1];
z=thermosensor_coordinate[2];


if ((x >= xmin) && (x <= xmax))
{
if ((y >= ymin) && (y <= ymax))
{
if ((z >= zmin) && (z <= zmax))
{
thermosensor_temperature=thermosensor_temperature + C_T(c,t);
nt=nt+1.0;       /* count number */
}
}
}
end_c_loop(c,t)
}
thermosensor_temperature=thermosensor_temperature/nt;
thermosensor_temperature1=thermosensor_temperature;
}
DEFINE_PROFILE(heater_bc,t,i)
{
real cutoff_temperature;
real heater_on;
real heater_off;


face_t f;
cutoff_temperature=293.15;


heater_off = 0.0;
heater_on = 454.0;   /* heating/cooling power of 1500W, area of the heater boundary condition
3.299m^2,*/


if (thermosensor_temperature1<=cutoff_temperature)
{
```

```
 begin_f_loop(f,t)
 {
  F_PROFILE(f,t,i) = heater_on;
 }
 end_f_loop(f,t)
 }
 else
 {
 begin_f_loop(f,t)
 {
  F_PROFILE(f,t,i) = heater_off;
 }
 end_f_loop(f,t)
 }


 }
```

## Appendix C

```
#include "udf.h"
real thermosensor_temperature1;
thermosensor_temperature1=293.15;
DEFINE_EXECUTE_AT_END(tsensor)
{
 real thermosensor_coordinate[ND_ND];
 real thermosensor_temperature;
 real xmin;
 real xmax;
 real ymin;
 real ymax;
 real zmin;
 real zmax;
 real x,y,z,nt;

 cell_t c;
 Domain *d;
 Thread *t;
 d = Get_Domain(1);
 xmin=0.90;
```

160

```
xmax=1.1;
ymin=0.90;
ymax=1.1;
zmin=1.4;
zmax=1.6;
thermosensor_temperature=0.0;
nt=0.0;
thread_loop_c(t,d)
{
begin_c_loop(c,t)
{
 C_CENTROID(thermosensor_coordinate,c,t);


 x=thermosensor_coordinate[0];
 y=thermosensor_coordinate[1];
 z=thermosensor_coordinate[2];


 if ((x >= xmin) && (x <= xmax))
 {
 if ((y >= ymin) && (y <= ymax))
 {
  if ((z >= zmin) && (z <= zmax))
  {
   thermosensor_temperature=thermosensor_temperature + C_T(c,t);
   nt=nt+1.0;      /* count number */
  }
 }
 }
}
end_c_loop(c,t)
}
thermosensor_temperature=thermosensor_temperature/nt;
thermosensor_temperature1=thermosensor_temperature;
}
DEFINE_PROFILE(cooler_bc,t,i)
{
 real cutoff_temperature;
 real cooler_on;
 real cooler_off;
```

```
face_t f;
cutoff_temperature=293.15;


cooler_off = 0.0;
cooler_on = -454.0;   /* heating/cooling power of 1500W, area of the heater boundary condition
3.299m^2,*/


if (thermosensor_temperature1>=cutoff_temperature)
{
 begin_f_loop(f,t)
 {
  F_PROFILE(f,t,i) = cooler_on;
 }
 end_f_loop(f,t)
}
else
{
 begin_f_loop(f,t)
 {
  F_PROFILE(f,t,i) = cooler_off;
 }
 end_f_loop(f,t)
}


}
```

162

# Bibliography

Abhat, A. (1983). "Low temperature latent heat thermal energy storage: heat storage materials." Solar Energy **4**: 313-331.

Ahmad, M., Bontemps A, Salle´e H and Quenard D (2006). "Thermal testing and numerical simulation of a prototype cell using light wallboards coupling vacuum isolation panels and phase change material." Energy and Buildings **38**: 673–681.

Al-Saadi, S. N. and Z. Zhai (2013). "Modeling phase change materials embedded in building enclosure: A review." Renewable and Sustainable Energy Reviews **21**: 659-673.

ANSYS FLUENT (2015). User guid Release 16.0.

ARGEX (2013). "Argila Expandida, S.A., national structural ceramics, Technical sheet for ARGILA EXPANDIDA, Portugal."

ASHRAE55 (2004). Thermal Environment Standards for Human Occupancy. 55. Atlanta, GA. .

Azenha M (2009). Numerical simulation of the structural behaviour of concrete since its early ages [PhD thesis]. PhD thesis, University of Porto.

Baetens, A., Petter J.B and Gustavsen A (2010). "Phase change materials for building applications: A state-of-the-art review." Energy and Buildings **42** (9): 1361–1368.

Barreneche, C., Miró L, Solé A, Martorell I, Fernández A and Cabeza L (2013). "Study on differential scanning calorimetry analysis with two operation modes and organic and inorganic phase change material (PCM)." Thermochimica Acta **553**: 23–26.

Barreneche, C., L. Navarro, A. de Gracia, A. I. Fernández and L. F. Cabeza (2016). "In situ thermal and acoustic performance and environmental impact of the introduction of a shape-stabilized PCM layer for building applications." Renewable Energy **85**: 281-286.

Bentz, D. P. and R. Turpin (2007). "Potential applications of phase change materials in concrete technology." Cement and Concrete Composites **29**(7): 527-532.

Biswas, K., J. Lu, P. Soroushian and S. Shrestha (2014). "Combined experimental and numerical evaluation of a prototype nano-PCM enhanced wallboard." Applied Energy **131**(0): 517-529.

Biwan, X. and Zongjin Li (2013). "Paraffin/diatomite composite phase change material incorporated cement-based composites for thermal energy storage." Applied Energy **105**: 229-237.

BRANCO, G. (2014). "Produções and Construções Ecológicas LDA, Edisol Group, Agglomerates of expanded cork products, Portugal."

Cabeza, L., A. Castell, C. Barreneche, A. de Gracia and A. I. Fernández (2011). "Materials used as PCM in thermal energy storage in buildings: A review." Renewable and Sustainable Energy Reviews **15**(3): 1675-1695.

Castell A, Martorell I, Medrano M, Pérez G and Cabeza L (2010). "Experimental study of using PCM in brick constructive solutions for passive cooling." Energy and Buildings **42**(4): 534–540.

Castellón, C., E. Günther, H. Mehling, S. Hiebler and L. Cabeza (2008). "Determination of the enthalpy of PCM as a function of temperature using a heat-flux DSC—A study of different measurement procedures and their accuracy." International Journal of Energy Research **32**(13): 1258-1265.

Castro, J., L. Keiser, M. Golias and J. Weiss (2011). "Absorption and desorption properties of fine lightweight aggregate for application to internally cured concrete mixtures." Cement and Concrete Composites **33**(10): 1001-1008.

Catalina, T., J. Virgone and F. Kuznik (2009). "Evaluation of thermal comfort using combined CFD and experimentation study in a test room equipped with a cooling ceiling." Building and Environment **44**(8): 1740-1750.

CEPSA (2010). ECM-2 (C67BF4), version nº5, Portuguesa Petróleos, S.A. . Portugal.

Chen Q (2009). "Ventilation performance prediction for buildings: A method overview and recent applications." Building and Environment **44**(4): 848-858.

Collins, F. and J. G. Sanjayan (2000). "Effect of pore size distribution on drying shrinking of alkali-activated slag concrete." cement and concrete research **30**(9): 1401-1406.

Cunha, S., Aguiar J, Kheradmand M and Bragansa L (2013). " Thermal mortars: Contribution of the incorporation of PCM microcapsules." Restoration of Buildings and Monuments **19**: 171-178.

Cunha, S., J. Aguiar, V. Ferreira and A. Tadeu (2015). "Mortars based in different binders with incorporation of phase-change materials: Physical and mechanical properties." European Journal of Environmental and Civil Engineering: 1-18.

Cunha, S., J. Aguiar, V. Ferreira, A. Tadeu and A. Garbacz (2015). Mortars with phase change materials-Part I: Physical and mechanical characterization. Key Engineering Materials, Trans Tech Publications Ltd. **634:** 22-32.

de Gracia, A., L. Navarro, A. Castell, Á. Ruiz-Pardo, S. Alvárez and L. F. Cabeza (2013). "Experimental study of a ventilated facade with PCM during winter period." Energy and Buildings **58**: 324-332.

Denner T (2012). "NETZSCH Proteus- thermal analysis - release 6.0.0, Gerätebau GmbH Wittelsbacherstraße 42."

Duffie J (1980). Solar Engineering Of Thermal Prpcess. New York, JOHN WILEY & SONS, INC. .

Dumas, J.-P., S. Gibout, L. Zalewski, K. Johannes, E. Franquet, S. Lassue, J.-P. Bédécarrats, P. Tittelein and F. Kuznik (2014). "Interpretation of calorimetry experiments to characterise phase change materials." International Journal of Thermal Sciences **78**(0): 48-55.

Dutil, Y., Rousse D, Salah N, Lassue S and Zalewski L (2011). "A review on phase-change materials: Mathematical modeling and simulations." Renewable and Sustainable Energy Reviews **15**: 112–130.

Eissenberg A (1980). "What's in store for phase change thermal storage materials for active and passive solar applications." 12-16.

EN 933-1 (2012). Tests for geometrical properties of aggregates - Part 1: Determination of particle size distribution - Sieving method.

EN 1015-10 (1999). Methods of test for mortar for masonry, Part 10: Determination of dry bulk density of hardened mortar. European Committee for Standardization.

EN 1015-11 (1999). "Methods of test for mortar for masonary, Part 11: Determination of flexural and compressive strength of hardened mortar, European Committee for standardization."

EN 1097-6 (2003). "Tests for mechanical and physical properties of aggregates – Part 6: Determination of particle density and water absorption." European Committee for standardization,.

EN ISO 11357-1 (1997). Plastics – Differential scanning calorimetry (DSC) Part 1:General principles. Berlin, DIN Deutsches Institut für Normung e.V.

Evola, G., L. Marletta and F. Sicurella (2014). "Simulation of a ventilated cavity to enhance the effectiveness of PCM wallboards for summer thermal comfort in buildings." Energy and Buildings **70**: 480-489.

FIBRANs. (2011). Energy Shield. Thermal insulation with extruded polystyrene FIBRANxps, , from http://www.fibran.com.pt/.

Gellings, C. W. (2009). The smart grid: enabling energy efficiency and demand response, The Fairmont Press, Inc.

Goldstein J, Newbury D, Echlin P, Joy D, Romig A, Lyman C, Fior C and Lifshin E (1992). Scanning Electron Microscopy and X-ray Microanalysis. New York, Plenum Press.

Gómez, M., Álvarez Feijoo M, Comesaña R and Eguía P (2012). "CFD Simulation of a Concrete Cubicle to Analyze the Thermal Effect of Phase Change Materials in Buildings " energies **5**(7): 2093-2111.

Gowreesunker, B. L. and Tassou S. A. (2013). "Effectiveness of CFD simulation for the performance prediction of phase change building boards in the thermal environment control of indoor spaces." Building and Environment **59**(0): 612-625.

Hassan A (2010). Phase Change Materials for Thermal Regulation of Building Integrated Photovoltaics PhD Thesis Dublin Institute of Technology.

Hassan E (1991). "Technical assessment of solar thermal energy storage technologies " Pergamon Renewable Energy.

Hawes, D. W., D. Banu and D. Feldman (1989). "Latent heat storage in concrete." Solar Energy Materials **19**(3–5): 335-348.

Hawladera, M., Uddin M and Khin M (2003). "Microencapsulated PCM thermal-energy storage system." Applied Energy **74**: 195-202.

Hensen J (2011). Computational optimization of passive use of phase change materials in lightweight Low-Energy houses. MSc Master thesis, Eindhoven university.

Hong, Y., H. Hanfeng and G. Xinshi (2004). "The comparative numerical investigations on the melting process of form-stable phase change material using enthalpy formulation method and effective heat capacity formulation method." Acta Energiae Solaris Sinica **25**: 488-491.

Incopera, F., Dewitt D, Bergman T and Lavine A (2007). Fundamentals of heat and mass transfer, John Wiley.

ISO6946 (2007). building components and building elements-Thermal resistance and thermal transmittance- Calculation method.

ISO:8301 (1991). Thermal insulation: determination of steady state thermal resistance and related properties, heat flow meter apparatus.

Jaworski, M. (2014). "Thermal performance of building element containing phase change material (PCM) integrated with ventilation system – An experimental study." Applied Thermal Engineering **70**(1): 665-674.

Jeong, S.-G., J. Jeon, J. Cha, J. Kim and S. Kim (2013). "Preparation and evaluation of thermal enhanced silica fume by incorporating organic PCM, for application to concrete." Energy and Buildings **62**: 190-195.

Jin, X., X. Xu, X. Zhang and Y. Yin (2014). "Determination of the PCM melting temperature range using DSC." Thermochimica Acta **595**(0): 17-21.

Kalnæs, S. E. and B. P. Jelle (2015). "Phase change materials and products for building applications: A state-of-the-art review and future research opportunities." Energy and Buildings **94**: 150-176.

Karaipekli, A. and A. Sarı (2009). "Capric–myristic acid/vermiculite composite as form-stable phase change material for thermal energy storage." Solar Energy **83**(3): 323-332.

Kheradmand, M. (2012). Experimental work and Numerical simulation of facade linings with incorporation of phase change materials. First workshop in civil engineering. University of Minho.

Kheradmand, M., M. Azenha, J. L. B. de Aguiar and K. J. Krakowiak (2014). "Thermal behavior of cement based plastering mortar containing hybrid microencapsulated phase change materials." Energy and Buildings **84**(0): 526-536.

Kheradmand, M., J. Castro-Gomes, M. Azenha, P. D. Silva, J. L. B. de Aguiar and S. E. Zoorob (2015). "Assessing the feasibility of impregnating phase change materials in lightweight aggregate for development of thermal energy storage systems." Construction and Building Materials **89**: 48-59.

Khudhair, A. M. and M. M. Farid (2004). "A review on energy conservation in building applications with thermal storage by latent heat using phase change materials." Energy Conversion and Management **45**(2): 263-275.

Kosny, J. and Yarbrough D (2010). Development and testing of ignition resistant microencapsulated phase change material. Oak Ridge National Laboratory, Oak Ridge.

kousksou T, Jamil A and Zeraouli Y (2012). "Enthalpy and apparent specific heat capacity of the binary solution during the melting process: DSC modelling." Thermochimica Acta **41**: 31-41.

Kousksou, T., Rhafiki T, Jamil A, Bruel P and Zeraouli Y (2013). "PCMs inside emulsions: Some specific aspects related to DSC (differential scanning calorimeter)-like configurations." Energy **56**: 175-183.

Kuznik F, Virgone J and Roux JJ (2008). " Energetic efficiency of room wall containing PCM wallboard: a full-scale experimental investigation." Energy and Buildings **40**(1): 48–56.

Kuznik, F. and Virgone J (2009). "Experimental assessment of a phase change material for wall building use." Applied Energy **86**: 2038–2046.

Lamberg, P., Lehtiniemi R and Henell A (2004). "Numerical and Experimental Investigation of Melting and Freezing Processes in Phase Change Material Storage." International Journal of Thermal Sciences **43**.

Lecompte, T., P. Le Bideau, P. Glouannec, D. Nortershauser and S. Le Masson (2015). "Mechanical and thermo-physical behaviour of concretes and mortars containing phase change material." Energy and Buildings **94**(0): 52-60.

Li M, Zhishen Wu and Tan J (2013). "Heat storage properties of the cement mortar incorporated with composite phase change material." Applied Energy **103**: 393–399.

Lu, Z., B. Xu, J. Zhang, Y. Zhu, G. Sun and Z. Li (2014). "Preparation and characterization of expanded perlite/paraffin composite as form-stable phase change material." Solar Energy **108**(0): 460-466.

Lucas, S. S., V. M. Ferreira and J. L. B. d. Aguiar (2013). "Latent heat storage in PCM containing mortars—Study of microstructural modifications." Energy and Buildings **66**(0): 724-731.

Madenci, E. and I. Guven (2015). The Finite Element Method and Applications in Engineering Using ANSYS, Springer.

Manie J (2010). DIANA Finite Element Analysis User's Manual—Release 9.4.3. Netherlands TNO DIANA BV, .

MC-Bauchemie (2011). technical data sheet for Makote 3. Portugal.

Melhing, H. and Cabeza L.F (2008). Heat and Cold Storage with PCM, An Up to Date Introduction into Basics and Applications. Dieter Mewes. Berlin, Germany., Springer.

Memon Shazim A (2014). "Phase change materials integrated in building walls: A state of the art review." Renewable and Sustainable Energy Reviews **31**: 870-906.

Microthermic (2012). DEVAN chemicals. THERMIC temperature regulation technology. Portugal.

Murphy C. B (1958). "Differential Thermal Analysis." Analytical Chemistry **30**(4): 867-872.

Nova Win (2008). "User manual, Quantachrome Instruments , Nova Series Windows-based operating and data. ."

Nóvoa, P. J. R. O., M. C. S. Ribeiro, A. J. M. Ferreira and A. T. Marques (2004). "Mechanical characterization of lightweight polymer mortar modified with cork granulates." Composites Science and Technology **64**(13–14): 2197-2205.

Pasupathy, A. (2008). "Effect of double layer phase  change material in building roof for year round thermal managment." Energy Build: 193-203.

Pires, L., Silva P and Castro Gomes J P (2013). "Experimental study of an innovative element for passive cooling of buildings." Sustainable Energy Technologies and Assessments **4**: 29-35.

Pointwise Inc. (2015). "Pointwise: Mesh Generation Software for CFD, Release 17.2, http://www.pointwise.com/."

Ravikumar, M. and Srinisavand D (2008). "Phase change material as a thermal energy storage material for cooling of building " Journal of Theoretical and Applied Information Technology. .

RCCTE (2006). Regulamento das Características de Comportamento Térmico dos Edifícios (RCCTE).

Robynne, E. and Dominic G (2011). Modeling Convection during Melting of a Phase Change Material  The COMSOL Conference 2011 Boston.

Rubitherm GmbH (2012). "Technologies is the leading manufacturer of innovative Phase Change Material - RT, Germany."

Sakulich, A. R. and Bentz D.P (2012). "Incorporation of phase change materials in cementitious systems via fine lightweight aggregate." Construction and Building Materials **35**: 483-490.

Sarı, Sarı  H and Önal  A (2004). "Thermal properties and thermal reliability of eutectic mixtures of some fatty acids as latent heat storage materials." Energy Conversion and Management **45**(3): 365–376.

Sayyar, M., R. R. Weerasiri, P. Soroushian and J. Lu (2014). "Experimental and numerical study of shape-stable phase-change nanocomposite toward energy-efficient building constructions." Energy and Buildings **75**: 249-255.

Shafie-khah M, Kheradmand M, Javadi S, Azenha  M, Aguiar J, Castro Gomes J P and Catalao J P S (2015). "Optimal Behavior of Responsive Residential Demand considering Hybrid Phase Change Materials." Applied Energy.

Sharma, A., Tyagi V.V, Chen C.R and Buddhi D (2009). "Review on thermal energy storage with phase change materials and applications." Renewable and Sustainable Energy Reviews **13**(3): 18–45.

Shilei L, Guohui F and Neng  Z (2007). "Experimental study and evaluation of latent heat storage in phase change materials wallboards." Energy and Buildings **39**.

Shrestha M (2012). PCM Application-Effect on Energy Use and IA Temperature. Master thesis, Norwegian university of science and technology

Sika (2011). Technical sheet for Sikalastic -490T, version nº 1. Portugal.

Silva, E. R., J. F. J. Coelho and J. C. Bordado (2013). "Strength improvement of mortar composites reinforced with newly hybrid-blended fibres: Influence of fibres geometry and morphology." Construction and Building Materials **40**: 473-480.

Soares, N., Costa J.J, Gaspar A.R and Santos P (2013). "Review of passive PCM latent heat thermal energy storage systems towards buildings' energy efficiency." Energy and Buildings **59**: 82–103.

Song, S., L. Dong, Y. Zhang, S. Chen, Q. Li, Y. Guo, S. Deng, S. Si and C. Xiong (2014). "Lauric acid/intercalated kaolinite as form-stable phase change material for thermal energy storage." Energy **76**: 385-389.

Sunliang, C. (2010). State of the art thermal energy storage. Master Thesis, University of Jyväskylä, .

Taylor H.F.W (1990). Cement chemistry. London, Academic Press - Harcourt Brace Jovanovich

The World Weather Online (2014). "Global weather forecast and weather content for websites businesses and the travel industry, http://www.worldweatheronline.com,." Retrieved 2014.

Tittelein, P., S. Gibout, E. Franquet, K. Johannes, L. Zalewski, F. Kuznik, J.-P. Dumas, S. Lassue, J.-P. Bédécarrats and D. David (2015). "Simulation of the thermal and energy behaviour of a composite material containing encapsulated-PCM: Influence of the thermodynamical modelling." Applied Energy **140**(0): 269-274.

Tyagi, V. V. and Buddhi D. (2007). "PCM thermal storage in buildings: A state of art." Renewable and Sustainable Energy Reviews **11**(6): 1146-1166.

Tyagi, V. V., Kaushik S, Tyagi S and Akiyama T (2011). "Development of phase change materials based microencapsulated technology for buildings: a review." Renewable and Sustainable Energy Reviews **15**(2): 1373–1391.

URBICULT (2012). "The URBICULT Unipessoal Co. − Vermiculite / Perlite products, Portugal."

Vaz Sá, A., Azenha Miguel, de Sousa Hipólito and Samagaio António (2012). "Thermal enhancement of plastering mortars with Phase Change Materials: Experimental and numerical approach." Energy and Buildings **49**: 16-27.

Velraj, R. and Pasupathy A (2009). "Phase Change Material Based Thermal Storage for Energy Conservation in Building Architecture." Institute for Energy Studies.

Ventolà, L., Vendrell M and Giraldez P (2013). "Newly-designed traditional lime mortar with a phase change material as an additive." Construction and Building Materials **47**: 1210-1216.

Vicente, R. and T. Silva (2014). "Brick masonry walls with PCM macrocapsules: An experimental approach." Applied Thermal Engineering **67**(1–2): 24-34.

Wang, Y.-H. and Y.-T. Yang (2011). "Three-dimensional transient cooling simulations of a portable electronic device using PCM (phase change materials) in multi-fin heat sink." Energy **36**(8): 5214-5224.

Weber, S.-G. (2009). Technical sheet for Weber Dry Lastic. Portugal.

Yinping, Z., Guobing Z and Kunping l (2006). Application of latent heat thermal energy storage in buildings: State-of-the-art and outlook, Report. Department of Building Sciences, School of Archtitecture, University Of Beijing.

Zhai, Z., Zhang W and Chen Q (2007). "Evaluation of various turbulence models in predicting airflow and turbulence in enclosed environments  by CFD: Part 1 - Summary of prevalent turbulence models. ." HVAC&R Research **13**: 853-870.

Zhang, D., Zhou J, Wu K and Li Z (2005). "Granular phase changing composites for thermal energy storage." Solar Energy **78**(3): 471-480.

Zhang, Y., K. Du, M. A. Medina and J. He (2014). "An experimental method for validating transient heat transfermathematical models used for phase change materials(PCMs) calculations." Phase Transitions **87**(6): 541-558.

Zhao, C. and Zhang G (2011). "Review on microencapsulated phase change materials (MEPCMs): Fabrication, characterization and applications." Renewable and Sustainable Energy Reviews **15**: 3813–3832.

Zhou, D., Zhao C and Tian Y (2012). "Review on thermal energy storage with phase change materials (PCMs) in building applications." Applied Energy **92**: 593–605.